Faculty of Engineering and Science

Complex Dynamics in Fed-Batch Systems: Modeling, Analysis and Control of Alcoholic Fermentations

Seer Qiu Han

This thesis is presented for the Degree of
Doctor of Philosophy
of
Curtin University

April 2017

Declaration

To the best of my knowledge and belief this dissertation contains no material previously published by any other person except where due acknowledgment has been made.

This dissertation contains no material which has been accepted for the award of any other degree or diploma in any university.

Signature: .....
Date: 24th May 2017

"Never cut a tree down in the wintertime. Never make a negative decision in the low time. Never make your most important decisions when you are in your worst moods. Wait. Be patient. The storm will pass. The spring will come."

- Robert H. Schuller

Abstract

Motivated by energy security, sustainable economic growth and greenhouse gas emission reduction goals, biofuels, such as bioethanol, have emerged as a potential renewable alternative to fossil fuels. Over the past few decades, there has been a tremendous growth in the use of the fermentation process to achieve efficiency with biofuels. Among several different types of fermentation techniques available, the fed-batch fermentation process has gained increasing popularity due to its ability in avoiding the presence of large surplus nutrients in the broth, which can act as kinetic inhibitors leading to low yields and productivity. While this problem can be overcome by using the fed-batch fermentation technique, one of the key challenges in the system operation lies in its difficult control design problem, which arises from the time-varying nature of the system. Hence, to alleviate this problem, the modeling and control of the fed-batch fermentation process has been a subject of great interest in order to realize high productivity and yields from the fermentation technique. In fed-batch modeling, the development of a microbial kinetics model, will in part demonstrate the complexity of the overall system dynamics, which in turn will affect the controllability of the system.

A part of the present study was to investigate how pH, aeration rate and stirrer speed affect ethanol production by Bakers yeast using combined cassava and fruit waste (rejected mango and durian seeds) as feedstock. The usage of fruit waste (e.g. damaged fruit, peels and seeds) helped to reduce the heavy reliance on agricultural crops and avoid expensive pretreatment as in the case of lignocellulosic materials with complex structure. One of the findings showed that a simple Monods model was unable to describe the fermentation kinetics, suggesting that complex carbohydrate sources can lead to a more complex microbial kinetics behavior. A modified model based on the combined Herbert-Haldane microbial kinetics model was developed, which seemed to fit the experimental data better. Also, this modified Herbert-Haldane microbial kinetics model can be further altered to incorporate the direct effects of pH, aeration rate (AR) and

stirrer speed (SS) into the microbial kinetics. The proposed microbial model should be sufficiently reliable especially in describing the death phase in biomass concentration towards the end of fermentation. Although simple in structure, the proposed model has been shown to be accurate enough for applications in simulation, design and control studies of alcoholic fermentation processes.

Another part of this study, which constitutes the major component of the dissertation, was to investigate the complex dynamic behaviors that can arise from the fed-batch fermentation process and the stability implications imposed by these complex dynamics on a standard single-loop PID controller. As the fed-batch complex dynamics can evolve throughout the fermentation process, it is important to identify several typical dynamic forms at different points along some possible operating trajectories. Many of these complex dynamics can be adequately represented by fourth-order integrating/unstable model with multiple RHP zeros. Detailed understanding of such a point-wise, complex dynamic behaviors should provide us with hints on how to tune or design a given controller with guaranteed stability from the linear system point of view. In turn, sufficient understanding of all the possible forms of the complex dynamics, which can occur during the fed-batch operation, will help to better design an effective nonlinear control system for the fed-batch fermentation process, thus guaranteeing closed-loop stability as well as providing improvements in productivity. It is important to focus on addressing these complex dynamics separately (point-wise) by using a conventional PID controller before trying to address the fed-batch nonlinearity problem by developing some advanced control strategies.

From this study, two new theorems (i.e. necessary and sufficient criteria for stability) have been developed based on the Routh-Hurwitz stability analysis. These theorems enable effective determination of all stabilizing PID parameter regions for a single-loop feedback structure applied to a given form of complex dynamics in the fed-batch process. One of the findings in this study showed that a low-order PID controller could assure the stability for some of the complex dynamics that may occur in the fed-batch system. Fortunately, for these complex dynamics there is no need to use advanced high-order controllers. However, in some cases where the fed-batch dynamics are too complex, which would preclude the application of a single-loop PID controller, two novel advanced control schemes unifying both the direct and indirect multi-scale control (MSC) principles have been proposed, namely double-loop MSC and triple-loop MSC control schemes. Extensive simulation studies have demonstrated that both schemes can provide effective control of high-order unstable/unstable-integrating systems with

multiple RHP zeros, which could not otherwise be stabilized using a single-loop feedback control structure.

One possible future research topic is to apply the proposed advanced MSC schemes in developing a novel nonlinear control strategy. This novel control strategy should be able to handle both nonlinearity and complex dynamics problems encountered in a typical fed-batch fermentation process.

Acknowledgments

First and foremost, I would like to express my sincerest gratitude to my supervisor, A/Prof. Jobrun Nandong, who has supported me throughout my research with his patience, knowledge, guidance and encouragement whilst gave me the freedom to explore and work in my own way. His uncompromising research attitude and stimulating advice helped me in overcoming obstacles throughout my PhD. Moreover, I would like to gratefully thank to my co-supervisor, A/Prof. Zhuquan Zang, for his advice and constructive comments that he has provided in this dissertation. I have been extremely lucky to have both supervisors who cared so much about my work, and who responded to my questions and queries so promptly. Moreover, I would like to express my gratitude to my dissertation chairperson, Prof. Chua Han Bing for his valuable comments.

I would like to acknowledge the Curtin Malaysia Research Institute for supporting this research study through the project no. CMRI6009. Moreover, I acknowledge the financial and other support from Curtin University, Sarawak campus.

In my daily work, I have been blessed with a friendly and cheerful group of fellow students. Completing this work would have been all the more difficult were it not for the support and friendship provided by the postgraduate students at Curtin University, Sarawak campus and all the members of Curtin Sarawak Research Institute for helping me keep things in perspective.

Most importantly, none of this would have been possible without the love and patience of my family. I would like to express my heart-felt gratitude to my family for their love, concern and support all these years. Last but not the least, I wish to thank Benjamin Chong Min Fui for his great support and loving care. He was always there cheering me up and stood by me through the good times and bad. I dedicate my dissertation to all of you.

Publications

Q. H. Seer, J. Nandong and Z. Zang. Decentralized Control Design for Ethanol Fermentation by Zymomonas Mobilis - Multi-scale Control Approach. *Applied Mechanics and Materials*, 625: 34-37, 2014. (Best Paper Award)

Q. H. Seer and J. Nandong. Experimental study of the impacts of pH and aeration on kinetics of ethanol fermentation using cassava and fruit waste. *Asia Pacific Confederation of Chemical Engineering Congress 2015: APCChE 2015, incorporating CHEMECA 2015*, 1905-1915, 2015.

Q. H. Seer and J. Nandong. Tuning method for double-loop control structure for nonminimum-phase integrating systems. *2015 IEEE Conference on Control Applications (CCA)*, 589-594, 2015.

Q. H. Seer and J. Nandong. A unified double-loop multi-scale control strategy for NMP integrating-unstable systems. *IOP Conference Series: Materials Science and Engineering*, 121 (1): 12-21, 2016.

Q. H. Seer and J. Nandong. Advanced Expanded Microbial Kinetics (EMK) Model for Ethanol Production from Mixed Cassava and Fruit Wastes. *Procedia Engineering*, 148: 417-425, 2016.

Q. H. Seer, J. Nandong and T. Shanon. Experimental Study of Bioethanol Production using Mixed Cassava and Durian Seed. *IOP Conference Series: Materials Science and Engineering*, 206 (1): 12-20, 2017.

Q. H. Seer and J. Nandong. Stabilization and PID tuning algorithms for second-order unstable processes with time-delays. *ISA Transactions*, 67: 233-245, 2017.

Q. H. Seer and J. Nandong. Stabilizing PID Tuning for a class of fourth-order integrating nonminimum-phase systems. *Submitted to International Journal of Control - under first revision May 2017.*

Q. H. Seer and J. Nandong. Multi-scale control scheme: stabilization of a class of fourth-order integrating-unstable systems. *Submitted to Journal of Franklin Institute - under first revision May 2017.*

Contents

List of Figures

List of Tables

Chapter 1

Introduction

1.1 Background

A wide variety of fermentation products, such as foods, chemicals (solvents, enzymes, acids and others), biofuels and pharmaceuticals can be produced from the fermentation process. The operational mode of the fermentation process can be classified into three types: batch, fed-batch and continuous culture. Fed-batch culture is widely employed in the fermentation industry as it can reduce inhibition by high substrate concentration and thereby achieve high productivity and yields.

In recent years, the development of alternative energy sources has been a subject of great interest due to climate change, rapid growth in world energy demand and fast depletion of fossil fuels reserves [1, 2]. Bioethanol has been recognized as one of the promising alternative renewable fuels, which can improve energy security and reduce greenhouse gas emissions [1–4]. There are two ways to produce bioethanol: (1) the petrochemical route from the hydration of ethylene and (2) the most frequent biotechnological route, via microbial fermentation of agricultural biomass [5]. Conventionally, bioethanol is produced based on the latter from the fermentation of carbohydrate sources, i.e. agricultural crops and lignocellulosic waste. The conventional ethanol fermentation production process has primarily utilized sugar-based and starch-based food crops, which will over the long-term; compete with humans' need for food. Meanwhile, the use of lignocellulosic waste avoids such competition, but requires costly pretreatment to break down the tough lignin structure which often leads to low productivity, hence preventing commercialization [6–8].

In fact, the control design for the fed-batch fermentation processes was in-

tended to improve the operational stability and productivity. Over the past three decades, most research has mainly focused on addressing the nonlinearity problem of fed-batch fermentation by using advanced control strategies, i.e., optimal control [9, 10], robust control [11–13] and adaptive control [14–16]. It should be noted, fed-batch dynamics not only vary nonlinearly with operating conditions, but are also known to be high-order with the presence of complex dynamics. In order to have a more integrated control system for the fed-batch fermentation process, more emphasis should be made in dealing with those challenging complex dynamics arising from a typical fed-batch fermentation process. The traditional proportional-integral-derivative (PID) controllers are still commonly used in industries due to their simplicity and effectiveness. For this reason, it is extremely important to design the PID controllers to deal with those complex dynamics effectively before the implementation of advanced control strategies.

The goal of this dissertation is to gain insights into how the complex dynamic behaviors exhibited in fed-batch fermentation systems affect the stability of standard single-loop as well as non-standard feedback control structures.

1.2 Motivation and Objectives

Fed-batch systems are challenging to control due to process variability and complexity of biological systems, which result in complex and strong nonlinear dynamics. Until now, there has been a limited number of studies on the mathematical forms of complex dynamics in fed-batch processes. The complex high-order dynamic behaviors in a fed-batch system vary depending on the nature of fermentation conditions (concentration, temperature and pH), substrate types, and microorganisms used. Some mathematical models known as microbial kinetics models commonly represent microbial behavior. In fed-batch modeling, the type of microbial kinetics model used will in part determine the complexity of the system dynamics and affect the controllability of the system. The following research gaps that have been identified are as follows:

i. Kinetics modeling of alcoholic fermentation using fruit waste.

ii. Detailed point-wise analysis on the dynamics behavior of the fed-batch fermentation process.

iii. The stabilization and control of some complex dynamics in fed-batch fermentation in the context of the linear system approach.

The first gap requires a fundamental study via experiment in order to develop fermentation kinetics modeling using fruit waste. A reliable kinetics model for the bioprocess modeling is a prerequisite in order to obtain satisfactory results in any optimization and control study. The following hypotheses were posed as a guide in carrying out the experimental study on fermentation kinetics using mixed fruit waste and cassava:

i. The standard well-known Monod and Haldane kinetics models are not suitable to represent fermentation kinetics because the cell death rate is ignored, which is not realistic.

ii. pH has the largest influence on fermentation kinetics of mixed fruit waste and cassava because substantial deviation of the extracellular pH from the intracellular pH will cause greater stress on yeast cells in order to maintain the intracellular pH within the optimal range.

iii. Under micro-aerobic fermentation, the effect of mixing intensity (aeration rate and stirrer speed) is critical to maintain metabolite production.

In this work, the notion on Complex Dynamics is given as follows:

"A nonlinear system is said to have complex dynamics if the linearized process behaviors at any given operating point are given by a high-order system (model) having at least one unstable or integrating pole and with at least one right-half plane (RHP) zero. This high-order model cannot simply be reduced to a low (first- or second-order) model without losing the main information on the process behaviors at the given operating point. These complex dynamics are often very difficult or even impossible to stabilize using a standard single-loop PID controller."

It has been found that, a nonlinear fed-batch process model with four state variables can yield several forms of complex dynamics along an operating trajectory where most of the dynamics are representable by fourth-order integrating/unstable models with multiple RHP zeros.

The work described in this dissertation is aimed to fill these research gaps where the issues of control structure in fed-batch fermentation are addressed. The main objectives of this dissertation are as follows:

i. To study the effect of pH, aeration rate and stirrer speed on the bioreactor performance (i.e. yield and productivity) of ethanol from mixed fruit waste and cassava.

ii. To develop a new kinetic model, which is simple to use and reliable for a fed-batch fermentation process using fruit waste by *Saccharomyces cerevisiae* Type II.

iii. To determine the stability of a standard single closed-loop PID control for some complex dynamic behaviors exhibited in the fed-batch fermentation process based on the Routh-Hurwitz stability criteria.

iv. To develop new control strategies based on the multi-scale control (MSC) theory - double-loop MSC and triple-loop MSC control schemes.

1.3 Novelty, Contribution and Significance

The fed-batch processes is widely used in fermentation industries. However, modeling and controlling the processes are still considered unaddressed problems, which are subject to on-going research with the goals to maximize the product yield and quality. In regards to the bioprocess control aspect, most of the research has focused on the controller design algorithms over the past few decades; the closed-loop stabilization by conventional PID controllers has received less attention from researchers. The notable feature of this research study is that, an advanced PID-type-control structure, which unifies the multi-scale control (MSC) schemes is proposed to address the current knowledge gap in dealing with some specific complex dynamic behaviors inherent in some fed-batch bioprocesses.

The novelty of this research can be summarized as follows:

i. Development of kinetic models which incorporate mixing conditions (due to aeration rate and stirrer speed) and pH for the fed-batch system using fruit waste as a feedstock for fermentation.

ii. Development of two new theorems based on Routh-Hurwitz stability criteria, i.e., necessary and sufficient conditions, in order to determine the closed-loop stability of a PID-type controller.

iii. Development of two new advanced multi-scale control schemes which use a combination of 2 to 3 conventional PID controllers. The proposed double-loop multi-scale control scheme adopts two conventional PID controllers while the triple-loop multi-scale control scheme uses three PID controllers.

The major contributions of this research can be viewed in two aspects, theoretical (academic) contributions and contributions to industry. The theoretical contributions of this research study are:

i. A new unstructured kinetic model was developed, which is simple to use and reliable for describing the microbial growth during ethanolic fermentation.

ii. Two new PID closed-loop stabilization theorems were developed, i.e. only 3 or 5 steps are required to establish the stabilizing PID regions for second-order unstable processes and fourth-order integrating-unstable processes respectively.

iii. A new framework for unifying multi-scale control (MSC) for fed-batch fermentation processes was proposed. The double-loop MSC and triple-loop MSC schemes aim to first decompose the complex dynamics into two or three simpler sub-systems, which are then separately addressed in a multi-scale structure.

As for the practical contribution, this research provides a new set of knowledge and methods in fed-batch control system and fed-batch fermentation system modeling.

This study is significant for four reasons. First, this study proposes a fermentable feedstock that is cheap and readily available, i.e. fruit waste, such as rejected mango fruit. The fruit waste is high in sugar content and nutrients, which can be used readily as a glucose source without any hydrolysis or pretreatment processing. Thus, the cost of using rejected fruit should be low compared to starch-based and lignocellulosic materials. Second, the modular design based on the fed-batch mode can be implemented in small-scale ethanol production in distributed locations. Small-scale production is more attractive to rural communities compared to the conventional large-scale continuous systems, due to lower construction and logistic costs (e.g. transportation and storage). Moreover, rural communities can reduce dependence on expensive gasoline via bioethanol production utilizing this modular system. Third, the performance of the ethanol fermentation process can be improved by employing a systematic approach to control system design. The key significance in this study is the development of an effective control system design of the fed-batch fermentation processes, which can overcome the complex dynamic behaviors encountered. The outcome will be determined in the longer term with evidence of increased productivity and overall cost efficiency of the entire system design.

Another key significance of this study is that the new PID closed-loop stabilization theorems can be effectively used to establish stability regions of PID parameters for any given process whose dynamics is representable by a linear model. This is useful as in process industry, many processes are represented by some linear models, which are used to design or tune PID controllers. Thus, these theorems shall facilitate the tuning or design of PID controllers in industries.

1.4 Dissertation Structure

Figure 1.1 shows the overview of the dissertation structure. This dissertation is outlined as follows:

Chapter 1 defines the background, motivation and objectives of this research and is followed by the significance and contributions, whereby the issues and knowledge gaps relevant to this study are highlighted. The structure of this dissertation is summarized in this chapter.

Chapter 2 covers the literature review on the background relevant to this research study. The first part covers the overview of the fermentation process. The second part includes a review of the mathematical model (i.e., dynamics of bioreactor and microbial kinetics model) of the fermentation process. Lastly, the existing advanced control techniques in the bioprocess and the key challenges of the control design problem of the fed-batch fermentation process are reviewed. As a result, this review aims to identify the existing achievements and also the research gaps relevant to this study.

Chapter 3 concentrates on the experimental and analytical techniques required in this study. The experiments using mixed mango waste and cassava as feedstock were conducted as a case study for ethanolic fermentation. Meanwhile, the dynamics and microbial kinetics were studied with respect to the pH and mixing intensity (i.e., aeration rate and stirrer speed) within a batch mode bioreactor.

Chapter 4 presents the examination of the stabilization by PID controller of second-order unstable processes, which can be represented as a second-order deadtime with an unstable pole (SODUP) and a second-order deadtime with two unstable poles (SODTUP), based on necessary and sufficient criteria of the Routh-Hurwitz stability analysis. In doing so, the stabilization of some complex

dynamics, such as time delay and unstable poles are discussed.

Chapter 5 discusses the different forms of complex dynamics inherent in the fed-batch fermentation process. The limitations of a standard single-loop PID controller in providing stabilization to such high-order and complex dynamics process are discussed.

Chapter 6 presents the applications of the multi-scale control (MSC) scheme, which are applicable to multi-inputs and multi-outputs (MIMO) and integrating processes by using a decentralized control and a double-loop control structure respectively.

Chapter 7 extends the basic idea of the MSC scheme. A double-loop MSC (DL-MSC) scheme was developed which unifies the direct and indirect MSC schemes via a double-loop control structure for controlling highly nonminimum-phase integrating processes.

Chapter 8 provides a new triple-loop MSC (TL-MSC) scheme to deal with the stabilization of fourth-order integrating-unstable systems.

Chapter 9 draws conclusions from this research study and suggests future directions for extending its application into different areas.

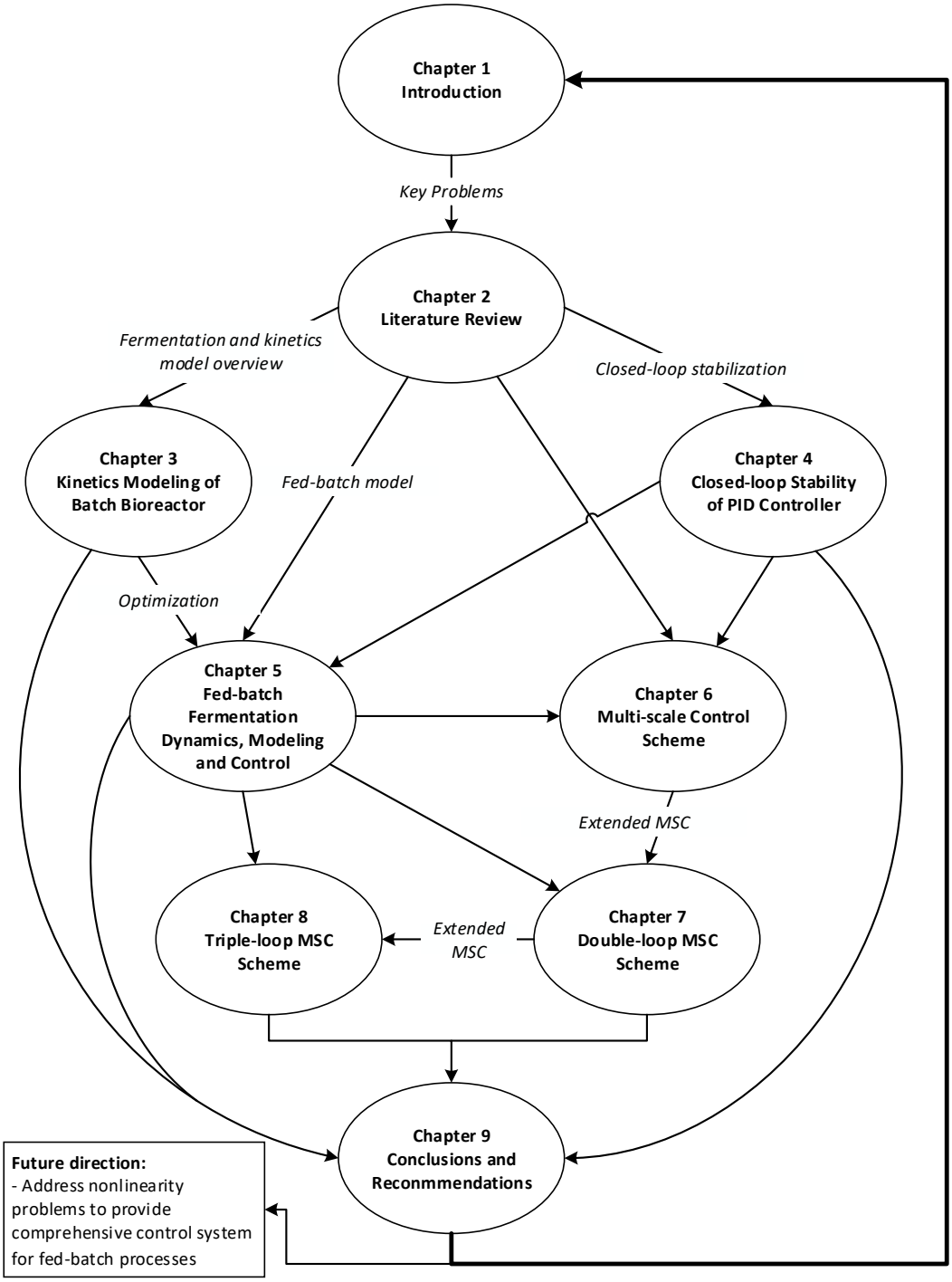

Figure 1.1: Dissertation structure overview

Chapter 2

Literature Review

A fed-batch fermentation process is commonly used in biotechnological industries to overcome substrate inhibition. The development of mathematical model (i.e., dynamics of bioreactor and kinetics modeling of microorganisms) of the fed-batch fermentation process is important for optimization and control study. Even when based on simple models, a fed-batch fermentation process can demonstrate high-order systems (at least fourth-order) with complex dynamic behaviors throughout the course of its operation. Most research has mainly focused on addressing the nonlinearity problem by using advanced control strategies, i.e., nonlinear PID. However, can a single-loop PID controller provides stabilization for such complex forms of dynamic behaviors? A high-order non-PID controller might be used instead, but it might be too complicated to be applied in a practical environment. To demonstrate the theoretical basis for this research, a concise literature review is presented in this chapter. The key points of the presentation are as follows:

- Overview of the alcoholic fermentation process.
- Modeling of fermentation process, i.e., kinetics modeling and bioreactor modeling.
- Key challenges in controller design of fed-batch fermentation process.
- Advanced control techniques in bioprocess.

2.1 Fermentation Process - Overview

Fermentation process is widely used within the food, pharmaceutical and biochemical industries. In recent years, a great interest in the production of some

commodity chemicals, such as ethanol, butanol, acetic acid, citric acid and etc, by fermentation processes has been observed.

Fermentation is a result of a complex reaction network characterizing certain metabolic activities carried out by yeast or bacterias that converts carbohydrate such as starch or sugar to acids, gases, and/or alcohol. When the medium is inoculated with microorganisms, there are four distinct phases of cell growth which have been observed as shown in Figure 2.1. Initially, the lag phase is a period without significant cell growth due to adaptation of the cells to new environment during which period enzymes are synthesized to employ nutrients in medium. Subsequently, it is followed by a log (exponential) phase, a period of rapid increase in the cell population in the presence of nutrients in excess. The growth is rapid and the cells multiply in an exponential order and most of the kinetic growth parameters are described in relation to this phase. In the next stationary phase, the cell growth becomes stagnant due to nutrient exhaustion. The microorganisms are still maintaining a certain metabolic activities by converting nutrients into secondary metabolites. Finally, the shortage of nutrient causes the decay of microorganisms, called death phase [17–19]. Acquiring basic understanding of the phases of cell growth is important in kinetics modeling.

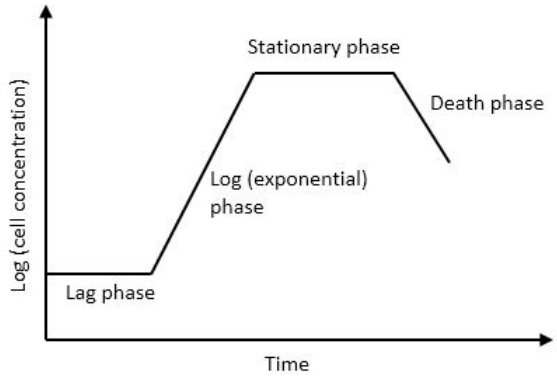

Figure 2.1: Phases of cell growth in a batch culture

A fermentation process is made up of bioreactor. Generally, there are three different types of mode of operation for bioreactor: (1) batch (2) fed-batch and (3) continuous culture. Batch and fed-batch are two modes of operation which are commonly used in fermentation industry. Over the past few decades, a fed-batch culture has been preferable as it can avoid the surplus nutrients which may inhibit microorganism growth, e.g., the concentration of glucose above 150 g/L would reduce the activity and growth of microorganisms in conventional alcoholic

fermentation [20, 21]. Moreover, the exponential phase can be extended and leads to high cell densities [22]. In so doing, the reaction can reach high yield and high production rate compared to batch fermentation [21, 23–26]. Thus, most studies in modeling and control in fermentation processes are now focused on fed-batch culture rather than batch and continuous culture.

2.1.1 Production of Bioethanol

Although many microbes, such as *Escherichia coli* and *Zymomonas mobilis*, have been used in ethanol production, *Saccharomyces cerevisiae* is the main yeast species used in ethanol production due to its active glucose transport system [4, 27–29]. Glycolysis (Embden-Meyerhof-Parnas or EMP pathway) is the main metabolic pathway in the ethanol fermentation process, whereby glucose is metabolized and convert into two molecules of pyruvate, two high-energy compounds ATP (adenosine triphosphate) and two NADH (reduced nicotinamide adenine dinucleotide) [4, 17, 27].

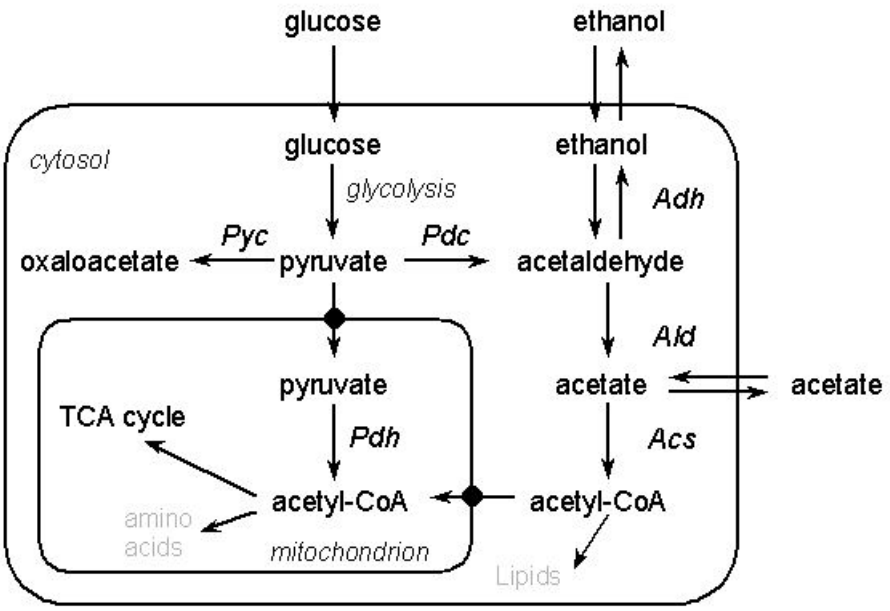

Figure 2.2: Pyruvate metabolism in *Saccharomyces cerevisiae*. Pyc: pyruvate carboxylase; Pdh: pyruvate-dehydrogenase complex; Pdc: pyruvate decarboxylase; Adh: alcohol dehydrogenase; Ald: acetaldehyde dehydrogenase; Acs: acetyl-coenzyme A synthetase

In Figure 2.2, the pyruvate formed in glycolysis pathway can be reduced into acetaldehyde or acetyl-CoA [30]. The acetaldehyde can be converted to ethanol

while the acetyle-CoA can be used for Tricarboxylic acid (TCA or Kreb's cycle) for cell respiration [17]. On the other hand, yeast cell growth requires two ATPs produced from glycolysis to drive the bio-synthesis, thus, ethanol production is tightly coupled with yeast cell growth [4]. Theoretically, 1g of glucose is able to produce 0.511g of ethanol and 0.489g of CO_2 base on mass basis. A yield of 90-93% of ethanol theoretical yield can be produced by *Saccharomyces cerevisiae* based on total sugar feeding [4]. Moreover, it is recognized as safe (GRAS) microorganism that can produce up to 20% (v/v) ethanol from mainly C6 carbon sources (e.g. glucose) by fermentation process [4, 29, 31]. In the current research project, *Saccharomyces cerevisiae* is used as a case study for bioethanol production in the experiments.

2.1.1.1 Bioethanol Feedstocks

In general, bioethanol can be extracted from the fermentation of various sorts of carbohydrate sources. The first generation feedstocks for bioethanol production refer to food crops, mainly from sugar-based and starch-based biomass. The second generation raw materials refer to non-food biomass sources, such as lignocellulosic biomass. The third generation feedstocks are focused on the fermentation from algae. The examples of each categorized feedstock are shown in Table 2.1.

Table 2.1: Bioethanol feedstocks

First Generation Feedstocks		Second Generation Feedstocks	Third Generation Feedstocks
Sugar-based Biomass	Starch-based Biomass	Lignocellulosic Biomass	Algae
Sugarcane	Cassava	Agricultural residues	Microalgae
Molasses	Corn	(straw, stover, baggase)	Macroalgae (seaweed)
Sugar beet	Potato	Forestry residues (wood)	
Fruits	Grains	Waste paper, paper pulp	
Sweet sorghum		Municipal solid waste	

The conventional ethanol production processes primarily refer to first generation feedstocks, which utilize easily fermentable biomass feedstocks to produce bioethanol [32]. Sugar-based crops represent a readily fermentable sugar source (mainly sucrose, fructose and glucose), whilst starch-based materials have to be undergoing simple pre-hydrolysis to break down the chains of carbohydrate for obtaining fermentable sugars (mainly glucose) [6, 33, 34]. However, one of the major concerns with the usage of first generation feedstocks exclusively for bioethanol production is potential competition with livestock and human food consumptions in the long term [1, 2, 35].

This dilemma has motivated extensive studies on the usage of lignocellulosic materials, mainly from agricultural residues, which have been categorized as second generation feedstocks. Second generation feedstocks are attractive as they are sufficiently abundant, renewable and low cost [7, 8, 35]. The bioethanol production from lignocellulosic materials helps to reduce pressure on the demand for food crops. Lignocellulosic biomass is a complex material composed of three main constituents, namely cellulose, hemicellulose and lignin. However, the costly and complicated pretreatment processes (e.g. physical, chemical, or biological) required to break down the complex structure of lignin often lead to low productivity, which has so far prevented commercialization [6–8]. An overview of the processes for various bioethanol feedstocks is shown in Figure 2.3.

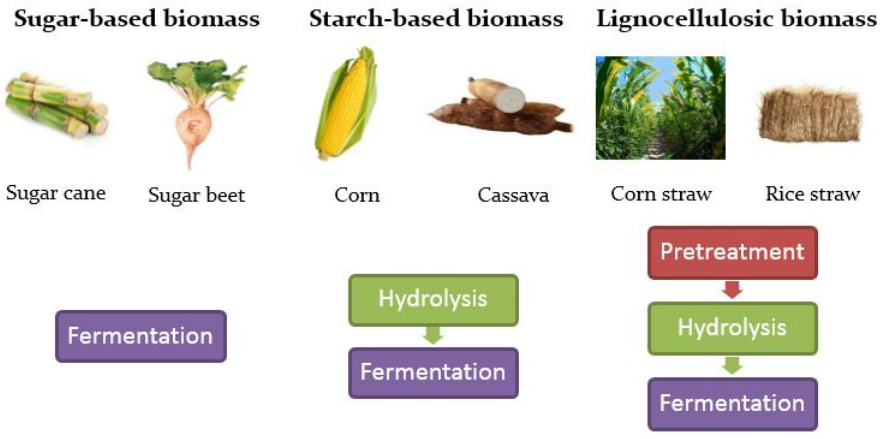

Figure 2.3: Overview process for bioethanol feedstocks

Fruit waste (e.g. damaged fruit and peels) has also been proposed as cheap fermentation feedstock. Fruit waste is often in the form of readily fermentable sugars. Thus, the hydrolysis pretreatment process can be exempted. For such fruit waste, mangoes are abundant in tropical countries, e.g., Malaysia, the re-

jected mangoes can be considered as a cheap source for the fermentation process compared to traditional lignocellulosic waste. In this study, the experimental study of batch fermentation of ethanol production using combined cassava and mango waste as feedstocks is studied.

In Malaysia, the tropical climate creates a luxuriant plant life and produces a wide diversity of edible and succulent fruit. Most of tropical fruits are available all year around (e.g., mangoes), but some are seasonal (e.g., durian). Moreover, cassava is widely harvested in most parts of Asia. Malaysia harvests about 400,000 t year^{-1} of cassava from an area of about 39,000 ha and most of the cassava is for starch production [36].

2.1.2 Fermentation Operating Conditions

The rate of fermentation depends on operating conditions, such as medium pH, temperature, agitation rate (stirrer speed) and aeration rate, which affect the specific rate of growth and ethanol yield [37, 38].

2.1.2.1 Temperature

Fermentation processes are highly sensitive to changes in temperature. At a higher temperature, the rate of yeast activity is higher because the collisions between the substrate and the enzymes active site are more frequent [39]. Thus, an increase of temperature often leads to higher fermentation rate [38, 40]. However, because of several other biological limitations, the increment of yeast activity is only up to a point where the cells are at the maximum efficiency. Beyond this optimum temperature, yeast cells begin to denature due to excessive kinetic energy which breaks the bonds eventually alters the active sites shape. This results in the rapid decrease or even complete halt of the enzymatic reactions involved. It is reported that the inhibition of cell growth could occur at 50℃ [38]. The inhibition of cell growth due to high temperature changes the transport activity or saturation level of soluble compounds and solvents in yeast cells, e.g. ethanol, which might cause a reduction of cell growth [38]. On the other hand, at lower temperatures the cells specific growth rate is lower which is due to their low ethanol tolerance at lower temperatures [41]. The influence of temperature in fermentation process has been studied extensively [37–43]. According to [38, 43], the optimum temperature of saccharifying enzymes for fermentation and microbial growth is 25-35℃.

2.1.2.2 pH

It has been widely recognized that the cultivation pH plays an important role in ethanol production [44]. *S. cerevisiae* is an acidophilic organism where a medium pH in the range of 4 to 6 has been known to be the optimal pH for yeast growth during fermentation. pH has a significant impact on microbial activities [45–47], where the chemical pathways of the biological reactions can be modified by pH parameter as well as their kinetics [45]. The specific growth rate of microorganism was reported to be related to the pH of the growth medium in [48–51]. A constant yeast intracellular pH has to be maintained during fermentation process [52]. When the difference between extracellular pH and intracellular pH becomes wider, greater stress is imposed on yeast cells and more energy is transformed to either pump in or pump out hydrogen ions in order to maintain the intracellular pH within the optimal range [53], which permits growth and survival of the yeast [52, 54], which in turn affect the efficiency of ethanol production.

2.1.2.3 Anaerobic and Aerobic Fermentation Process

Fermentation processes can be carried out in anaerobic process or aerobic process. Aeration rate and stirrer speed are important factors in the fermentation processes, as both of the parameters will affect the mixing mechanisms between the culture medium and microorganism [31, 55]. Aeration is an important factor for growth and ethanol production by *S. cerevisiae*. In practice, most of the fermentation process for ethanol production is carried out under anaerobic condition. The *S. cerevisiae* yeast has the ability to grow under anaerobic conditions, however, it is interesting to point out that a certain amount of delivery of oxygen to culture broth is important to maintain metabolite production and growth of microorganisms [56]. Under anaerobic conditions, small amount of oxygen is required to favor the synthesis of sterols and unsaturated fatty acids, which are necessary for plasma membrane coherence [57–60]. Additionally, the synthesis of unsaturated fatty acids counteracts ethanol inhibition by increasing the fluidity of plasma membrane [4]. Thus, the increasing of aeration rates from very low value leads to improved cell viability and enhancing the formation of ethanol by yeast [31, 61, 62]. A fermentation where limited amount of oxygen is supplied is called micro-aerobic fermentation.

2.1.2.4 Stirrer Speed

In fermentation process, the stirrer speed is an important factor to induce turbulence and shear, which favors homogeneity of yeasts and substrates in broth [63] and prevents the sedimentation of yeasts [64]. Under micro-anaerobic condition with small amount of oxygen delivered to culture broth, stirring breaks up the bubbles [56] while the oxygen transfer is enhanced [65]. Moreover, mixing induces better coupling between catabolism and anabolism [66]. Thus, higher mass transfer rate within the bioreactor is achieved by higher stirrer speed, thereby resulting in higher ethanol yield [31, 64].

2.2 Modeling of Fermentation Process

The mathematical model is defined as a representation in mathematical terms of the behavior of a real process, which is important and useful for design, optimization, control, safety and etc. There are five key reasons why models are required in process engineering [67]:

- To organize disparate information into a coherent whole.
- To think and calculate logically about what components and interactions are important in a complex system (i.e. from DNA sequence to phenotype).
- To discover new strategies.
- To make important corrections in the conventional wisdom.
- To understand the essential, qualitative features.

The basic idea of making models is to be able to bring a measure of order to our experience and observations, as well as to make specific predictions about certain aspects of the world we experience [68]. In Figure 2.4, three stages: observation, modeling and prediction, can be observed in the conceptual world [69]. In observation stage, what is happening in the real world is measured. Modeling stage is to analyze the observations. Validation of a model is integral to the modeling process, i.e., graphical presentations of experimental results are the most convenient and informative method. In fact, modeling or model development for a given process is an iterative procedure: data fitting to a specific model structure and followed by validation. If the validation is not satisfactory, then the model

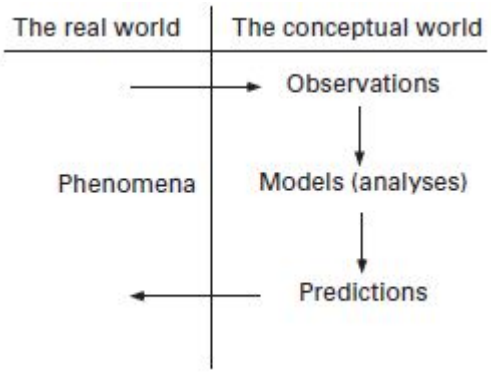

Figure 2.4: Basic idea of making models

structure will be revised and then followed by data fitting and re-validation. The iterative process will go on until satisfactory validation result is obtained. Lastly, the models are exercised and what will happen in a yet-to-be conducted experiment will be revealed on prediction stage. Therefore, mathematical modeling does not make sense without defining, before making the model, what its use is and what problem it is intended to help to solve [68].

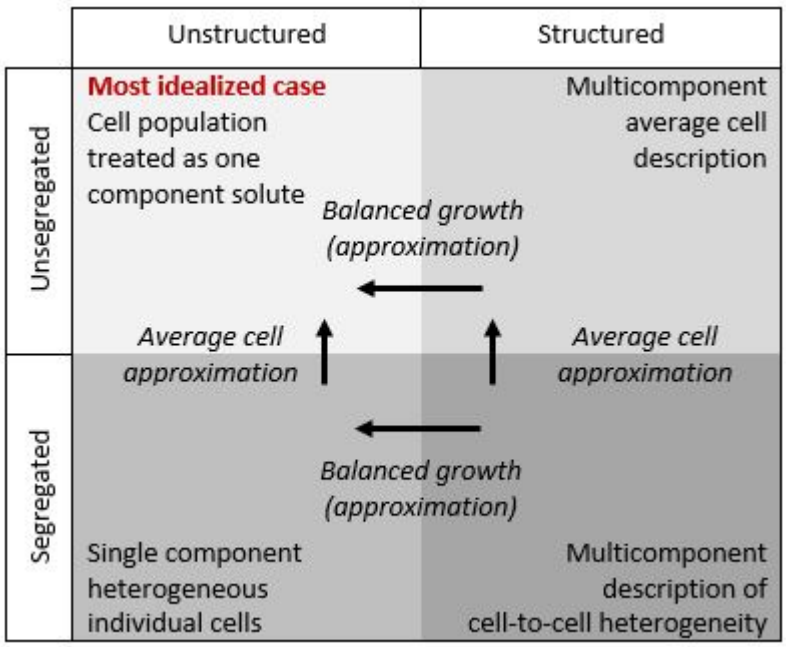

Figure 2.5: Mathematical (and other) representation of cell populations

The models of cell populations can be divided into structured/unstructured and segregated/unsegregated [67]. Figure 2.5 shows the classification of mathe-

matical and other representation of cell populations introduced by A. G. Fredrickson [67]. The 'segregated' term represents explicit accounting for the presence of heterogeneous individuals in a population of cells, whereby the 'structured' term represents a formulation in which a cell material is composed of multiple chemical components. In modeling of bioprocesses, the majority of the kinetic models of cell populations is described by using unsegregated and unstructured model, which consider the cell population as one component solute.

There are two component models involved in the modeling of a bioreactor, which are: (1) dynamics (mass and energy balances) of bioreactor, and (2) kinetics modeling of microorganisms involved. Generally, the macro-scale (black box) approach is used for bioreactor modeling. The black box models are frequently used in process optimization and control, which provide the functionality relations between input factors and output responses. The schematic diagram of macro-scale bioreactor modeling is shown in Figure 2.6, where U_{mac} and Y_{mac} represent the input and output variables of the process respectively.

Figure 2.6: Schematic diagram of macro-scale bioreactor modeling

Kinetics model is critical in the mathematical modeling of a whole bioprocess of interest, where the bioreactor model can be used for optimization and control study. In the modeling of the fermentation process, the behaviors of cell population are the main idea of the complex kinetic description. An unstructured kinetic model is often used in bioreactor modeling, which represent a simple overview of the metabolism of cell over the course of time [18]. Nevertheless, the kinetics modeling also incorporate with cell growth, substrates consumption, products synthesis and sometimes with the cell death [18]. The majority of kinetic models describing microbial growth during alcoholic fermentation follows a formal unstructured (macro) approach to bioprocessing. Various studies have been dedicated to the modeling of the key parameters affecting alcoholic fermentation. Table 2.2 summarizes some of the modeling of key behaviors in alcoholic fermentation obtained from open literature.

Table 2.2: Summaries on modeling of key parameters in alcoholic fermentation

Key Parameters	**Remarks**	**References**
High substrate or product or biomass concentration	Inhibition effects due to high substrate, product or biomass concentrations and lead to low yield.	[70–75]
Temperature	High temperature changes the transport activity or saturation level of soluble compounds and solvents in cell.	[46, 47, 76, 77]
pH	Different yeast has its optimal pH for yeast growth. Significant deviation of extracellular pH from the optimal intracellular pH leads to low yield.	[45–47, 76, 78]
Oxygen supply	Small amount of oxygen supply could increase cell viability. Mirco-aerobic improves cell viability under stress conditions.	[79–81]

2.2.1 Bioreactor Modeling

In general, the macro-scale model of a bioreactor can be represented by a set of mass balance differential equations. A set of differential equations of a bioreactor with respect to state variables and output variables can be described as:

$$\dot{Z}_{mac}(t) = f(Z_{mac}(t), U_{mac}(t), \beta) \tag{2.1}$$

$$\dot{Y}_{mac}(t) = g(Z_{mac}(t), U_{mac}(t)) \tag{2.2}$$

where $Z_{mac}(t) \in \mathbb{R}^{n_x}$, $U_{mac}(t) \in \mathbb{R}^{n_u}$, $Y_{mac}(t) \in \mathbb{R}^{n_y}$ are vectors of state variables, input variables and output variables respectively. The β is kinetic parameters which being constant values (real parameters) and t is time. Notice that, the $f = [f_1, f_2, \ldots f_n]^\intercal$ and $g = [g_1, g_2, \ldots g_n]^\intercal$ are nonlinear vector functions.

2.2.2 Unstructured Fermentation Kinetics Modeling

Unstructured (macro) models have widely been used for modeling of microbial kinetics to describe the microbial growth during ethanol fermentation. The models are empirical and provide the most fundamental observations concerning microbial metabolic processes [78, 82, 83]. A functional relationship between the specific growth rate and an essential substrate concentration is often expressed by Monod's equation [72, 84].

$$\mu = \frac{\mu_m S}{k_s + S} \tag{2.3}$$

where μ_m is the maximum specific growth rate of the microorganisms, k_s is the value of S when $\mu/\mu_m = 0.5$ (referred as saturation constant), S is the concentration of the limiting substrate for growth.

However, some limitations arise from the Monod's equation due to: (1) substrate and product inhibition are excluded, (2) cell death rate is ignored, and (3) well-mixed conditions are assumed in bioreactor [72, 84]. These limitations of Monod's equation often make it not suitable to fit in real bioprocess behaviours. In general, there are three types of inhibitory effects which are frequently encountered in a fermentation process, which are substrate inhibition, product inhibition and biomass inhibition.

Numerous modifications based on Monod's equation have been developed which take into account the inhibition of microbial growth under a high concentration of substrate and/or product [78]. The inhibition by high concentration of substrate result in lag time increment in a batch fermentation culture whereby it may result in process instability in continuous fermentation culture [85]. The kinetics of substrate inhibition usually described by general mechanism of competitive, e.g. hyperbolic [47, 85–89] and non-competitive based on exponential relation, i.e., Aiba [90].

$$\text{Hyperbolic form:} \quad \mu_i = \mu_m \frac{S}{k_s + S + k_{ss} S^2} \tag{2.4}$$

$$\text{Exponential form:} \quad \mu_i = \mu_m \exp\left(-k_s S\right) \tag{2.5}$$

where S is the substrate concentration while K_s and K_{ss} are parameters

Most of the kinetics under product inhibition often described by non-competitive approach such as linear form, i.e., Hinshelwood [91, 92], exponential, i.e., Aiba

[90], hyperbolic, i.e., Jerusalimsky [71, 93] and parabolic, i.e., Levenspiel [86, 94].

$$\text{Linear form:} \quad \mu_i = \mu_m\Big(1 - \frac{E}{E_m}\Big) \tag{2.6}$$

$$\text{Exponential form:} \quad \mu_i = \mu_m \exp\left(-k_e E\right) \tag{2.7}$$

$$\text{Hyperbolic form:} \quad \mu_i = \mu_m \frac{1}{1 + E/k_e} \tag{2.8}$$

$$\text{Parabolic form:} \quad \mu_i = \mu_m\Big(1 - \frac{E}{E_m}\Big)^n \tag{2.9}$$

where E is the product concentration, E_m is the maximum concentration of product and k_e denotes as a parameter.

Moreover, the specific growth rate of cells is expressed by Monod type kinetics extended to allow the inhibition effect due to biomass concentration(X) on the kinetics. A modified model which incorporates both product and biomass inhibition is proposed by [75] as follows:

$$\mu_i = \mu_m\Big[1 - \Big(\frac{E}{E_m}\Big)^m\Big]\Big[1 - \Big(\frac{X}{X_m}\Big)^n\Big] \tag{2.10}$$

where m and n are parameters of cellular and product inhibitions respectively. Furthermore, [77, 95] proposed the combined inhibition effects on substrate, product and biomass as follows:

$$\mu_i = \mu_m \frac{S}{k_s + S} \exp\left(-k_i S\right)\Big(1 - \frac{X}{X_m}\Big)^m\Big(1 - \frac{E}{E_m}\Big)^n \tag{2.11}$$

The rate of substrate consumption can be modified following the *Pirt* equation [96].

$$r_s = -\frac{r_x}{Y_{x/s}} - m_s X \tag{2.12}$$

where $Y_{x/s}$ and m_s denote the biomass yield referred to substrate consumed and maintenance parameter respectively.

Meanwhile, the rate of product formation can be defined as *Luedeking-Piret* equation [96].

$$r_p = r_x Y_{e/x} + m_e X \tag{2.13}$$

where, $Y_{e/x}$ is the product yield based on biomass growth and m_e denotes coefficient for the ethanol production associated with the microbial growth.

2.3 Bioprocess Systems

Generally, there are three different types of fermentation process: (1) Batch fermentation process (2) Fed batch fermentation process and (3) Continuous fermentation process, which are shown in Figure 2.7 [19].

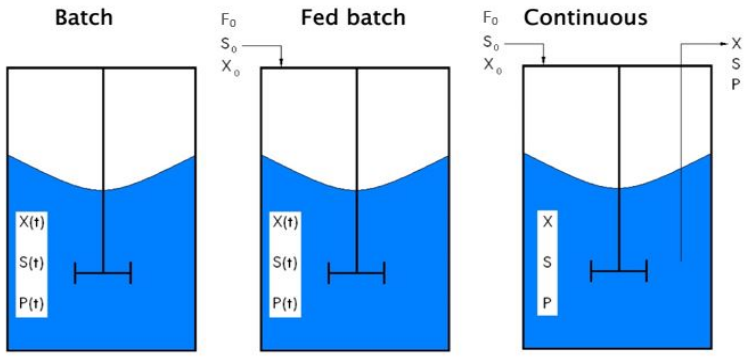

Figure 2.7: Batch, fed-batch and continuous fermentation process; X:biomass, S:substrate, P:product, t:time

In Figure 2.7, the notations F_0, S_0 and X_0 represent the feed flow rate, substrate concentration in the feed and biomass concentration in the feed. Batch fermentation system is a closed system. The basic idea of batch fermentation is that all substrate components and inoculum are added at the beginning of fermentation and nothing is added throughout until the end of the process, except oxygen (for aerobic and micro-aerobic fermentation), antifoam agent, acid or base to control pH. The composition of the medium, the biomass concentration and the metabolite concentration generally change constantly as a result of the metabolism of the cells [19]. Continuous fermentation system is an open system, which the substrates are fed continuously while the effluent stream containing the cells, products and residual is withdrawn at the same flow rate of inlet flow, which establish a steady state condition. By maintaining a constant volume of culture, the continuous fermentation can be monitored in either constant substrate concentration or constant cell growth. Continuous system is frequently used in large scale production. Fed-batch fermentation system is a technique in between batch and continuous process, in which the nutrients are fed intermittently or continuously while the culture broth is collected at the end of the process. The fed-batch system is a dynamic operation. An advantage of fed-batch fermentation is that it can avoid the surplus nutrients (due to overfeeding in batch culture) which may inhibit microorganism growth. In so doing, the reaction can reach high yield

and high production rate, maintain sterile culture and assure operational flexibility in keeping pace with the changing market requirements [97, 98]. In view of an increase in productivity, fed-batch system is widely employed in bioprocesses industry. Apart from bioethanol production, fed-batch culture is used for production of various products such as penicillin [99–101], spirulina [102–105], amino acids [106], antibiotics [107, 108], lovastatin [109, 110], recombinant proteins [111], etc. In fact fed-batch culture does not require special amendment to the existing equipment required by batch culture [112], whereas it is beneficial in increasing yield and productivity of the fermentation process. Table 2.3 shows some pros and cons of these three fermentation system [17–19, 21, 23–26, 113, 114].

Table 2.3: Batch, fed-batch and continuous fermentation

Fermentation System	**Advantages**	**Disadvantages**
Batch	Simple process. Reduced risk of contamination. Complete substrate conversion.	Low productivity. Labour intensive. Low cell concentration.
Fed-batch	Reduced inhibition by the substrate. Extension of the exponential growth phase. Higher biomass concentration and yield (compared to batch system).	Labour intensive. Risk of contamination.
Continuous	Steady-state system. No dead-times. High productivity. Cost efficient (low labour cost). Less sensitive to human error.	Interruptions due to contamination and mutation of yeasts. Difficulty in control. Risk of contamination.

2.3.1 Key Challenges in Controller Design for Fed-batch Fermentation Process

Fed-batch processes are technically challenging to control due to process variability and complexity of biological systems [115], which resulted in complex and

strong nonlinear dynamics. On the other hand, the process variables are time-varying and difficult to measure on-line. Thus, the development and application of advanced control strategies for fed-batch fermentation system are mainly focused on addressing the nonlinear dynamics. Most of the manipulated variables reported in the open literature are substrate feed rate and aeration rate (for micro-aerobic fermentation) for fed-batch fermentation system in order to maximize the production of the microorganisms (biomass) and/or formation of the product. Table 2.4 shows the review of advanced control strategies for fed-batch fermentation system.

Table 2.4: Fed-batch control strategies review

Methods	**Remarks**	**References**
Model reference adaptive control (MRAC)	Control DO variable using closed-loop approach by manipulating F to obtain maximum oxygen transfer capacity.	[116, 117]
	Closed-loop adaptive PI controller was designed to control the specific growth rate by manipulating F.	[118]
	In this 2×2 system, manipulated variables are substrate feed rate and the airflow rate; control variables are DO and substrate concentration.	[119]
Nonlinear model predictive control (MPC)	Regulate the acetate concentration, constraining the feed rate to follow an optimal reference profile which maximizes the biomass growth.	[120]
	Obtain high concentration of product using open-loop approach by regulating temperature and pH.	[121]
	Control the glucose concentration using closed-loop approach by manipulating F.	[122]

Table 2.4: continued

Methods	Remarks	References
Fuzzy logic controller	Linguistic variables: the error in the product concentration and the feed flow rate, F was manipulated to control product concentration.	[123]
	Control the difference between the specific carbon dioxide evolution rate (Q_c) and specific oxygen uptake rate (Q_o) using closed-loop approach by manipulating F.	[124]
Neural network	Fermentation time, pH, dissolved oxygen level, temperature and turbidity were used to identify the nonlinear relationship between fermentation parameters (input vector) and bacterial inhibition diameter (output vector).	[125]

To date, in spite of the availability of several advanced control laws for process control applications, the fixed structure low-order Proportional-Integral-Derivative (PID) controllers are still widely used in industries due to the simplicity, reliability and robustness of the controllers [126, 127]. More than 95% of the controllers in process control applications are of PID type. Because of the industrial importance of PID control, numerous methods of PID controller synthesis and tuning have been developed over the past few decades, such as Ziegler-Nicholas based tuning methods [128, 129], IMC design methods [127, 130, 131], frequency-domain method [132] and decomposition method based on multi-scale control (MSC) scheme [133]. A vast collection of existing PID tuning rules can be found in a PID controller handbook [134].

It should be noted that for some complex processes, higher order controllers can provide better performance than the low-order PID controllers [135]. Unfortunately, a higher order controller is more difficult to design than a PID controller where the methods available for the higher order controller design are often lim-

ited and some of them might be too complicated to be applied in practice. The PID controller design for a fed-batch fermentation process can be very challenging due to the presence of a variety of dynamics such as

1. Time-varying dynamics.
2. Higher order, i.e., to capture delicate dynamic behaviors of the process with higher accuracy [136].
3. Unstable dynamics.
4. Integrating dynamics.
5. Time delay (deadtime).

Table 2.5 summarizes the key challenges in controller design for fed-batch fermentation process,

Table 2.5: Key challenges in controller design for fed-batch fermentation process

Key Challenges	**Remarks**
Time-varying	Process variables are time-varying as nutrients are fed intermittently or continuously.
Higher order	Model reduction technique leads to the loss of some information on the system dynamics [137, 138]. Imposes more upper limits on control aggressiveness [139].
Unstable pole	Imposes a minimum limit on control performance (could lead to an excessive overshoot and long settling time). Unstable pole moves further away from the imaginary axis to the right-hand side in the complex plane (i.e., faster unstable pole), the maximum lower limit on controller aggressiveness is increased.
Integrating	Inverse-response behaviors. Never settles to a steady state when a step input change is made.
Time delay (deadtime)	Imposes an upper limit on the controller aggressiveness. Deadtime grows larger, the minimum upper limit on controller aggressiveness is reduced.

The difficulty in stabilizing such a process will no doubt require sufficient knowledge on the process of interest, i.e., a process model is useful to controller

design. As a result of this limitation on closed-loop stability, it is a crucial first step in PID controller design to establish the stabilizing PID parameter regions for the given unstable process. Therefore, fed-batch bioprocesses require advanced regulatory procedures to ensure acceptable bioprocesses performances and efficiency.

2.3.2 PID Closed-loop Stabilization

The output feedback stabilization of a linear time invariant (LTI) system is one of the most important open questions in control engineering [140, 141]. Computational methods of the set of stabilizing PID parameters have been reported in several literature. One of the well-known approaches to computing the stabilizing PID controller region is based on a generalization of Hermite-Biehler theorem [142, 143]. However, this approach requires sweeping over the proportional gain as to find all stabilizing regions of PID parameters [144, 145]. The Hermite-Biehler theorem has become the basis of extended theorem used to find the PID stabilizing parameter regions, e.g., in [146] and [147] where the complete stabilizing set of the classical PI and PID controller parameter regions for the first-order time-delay plants were derived.

In addition to the methods based on the Hermite-Biehler theorem, the use of Nyquist plot has also been adopted by several researchers. For examples, the graphical approach to compute the set of all stabilizing PID parameters [148]. The Nyquist plot approach was adopted in [149] to compute the stabilizing PID parameter regions for high-order unstable time-delay processes with one unstable pole. In [145], the design of PI and PID controllers has been developed based on a stability boundary locus approach where the regions are expressed in the proportional, integral gain, i.e., (k_p, k_i)-plane. However, it was noted that one of the difficulties of this approach is related to the constraint for frequency gridding [145]. Another interesting graphical approach is based on the so-called dual-locus diagram, which was adopted in [150] to construct robust stability regions of optimization-based PID controllers.

Another well-known approach to constructing the stabilizing PID parameter regions is based on the Gain-Phase Margin (GPM) specification, e.g., in [151] the GPM approach was used to determine the feasible range of GPM for the first-order unstable time-delay processes. Also, in [152] the GPM specification approach was used to establish the set of PI/PID parameters, which meets desired closed-loop time response measured in term of the dominant pole placement - the method

was applied to first- and second-order stable time-delay processes. A review on the PID controller design based on GPM specifications can be found in [153].

Remark 1. *Root locus and pole placement method are often applicable to simple P-only controller analysis applied to simple systems, i.e., those systems which are representable by low-order models. For a high-order complex system using PID controller, these methods are not convenient because of the existence of more than one dominant poles (both real and complex); thus, one cannot simply adjust one dominant pole without affecting the others. For this reason, the root locus and pole placement methods can lead to tedious PID tuning procedures for complex high-order systems.*

2.3.3 Multi-scale Control Scheme

Due to the widely industrial application of PID control, PID controller synthesis and tuning have been developed over the past few decades. The multi-scale control (MSC) scheme has been reported in [154–157], which offers a systematic approach to designing multi-loop PID controllers (sometimes augmented with filters). Figure 2.8 shows the realization block diagram for a two-layer multi-scale control (MSC) scheme [154].

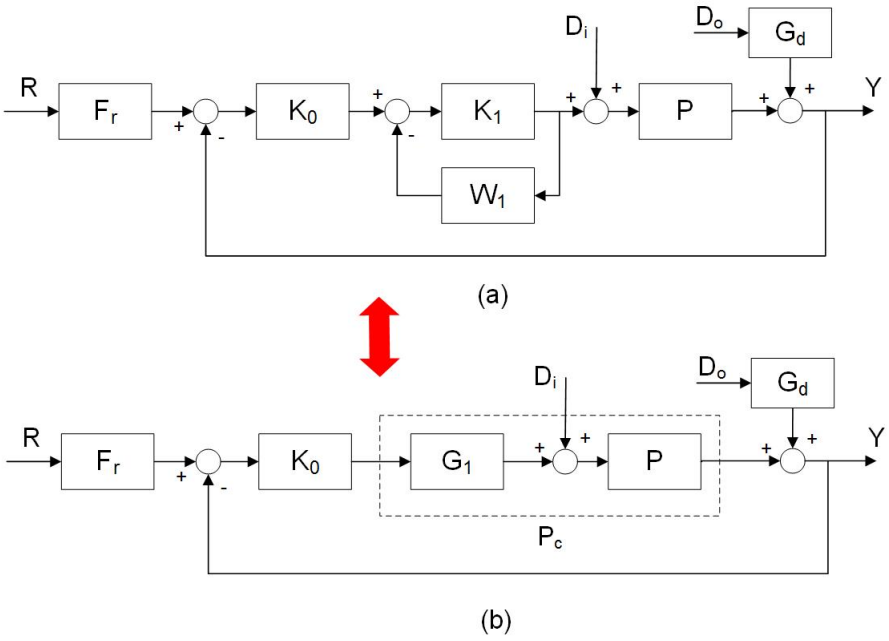

Figure 2.8: MSC scheme: (a) 2-layer and (b) reduced single-loop feedback

The basic idea of multi-scale control (MSC) scheme is to decompose a given plant P via partial fraction expansion into a sum of basic modes as follows:

$$P(s) = m_0(s) + m_1(s) + \cdots + m_n(s) \tag{2.14}$$

where m_i, $\forall i \in 0, 1, 2, ..., n$ is the plant factor, which can be first or second order system with real coefficients. m_0 is the outermost (slowest) factor while m_i, $\forall i \in 0, 1, 2, ..., n$ is the inner-layer factor, where the response of m_j is slower that m_{j+1}, $\forall j \in 0, 1, 2, ..., n-1$. A set of individual sub-controllers is designed based on the basic modes, which are then combined in such a way to enhance cooperation among these different modes.

The unifying MSC scheme has been reported in [154, 155] to controlling the first- and second-order plus time-delay processes, which is applicable to both stable and unstable integrating processes.

2.4 Bioprocess Control

Due to the rapid growth of the biotechnology industry, the development of a cost-effective production of bioproducts has been a subject of great interest with a shift in focus towards the production with high productivity and yields. Three reasons why process control is required in bioprocesses [115].

- To reduce process variability.
- To improve the productivity.
- To increase monitoring and troubleshooting capability.

From the control engineer's viewpoint, the control of fed-batch fermentation system is challenging as the optimization of the substrate feed rate is a dynamic problem [158], which causes the nonlinearity in bioprocesses. The nonlinearity problem has been considered as one of the key challenges to control performance. To overcome this limitation, various types of advanced control techniques have received a widespread research attention in the area of bioprocess control such as (a) adaptive control, (b) fuzzy control, (c) robust control, and (d) nonlinear PID. It can be noticed that, some of the advanced control techniques are adopted with the implementation of PID controller.

2.4.1 Adaptive Control

There are two dilemmas motivate the application of adaptive control technique in fermentation processes, i.e., (1) complex and nonlinear dynamics of the processes, and (2) lack of reliable sensors for real-time monitoring of the process parameters [159]. The application of adaptive control can deal with the dynamic systems which have constant or slowly-varying uncertain parameters. The basic idea of adaptive controller is parameter estimation, i.e., estimate the uncertain process parameters on-line and used it in the control input computation, which is able to maintain the control performance of uncertain or time-varying systems [160].

Recently, much effort has been placed in adaptive control in both theory and applications. The model-reference adaptive PI controller has an outstanding performance in controlling the specific growth rate in the production of vaccine [118]. There are various control techniques have been proposed to be combined with basic adaptive control techniques for fermentation process, such as robust [161], optimal [159], fuzzy [162] and neural network [163] control techniques.

2.4.2 Fuzzy Control

Fuzzy control is designed to deal with uncertainties and non-quantitative knowledge in complex bioprocess systems, which control a system based on human's heuristic knowledge on a real plant. It is suitable to be applied in the nonlinear bioprocesses with poor measurements of process parameters. Moreover, fuzzy control technique can be used to improve the closed-loop control performance for linear or nonlinear processes when the simple process model is available [164].

Some implementations of fuzzy control technique to fed-batch bioreactor are presented by [123, 124]. An improved fuzzy control system with feedforward/ feedback structure was used in glutathione production to indirectly control specific growth rate by manipulating the glucose feed rate [165].

2.4.3 Robust Control

Robust control has advantages in dealing with disturbances, quickly varying parameters, and unmodeled dynamics, which requires a prior information about the bounds on these uncertain or time-varying parameters.

The H_∞ robust multivariate control achieved a promising results in maintaining both closed-loop stability and specific performance over a range of operating conditions [13]. A robust controller can be employed in fed-batch fermentation

cultures with minimal process knowledge and minimal measurement information [11].

2.4.4 Nonlinear PID

PID controllers are conventionally preferred in bioprocess industry. However, the highly nonlinear and time varying bioprocesses pose a great challenge to the PID controller design. Many model-based strategies adopted in bioprocesses are still relying on non-mechanistic model such as fuzzy system, neural network and etc.

The fuzzy self-tuning PID control of the operating temperatures in a two-staged membrane separation process was studied in [166], which the PID parameters can be tuned on-line to solve nonlinear problems in the process. The self-tuning PID controller with genetic algorithm was proposed in [167] to obtain optimal tuning parameters. In [168], the concepts of invariant control and system immersion are combined to design nonlinear PI controllers. The predictive approach was proposed and the auto-tuned PID controller was used to control a fed-batch culture penicillin production [121].

2.5 Summary

- Alcoholic fermentation plays significant roles in developing alternative renewable energy sources, especially, where they are used as additive for gasoline. A fed-batch culture is commonly used to overcome substrate inhibition, which can be applied to developing modular distributed system for bioethanol production. This modular system can adopt in across rural areas, where bioethanol can be produced from fermentation agricultural waste.

- Mathematical model of fed-batch fermentation process includes (1) dynamics of bioreactor, and (2) kinetics modeling of microorganisms, which can be used for optimization and control study. Numerous modified Monod's equations which have been developed to express the specific growth rate based on substrate, product and biomass inhibitions.

- Fed-batch system is a dynamic system, which causes the nonlinearity and it may exhibit complex form of dynamics at some points of its operation. Over the past few decades, various types of advanced control techniques have been reported to address the nonlinearity problem, however, the performance of

the practical applications of these advanced control strategies is limited by inappropriate PID controller settings. The conventional single-loop PID controller has its limitation on providing stabilization to such a complex dynamic process.

- The multi-scale control (MSC) scheme can be used to address complex forms of fed-batch dynamics, which could not be solved using the single-loop PID control methods. The two advanced MSC schemes will be presented in Section 7-8.

Chapter 3

Kinetics Modeling of Batch Bioreactor

In the modeling of a fed-batch fermentation process, there are two component models which must be included: (1) dynamics of bioreactor, and (2) kinetics model of microorganisms. In this chapter, we have focused on addressing the microbial kinetics developed in a batch mode bioreactor based on modified Monod's equation, which can provide better fitting to experimental data. In this work, a batch mode experimental study was conducted on ethanol production using combined cassava and mango waste as feedstock. The usage of fruit waste is proposed to avoid long-term competition with food consumption and costly pretreatment process by using conventional feedstock, i.e., agricultural crops and lignocellulosic materials. The development of microbial kinetics of the ethanolic fermentation process is useful and can be used as a basis for the control study.

3.1 Factorial Design

In general, factorial design can be considered as one of the most efficient and suitable methods in the screening of experiments involving several factors. It is beneficial to investigate the joint effect of the factors in the early stages of experimental work. 2^k factorial design provides the smallest number of runs with k factors at only two levels (high and low) each. The effects of each factor on the response variable, as well as the effects of interactions between factors on the response variable, are studied in the experiments.

In this section, a 2^3 factorial design is shown as an example. There are three factors, pH (A), stirrer speed (B), and aeration rate (C) of the experiment with

only two levels (high or low) to be investigated. The pH of the medium has a significant impact on microorganism activities. The changes of pH in the medium will modify the chemical pathways of the biological reactions as well as their kinetics [45]. In a micro-aerobic fermentation, the aeration rate and stirrer speed are important factors, as both of the parameters will affect the mixing intensity of a bioreactor.

It is assumed that the observed response is approximately linear over the range of factor level chosen. There are eight treatment combinations and it can be displayed geometrically as a cube, as shown in Figure 3.1. The "+" and "-" notation represent the high and low levels of the factors. The design matrix of 2^3 factorial design is shown in Table 3.1 and the standard order of treatment combinations is given as (1), a, b, ab, c, ac, ab, and abc.

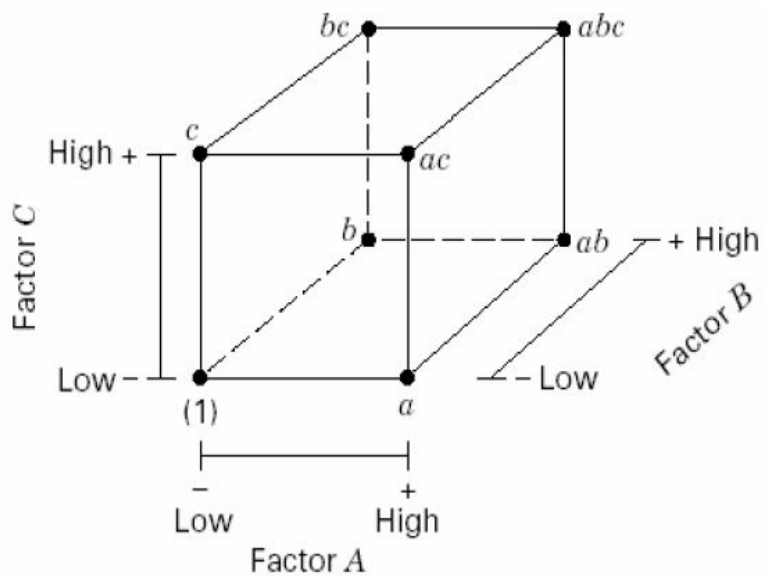

Figure 3.1: Geometric view of 2^3 factorial design

There are seven degrees of freedom for eight treatment combinations in 2^3 factorial design. There are three degrees of freedom which are associated with main effects: A, B and C; four degrees of freedom are associated with interactions: AB, AC, BC and ABC. Figure 3.2 shows the geometric presentation of contrasts to main effects (A, B and C) and interactions (AB, AC, BC and ABC) in 2^3 factorial design.

First, consider estimating the main effects. For example, the average effect of A can be calculated with the average of four runs where A is at the high level ($\bar{y}_{A^+}$) minus the average of the four runs where A is at the low level ($\bar{y}_{A^-}$).

Table 3.1: Design matrix of 2^3 factorial design

Run	A	B	C	Labels	A	B	C
1	-	-	-	(1)	0	0	0
2	+	-	-	a	1	0	0
3	-	+	-	b	0	1	0
4	+	+	-	ab	1	1	0
5	-	-	+	c	0	0	1
6	+	-	+	ac	1	0	1
7	-	+	+	bc	0	1	1
8	+	+	+	abc	1	1	1

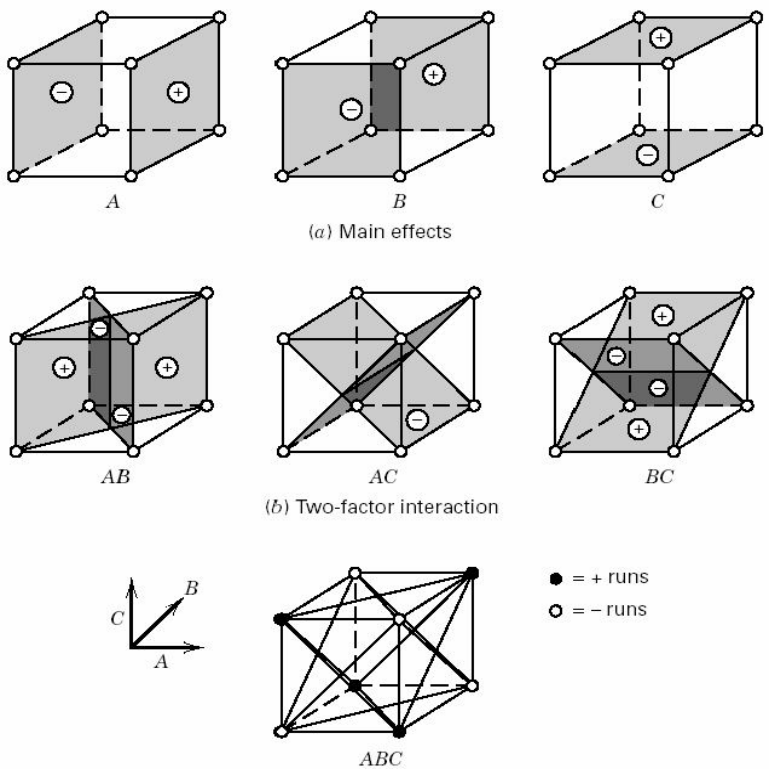

Figure 3.2: Geometric presentation of contrasts to main effects and interactions in 2^3 factorial design

The average effect of B and C can be estimated in similar way. The equation of

average effect of A is shown as follows:

$$\begin{aligned} A &= \bar{y}_{A^+} - \bar{y}_{A^-} \\ &= \frac{a + ab + ac + abc}{4n} - \frac{(1) + b + c + bc}{4n} \\ &= \frac{1}{4n}[a + ab + ac + abc - (1) - b - c - bc] \end{aligned} \tag{3.1}$$

The two factor interaction effect between A and B can be calculated with one half of the difference between the average A effects at the two levels of B. The AC and BC interactions can be estimated in the similar method. The equation of AB interaction is denoted as follows:

$$\begin{aligned} AB &= \frac{1}{2}\Big[\frac{ab + abc - b - bc}{2n} - \frac{ac + a - (1) - c}{2n}\Big] \\ &= \frac{abc + ab + c + (1) - a - ac - bc - b}{4n} \end{aligned} \tag{3.2}$$

The three-factor interaction effect between A, B and C is defined as the average difference between the AB interaction for the two different levels of C, which is given by

$$\begin{aligned} ABC &= \Big[\frac{(abc - bc) - (ac - c)}{4n} - \frac{(ab - b) - (a - (1))}{4n}\Big] \\ &= \frac{abc + a + b + c - ab - ac - bc - (1)}{4n} \end{aligned} \tag{3.3}$$

Each effect has a corresponding single-degree-of-freedom contrast. The sums of squares associated with each effect in 2^3 factorial design with n replicated is defined as

$$SS = \frac{(Contrast)^2}{8n} \tag{3.4}$$

It is usually interesting to build a model to relate the response to process variables for prediction, process optimization, and process control. A regression model is a mathematical model which fits to a set of sample data to approximate the exact appropriate relation. In general, the response variable y may be fitted to k factor variables and factor interaction terms by a linear (first order) regression model, and the k factors in the experiment are quantitative [169].

Since there are three manipulated variables taken into account in this research study, i.e. pH, stirrer speed (SS) and aeration rate (AR), as a 2^3 design, the first order regression model with interaction terms are added to a main effects can be written as follows:

$$\begin{aligned} y = \beta_0 + \beta_1 X_1 + \beta_2 X_2 + \beta_3 X_3 + \beta_1 2 X_1 X_2 \\ + \beta_1 3 X_1 X_3 + \beta_2 3 X_2 X_3 + \beta_1 23 X_1 X_2 X_3 + \epsilon \end{aligned} \tag{3.5}$$

where y is the response, the β's are the parameters whose values are to be determined, X_1, X_2 and X_3 are the variable that represents factor A, B and C respectively, ϵ is a random error term.

3.2 Experimental Setup

A set of experiments was executed in batch mode by using a BIOSTAT A-plus 2 L, MO-Assembly bioreactor. In this study, a 2^3 factorial design experiment is implemented in order to study the effect of pH (X_1), stirrer speed (SS = X_2, rpm) and aeration rate (AR = X_3, v/v.min) on fermentation kinetics and performance in bioreactor corresponding to lower (-1), middle (0) and higher (+1) levels. pH (X_1) value is in between 4.5 to 5.5, stirrer speed (SS, X_2) varied between 160 rpm and 240 rpm and aeration rate (AR, X_3) ranged between 0.033 v/v.min and 0.1 v/v.min. The values of input variables are shown in Table 3.2.

Table 3.2: Input variables and levels in 2^3 factorial design

Factor	Variable	Units	Low level (-)	Middle level (0)	High level (+)
X_1	pH	-	4.5	5.0	5.5
X_2	Stirrer speed (SS)	rpm	160	200	240
X_3	Aeration rate (AR)	v/v.min	0.033	0.067	0.1

A total of nine experiments (including the baseline) are conducted based on 2^3 factorial design. Table 3.3 shows the experimental runs corresponding to different combinations of pH, aeration rate and stirrer speed, where run 0 denotes the baseline run.

The glucose, ethanol and biomass concentration are recorded throughout the experiments. The impact of pH, aeration rate and stirrer speed on micro-aerobic batch fermentation by using wasted mango fruit are investigated via the analysis of the experimental data, i.e. rate of substrate consumption, rate of ethanol production and rate of biomass growth. The research materials and methods can be referred to Appendix A.1-A.3. The experimental procedures are available in Appendix A.

Table 3.3: Experimental run

Experimental Run	X_1: pH	X_2: Stirrer Speed	X_3: Aeration Rate
Baseline (0)	0	0	0
1	-	-	-
2	-	+	-
3	-	-	+
4	-	+	+
5	+	-	-
6	+	+	-
7	+	-	+
8	+	+	+

3.3 Experimental Study on Bioreactor Performance

Generally, the decrease in glucose concentrations and the increase in ethanol concentrations is expected due to the consumption of glucose as substrate with oxygen consumption to produce ethanol throughout the fermentation process. It was observed that the microorganism growth increased throughout the experiment, but dropped towards the end of the experiment. The decrease in cell viability could be due to the exhaustion of substrate and this led to the inhibition of ATP synthesis, or it could be because of the yeast cells were metabolically inactive due to the higher rate of ethanol formation and this led to the leakage of intracellular metabolites into the growth medium [29]. Both of these situations led to the loss of plasma membrane integrity and a reduction in the ethanol tolerance of yeast cells which in turn caused increased cell death [29, 170].

3.3.1 Effects of pH, Aeration Rate and Stirrer Speed on Glucose Concentration

Figure 3.3 shows the substrate concentration profiles under various experimental conditions. Under low pH 4.5 medium, the substrate (glucose) was almost completely consumed, leaving only 2 kg/m^3 left at the end of the experiment for about 50 hours, whereas the substrate remaining at the end of the experiment was around 8-19 kg/m^3 for fermentation process with high pH 5.5. Also, some of

the ethanol that was produced started to oxidize and used as substrate before the glucose finished up. It was observed that the glucose concentrations were fairly comparable under different conditions of aeration rate and stirrer speed either in pH 4.5 or pH 5.5. The results of the experiments showed that the effect of pH on glucose concentration profiles was significant.

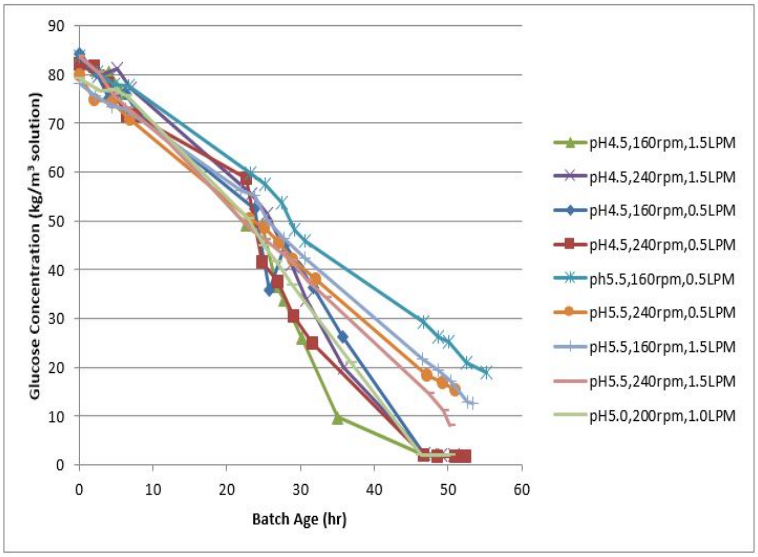

Figure 3.3: Substrate concentration profiles under various experimental conditions

3.3.2 Effects of pH, Aeration Rate and Stirrer Speed on Biomass Concentration

Figure 3.4 shows the biomass concentration profiles under various experimental conditions. In Figure 3.4, the fermentation process under low pH 4.5 gave a higher maximum biomass concentration towards the end of the fermentation, with a range of 5.9 kg/m^3 to 6.8 kg/m^3. Note that, the biomass concentrations were relatively lower under high pH 5.5, ranging from around 1.8 kg/m^3 to 2.4 kg/m^3 compared to the fermentation process at low pH 4.5. It was observed that the medium condition under pH 4.5 was more optimum for the growth of *S. cerevisiae* instead of high pH 5.5. It should be noted that, the increase in biomass concentration also resulted in higher ethanol production.

On the other hand, the effect of aeration rate has the significant effect on biomass concentration profiles. At low pH 4.5 and high pH 5.5, an increase

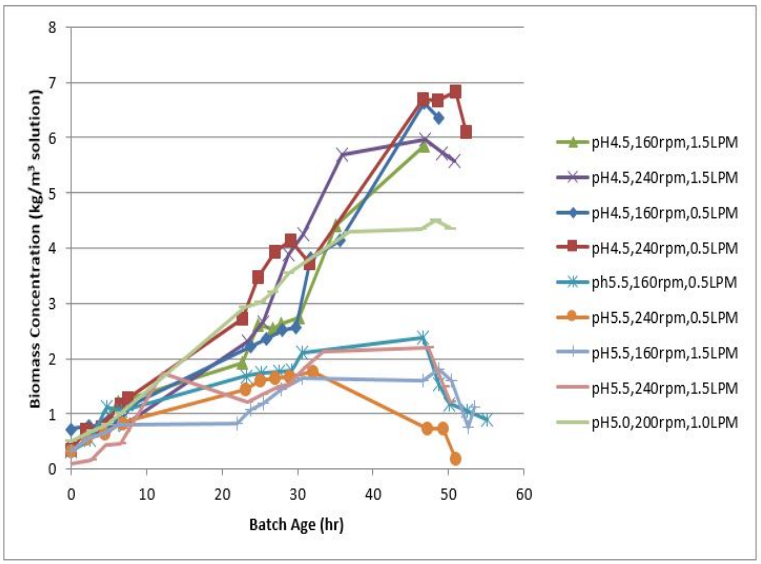

Figure 3.4: Biomass concentration profiles under various experimental conditions

in AR from 0.033 v/v.min to 0.1 v/v.min led to a reduction in the biomass concentration, i.e., from 6.6-6.8 kg/m^3 at run 1 and run 2 to 5.9-6 kg/m^3 at run 3 and run 4; and 2.4 kg/m^3 at run 3 to 1.8 kg/m^3 at run 4 respectively. At high pH 5.5 and SS = 240 rpm, the reduction in biomass concentration was not observed with the increase of AR might due to analytical error. It is observed that under different conditions of stirrer speed either in pH 4.5 or pH 5.5, the biomass concentrations were quite similar. The pH and aeration rate have most influence on biomass concentration profiles rather than stirrer speed.

3.3.3 Effects of pH, Aeration Rate and Stirrer Speed on Ethanol Concentration

The ethanol production is always followed with interest in the fermentation process. Figure 3.5 shows the ethanol concentration profiles under various experimental conditions.

In Figure 3.5, the ethanol production can reach up to 17.5 kg/m^3 at run 3 to 24.5 kg/m^3 at run 1 under pH 4.5 while the higher pH 5.5 gave a lower ethanol production, i.e., 12 kg/m^3 at run 7 to 15.5 kg/m^3 at run 5. A reduction range from 31% to 35% was observed with the increase of pH from 4.5 to pH 5.5. It was observed that a higher ethanol production can be achieved under the pH 4.5 medium than under the pH 5.5.

Note that, the ethanol concentration profiles were affected more significantly

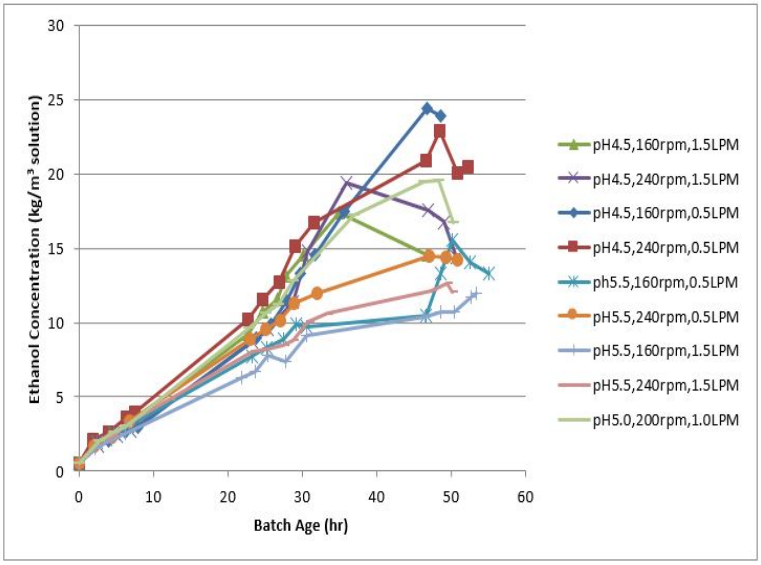

Figure 3.5: Ethanol concentration profiles under various experimental conditions

than that of the substrate and biomass concentration profiles by the changes in aeration rate (AR). At pH 4.5 and SS = 160 rpm, an increase in AR from 0.033 v/v.min to 0.1 v/v.min led to a significant reduction in the maximum ethanol concentration, i.e., from about 24.5 kg/m^3 to 17.5 kg/m^3 (27% reduction). At pH 4.5 and SS = 240 rpm, the maximum ethanol concentration dropped from 23 kg/m^3 to 19.5 kg/m^3 (15% reduction) with an increase of AR from 0.033 v/v.min to 0.1 v/v.min. There was a similar trend observed with the reduction in the maximum ethanol condition that occurred at high pH 5.5 as well. At pH 5.5 and SS = 160 rpm, the maximum ethanol concentration dropped from 15.5 kg/m^3 to 12 kg/m^3 (23% reduction) with an increase of AR from 0.033 v/v.min to 0.1 v/v.min; at pH 5.5 and SS = 160 rpm, the maximum ethanol concentration dropped from 14.5 kg/m^3 to 12.5 kg/m^3 (14% reduction) with an increase of AR from 0.033 v/v.min to 0.1 v/v.min.

Moreover, at pH 4.5 and AR = 0.033 v/v.min, the ethanol concentration reached the maximum in a shorter experiment time of about 36 hours. While at pH 4.5 and AR = 0.1 v/v.min, a maximum ethanol concentration was reached between 47-49 hours. At high pH 5.5, the effect of the aeration rate on the experiment time to reach a maximum ethanol concentration was not that significant compared to that at low pH 4.5. It was observed that the ethanol concentration dropped towards the end of the fermentation, i.e., as the substrate concentration reached exhaustion - some of the ethanol produced was oxidized at high aera-

tion rate. Moreover, it was observed that the ethanol concentrations are fairly comparable under different conditions of stirrer speed.

The experiment showed that the impact of stirrer speed on ethanol production can be as significant as that of pH and aeration rate. Note that, stirrer speed is important in the fermentation process because it provides a homogenous medium broth [63] and induces better coupling between catabolism and anabolism [66].

3.4 Modeling and Identification

3.4.1 Batch Bioreactor Model

A batch bioreactor can be modeled dynamically as follows [86]:

$$\frac{dX_v}{dt} = r_x \tag{3.6}$$

$$\frac{dS}{dt} = -r_s \tag{3.7}$$

$$\frac{dE}{dt} = r_p \tag{3.8}$$

The microbial kinetics include 3 components, i.e. rate of biomass formation r_x, rate of substrate consumption r_s and rate of product formation r_p, where the state variables consist of the concentrations of substrate (glucose) S, product (ethanol) E and viable cell (biomass) X_v. It was assumed that the rate of substrate consumption r_s and rate of product formation r_p are proportional to the rate of biomass formation r_x.

3.4.2 Microbial Kinetics Model

In this work, the kinetic parameters were estimated using the experimental data of substrate, product and biomass concentrations based on the batch fermentation by *S. cerevisiae* of ethanol production from mixed cassava and fruit waste. Three kinetic models were compared. Firstly, the Herbert's concept was proposed which assumed that the observed rate of biomass formation r_x comprised the growth rate $(r_x)_{growth}$ and the death rate of biomass via catabolism, which represents the rate of endogenous metabolism $(r_x)_{end}$ [171]. The rate of growth based on Herbert's concept is as follows:

$$r_x = (r_x)_{growth} + (r_x)_{end} \tag{3.9}$$

where, the growth rate comprised the effects of the inhibition imposed by high substrate concentration, i.e. Haldane model [86–88], during ethanol fermentation.

$$(r_x)_{growth} = k_1 X_v \frac{S}{k_2 + S + k_5 S^2} \tag{3.10}$$

The rates of substrate consumption and product formation were assumed to be proportional to the biomass growth rate:

$$r_s = -k_3 (r_x)_{growth} \tag{3.11}$$

$$r_p = k_4 (r_x)_{growth} \tag{3.12}$$

The rate of endogenous metabolism $(r_x)_{end}$ by linear dependence is shown as follows:

$$(r_x)_{end} = -k_6 X_v \tag{3.13}$$

In order to justify the proposed microbial kinetic model, two popular models were adopted, i.e. Andrade [77, 95] and Phisalaphong [86] for comparison. In Andrade model, the growth rate is given by (3.14) and considers the substrate (S) as limiting yeast growth, and ethanol (E), substrate (S) and cell concentrations (X_v) as inhibitors:

$$r_x = \mu_{max} X_v \frac{S}{k_s + S} \exp -k_i S \Big(1 - \frac{X_v}{X_{v_{max}}}\Big)^m \Big(1 - \frac{E}{E_{max}}\Big)^n \tag{3.14}$$

where, μ_{max} is the maximum specific growth rate (h^{-1}), k_s the substrate saturation parameter (kg/m^3), k_i is the substrate inhibition parameter (m^3/kg), $X_{v_{max}}$ is the biomass concentration when cell growth ceases (kg/m^3), E_{max} is the product concentration when cell growth ceases (kg/m^3), and m and n are parameters of cellular and product inhibitions, respectively. The rates of substrate consumption and ethanol formation is given by (3.15) and (3.16).

$$r_s = -\frac{r_x}{Y_x} - m_s X_v \tag{3.15}$$

$$r_p = r_x Y_{p/x} + m_p X_v \tag{3.16}$$

In (3.15), Y_x (kg/kg) and m_s (kg/kg h) denote the limit cellular yield and maintenance parameter respectively whilst In (3.16), $Y_{p/x}$ (kg/kg) is the product yield based on cell growth and m_p denotes the ethanol production associated with growth (kg/kg h).

The Phisalaphong model proposed by [86], the growth rate considers the substrate (S) as limiting yeast growth, and ethanol (E) as inhibitors, is given by (3.17):

$$r_x = \mu_{max} X_v \frac{S}{k_s + S + k_{ss} S^2} \left(1 - \frac{E}{E_{max}}\right) \tag{3.17}$$

where, μ_{max} is the maximum specific growth rate (h^{-1}), k_s the substrate saturation parameter (kg/m^3), k_{ss} is the substrate inhibition term (kg/m^3), E_{max} is the product inhibition parameter (kg/m^3). The rates of substrate consumption and ethanol formation is shown as follows:

$$r_s = -\frac{r_x}{Y_x} + m_s X_v \tag{3.18}$$

$$r_p = r_x Y_{p/x} + m_p X_v \tag{3.19}$$

where, Y_x (kg/kg) and m_s (kg/kg h) represent the limit cellular yield and maintenance parameter respectively whilst $Y_{p/x}$ (kg/kg) is the product yield based on cell growth and m_p denotes the ethanol production associated with growth (kg/kg h).

3.4.3 Kinetic Model Parameter Identification

The kinetic model parameter identification can be determined by Sum of Square Error (SSE), given by (3.20). The proposed SSE method is used to obtain optimum values for the parameters, which corresponds to the best model fitting between the experimental observations and model predictions [172].

$$E(\theta) = \sum_{n=1}^{np} \left[\frac{(X_{v_n} - X_{ve_n})^2}{X_{ve_{max}}^2} + \frac{(S_n - S_{e_n})^2}{S_{e_{max}}^2} + \frac{(E_n - E_{e_n})^2}{E_{e_{max}}^2} \right] \tag{3.20}$$

where θ is the vector of kinetic model parameters, which is constrained by bounds within a realistic range, $\theta = [k_1, k_2 ... k_n]^T$. X_{ve_n}, S_{e_n} and E_{e_n} are the experimental value of concentrations of cell, substrate and ethanol at the sampling time n, while X_{v_n}, S_n and E_n are the concentration of cell, substrate and ethanol computed by the model 1-6 at the sampling time n. $X_{ve_{max}}$, $S_{e_{max}}$ and $E_{e_{max}}$ are the maximum measured concentration; np is the number of samples [172].

3.4.4 Results and Discussion

The proposed model and another two models were fitted to the experimental data for runs 0 to run 8 (see Table 3.3). Table 3.4 shows the proposed model (Herbert-Haldane) parameters obtained from this study.

Table 3.4: Herbert-Haldane kinetic parameters for each run

Experimental Run	k_1	k_2	k_3	k_4	k_5	k_6
Run 0	1.4162	800.0	11.7442	3.0156	0.0388	0.0174
Run 1	2.1111	800.0	15.0760	4.4871	0.4002	0.0010
Run 2	1.1869	800.0	12.5627	3.4196	0.0010	0.0010
Run 3	1.9369	800.0	17.5728	4.0315	0.1871	0.0010
Run 4	3.0117	800.0	12.7786	2.7784	0.3385	0.0071
Run 5	22.6987	10000.0	7.7269	1.7466	0.0010	0.0938
Run 6	5.6469	1300.0	6.7017	1.6351	0.0631	0.1602
Run 7	2.3389	1300.0	15.4493	2.8930	0.0184	0.0508
Run 8	22.6401	10000.0	17.2943	3.0020	0.0010	0.0502

Table 3.5 shows the Andrade model parameters obtained from this study. Note that, the remaining parameters were fixed in the previous values determined by [77, 95], where $k_s = 4.1$ kg/m^3, $m_p = 0.1$ kg/kg h, $m_s = 0.2$ kg/kg h, $k_i = 0.004$ m^3/kg, $m = 1.0$ and $n = 1.5$ respectively. Table 3.6 shows the Phisalaphong model parameters obtained from this study.

Table 3.5: Andrade kinetic parameters for each run

Experimental Run	μ_{max}	$X_{v_{max}}$	$P_{r_{max}}$	Y_x	$Y_{p/x}$
Run 0	0.1549	4.5064	40676.6996	0.0836	1.7873
Run 1	0.0824	15.3151	76.5619	0.0910	2.2803
Run 2	0.1702	6.5746	75.1453	0.1170	1.2145
Run 3	0.1349	5.9583	99.9951	0.0690	2.3568
Run 4	0.1270	10.1555	88.2144	0.0965	1.0180
Run 5	0.1515	2.3789	13.1715	0.0346	4.8366
Run 6	0.1388	1.6694	15.4118	0.0214	9.7121
Run 7	0.1064	1.6133	99.9866	0.0242	5.5415
Run 8	0.2617	1.9081	14.4644	0.0332	4.1605

According to Table 3.4, six parameters were optimized using Herbert-Haldane model at each experimental run, which is considered a simpler model than the Andrade and Phisalaphong models, which have 11 (include the fixed parameters) and eight parameters, respectively (refer to Table 3.5 and Table 3.6). For illustration, the fitting of the models for run 1, run 3, run 5 and run 7 are provided.

Table 3.6: Phisalaphong kinetic parameters for each run

Experimental Run	μ_{max}	k_s	$k_s s$	$P_{r_{max}}$	$Y_{p/x}$	m_p	Y_x	m_s
Run 0	4.865	1001.6	0.618	22.006	4.410	0.001	0.058	0.001
Run 1	3.461	1000.0	0.715	99.943	4.557	0.001	0.041	0.385
Run 2	1.421	976.9	0.001	10000	3.477	0.001	0.078	0.001
Run 3	14.582	993.4	2.174	21.659	4.083	0.001	0.051	0.082
Run 4	1000	992.6	151.753	17.895	3.213	0.001	0.071	0.001
Run 5	1.123	1003.2	0.001	17.215	8.484	0.010	0.026	0.001
Run 6	1.002	1003.3	0.001	20.875	14.303	0.001	0.017	0.001
Run 7	0.836	1003.3	0.001	30.708	9.126	0.001	0.021	0.001
Run 8	20.818	10000.0	0.001	15.020	6.408	0.001	0.028	0.001

Figure 3.6 and Figure 3.7 show the fitting of the models for run 1 (pH 4.5 and AR = 0.033 v/v.min) and run 3 (pH 4.5 and AR = 0.1 v/v.min), whilst Figure 3.8 and Figure 3.9 show the fitting of the models for run 5 (pH 5.5 and AR = 0.033 v/v.min) and run 7 (pH 5.5 and AR = 0.1 v/v.min), respectively.

In Figure 3.6 and Figure 3.7, the three models, i.e. Herbert-Haldane, Andrade and Phisalaphong, provided a good fitting for run 1 and run 3 to the experimental data of biomass, substrate and ethanol. The results showed that the three models were capable of predicting the fermentation kinetics under conditions of low pH 4.5 either at high or low aeration rate.

From Figure 3.8 and Figure 3.9, it was observed that the Andrade and Phisalaphong models were not capable of predicting the cell death phase at the end of the experiment under condition of high pH 5.5, thereby resulting in a bad fitting of the experimental data especially in biomass growth. The reason for poor fitting might be due to the neglect of endogenous metabolic behavior in these two models, which tend to give a straight curve in the kinetics of biomass growth. On the other hand, the Herbert-Haldane model was observed to give a smooth curve in biomass growth, especially in describing the endogenous metabolism behavior at the end of the experiment. In addition, the three models provided a similar trend on substrate and ethanol concentration profiles.

Based on Table 3.4, Herbert-Haldane can be considered as a simple kinetic model with the least number of parameters where it provided a better fitting among the three models. On the other hand, it showed that the variations of

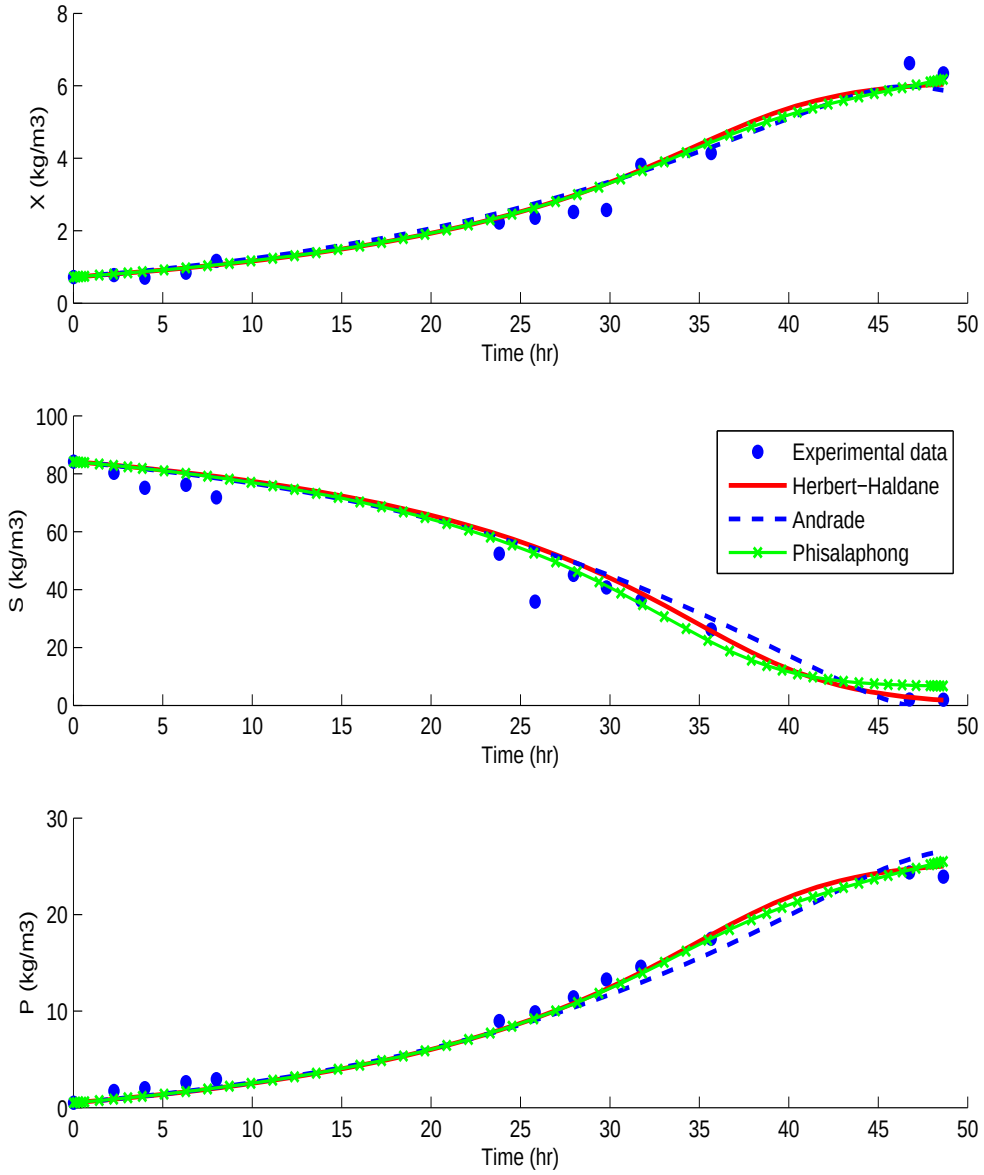

Figure 3.6: Comparison of kinetic models and experimental data on the concentrations of biomass (X), glucose (S) and ethanol (P) for run 1

these six parameters were very significant over the experimental ranges of pH and aeration rate. It was observed that k_1, k_2, k_3, k_4, k_5 and k_6 were heavily influenced by the changes in pH, stirrer speed and aeration rate while k_6 was directly related to endogenous metabolism.

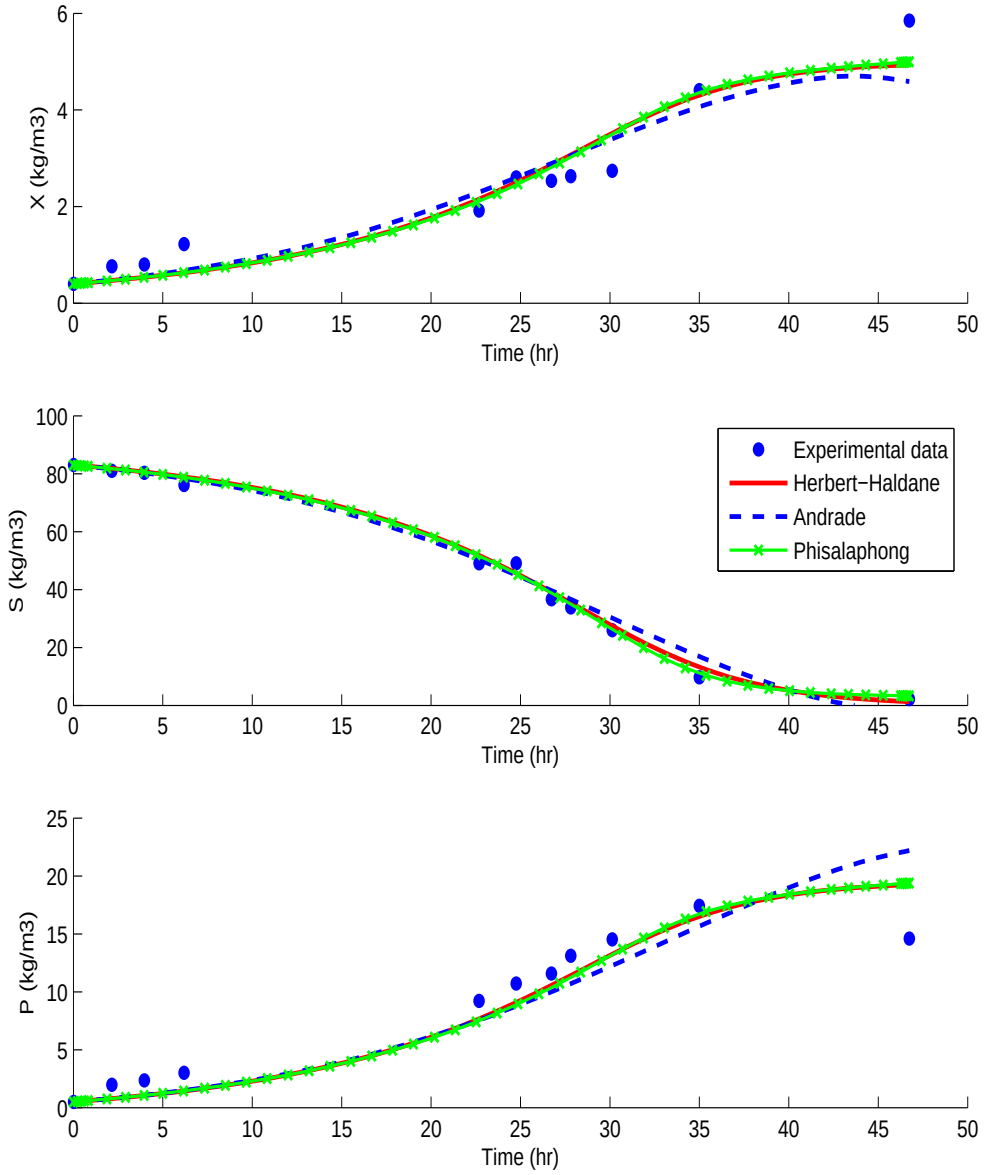

Figure 3.7: Comparison of kinetic models and experimental data on the concentrations of biomass (X), glucose (S) and ethanol (P) for run 3

Based on the discussion above, the result supports that the proposed Herbert-Haldane model fits well into the experimental data for run 0 to run 8 within the given experimental ranges for pH, stirrer speed and aeration rate by using the combined cassava and mango waste as carbon sources. Furthermore, it is worth

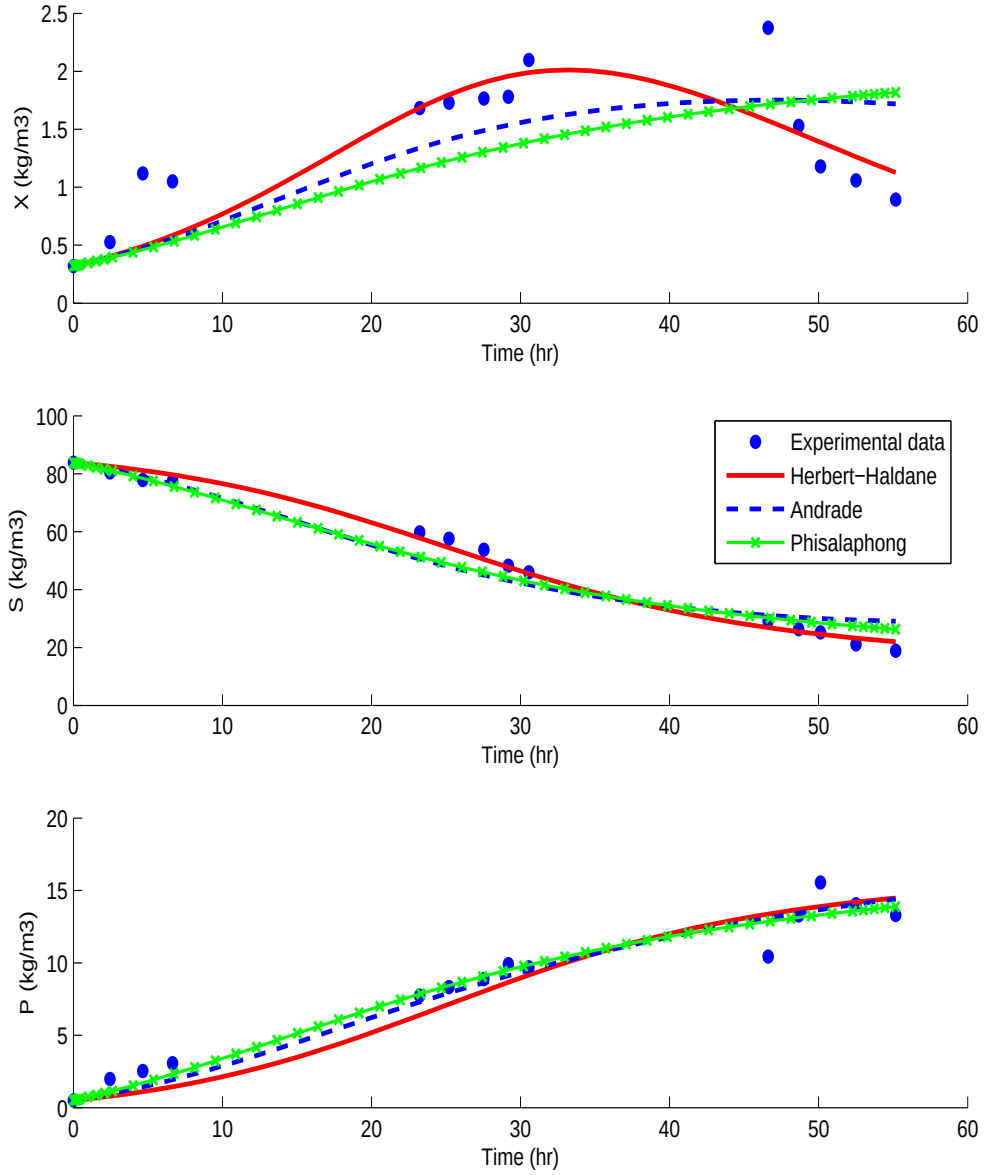

Figure 3.8: Comparison of kinetic models and experimental data on the concentrations of biomass (X), glucose (S) and ethanol (P) for run 5

highlighting that the Herbert-Haldane model was capable of capturing the death phase in the viable biomass concentration towards the end of the batch process and this is important for long batch process where cell death cannot be ignored.

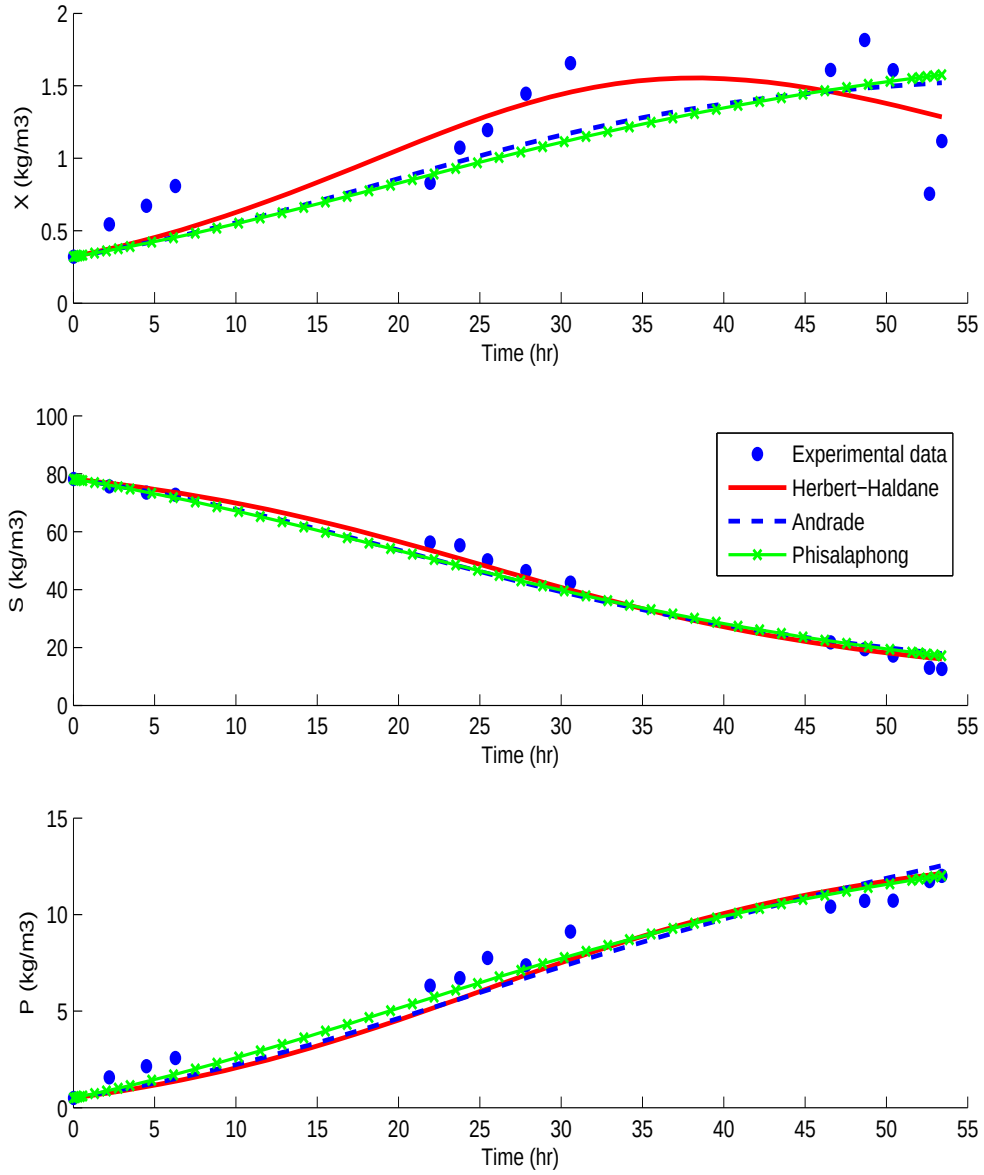

Figure 3.9: Comparison of kinetic models and experimental data on the concentrations of biomass (X), glucose (S) and ethanol (P) for run 7

3.5 Discussion

It can be noticed that, the modified Herbert-Haldane model (incorporating pH and aeration rate) was used to construct an advanced expanded microbial kinetics

(EMK) model, which has been presented to predict the kinetic parameters of a highly nonlinear dynamic fermentation process [173]. The model provides a higher accuracy in estimating the kinetic parameter value in a case when it is highly nonlinear function of certain input parameters. It is worth highlighting that, the advanced EMK model is easy and inexpensive to construct (in comparison with a neural network model), thus it can be used in bioreactor simulation, optimization and control studies. The detailed modeling approach can be referred to [173].

The experiment to evaluate product inhibition was not conducted in this research study. The kinetics of ethanol inhibition in alcoholic fermentation process have been reported in many literature [70, 78, 83]. The conventional alcoholic fermentation is typically inhibited by high ethanol concentration. The concentration of ethanol above 112 kg/m^3 (about 12% v/v) would reduce the activity and growth of microorganisms [20, 21, 70]. In general, for *S. cerevisiae*, the ethanol inhibition is small or negligible when the ethanol concentration is below 40 kg/m^3.

3.6 Summary

- The hypothesis has been supported by the results of experiments. The modified Herbert-Haldane model can fit the experimental data well as the model is capable of capturing the death phase in biomass concentration towards the end of fermentation.

- The development of a microbial kinetics model, will in part demonstrate the complexity of the overall system dynamics (e.g., in fed-batch modeling) and affect the controllability of the system.

- The fermentation was affected more significantly by the changes in pH and aeration rate compared to stirrer speed. The experimental results suggested that ethanol production was highest at pH 4.5, SS = 160 rpm and AR = 0.033 v/v.min with 24.5 kg/m^3 final ethanol concentration.

- The works described in this chapter have been published in Asia Pacific Confederation of Chemical Engineering Congress 2015[1], Procedia Engineering[2]

[1]Qiu Han Seer and Jobrun Nandong. Experimental study of the impacts of pH and aeration on kinetics of ethanol fermentation using cassava and fruit waste. *Asia Pacific Confederation of Chemical Engineering Congress 2015: APCChE 2015, incorporating CHEMECA 2015*, 1905-1915, 2015.

[2]Qiu Han Seer and Jobrun Nandong. Advanced Expanded Microbial Kinetics (EMK) Model

and IOP Conference Series: Materials Science and Engineering[3]. The modified Herbert-Haldane model was used to construct an advanced expanded microbial kinetics (EMK) model. The proposed EMK model can be used to predict the kinetic parameters of a highly nonlinear dynamic fermentation process using much less experimental data compared to neural network model.

- The fruit waste (e.g., rejected mango) appear to be a promising alternative to agricultural crops and lignocellulosic materials for alcoholic fermentation process. The bioethanol production from fruit waste helps to reduce the competition with food consumption and avoids costly pretreatment process.

for Ethanol Production from Mixed Cassava and Fruit Wastes. *Procedia Engineering*, 148: 417-425, 2016.

[3]Qiu Han Seer, Jobrun Nandong and Thomas Shanon. Experimental Study of Bioethanol Production using Mixed Cassava and Durian Seed. *29th Symposium of Malaysian Chemical Engineers (SOMChE 2016).*

Chapter 4

Closed-loop Stability of PID Controller

In some common cases of fermentation, the process involved can be simplified to a second- or even first-order system with delay. The nature of fermentation dynamics depends on the types of applications and microorganisms involved. In the process industry, open-loop unstable systems with time delays are often encountered which pose a relatively challenging problem to controller design compared to that of stable open-loop systems. In this chapter, the stabilization by a PID controller of second-order unstable processes, which can be represented as second-order deadtime with an unstable pole (SODUP) and second-order deadtime with two unstable poles (SODTUP), is performed via the necessary and sufficient criteria of the Routh-Hurwitz stability analysis. Two novel theorems are proposed which can be applied to the closed-loop characteristic equation in order to analyze the existence of stabilizing regions of each PID parameter based on the Routh-Hurwitz stability criteria.

4.1 Preliminaries

4.1.1 Feedback Control

Figure 4.1 shows a single-loop feedback control structure. Here, P, G_c and F_r denote the plant, controller and setpoint pre-filter transfer functions; R, D_i, D_o and Y represent setpoint, input disturbance, output disturbance and controlled variable signals respectively.

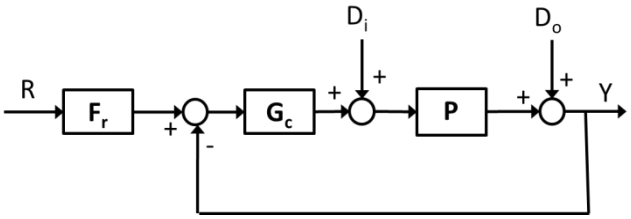

Figure 4.1: Block diagram of a feedback control structure

The closed-loop feedback transfer function from R to Y is written as

$$P_a(s) = \frac{Y}{R} = \frac{F_r G_c P}{1 + G_c P} \tag{4.1}$$

With regard to Figure 4.1, the closed-loop characteristic equation is written as $1 + G_c P = 0$, which can be rearranged in a polynomial form as

$$a_q s^q + a_{q-1} s^{q-1} + \ldots a_1 s + a_0 = 0 \tag{4.2}$$

where a_i, $i = 0, 1, 2, \ldots q$ are the coefficients of the closed-loop characteristic polynomial. For closed-loop stability, the necessary criterion of Routh stability states that all of the coefficients in the characteristic equation must be positive, i.e., $a_i > 0$, $i = 0, 1, 2, \ldots q$. Furthermore, the sufficient condition can be inferred from the Routh array **RA**, which has $q + 1$ rows. The first two rows are the coefficients of the characteristic polynomial (4.2). The Routh array for (4.2) is written as

$$\mathbf{RA} = \begin{vmatrix} a_q & a_{q-2} & a_{q-4} & \ldots \\ a_{q-1} & a_{q-3} & a_{q-5} & \ldots \\ b_1 & b_2 & \ldots & \\ c_1 & \ldots & & \\ \vdots & & & \end{vmatrix} \tag{4.3}$$

where the elements b_i and c_i can be computed as follows:

$$b_i = \frac{a_{q-1} a_{q-2i} - a_q a_{q-2i-1}}{a_{q-1}} \tag{4.4}$$

$$c_i = \frac{b_1 a_{q-2i-1} - a_{q-1} b_{i+1}}{b_{i+1}} \tag{4.5}$$

The necessary and sufficient conditions for closed-loop stability are that all of the elements in the left column of the Routh array (4.3) are positive [174]. In process industry, several forms of proportional-integral-derivative (PID) controllers are adopted. One of the common forms is the ideal PID controller given by

$$G_c(s) = K_c(1 + \frac{1}{\tau_I s} + \tau_D s) \tag{4.6}$$

where K_c, τ_I and τ_D are the tuning parameters known as the controller gain, integral or reset time and derivative time respectively.

4.1.2 Unstable Processes

In the present work, we consider two types of models commonly used to represent second-order unstable processes. The first one is called the second-order deadtime unstable pole (SODUP) model given by

$$P(s) = \frac{K_p e^{-\theta s}}{(\tau_u s - 1)(\tau_a s + 1)} \tag{4.7}$$

Here, K_p, θ and τ_j, $j = u, a$ are called the process gain, deadtime and time constants, respectively. It is assumed that $\theta > 0$, $\tau_u > 0$ and $\tau_a > 0$.

Another type is the second-order deadtime two-unstable pole (SODTUP) model

$$P(s) = \frac{K_p e^{-\theta s}}{(\tau_1 s - 1)(\tau_2 s - 1)} \tag{4.8}$$

where both time constants take positive values, i.e., $\tau_1 > 0$ and $\tau_2 > 0$. This process has two poles which are on the right-hand side of complex plane.

4.2 Theorem

Theorem 4.2.1. *For a given open-loop process there exists a set of ranges of K_c, τ_I and τ_D forming a region Ω^{nc} within which the necessary criterion of Routh stability can be fulfilled, otherwise, the PID controller cannot stabilize the process. A region based on the necessary criterion exists if and only if*

$$\Omega^{nc} := \begin{cases} \tau^{nc}_{D,min} < \tau_D < \tau^{nc}_{D,max} \\ \tau^{nc}_{I,min} < \tau_I < \tau^{nc}_{I,max} \\ K^{nc}_{min} < K < K^{nc}_{max} \end{cases}$$

where $\tau^{nc}_{D,min} = max[\underline{D}^{nc}_1, \underline{D}^{nc}_2, \ldots \underline{D}^{nc}_m]$ denotes the maximum lower limit on the derivative time, $\tau^{nc}_{D,max} = min[\overline{D}^{nc}_1, \overline{D}^{nc}_2, \ldots \overline{D}^{nc}_m]$ the minimum upper limit on the derivative time, $\tau^{nc}_{I,min} = max[\underline{I}^{nc}_1, \underline{I}^{nc}_2, \ldots \underline{I}^{nc}_m]$ the maximum lower limit on the integral time, $\tau^{nc}_{I,max} = min[\overline{I}^{nc}_1, \overline{I}^{nc}_2, \ldots \overline{I}^{nc}_m]$ the minimum upper limit on the integral time, $K^{nc}_{min} = max[\underline{K}^{nc}_1, \underline{K}^{nc}_2, \ldots \underline{K}^{nc}_m]$ the maximum lower limit on the loop gain, and $K^{nc}_{max} = min[\overline{K}^{nc}_1, \overline{K}^{nc}_2, \ldots \overline{K}^{nc}_m]$ the minimum upper limit on the

loop gain all of which are established from the coefficients of the closed-loop characteristic polynomial equation (4.2)*. Thus, the superscript "nc" indicates the limit is established from the necessary criterion.*

Proof. Consider a given process $P(s) = N(s)/D(s)$ where $N(s) = \alpha_m s^m + \alpha_{(m-1)}s^{m-1} + \ldots \alpha_1 s + \alpha_0$ and $D(s) = \beta_n s^n + \beta_{n-1}s^{n-1} + \ldots \beta_1 s + \beta_0$ are polynomial equations with real coefficients of α_i, $i = 0, 1, \ldots m$ and β_j, $j = 0, 1, \ldots n$. The system is assumed to be a proper transfer function, i.e., $m \leq n$. Let us assume that the closed-loop characteristic equation with an ideal PID controller (4.6) can be written in the following form

$$E(s, \Phi) = \underbrace{(f_q + h_q K)}_{a_q} s^q + \underbrace{(f_{q-1} + h_{q-1} K)}_{a_{q-1}} s^{q-1} + \ldots \underbrace{(f_1 + h_1 K)}_{a_1} s^1 + \underbrace{(f_0 + h_0 K)}_{a_0} = 0 \quad (4.9)$$

Further assume that $f_i = F_i(\tau_I, \tau_D, \Theta)$ and $h_i = H_i(\tau_I, \tau_D, \Theta)$ are functions of the integral time τ_I, derivative time τ_D and model parameters only. h_i, $i = 1, 2, \ldots q$ are the coefficients of loop gain in the closed-loop characteristic equation. Note that, $K = K_c K_p$, $\Phi = \{K_c, \tau_I, \tau_D\}$ and Θ denote the loop gain, a set of PID controller parameters and a set of model parameters respectively. The set of lower limits on the loop gain $\Psi^K_{lm} = \{\underline{K}^{nc}_1, \underline{K}^{nc}_2, \ldots \underline{K}^{nc}_k\}$ and the set of upper limits on the loop gain $\Psi^K_{ul} = \{\overline{K}^{nc}_1, \overline{K}^{nc}_2, \ldots \overline{K}^{nc}_k\}$ depend on the values selected for τ_D and τ_I which can either cause $h_i > 0$ or $h_i < 0$.

Thus for a given coefficient a_i in the characteristic polynomial (4.9), a lower limit on the loop gain will be given by $\underline{K}^{nc}_i = -f_i/h_i$ if $h_i > 0$. Otherwise, an upper limit on the loop gain will be obtained instead as $\overline{K}^{nc}_i = f_i/|h_i|$ if $h_i < 0$. As different ranges of τ_D and τ_I lead to either $h_i > 0$ or $h_i < 0$, we can divide the entire stabilization problem into a number of finite cases, e.g., z number of cases: $C.1$, $C.2$,...$C.z$.

Consider a particular case $C.j$ where $j \in \{1, 2, \ldots z\}$. First to establish either a lower limit or an upper limit on the loop gain, we need to determine the upper and lower limit on the integral time as functions of derivative time and process model parameters, e.g., for a given $h_1 > 0$ or $h_1 < 0$ the integral time is bounded as

$$\underline{I}^{nc}_1 < \tau_I < \overline{I}^{nc}_1$$

s.t.:

$$\underline{D}^{nc}_1 = max[\underline{D}_a, \underline{D}^*] < \tau_D < \overline{D}^{nc}_1 = min[\overline{D}_a, \overline{D}^*]$$

Here, $\underline{I}_1^{nc} = g_{lm,1}(\tau_D, \Theta)$ and $\overline{I}_1^{nc} = g_{ul,1}(\tau_D, \Theta)$ are both functions of τ_D and a set of model parameters Θ. Note that, $\underline{D}_a$ and $\overline{D}_a$ represent the lower and upper limits on the derivative time respectively, where any value of $\tau_D \in (\underline{D}_a, \overline{D}_a)$ will lead to the above given range of the integral time. Meanwhile, $\underline{D}^*$ and $\overline{D}^*$ denote the lower and upper limits on the derivative time where any value of $\tau_D \in (\underline{D}^*, \overline{D}^*)$ will ensure that the upper limit of the integral time is always larger than its lower limit, i.e., $\overline{I}_1^{nc} > \underline{I}_1^{nc}$. Hence, the derivative time must be within the range given above, otherwise, the range of integral time is not valid leading to a negative coefficient of the characteristic polynomial. All of the limits on the derivative time are assumed as functions of model parameters only, e.g., $\underline{D}_a = f_{lm,a}(\Theta)$, etc.

If the ranges of τ_D and τ_I are met, then the loop gain will be either bounded from below or above

$$K > \underline{K}_1^{nc} = -f_1/h_1 \quad \text{if} \quad h_1 > 0$$

or

$$K < \overline{K}_1^{nc} = f_1/|h_1| \quad \text{if} \quad h_1 < 0$$

The same procedure is repeated for $h_0, h_2, \ldots h_q$ under the given case $C.j$, which upon collections of all the limits leads to sets of lower and upper limits on the integral time $(\Psi_{lm}^I, \Psi_{ul}^I)$, derivative time $(\Psi_{lm}^D, \Psi_{ul}^D)$ and loop gain $(\Psi_{lm}^K, \Psi_{ul}^K)$.

Next, we need to check whether there is a violation of any limit in the derivative time set $(\Psi_{lm}^D, \Psi_{ul}^D)$. The basic requirement for fulfilling the necessary criterion of Routh stability is that the derivative time must be bounded by the following range

$$\tau_{D,min}^{nc} < \tau_D < \tau_{D,max}^{nc}$$

where $\tau_{D,min}^{nc} = max\{\Psi_{lm}^D\}$ and $\tau_{D,max}^{nc} = min\{\Psi_{ul}^D\}$ are the maximum lower limit and minimum upper limit on the derivative time respectively. Note that, if $\tau_{D,max}^{nc} < \tau_{D,min}^{nc}$, then this indicates that at least one of the lower limits of integral time will switch to an upper limit, which in turn will lead to at least one of the lower limit on the loop gain to become an upper limit. This shall cause at least one of the coefficients of closed-loop characteristic polynomial (4.9) to become negative, hence leading to the non-existence of a stabilizing PID controller under the given case $C.j$. On the other hand, if $\tau_{D,max}^{nc} > \tau_{D,min}^{nc}$, then this will ensure that $\tau_{I,max}^{nc} > \tau_{I,min}^{nc}$ which in turn will lead to $K_{max}^{nc} > K_{min}^{nc}$. If this happens, then all of the coefficients in the characteristic polynomial (4.9) are guaranteed to be positive (necessary criterion of Routh stability is achieved) if and only if the derivative time, integral time and loop gain are respectively bounded in the

ranges of $\tau_{D,min}^{nc} < \tau_D < \tau_{D,max}^{nc}$, $\tau_{I,min}^{nc} < \tau_I < \tau_{I,max}^{nc}$ and $K_{min}^{nc} < K < K_{max}^{nc}$. This completes the proof of Theorem 4.2.1.

□

Theorem 4.2.2. *For the given values of τ_D and K such that $\tau_D \in (\tau_{D,min}^{nc}, \tau_{D,max}^{nc})$ and $K \in (K_{min}^{nc}, K_{max}^{nc})$, the closed-loop characteristic polynomial is Hurwitz if and only if a value of τ_I is within*

$$\Omega^{sc} := \begin{cases} for\ K, \tau_D \in \Omega^{nc} \\ max[\tau_{I,min}^{nc}, \tau_{I,min}^{sc}] < \tau_I < min[\tau_{I,max}^{nc}, \tau_{I,max}^{sc}] \end{cases}$$

where $\tau_{I,min}^{sc} = max[\underline{I}_1^{sc}, \underline{I}_2^{sc}, \ldots \underline{I}_m^{sc}]$ denotes the maximum lower limit on the integral time and $\tau_{I,max}^{sc} = min[\overline{I}_1^{sc}, \overline{I}_2^{sc}, \ldots \overline{I}_m^{sc}]$ the minimum upper limit on the integral time all of which are obtained based on the elements in the left column of Routh array (4.3)*. Here, the superscript "sc" indicates the limit is based on the sufficient criterion.*

Proof. Suppose that the conditions given by the Theorem 4.2.1 are completely fulfilled, and then all of the coefficients of the closed-loop characteristic polynomial (4.9) are positive, i.e., the necessary (but not sufficient) criterion of Routh stability is met. However, this does not guarantee that the sufficient criterion for closed-loop stability is met because some of the elements in the left column of Routh array might be negative. Note that, the elements in the Routh array are functions of K, τ_D and τ_I but we can fix the values of the K and τ_D first to be within the ranges established in the Theorem 4.2.1. Hence, based on each element in the left column of Routh array excluding those in the first two rows, we can express the limit on τ_I as a function of K, τ_D and Θ whose values already fixed. It follows that, we may establish a minimum upper limit $\tau_{I,max}^{sc}$ and maximum lower limit $\tau_{I,min}^{sc}$ based on the elements of Routh array. Finally, to fulfill the sufficient criterion of Routh stability, we have to set a value for the integral time within $max[\tau_{I,min}^{nc}, \tau_{I,min}^{sc}] < \tau_I < min[\tau_{I,max}^{nc}, \tau_{I,max}^{sc}]$ so as to achieve both necessary and sufficient criteria of Routh stability. This completes the proof of Theorem 4.2.2.

□

The application of the Theorems 4.2.1 and 4.2.2 to establishing the stabilizing regions of PID tuning parameters for a class of second-order unstable processes will be demonstrated in the following sections.

4.3 Stability Analysis of SODUP

Upon the approximation of the deadtime in the process (4.7) by using the first-order Taylor series

$$P(s) \cong \frac{K_p(-\theta s + 1)}{(\tau_u s - 1)(\tau_a s + 1)} \tag{4.10}$$

Then, by using the ideal PID controller (4.6), the closed-loop characteristic polynomial becomes

$$\underbrace{\tau_I(\tau_u\tau_a - K\theta\tau_D)}_{a_3} s^3 + \underbrace{\tau_I[\tau_u - \tau_a + K(\tau_D - \theta)]}_{a_2} s^2 + \underbrace{[-\tau_I + K(\tau_I - \theta)]}_{a_1} s + \underbrace{K}_{a_0} = 0 \tag{4.11}$$

4.3.1 Necessary Stability Conditions for SODUP

Theorem 4.2.1 is applied in order to establish the ranges or limits on the loop gain, derivative time and integral time which render all the coefficients in the characteristic equation (4.11) positive. From the characteristic equation (4.11) and based on the coefficient of s^0, we can readily establish one of the lower limits on the loop gain $K = K_c K_p$ as follows

$$K > \underline{K}_o^{nc} = 0$$

and an upper limit based on the coefficient of s^3

$$K < \overline{K}_o^{nc} = \frac{\tau_u\tau_a}{\theta\tau_D}$$

The notations $\underline{K}_o^{nc}$ and $\overline{K}_o^{nc}$ indicate the lower and upper limits on the loop gain based on the necessary criterion of Routh stability, respectively. It is important to point out that for a PID controller, a few extra conditions have to be fulfilled so that the necessary criterion of Routh stability is obeyed.

Remark 2. *As the Theorem 4.2.1 states, the maximum lower limit of the loop gain must always be smaller than the upper limit to ensure that the necessary criterion of the Routh stability is obeyed, otherwise, the PID controller is deemed unstable.*

4.3.1.1 Case 1: $\tau_u > \tau_a$

Case 1.1: $\tau_D > \theta$, $\tau_I > \theta$

For this case 1.1, in addition to $\underline{K}_o^{nc}$ there are two extra lower limits on the K which are obtained from the coefficients of s^2 and s in the characteristic equation (4.11):

$$K > \underline{K}_{1.1a}^{nc} = \frac{\tau_a - \tau_u}{\tau_D - \theta} < 0$$

$$K > \underline{K}_{1.1b}^{nc} = \frac{\tau_I}{\tau_I - \theta} > 0$$

Remark 3. *For this case 1.1, the maximum lower limit is always given by* $\underline{K}_{1.1b}^{nc}$ *since another lower limit* $\underline{K}_{1.1a}^{nc}$ *is always less than zero, i.e., since* $\tau_u > \tau_a$. *Based on Theorem 4.2.1, we must ensure that the only upper limit on the loop gain* $(\overline{K}_o^{nc})$ *must always be larger than its maximum lower limit, i.e.,* $\overline{K}_o^{nc} > \underline{K}_{1.1b}^{nc}$.

In view of the remark 3, let $\overline{K}_o^{nc} > \underline{K}_{1.1b}^{nc}$ so that we have the following inequality

$$\frac{\tau_u \tau_a}{\theta \tau_D} > \frac{\tau_I}{\tau_I - \theta}$$

For the inequality above to hold, it can be easily shown that the integral time must be bounded by a lower limit

$$\tau_I > \underline{I}_{1.1}^{nc} = \frac{\theta \tau_u \tau_a}{\tau_u \tau_a - \theta \tau_D} \tag{4.12}$$

It should be pointed out that for the lower limit on the integral time (4.12) to be valid, the derivative time must be bounded from above and as a result the denominator of (4.12) must be positive. Otherwise, the inequality leads to a lower limit on the derivative time while the integral time will then be bounded from above - such a switch is not allowed by the Theorem 4.2.1. Hence, by assuming that the denominator of (4.12) is always positive, i.e., $\tau_u \tau_a - \theta \tau_D > 0$, the upper bound on the derivative time is obtained

$$\tau_D < \overline{D}_{1.1}^{nc} = \frac{\tau_u \tau_a}{\theta} \tag{4.13}$$

In view of the fact that the case 1.1 requires $\tau_D > \theta$, the upper limit on the derivative time must be larger than the deadtime θ, that is

$$\overline{D}_{1.1}^{nc} > \theta \quad \Rightarrow \quad \theta < \overline{\theta}_{1.1} = \sqrt{\tau_u \tau_a}$$

Hence, if the process deadtime is larger than the upper limit $\overline{\theta}_{1.1}$, then there is no PID controller that can stabilize the SODUP (4.7) under the case 1.1.

Assuming that the limit on integral time (4.12) and the limit on derivative time (4.13) are obeyed, then the loop gain is guaranteed to be bounded between its maximum lower and upper limits as

$$\frac{\tau_I}{\tau_I - \theta} < K < \frac{\tau_u \tau_a}{\theta \tau_D} \tag{4.14}$$

In other words, the necessary criterion for stability can only be fulfilled for the case 1.1, if and only if all the limits or ranges for τ_I, τ_D and K are met, i.e., in (4.12) - (4.14).

Case 1.2: $\tau_D < \theta$, $\tau_I > \theta$

Under the case 1.2, the following additional limits (in addition to $\underline{K}_o^{nc}$ and $\overline{K}_o^{nc}$) are established:

$$K < \overline{K}_{1.2}^{nc} = \frac{\tau_u - \tau_a}{\theta - \tau_D} > 0$$

$$K > \underline{K}_{1.2}^{nc} = \underline{K}_{1.1b}^{nc}$$

Since we have two upper limits on the loop gain ($\overline{K}_o^{nc}$ and $\overline{K}_{1.2}^{nc}$), to fulfill the necessary criterion of Routh stability, the minimum upper limit must be larger than the maximum lower limit (Theorem 4.2.1). First, consider that the minimum upper limit is $\overline{K}_o^{nc}$, so that we get the following inequality

$$\underbrace{\frac{\tau_u \tau_a}{\theta \tau_D}}_{\overline{K}_o^{nc}} < \underbrace{\frac{\tau_u - \tau_a}{\theta - \tau_D}}_{\overline{K}_{1.2}^{nc}}$$

For the inequality above to hold, the derivative time must be bounded from below

$$\tau_D > \underline{D}_{1.2}^{nc} = \frac{\theta \tau_u \tau_a}{\tau_u \tau_a + \theta(\tau_u - \tau_a)} \tag{4.15}$$

Based on the Theorem 4.2.1, the minimum upper limit on the loop gain $\overline{K}_o^{nc}$ must always be larger than its maximum lower limit (same as case 1.1), i.e.

$$\underbrace{\frac{\tau_u \tau_a}{\theta \tau_D}}_{\overline{K}_o^{nc}} > \underbrace{\frac{\tau_I}{\tau_I - \theta}}_{\underline{K}_{1.2}^{nc}}$$

From the inequality above, it can be readily shown that the integral time is bounded from below:

$$\tau_I > \underline{I}_{1.2}^{nc} = \underline{I}_{1.1}^{nc} = \frac{\theta \tau_u \tau_a}{\tau_u \tau_a - \theta \tau_D} \tag{4.16}$$

Note that, the denominator of (4.16) must be positive, otherwise, the integral time is bounded from above instead leading to a condition where there is no stable

PID controller exits for stabilizing the SODUP (violation of the Theorem 4.2.1). For the denominator to be positive, the derivative time must be limited by an upper limit

$$\tau_D < \overline{D}_{1.2}^{nc} = \overline{D}_{1.1}^{nc} = \frac{\tau_u \tau_a}{\theta} \tag{4.17}$$

In view of case 1.2, $\tau_D < \theta$, the upper limit on derivative time under the case 1.2 (4.17) must lie in the range between the deadtime θ and the lower limit on derivative time under the case 1.2 (4.15). Since the upper limit on derivative time (4.17) must be less than the deadtime θ, the lower limit on deadtime $\theta > \underline{\theta}_{1.2} = \sqrt{\tau_u \tau_a}$ is given. Meanwhile, a maximum value of deadtime $\theta < \overline{\theta}_{1.2} = \tau_u$ is obtained since the upper limit on derivative time (4.17) must be larger than the lower limit on derivative time (4.15). We can show that the value of deadtime beyond which there is no stable PID exists for stabilizing SODUP is

$$\sqrt{\tau_u \tau_a} = \underline{\theta}_{1.2} < \theta < \overline{\theta}_{1.2} = \tau_u \tag{4.18}$$

Hence, the range of deadtime is given in (4.18) associated with the unstable pole, beyond this value there is no stabilizing PID controller exists under the case 1.2.

If all the ranges or limits of τ_I, τ_D and θ given in (4.15) - (4.18) respectively are obeyed, then the loop gain is bounded as follows

$$\frac{\tau_I}{\tau_I - \theta} < K < \frac{\tau_u \tau_a}{\theta \tau_D} \tag{4.19}$$

Remark 4. *If the minimum upper limit on the loop gain is given by $\overline{K}_{1.2}^{nc}$, then the range of τ_I and τ_D are given by*

$$\tau_I > \underline{I}_{1.2b}^{nc} = \frac{\theta(\tau_u - \tau_a)}{\tau_u + \tau_D - (\theta + \tau_a)}$$

$$\tau_D < \overline{D}_{1.2b}^{nc} = \frac{\theta \tau_u \tau_a}{\tau_u \tau_a + \theta(\tau_u - \tau_a)}$$

Since the denominator of the lower limit of integral time is always positive, the lower bound on the derivative time is given by

$$\tau_D > \underline{D}_{1.2b}^{nc} = \theta + \tau_a - \tau_u$$

Note that, the upper limit of τ_D must be greater than its lower limit, thus the upper limit of deadtime is established, i.e.,

$$\theta < \overline{\theta}_{1.2b} = \tau_u$$

Thus under this case, there is only an upper limit on deadtime given by $\overline{\theta}_{1.2b}$ *in order for* $\overline{K}_{1.2}^{nc} < \overline{K}_{o}^{nc}$*, this implies that for* $0 < \theta < \sqrt{\tau_u \tau_a}$*, the minimum upper limit is always* $\overline{K}_{1.2}^{nc}$*. However, above the lower limit on deadtime* $\underline{\theta}_{1.2}$ (4.18) *which leads to* $\overline{K}_{o}^{nc} < \overline{K}_{1.2}^{nc}$*, the minimum upper limit is always* $\overline{K}_{o}^{nc}$*. It should be noted that, above the lower limit of deadtime* $\underline{\theta}_{1.2}$ *a stable PID controller can be obtained under the case 1.2; below this lower limit, a stable PID controller can be obtained under both cases 1.1 and 1.2.*

Remark 5. *If* $\tau_I < \theta$ *while* $\tau_D > \theta$ *or* $\tau_D < \theta$ *, then there is no stable PID controller exists for the SODUP. The reason is that, when* $\tau_I < \theta$ *we have an upper limit on the loop gain based on the coefficient of* s *in the characteristic equation as follows*

$$K < \overline{K}_{1}^{nc} = -\frac{\tau_I}{\theta - \tau_I} < 0$$

Since the maximum lower limit on the loop gain based on the necessary condition is always greater than zero, i.e., $\underline{K}_{o}^{nc} > 0$*, so this means that the minimum upper limit of the loop gain is always less than its maximum lower limit leading to the violation of the Theorem 4.2.1, which means the necessary criterion of Routh stability is impossible to fulfill. Therefore, for* $\tau_I < \theta$ *there is no stable PID controller exists to stabilize the SODUP* (4.7) *for all values of model parameters.*

4.3.1.2 Case 2: $\tau_u < \tau_a$, $\tau_D > \theta$, $\tau_I > \theta$

For this case 2, in addition to the previously given upper limit $\overline{K}_{o}^{nc}$ and lower limit $\underline{K}_{o}^{nc}$, there are two extra positive lower limits

$$K > \underline{K}_{2a}^{nc} = \underline{K}_{1.1a}^{nc} > 0$$

$$K > \underline{K}_{2b}^{nc} = \underline{K}_{1.1b}^{nc} > 0$$

The first step is to examine which one of these positive lower limits is the maximum and under what condition it occurs. Hence, for the case 2 we further divide it into two sub cases as described below.

Remark 6. *For case 2, there is no stable PID controller exists for the SODUP when* $\tau_D < \theta$ *or* $\tau_I < \theta$*. When* $\tau_D < \theta$*, an upper limit on the loop gain is given based on the coefficient of* s^2 *in the characteristic equation as follows*

$$K < \overline{K}_{2}^{nc} = \frac{\tau_u - \tau_a}{\theta - \tau_D} < 0$$

On the other hand, if $\tau_I < \theta$, an upper limit on the loop gain based on the coefficient of s is given by

$$K < \overline{K}_3^{nc} = -\frac{\tau_I}{\theta - \tau_I} < 0$$

Both of the minimum upper limits is always less than zero, this means that the minimum upper limit of the loop gain is always less than its maximum lower limit based on the necessary condition, i.e., $\underline{K}_o^{nc} > 0$, which leads to the violation of the Theorem 4.2.1.

Case 2.1: $\underline{K}_{2a}^{nc} > \underline{K}_{2b}^{nc}$

For this case 2.1 to occur, the maximum lower limit on the loop gain is given by $\underline{K}_{2a}^{nc}$, i.e.:

$$\underbrace{\frac{\tau_a - \tau_u}{\tau_D - \theta}}_{\underline{K}_{2a}^{nc}} > \underbrace{\frac{\tau_I}{\tau_I - \theta}}_{\underline{K}_{2b}^{nc}}$$

It is required that the integral time must be bounded from below

$$\tau_I > \underline{I}_{2.1}^{nc} = \frac{\theta(\tau_a - \tau_u)}{\tau_a + \theta - (\tau_u + \tau_D)} \tag{4.20}$$

But to ensure this lower limit on integral time (4.20) holds, the denominator must be positive, which means that the derivative time has to be restricted by an upper limit given by

$$\tau_D < \overline{D}_{2.1}^{nc} = \tau_a - \tau_u + \theta \tag{4.21}$$

The second step is to meet the Theorem 4.2.1, which stipulates that the upper limit of the loop gain must always be larger than its maximum lower limit, so

$$\underbrace{\frac{\tau_a - \tau_u}{\tau_D - \theta}}_{\underline{K}_{2a}^{nc}} < \underbrace{\frac{\tau_u \tau_a}{\theta \tau_D}}_{\overline{K}_o^{nc}}$$

For the inequality above to hold, the derivative time must be imposed by a lower limit as

$$\tau_D > \underline{D}_{2.1}^{nc} = \frac{\theta \tau_u \tau_a}{\tau_u \tau_a - \theta(\tau_a - \tau_u)} \tag{4.22}$$

Since the denominator of the inequality in (4.22) must be positive, this suggests that the deadtime must have an upper limit beyond which the Theorem 4.2.1 cannot be fulfilled. By setting the denominator in (4.22) greater than zero, this upper limit is established as follows

$$\theta < \overline{\theta}_{2.1a} = \frac{\tau_u \tau_a}{\tau_a - \tau_u}$$

Additionally, because the upper limit of derivative time must be larger than its lower limit, another upper limit on the deadtime can be further established by first noting that

$$\underbrace{\frac{\theta\tau_u\tau_a}{\tau_u\tau_a - \theta(\tau_a - \tau_u)}}_{\underline{D}^{nc}_{2.1}} < \underbrace{\tau_a - \tau_u + \theta}_{\overline{D}^{nc}_{2.1}}$$

By rearranging the inequality above, we establish another upper limit on the deadtime:

$$\theta < \overline{\theta}_{2.1b} = \tau_u$$

To fulfill the Theorem 4.2.1, one of the conditions is that the minimum upper limit on the deadtime is not violated where in the case of $\tau_u < \tau_a$, this minimum upper limit can be shown as

$$\overline{\theta}^{min}_{2.1} < min(\overline{\theta}_{2.1a}, \overline{\theta}_{2.1b}) = \tau_u, \quad \tau_u < \tau_a \tag{4.23}$$

In summary, for a closed-loop stability to occur, the lower limit on the integral time in (4.20) must not be violated in addition to the derivative time and loop gain must be bounded as follows

$$\underline{D}^{nc}_{2.1} < \tau_D < \overline{D}^{nc}_{2.1} \tag{4.24}$$

$$\underline{K}^{nc}_{2a} < K < \overline{K}^{nc}_{o} \tag{4.25}$$

Case 2.2: $\underline{K}^{nc}_{2a} < \underline{K}^{nc}_{2b}$

The case 2.2 leads to the following inequality

$$\underbrace{\frac{\tau_a - \tau_u}{\tau_D - \theta}}_{\underline{K}^{nc}_{2a}} < \underbrace{\frac{\tau_I}{\tau_I - \theta}}_{\underline{K}^{nc}_{2b}}$$

There are two possible sets of conditions that can lead to $\underline{K}^{nc}_{2a} < \underline{K}^{nc}_{2b}$. One of the sets of conditions (C.2.2.I) is given by

$$\tau_I > \underline{I}^{nc}_{2.2a} = \frac{-\theta(\tau_a - \tau_u)}{\tau_u + \tau_D - (\tau_a + \theta)} \tag{4.26}$$

$$\tau_D > \underline{D}^{nc}_{2.2} = \tau_a - \tau_u + \theta \tag{4.27}$$

Another set of conditions (C.2.2.II) is given as follows

$$\tau_I < \overline{I}^{nc}_{2.2.II} = \frac{\theta(\tau_a - \tau_u)}{(\tau_a - \tau_u) + (\theta - \tau_D)} \tag{4.28}$$

$$\tau_D < \overline{D}^{nc}_{2.2.II} = \tau_a - \tau_u + \theta \tag{4.29}$$

It should be noted that, the second set of conditions (C.2.2.II) often leads to unstable or marginally stable PID controller for the SODUP under the case 2.2 because of the existence of an upper limit on the integral time. The reason for this is that, the upper limit on the integral time $\overline{I}^{nc}_{2.2.II}$ can often be lower than the lower limit on the integral time imposed by the sufficient condition $\underline{I}^{sc}$ (to be described in the next section).

Assuming the condition C.2.2.I is met, then to ensure that the necessary criterion of Routh stability is fulfilled, the following extra limits must be applied. According to the Theorem 4.2.1, the upper limit on the loop gain must be smaller than its maximum lower limit leading to an inequality

$$\underbrace{\frac{\tau_I}{\tau_I - \theta}}_{\underline{K}^{nc}_{2b}} < \underbrace{\frac{\tau_u \tau_a}{\theta \tau_D}}_{\overline{K}^{nc}_{o}}$$

which stipulates the integral time must be bounded from below, hence

$$\tau_I > \underline{I}^{nc}_{2.2b} = \frac{\theta \tau_u \tau_a}{\tau_u \tau_a - \theta \tau_D} \tag{4.30}$$

$$\tau_D < \overline{D}^{nc}_{2.2} = \frac{\tau_u \tau_a}{\theta} \tag{4.31}$$

Note that, $\underline{I}^{nc}_{2.2b} > 0 > \underline{I}^{nc}_{2.2a}$ provided that $\underline{D}^{nc}_{2.2} < \tau_D < \overline{D}^{nc}_{2.2}$. Furthermore, it is necessary to ensure that $\overline{D}^{nc}_{2.2} > \underline{D}^{nc}_{2.2}$ a requirement that leads to another upper limit on the deadtime, i.e.:

$$\theta < \overline{\theta}_{2.2} = \tau_u$$

Hence, the loop gain is bounded between its maximum lower and minimum upper limit as

$$\frac{\tau_I}{\tau_I - \theta} < K < \frac{\tau_u \tau_a}{\theta \tau_D}$$

4.3.2 Sufficient Stability Criterion for SODUP

Remark 7. *All the coefficients of the closed-loop characteristic polynomial are positive when the conditions given by the Theorem 4.2.1 are fulfilled. However, the sufficient criterion for closed-loop stability are not guaranteed, i.e., some of the elements in the left column of Routh array might still in negative value. Thus, the Theorem 4.2.2 is applied in order to establish the limit on integral time which render the closed-loop characteristic polynomial Hurwitz (sufficient criterion for closed-loop stability).*

From the characteristic equation (4.11), we have only a single element in the left column of the Routh array:

$$b = a_1 - \frac{a_3 a_0}{a_2} > 0$$

From the above inequality, it can be readily shown that a lower limit on the integral time is given by

$$\tau_I > \underline{I}^{sc} = \underbrace{\left(\frac{K}{K-1}\right)}_{g_1} \underbrace{\left(\theta + \frac{\tau_u \tau_a - K\theta\tau_D}{\tau_u - \tau_a + K(\tau_D - \theta)}\right)}_{g_2} \tag{4.32}$$

Remark 8. *Form the g_1 term, when $K < 1$ we have an upper limit on the integral time*

$$\tau_I < \overline{I}^{sc} = -\left(\frac{K}{1-K}\right)\left(\theta + \frac{\tau_u \tau_a - K\theta\tau_D}{\tau_u - \tau_a + K(\tau_D - \theta)}\right) < 0 \tag{4.33}$$

Because the upper limit now becomes negative, this suggest that for $K < 1$, a PID controller cannot provide closed-loop stability for SODUP (4.7)*. Based on the sufficient condition of Routh stability, the loop gain must be bounded from below by a lower limit $\underline{K}_1^{sc} > 1$. From the g_2 term, if the denominator becomes negative for $K > 1$, then the negative value of upper limit on the integral time will also be present. Thus, this leads to another lower limit on the loop gain based on the sufficient condition, which is $K > (\tau_a - \tau_u)/(\tau_D - \theta) = \underline{K}_{2a}^{nc}$, i.e., similar to one of the lower limits in the case 2 obtained based on the necessary criterion.*

Remark 9. *The lower limit on the integral time* (4.32) *represents a necessary and sufficient condition for closed-loop stability to occur given that both loop gain and derivative time are set in such a way to fulfilling the necessary conditions from Theorem 4.2.1. This is because the maximum lower limit on the loop gain arises from the necessary condition (Theorem 4.2.1) where the sufficient condition does not impose any new upper limit in addition to those obtained via the necessary criterion.*

The results of stabilizing regions of PID parameters for SODUP processes obtained through the Theorems 4.2.1 and 4.2.2 are summarized in the Table 4.1.

Table 4.1: Summary of the PID parameter regions for SODUP processes

Case	θ	K	τ_I	τ_D
case 1: $\tau_u > \tau_a$				
1.1 $\tau_D > \theta$ $\tau_I > \theta$	$0 < \theta < \sqrt{\tau_u \tau_a}$	$\frac{\tau_I}{\tau_I - \theta} < K < \frac{\tau_u \tau_a}{\theta \tau_D}$	$\tau_I > max(\underline{I}^{nc}_{1.1}, \underline{I}^{sc})$ $\underline{I}^{nc}_{1.1} = \frac{\theta \tau_u \tau_a}{\tau_u \tau_a - \theta \tau_D}$ $\underline{I}^{sc} = \left(\frac{K}{K-1}\right)\left(\theta + \frac{\tau_u \tau_a - K\theta\tau_D}{\tau_u - \tau_a + K(\tau_D - \theta)}\right)$	$\theta < \tau_D < \frac{\tau_u \tau_a}{\theta}$
1.2a $\tau_D < \theta$ $\tau_I > \theta$	$\sqrt{\tau_u \tau_a} < \theta < \tau_u$	$\frac{\tau_I}{\tau_I - \theta} < K < \frac{\tau_u \tau_a}{\theta \tau_D}$	$\tau_I > max(\underline{I}^{nc}_{1.2}, \underline{I}^{sc})$ $\underline{I}^{nc}_{1.2} = \frac{\theta \tau_u \tau_a}{\tau_u \tau_a - \theta \tau_D}$	$\frac{\theta \tau_u \tau_a}{\tau_u \tau_a + \theta(\tau_u - \tau_a)} <$ $\tau_D < \frac{\tau_u \tau_a}{\theta}$
1.2b $\tau_D < \theta$ $\tau_I > \theta$	$0 < \theta < \sqrt{\tau_u \tau_a}$	$\frac{\tau_I}{\tau_I - \theta} < K <$ $\frac{\tau_u - \tau_a}{\theta - \tau_D}$	$\tau_I > max(\underline{I}^{nc}_{1.2b}, \underline{I}^{sc})$ $\underline{I}^{nc}_{1.2b} = \frac{\theta(\tau_u - \tau_a)}{\tau_u + \tau_D - (\theta + \tau_a)}$	$\theta + \tau_a - \tau_u <$ $\tau_D < \frac{\theta \tau_u \tau_a}{\tau_u \tau_a + \theta(\tau_u - \tau_a)}$
case 2: $\tau_u < \tau_a$				
2.1 $\tau_D > \theta$ $\tau_I > \theta$	$0 < \theta < \tau_u$	$\frac{\tau_a - \tau_u}{\tau_D - \theta} < K < \frac{\tau_u \tau_a}{\theta \tau_D}$	$\tau_I > max(\underline{I}^{nc}_{2.1}, \underline{I}^{sc})$ $\underline{I}^{nc}_{2.1} = \frac{\theta(\tau_a - \tau_u)}{\tau_a + \theta - (\tau_u + \tau_D)}$	$\frac{\theta \tau_u \tau_a}{\tau_u \tau_a - \theta(\tau_a - \tau_u)} <$ $\tau_D < \tau_a - \tau_u + \theta$
2.2 $\tau_D > \theta$ $\tau_I > \theta$	$0 < \theta < \tau_u$	$\frac{\tau_I}{\tau_I - \theta} < K < \frac{\tau_u \tau_a}{\theta \tau_D}$	$\tau_I > max(\underline{I}^{nc}_{2.2b}, \underline{I}^{sc})$ $\underline{I}^{nc}_{2.2b} = \frac{\theta \tau_u \tau_a}{\tau_u \tau_a - \theta \tau_D}$	$\tau_a - \tau_u + \theta <$ $\tau_D < \frac{\tau_u \tau_a}{\theta}$

4.4 Stability Analysis of SODTUP

After approximating the deadtime in (4.8) using the first-order Taylor series

$$P(s) = \frac{K_p(1-\theta s)}{(\tau_1 s - 1)(\tau_2 s - 1)} \tag{4.34}$$

Assuming the PID controller (4.6) is used, the characteristic equation can be expressed as

$$\underbrace{(\tau_I\tau_1\tau_2 - K\theta\tau_I\tau_D)}_{a_3}\, s^3 + \underbrace{[K\tau_I(\tau_D-\theta) - \tau_I(\tau_1+\tau_2)]}_{a_2}\, s^2 + \underbrace{[\tau_I + K(\tau_I - \theta)]}_{a_1}\, s + \underbrace{K}_{a_0} = 0 \tag{4.35}$$

where $K = K_c K_p$ denotes the loop gain.

4.4.1 Necessary Stability Conditions for SODTUP

From the characteristic equation (4.35), we can directly identify the upper and lower limits on the loop gain from the coefficients of s^3 and s^0 respectively:

$$K < \overline{K}_o^{nc} = \frac{\tau_1\tau_2}{\theta\tau_D}$$

$$K > \underline{K}_o^{nc} = 0$$

Based on the coefficients of s^2 and s, we can further obtain either upper or lower limits on the loop gain depending on the values of τ_D and τ_I with respect to the value of θ.

4.4.1.1 Case 1: $\tau_D > \theta$ and $\tau_I > \theta$

For this case 1, we can get two extra lower limits on the loop gain given as follows

$$K > \underline{K}_{1a}^{nc} = \frac{\tau_1 + \tau_2}{\tau_D - \theta}$$

$$K > \underline{K}_{1b}^{nc} = -\frac{\tau_I}{\tau_I - \theta}$$

It is obvious that the maximum lower limit on the loop gain is given by $\underline{K}_{1a}^{nc}$ when $\tau_D > \theta$ and $\tau_I > \theta$.

Remark 10. *If $\tau_D < \theta$, then from the coefficient of s^2 in the characteristic equation* (4.35) *we will get an upper limit given by*

$$K < \overline{K}_{1c}^{nc} = -\frac{\tau_1 + \tau_2}{\theta - \tau_D}$$

Since $\tau_D < \theta$ leads to a minimum upper limit on the loop gain ($\overline{K}_{1c}^{nc}$) which is always lower than the lower limit of the loop gain, i.e., $\underline{K}_o^{nc} = 0$, this means that there is no stable PID controller exists for stabilizing the SODTUP process under the conditions of case 1.

Following the remark 2, for the closed-loop stability to occur the upper limit of the loop gain must always be larger than its maximum lower limit, thus $\underline{K}_{1a}^{nc} > 0$. In order for $\overline{K}_o^{nc} > \underline{K}_{1a}^{nc}$, the derivative time must be bounded from below

$$\tau_D > \underline{D}_1^{nc} = \frac{\theta\tau_1\tau_2}{\tau_1\tau_2 - \theta(\tau_1 + \tau_2)} \tag{4.36}$$

For the limit (4.36) to be valid, the process deadtime has to be less than a certain value given by

$$\theta < \overline{\theta}_1 = \frac{\tau_1\tau_2}{\tau_1 + \tau_2} \tag{4.37}$$

If the lower limit on the derivative time (4.36) and upper limit on the deadtime (4.37) are not violated, then the loop gain will be bounded as follows

$$\frac{\tau_1 + \tau_2}{\tau_D - \theta} < K < \frac{\tau_1\tau_2}{\theta\tau_D} \tag{4.38}$$

4.4.1.2 Case 2: $\tau_D > \theta$ and $\tau_I < \theta$

Under the conditions of case 2, in addition to the previous $\overline{K}_o^{nc}$ and $\underline{K}_o^{nc}$ there are two more limits given as follows

$$K > \underline{K}_2^{nc} = \frac{\tau_1 + \tau_2}{\tau_D - \theta}$$

$$K < \overline{K}_2^{nc} = \frac{\tau_I}{\theta - \tau_I}$$

Assuming that $\overline{K}_2^{nc} > \overline{K}_o^{nc} > 0$, the integral time must take a lower limit given by

$$\tau_I > \underline{I}_2^{nc} = \frac{\theta\tau_1\tau_2}{\theta\tau_D + \tau_1\tau_2} \tag{4.39}$$

Furthermore, if the derivative time takes a lower limit as follows

$$\tau_D > \underline{D}_1^{nc} = \frac{\theta\tau_1\tau_2}{\tau_1\tau_2 - \theta(\tau_1 + \tau_2)}$$

then, the loop gain must be bounded within a range of

$$\frac{\tau_1 + \tau_2}{\tau_D - \theta} < K < \frac{\tau_1 \tau_2}{\theta \tau_D}$$

Remark 11. *Notice that in both cases 1 and 2, similar ranges for τ_D and K are applied, but for the case 2 there exists a lower limit on the integral time* (4.39) *based on the necessary condition of Routh stability. It should be noted that, another lower limit on the integral time which is applied to both cases can also be established based on the sufficient condition of Routh stability as will be shown in the next section. Hence, cases 1 and 2 can be merged together in the sense that the integral time can be greater or less than the deadtime, so long its maximum lower limit is not violated.*

4.4.2 Sufficient Stability Conditions for SODTUP

In view of remark 7, the sufficient criterion of Routh stability stipulates that $b > 0$ in the Routh matrix, which leads to the minimum limit on integral time

$$\tau_I > \underline{I}^{sc} = \left(\frac{K}{1+K}\right)\left(\theta + \frac{\tau_1\tau_2 - K\theta\tau_D}{K(\tau_D - \theta) - (\tau_1 + \tau_2)}\right) \tag{4.40}$$

From (4.40), we can deduce two lower limits on the loop gain: $\underline{K}_1^{sc} = -1$ and $\underline{K}_2^{sc} = (\tau_1 + \tau_2)/(\tau_D - \theta)$ and obviously the second one is similar to the maximum lower limit on the loop gain based on the necessary criterion of Routh stability. Thus, for $\tau_I > \theta$ (i.e., case 1), it is sufficient for closed-loop stability to occur, we require that the minimum limit on the integral time (4.40) must not be violated in addition to fulfilling the limits on the derivative time and loop gain obtained based on necessary criterion of stability. However, when $\tau_I < \theta$ (i.e., case 2) there are two lower limits on the integral time, one imposed by the necessary criterion of stability (4.39) and the one imposed by the sufficient condition (4.40). Sufficient conditions for closed-loop stability are attained if the maximum lower limit of the integral time is not violated in addition to fulfilling the limits on the derivative time and loop gain imposed by the necessary criterion of Routh stability. Table 4.2 shows the ranges of K, τ_I and τ_D within which one can find the values of PID parameters leading to closed-loop stability of a given SODTUP process.

Table 4.2: Summary of the PID parameter regions for SODTUP processes

Case	θ	K	τ_I	τ_D
1 $\tau_D > \theta$ $\tau_I > \theta$	$0 < \theta < \frac{\tau_1\tau_2}{\tau_1+\tau_2}$	$\frac{\tau_1+\tau_2}{\tau_D-\theta} < K < \frac{\tau_1\tau_2}{\theta\tau_D}$	$\tau_I >$ $\left(\frac{K}{1+K}\right)\left(\theta + \frac{\tau_1\tau_2 - K\theta\tau_D}{K(\tau_D-\theta)-(\tau_1+\tau_2)}\right)$	$\tau_D > \frac{\theta\tau_1\tau_2}{\tau_1\tau_2-\theta(\tau_1+\tau_2)}$
2 $\tau_D > \theta$ $\tau_I < \theta$	$0 < \theta < \frac{\tau_1\tau_2}{\tau_1+\tau_2}$	$\frac{\tau_1+\tau_2}{\tau_D-\theta} < K < \frac{\tau_1\tau_2}{\theta\tau_D}$	$\tau_I > max(\underline{I}_2^{nc}, \underline{I}^{sc})$ $\underline{I}_2^{nc} = \frac{\theta\tau_1\tau_2}{\theta\tau_D+\tau_1\tau_2}$ $\underline{I}^{sc} >$ $\left(\frac{K}{1+K}\right)\left(\theta + \frac{\tau_1\tau_2 - K\theta\tau_D}{K(\tau_D-\theta)-(\tau_1+\tau_2)}\right)$	$\tau_D > \frac{\theta\tau_1\tau_2}{\tau_1\tau_2-\theta(\tau_1+\tau_2)}$

4.5 PID Tuning Algorithms

As a prerequisite for the proposed tuning algorithms, we introduce 3 new tuning or scaling parameters, namely r_c, r_d and r_i which are used to calculate for the values of conventional PID parameters, K_c, τ_D and τ_I respectively. The manners of using these new tuning parameters will be described alongside the proposed tuning rules in the following sections.

4.5.1 SODUP: PID Tuning Algorithm 1

This tuning rule is proposed in order to obtain tuning values within the stable regions (see Table 4.1) corresponding to the cases 1.1 and 1.2.
Step 1: Initialization of tuning values; set $r_c = 0.7$, $r_d = 0.5$ and $r_i = 3$.
Step 2: Calculate the following:

i Minimum of the derivative time $\tau_{D,min}$

$$\tau_{D,min} = \begin{cases} \theta & \text{for } 0 < \theta < \sqrt{\tau_u \tau_a} \\ \dfrac{\theta \tau_u \tau_a}{\tau_u \tau_a + \theta(\tau_u - \tau_a)} & \text{for } \sqrt{\tau_u \tau_a} < \theta < \tau_u \end{cases}$$

ii Maximum of the derivative time $\tau_{D,max}$

$$\tau_{D,max} = \frac{\tau_u \tau_a}{\theta}$$

iii Actual value of the derivative time τ_D

$$\tau_D = r_d(\tau_{D,max} - \tau_{D,min}) + \tau_{D,min}, \quad 0 < r_d < 1$$

iv Minimum of the integral time $\tau_{I,min}$ based on the necessary condition

$$\tau_{I,min} = \frac{\theta \tau_u \tau_a}{\tau_u \tau_a - \theta \tau_D}$$

v Actual value of the integral time τ_I

$$\tau_I = r_i(\tau_{I,min}), \quad r_i > 1$$

vi Minimum of the loop gain K_{min}

$$K_{min} = \frac{\tau_I}{\tau_I - \theta}$$

vii Maximum of the loop gain K_{max}

$$K_{max} = \frac{\tau_u \tau_a}{\theta \tau_D}$$

viii Actual value of the controller gain K_c

$$K_c = \frac{r_c(K_{max} - K_{min}) + K_{min}}{K_p}, \quad 0 < r_c < 1$$

ix Calculate the minimum of integral time based on the sufficient condition, i.e., $\underline{I}^{sc}$; if $\tau_I > \underline{I}^{sc}$, then go to next Step 3, otherwise $\tau_I < \underline{I}^{sc}$, go back to Step 2(v) and increase the value of r_i such that the integral time is larger than its lower limit based on the sufficient condition. Repeat Step 2(vi)-(ix).

Step 3: Evaluate the closed-loop robustness via gain margin (GM) and phase margin (PM) analysis using Nyquist diagram. Evaluate the responses to step changes in setpoint and disturbance. If the robustness and performance meet desired specifications, then the tuning task is completed, otherwise, repeat Step 2(iii)-(ix) by adjusting the values of r_c, r_d and r_i until acceptable or desired robustness-performance is obtained. Moreover, a set point pre-filter (F_r) is suggested in order to reduce the overshoot response in setpoint tracking. The setpoint pre-filter is expressed by

$$F_r = \frac{\frac{\tau_I}{\epsilon}s + 1}{\tau_I s + 1}, \quad 1.5 < \epsilon < 5 \tag{4.41}$$

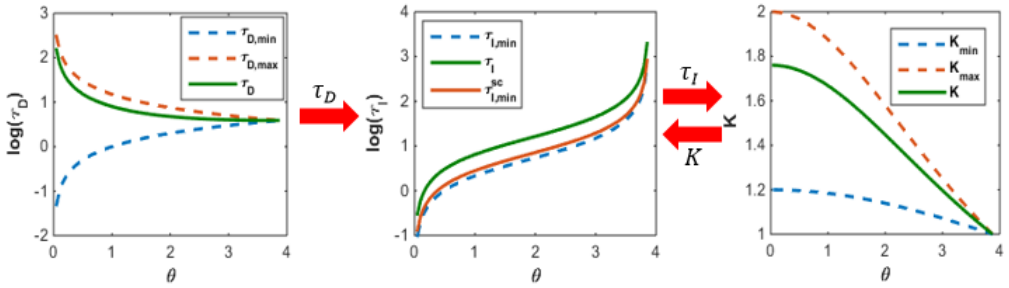

Figure 4.2: Closed-loop stability regions of PID parameters when $\tau_u = 5$ and $\tau_a = 3$ by setting $r_c = 0.7$, $r_d = 0.5$ and $r_i = 3$

In Figure 4.2, the closed-loop stability regions of PID parameters are shown when $\tau_u = 5$ and $\tau_a = 3$. The $\tau_{D,min}$ and $\tau_{D,max}$ are determined based on the necessary criterion, where any value $\tau_D \in (\tau_{D,min}, \tau_{D,max})$ is considered as stabilizing τ_D boundary. By setting $r_d = 0.5$, the actual value of τ_D is obtained

which lead to the given range of the integral time $\tau_{I,min}$ based on the necessary criterion. Notice that, any value above the $\tau_{I,min}$ is considered as stabilizing τ_I boundary. The actual value of τ_I is determined by setting $r_i = 3$, which can be used to determine the stabilizing K boundary based on the necessary condition, i.e. K_{min} and K_{max}. The actual value of K is obtained by setting $r_c = 0.7$ and calculate the minimum of integral time $\tau^{sc}_{I,min}$ based on the sufficient condition. From Figure 4.2, $\tau_I > \tau^{sc}_{I,min}$, thus the closed-loop stability is satisfied.

4.5.2 SODUP: PID Tuning Algorithm 2

This tuning rule is developed based on the case 2 (Table 4.1) for a SODUP process in which $\tau_u < \tau_a$.

Step 1: Initialization of tuning values; set $r_c = 0.7$, $r_d = 0.9$ and $r_i = 3$.

Step 2: Calculate the following:

i Minimum of the derivative time $\tau_{D,min}$

$$\tau_{D,min} = \begin{cases} \dfrac{\theta\tau_u\tau_a}{\tau_u\tau_a - \theta(\tau_a - \tau_u)} & \text{for } \underline{K}^{nc}_{2a} > \underline{K}^{nc}_{2b} \\ \tau_a - \tau_u + \theta & \text{for } \underline{K}^{nc}_{2a} < \underline{K}^{nc}_{2b} \end{cases}$$

ii Maximum of the derivative time $\tau_{D,max}$

$$\tau_{D,max} = \begin{cases} \tau_a - \tau_u + \theta & \text{for } \underline{K}^{nc}_{2a} > \underline{K}^{nc}_{2b} \\ \dfrac{\tau_u\tau_a}{\theta} & \text{for } \underline{K}^{nc}_{2a} < \underline{K}^{nc}_{2b} \end{cases}$$

iii Actual value of the derivative time τ_D

$$\tau_D = r_d(\tau_{D,max} - \tau_{D,min}) + \tau_{D,min}, \quad 0 < r_d < 1$$

iv Minimum of the loop gain K_{min}

$$K_{min} = \begin{cases} \dfrac{\tau_a - \tau_u}{\tau_D - \theta} & \text{for } \underline{K}^{nc}_{2a} > \underline{K}^{nc}_{2b} \\ \dfrac{\tau_I}{\tau_I - \theta} & \text{for } \underline{K}^{nc}_{2a} < \underline{K}^{nc}_{2b} \end{cases}$$

v Maximum of the loop gain K_{max}

$$K_{max} = \frac{\tau_u\tau_a}{\theta\tau_D}$$

vi Actual value of the controller gain K_c

$$K_c = \frac{r_c(K_{max} - K_{min}) + K_{min}}{K_p}, \quad 0 < r_c < 1$$

vii Minimum of the integral time $\tau_{I,min}$

$$\tau_{I,min} = \begin{cases} max(\underline{I}^{nc}_{2.1}, \underline{I}^{sc}) & \text{for } \underline{K}^{nc}_{2a} > \underline{K}^{nc}_{2b} \\ max(\underline{I}^{nc}_{2.2b}, \underline{I}^{sc}) & \text{for } \underline{K}^{nc}_{2a} < \underline{K}^{nc}_{2b} \end{cases}$$

viii Actual value of the integral time τ_I

$$\tau_I = r_i(\tau_{I,min}), \quad r_i > 1$$

Step 3: Evaluate the closed-loop robustness via gain margin (GM) and phase margin (PM) analysis using Nyquist diagram. Evaluate the responses to step changes in setpoint and disturbance. If the robustness and performance meet desired specifications, then the tuning task is completed, otherwise, repeat Step 2(iii)-(viii) by adjusting the values of r_c, r_d and r_i until acceptable or desired robustness-performance is obtained. The augmented lag filter as (4.42) is suggested to reduce the impulsive spikes on the manipulated variable with setpoint tracking and output disturbance rejection. The setpoint pre-filter as (4.41) can be used to reduce the overshoot.

4.5.3 SODTUP: PID Tuning Algorithm 3

This tuning rule is developed based on the stabilizing region shown in Table 4.2.
Step 1: Initialization of tuning values; set $r_c = 0.8$, $r_d = 10$ and $r_i = 10$.
Step 2: Calculate the following:

i Minimum of the derivative time $\tau_{D,min}$

$$\tau_{D,min} = \frac{\theta\tau_1\tau_2}{\tau_1\tau_2 - \theta(\tau_1 + \tau_2)}$$

ii Actual value of the derivative time τ_D

$$\tau_D = r_d(\tau_{D,min}), \quad r_d > 1$$

iii Minimum of the loop gain K_{min}

$$K_{min} = \frac{\tau_1 + \tau_2}{\tau_D - \theta}$$

iv Maximum of the loop gain K_{max}

$$K_{max} = \frac{\tau_1 \tau_2}{\theta \tau_D}$$

v Actual value of the controller gain K_c

$$K_c = \frac{r_c(K_{max} - K_{min}) + K_{min}}{K_p}, \quad 0 < r_c < 1$$

vi Minimum of the integral time $\tau_{I,min}$

$$\tau_{I,min} = \left(\frac{K}{1+K}\right)\left(\theta + \frac{\tau_1\tau_2 - K\theta\tau_D}{K(\tau_D - \theta) - (\tau_1 + \tau_2)}\right)$$

vii Actual value of the integral time τ_I

$$\tau_I = r_i(\tau_{I,min}), \quad r_i > 1$$

Step 3: Evaluate the closed-loop robustness via gain margin (GM) and phase margin (PM) analysis using Nyquist diagram. Evaluate the responses to step changes in setpoint and disturbance. If the robustness and performance meet desired or acceptable specifications, then the tuning task is completed, otherwise, repeat Step 2(ii)-(vii) by adjusting the values of r_c, r_d and r_i until acceptable or desired robustness-performance is obtained. Note that, a set point pre-filter (F_r) is suggested in order to reduce the overshoot response in setpoint tracking. The augmented lag filter as (4.42) is suggested to reduce the impulsive spikes on the manipulated variable with setpoint tracking and output disturbance rejection. The setpoint pre-filter is given by (4.41).

Remark 12. *If there are impulsive spikes on the manipulated variable with set-point tracking and output disturbance rejection, a lag filter is suggested to augment with the proposed PID controller in order to reduce the impulsive spikes as follows:*

$$F_a = \frac{1}{\tau_f s + 1}, \quad 0.01 < \tau_f < 0.1 \tag{4.42}$$

4.6 Illustrative Examples

4.6.1 Example 1: SODUP ($\tau_u > \tau_a$)

Consider an example used in [175]:

$$P(s) = \frac{\exp(-0.5s)}{(5s-1)(2s+1)(0.5s+1)}$$

This example has been widely used by researchers to evaluate the performance of a PID controller based on several different tuning or design methods. In [175], the researchers compared their simple analytical method with two different methods proposed in [130] and [131] and it was shown that the simple analytical tuning rule led to improved performance of the PID controller. Researchers in [175] also proposed a method of designing the setpoint pre-filter. For this example, the PID controller and setpoint pre-filter based on Cho, Lee, and Edgar (2014) [175] are $G_c(s) = 4.7408(1 + 1/9.1627s + 1.6975s)$ and $F_r(s) = (4.6656s^2 + 4.32s + 1)(15.5539s^2 + 9.1627s + 1)$ respectively. This PID controller produces a maximum peak of sensitivity function equals to 4.3. We use the proposed PID controller tuning algorithm 1 in order to design a PID controller for the given process. Before we can applying the PID tuning algorithm 1, we need to reduce the third-order process to a SODUP form. We reduce the third-order process to a SODUP form by approximating the third (smallest) time constant in the denominator using the first-order Taylors series, which gives

$$P(s) = \frac{\exp(-s)}{(5s-1)(2s+1)}$$

By dint of trial-and-error, we find that by settings $r_c = 0.8$, $r_d = 0.11$ and $r_i = 7.7$, where the resulting PID controller stability margin and performance are quite satisfactory. Corresponding to these settings, the PID controller obtained is $G_c(s) = 4.2433(1 + 1/9.613s + 1.99s)$ augmented with a lag filter $F_a = (1/(0.05s + 1))$ to reduce the impulsive spikes on manipulated variable with setpoint tracking and output disturbance rejection. In order to reduce the setpoint tracking overshoot, we apply the simple rule presented in the Section 4.5.1 to design a lead-lag filter. By setting $\epsilon = 2.5$, we get $F_r(s) = (3.8452s+1)/(9.613s+1)$ which produces satisfactorily smooth setpoint tracking response. The proposed PID controller has a gain margin (GM), phase margin (PM) and maximum peak of sensitivity function (M_s) of 4.37 dB, 26.6° and 2.63 respectively. Based on the values of M_s, the proposed PID controller seems to be more robust than the PID controller designed in [175]. The performance robustness of the two different PID controllers are evaluated at a perturbed condition represented as

$$P_{\triangle}(s) = 1.1\left[\frac{(-0.05s+1)\exp(-0.6s)}{(3.5s-1)(3s+1)(0.4s+1)}\right]$$

The closed-loop performances of the PID controllers are evaluated based on a sequential 1 unit step changes in the setpoint at $t = 1$ unit, input disturbance at

$t = 50$ units and output disturbance at $t = 100$ units. Figure 4.3 shows the closed-loop responses at the nominal condition while Figure 4.4 shows the responses at the perturbed condition. Whilst at the nominal condition both PID controllers shows almost similar responses but at the perturbed condition, the proposed PID controller demonstrates improved performance robustness over that of PID designed via [175].

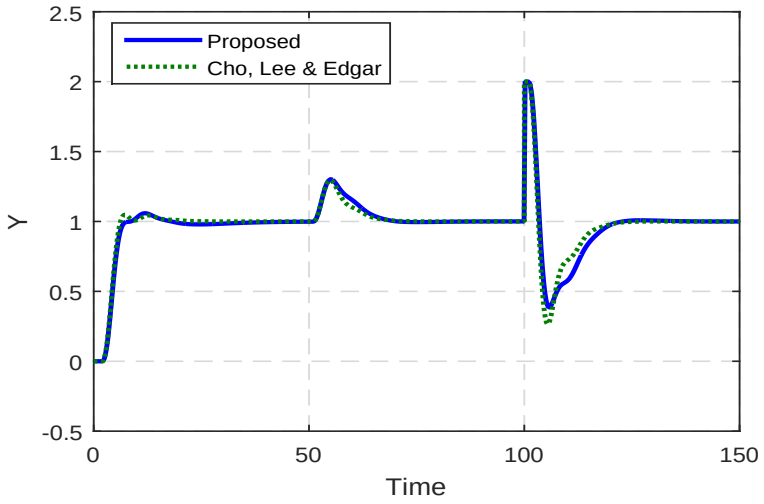

Figure 4.3: Closed-loop responses at the nominal condition for example 1

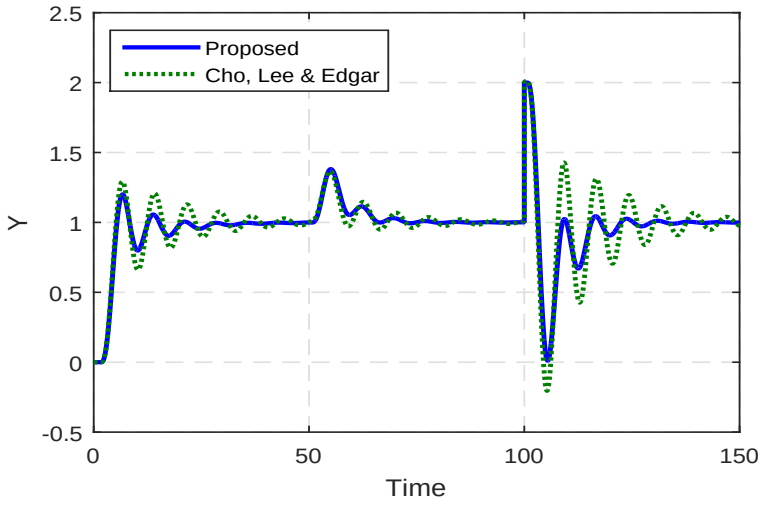

Figure 4.4: Closed-loop response at the perturbed condition for example 1

The responses of manipulated variable for setpoint tracking, input disturbance rejection and output disturbance rejection are shown in Figure 4.5, which

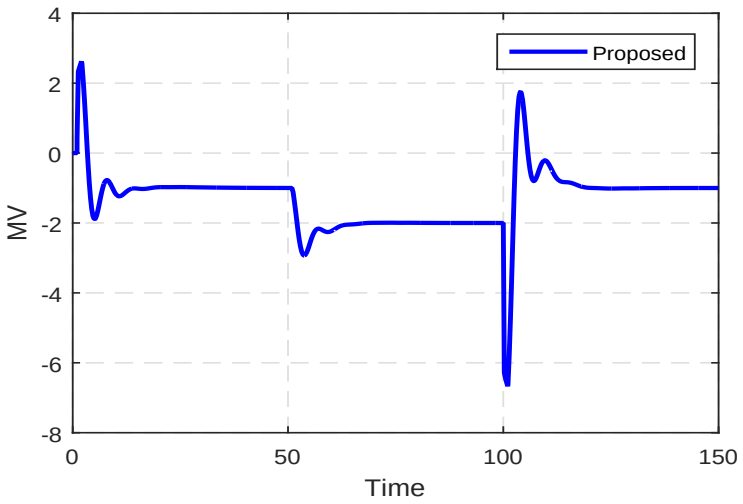

Figure 4.5: Response of manipulated variable

shows no obvious impulsive spikes occurred on the manipulated variable for the proposed PID controller. It is interesting to note that, the impulsive spikes on the manipulated variable for setpoint tracking and output disturbance rejection has been reduced significantly by augmenting the lag filter to the proposed PID controller. In contrast, the PID controller based on Cho, Lee, and Edgar (2014) [175] shows huge spikes on the manipulated variable for setpoint tracking, input disturbance rejection and output disturbance rejection.

4.6.2 Example 2: SODTUP

To demonstrate the effectiveness of the PID tuning rule 3 (refer to Section 4.5.3), we use an example (SODTUP process) cited in Panda (2009) [127] given as

$$P(s) = \frac{2\exp(-0.3s)}{(3s-1)(s-1)}$$

Based on the PID synthesis in [127], a PID controller obtained is $G_c(s) = 0.881(1 + 1/5.1103s + 3.42s)$. By using the PID tuning algorithm 3, we obtain $G_c(s) = 0.8277(1 + 1/4.0843s + 5s)$ after a trial-and-error tuning with $r_c = 0.7$, $r_d = 10$ and $r_i = 15$ augmented with a lag filter $F_a = (1/(0.02s + 1))$ to reduce the impulsive spikes on manipulated variable with setpoint tracking and output disturbance rejection. The proposed PID controller has a GM and PM of 3.48 dB and 12.9° respectively. For this example, the setpoint pre-filter is not needed as the setpoint tracking shows no severe overshoot. To evaluate the performance

robustness of the two PID controllers, we adopt a perturbed condition represented by

$$P_{\triangle}(s) = \frac{1.9(-0.1s+1)\exp(-0.2s)}{(2.8s-1)(1.3s-1)(0.1s+1)}$$

The closed-loop responses of the two PID controllers are compared on the basis of sequential step changes of magnitude 1 unit each in the setpoint, input disturbance and output disturbance. Figure 4.6 displays the responses at the nominal condition and Figure 4.7 shows the responses at the perturbed conditions. Moreover, the simulation of the responses of manipulated variable for setpoint tracking and disturbance rejection has been done but no impulsive spikes were observed. It is worth noting that the proposed PID controller outperforms that of [127] both in terms of nominal performance and performance robustness.

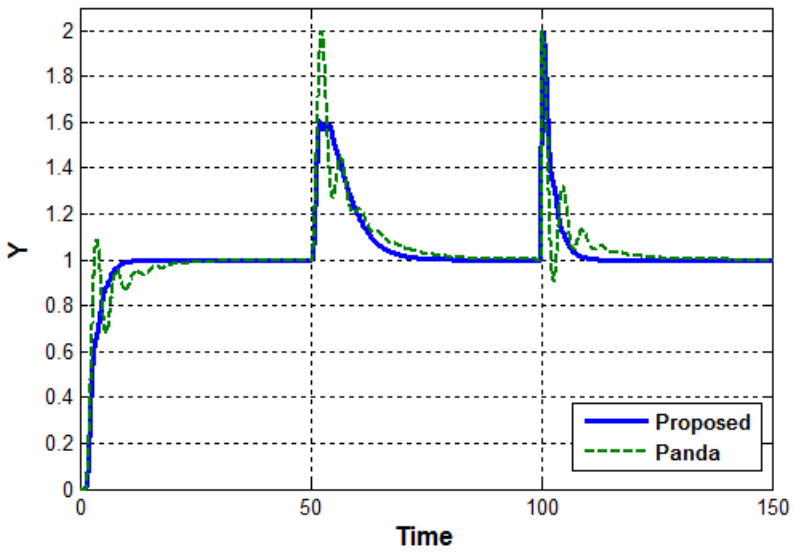

Figure 4.6: Closed-loop responses at the nominal condition for example 2

4.6.3 Example 3: SODUP ($\tau_u < \tau_a$)

In this example, we consider a SODUP process where $\tau_u < \tau_a$ as follows

$$P(s) = \frac{\exp(-s)}{(3s-1)(10s+1)}$$

Since PID controller tuning or synthesis for this type of SODUP has never been reported in the open literature, we use the LQG controller to compare the proposed PID controller designed using the tuning algorithm 2 in Section 4.5.2.

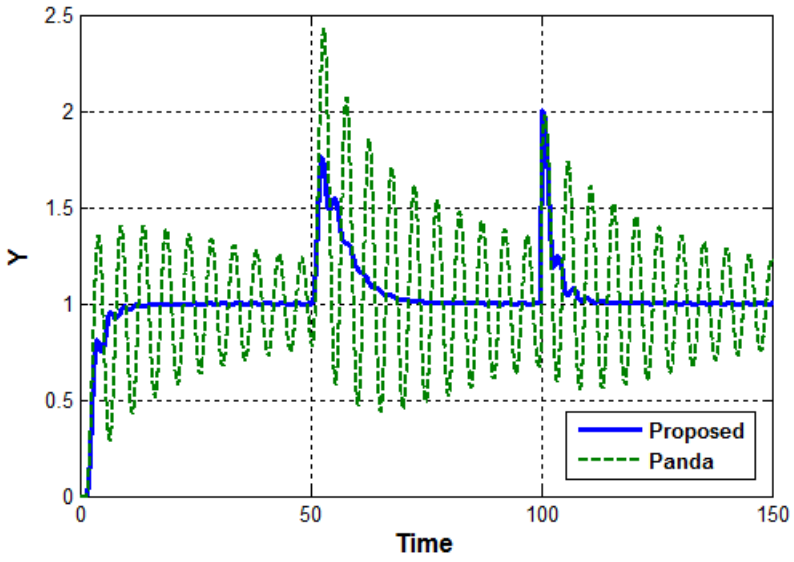

Figure 4.7: Closed-loop response at the perturbed condition for example 2

By settings (through a trial-and-error) $r_c = 0.7$, $r_d = 0.9$ and $r_i = 2$, we get a PID controller $G_c(s) = 3.1998(1 + 1/20.886s + 7.3294s)$ augmented with a lag filter $F_a = (1/(0.02s+1))$ to reduce the impulsive spikes on manipulated variable with setpoint tracking and output disturbance rejection. Since the setpoint tracking response shows severe overshoot, we propose to use a lead-lag filter given as $F_r(s) = (6.962s+1)/(20.886s+1)$ by setting $\epsilon = 3$. This proposed PID controller has a GM and PM of 4.65 dB and 21.4° respectively. For the LQG controller synthesis, we use the Matlab Controller System Design tool which produces a stabilizing 5^{th} order controller given as follows

$$G_c(s) = 0.03849\left[\frac{(0.0841s^2 + 0.5s + 1)(31s + 1)(11s + 1)}{s(0.5476s^2 + 0.62s + 1)(0.0729s^2 + 0.46s + 1)}\right]$$

To evaluate the performance robustness, we consider a perturbed condition given by

$$P_{\triangle}(s) = \frac{1.1(-0.1s + 1)\exp(-1.1s)}{(4.5s - 1)(7s + 1)(0.1s + 1)}$$

Again the closed-loop responses of the two different controllers are compared on the basis of 1 unit sequential step changes in the setpoint, input disturbance and output disturbance. Figure 4.8 displays the closed-loop responses at the nominal condition while Figure 4.9 demonstrates the responses at the perturbed condition. The simulation of the responses of manipulated variable for setpoint tracking and disturbance rejection has been done but no impulsive spikes were

observed. It is worth mentioning that, the proposed PID controller outperforms the high-order LQG controller both in terms of nominal performance and performance robustness.

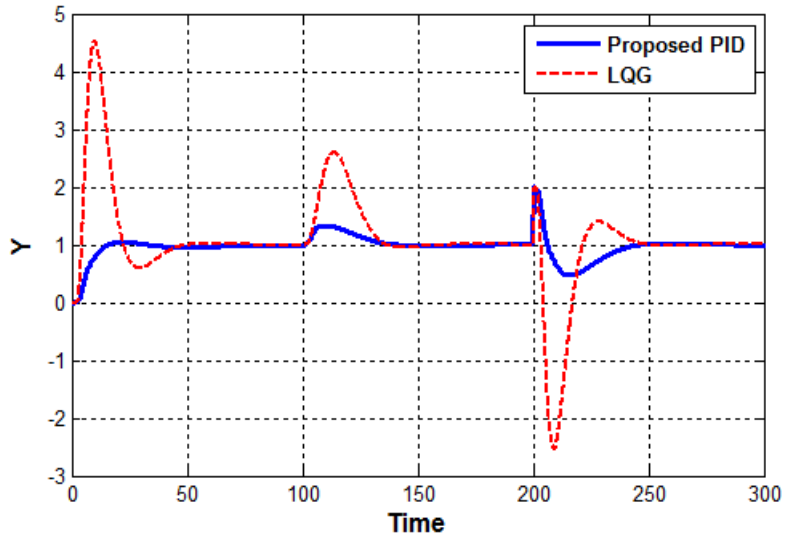

Figure 4.8: Closed-loop responses at the nominal condition for example 3

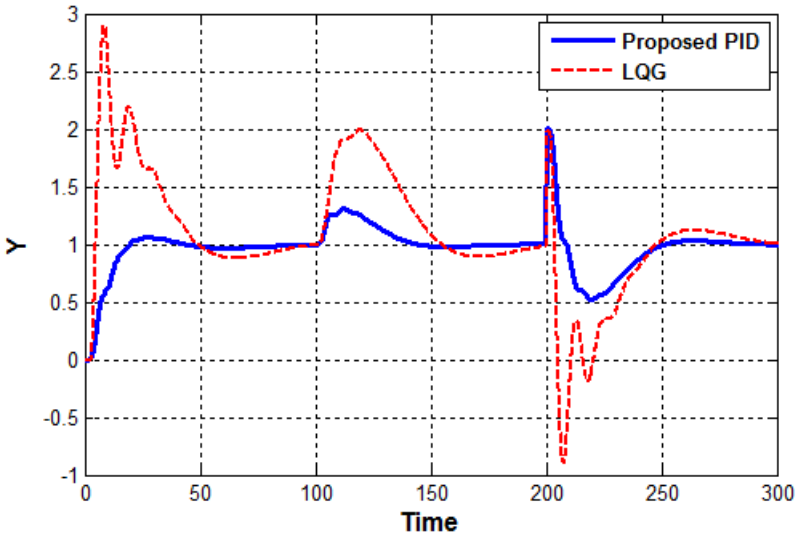

Figure 4.9: Closed-loop response at the perturbed condition for example 3

4.6.4 Example 4: Simulation Example

The simulation example is taken from [176] based on a nonlinear bioreactor. The models equation are obtained from [177], which are given as

$$\frac{dX_v}{dt} = (\mu - D)X_v$$

$$\frac{dS}{dt} = (S_f - S)D - \frac{\mu X_v}{\gamma}$$

$$\mu = \frac{\mu_m S}{K_m + S + K_I S^2}$$

where the model parameters are given as: $\gamma = 0.4g/g$, $S_f = 4g/L$, $\mu_m = 0.53h^{-1}$, $D = 0.3h^{-1}$, $K_m = 0.12g/L$ and $K_I = 0.4545L/g$. The bioreactor operated at an unstable operating condition: biomass concentration $X_v = 0.9951g/L$ and substrate concentration $S = 1.5122g/L$. For controller design, a linearized model is obtained at the operating condition:

$$P(s) = \frac{X_v(s)}{D(s)} = \frac{-5.89\exp(-2.4s)}{5.86s - 1}$$

In order to use the proposed PID tuning algorithm which is developed for the second-order unstable model, the process model above is approximated as follows

$$P(s) = \frac{-5.89\exp(-2.4s)}{5.86s - 1} \cong \frac{-5.89\exp[-2.4(1-\beta)s]}{(5.86s - 1)(2.4\beta s + 1)}$$

Here, we take β value to be a fraction of the dead-time value, i.e., 1/6 to 1/2 of the dead-time. In this case, let us take $\beta = 1/2$, so that $\tau_u = 5.86$, $\tau_a = 1.2$ and the modified delay $\theta_m = 1.2$. By using the PID tuning algorithm 1, and by setting $r_p = 0.4$, $r_i = 12$ and $r_d = 0.1$, we get a PID controller tuning values: $K_c = -0.3472$, $\tau_I = 20.1202$ and $\tau_D = 1.666$ augmented with a lag filter $F_a = (1/(0.05s+1))$ to reduce the impulsive spikes on manipulated variable with setpoint tracking and output disturbance rejection. For the setpoint pre-filter, we set $\epsilon = 4.5$ which gives $F_r = (4.47s + 1)/(20.12s + 1)$. Meanwhile, based on Jhunjhunwala and Chidambaram (2001) [176], the PID tuning values: $K_c = -0.4787$, $\tau_I = 11.4932$ and $\tau_D = 1.3671$. Additionally, for further comparison purpose we also use the PID tuning formula based on the multi-scale control (MSC-PID) scheme proposed in [178]. The resulting ideal PID augmented with a filter is obtained as follows

$$G_c(s) = 0.4018\left(1 + \frac{1}{17.4185s} + 1.1008s\right)\left(\frac{1}{0.0195s + 1}\right)$$

Additionally, a setpoint pre-filter is also obtained: $F_r = (3.1395s + 1)/(16.3434s + 1)$. The performances of the 3 different PID controllers are evaluated for setpoint tracking and disturbance rejection under a step change in biomass concentration setpoint by 0.3 g/L and step change in feed substrate concentration by -1.4 g/L. Figures 4.10 and 4.11 demonstrate the closed-loop responses of the 3 different controllers. Figure 4.12 shows the responses of manipulated variable for proposed PID and MSC-PID controllers with setpoint tracking. There are no obvious impulsive spikes occurred on the manipulated variable for both control schemes. However, the PID controller based on Jhunjhunwala and Chidambaram (2001) [176] shows impulsive spikes on the manipulated variable with setpoint tracking. Meanwhile, the simulation of the responses of manipulated variable with disturbance rejection for both control schemes has been done but no impulsive spikes were observed instead. It is worth noting that, the proposed PID controller gives a better response than that of the [176] both in terms of setpoint tracking and disturbance rejection. Also, the response of the proposed PID controller is as good as the advanced decomposition method - MSC-PID scheme designed by [178].

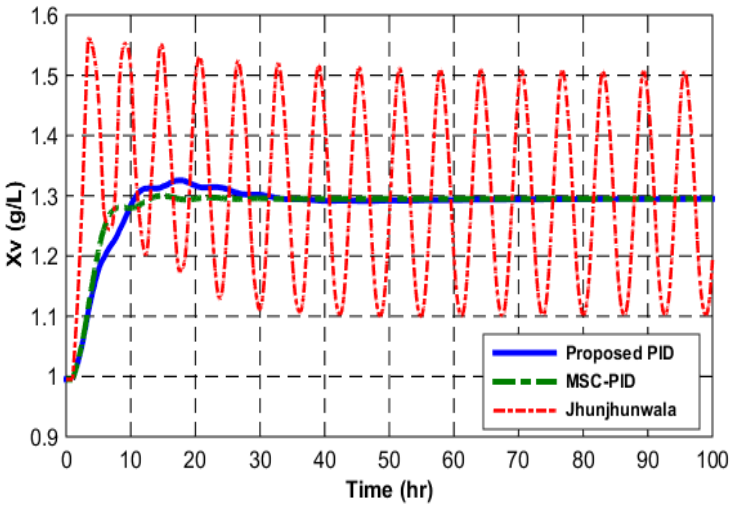

Figure 4.10: Setpoint tracking responses (step change in biomass setpoint = 0.3 g/L)

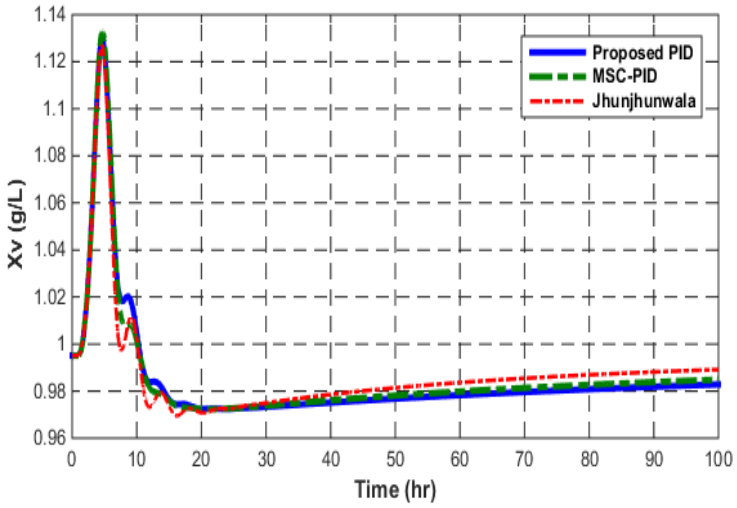

Figure 4.11: Disturbance rejection responses (step change in feed concentration = -1.4 g/L)

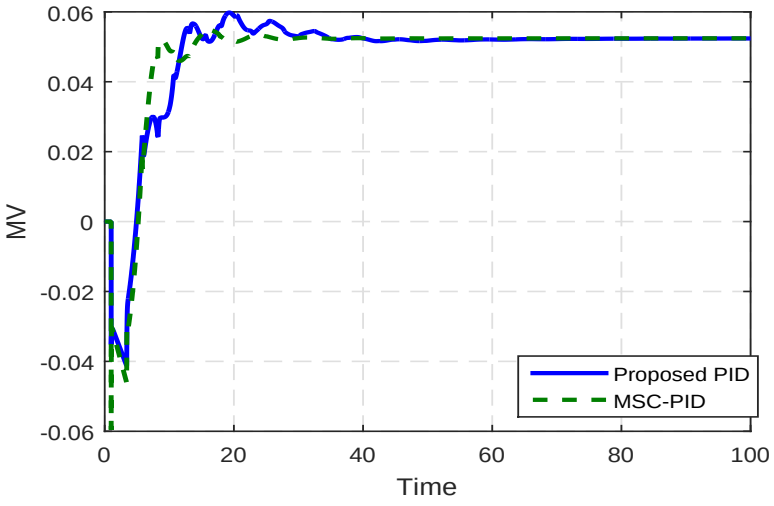

Figure 4.12: Responses of manipulated variable for setpoint tracking

4.7 Summary

In this chapter, the characterization of the boundaries of stabilizing PID parameter regions was evaluated based on the necessary criterion and sufficient criterion of Routh stability. Three simple controller tuning algorithms for two types of common second-order unstable processes, i.e., SODUP and SODTUP, have been proposed. All of the algorithms have been constructed based on the obtained boundaries of stabilizing PID controller parameter regions. Thus, the resulting

PID controller is guaranteed to deliver stable closed-loop response. Moreover, PID tuning algorithms are implemented to obtain tuning values within the stable regions to achieve optimum closed-loop performance-robustness. It is worth mentioning that, the performances of proposed PID controllers are relatively enhanced compared to some established controller design methods. The Theorems 4.2.1 and 4.2.2 will be applied to the higher-order system in Chapter 5. The work described in this chapter has been published in ISA Transactions[1].

[1]Qiu Han Seer and Jobrun Nandong. Stabilization and PID tuning algorithms for second-order unstable processes with time-delays. *ISA transactions*, 67: 233-245, 2017.

Chapter 5

Fed-Batch Fermentation Dynamics, Modeling and Control

Fed-batch dynamics are known to be of high-order and often vary nonlinearly with the operating conditions. Several different forms of complex dynamics can arise from a typical fed-batch fermentation process. At some points the process can exhibit relatively simple dynamics, which can be simplified to a second- or first-order system with delay (the PID stabilization of the second-order unstable processes has been reported in Chapter 4). It should be pointed out that at some points during the fed-batch fermentation, the process can simultaneously exhibit complex inverse-responses and integrating plus unstable underdamped dynamics, which could not be easily stabilized using the single-loop feedback control structure. In this chapter, a class of fourth-order integrating model can be used to adequately represent such a complex dynamics of the fed-batch fermentation process. The rigorous stability analysis of PID controller based on the Routh-Hurwitz criteria for the fourth-order integrating system is presented.

5.1 Ethanolic Fed-batch Fermentation

A fed-batch fermentation process is commonly used in biotechnological industries where it is desired to overcome substrate inhibition, which is responsible for low productivity in a batch fermentation [97, 98]. Like most modeling of common chemical reactors, the fed-batch bioreactor can be represented by using a set of mass balance equations or sometimes coupled with energy balances when the thermal generation of microrganisms involved is significant. In a simplest case under isothermal conditions, the application of mass balance often leads to a

system of differential-algebraic equation (DAE) as follows

$$\frac{dZ}{dt} = f(Z, U, R_r, T) \tag{5.1}$$

$$R_r = g(Z) \tag{5.2}$$

where $Z \in \Re^n$, $U \in \Re^m$ and $R_r \in \Re^q$ are vectors of state variables, input variables and reaction rates respectively; meanwhile f and g are nonlinear functions of their arguments. For a realistic modeling of the fed-batch bioreactor, a minimum of four state variables is often required together with at least three kinetics or rate equations. In many cases, only one input variable is available for manipulation, i.e., the fresh feed flow rate.

5.1.1 System Model

A typical mechanistic model of fed-batch fermentation comprises of mass balance differential equations, couple with constitutive rate equations on microorganism growth and death, substrate consumption and product formation. According to the mass balances for bioreactor volume, active biomass, substrate and product, the dynamic model of a typical fed-batch bioreactor system of ethanol fermentation are shown as follows [172]:

$$\frac{dV}{dt} = F \tag{5.3a}$$

$$\frac{dX_v}{dt} = r_x - r_d - \frac{FX_v}{V} \tag{5.3b}$$

$$\frac{dGl}{dt} = -r_s + \frac{F(Gl_{in} - Gl)}{V} \tag{5.3c}$$

$$\frac{dEt}{dt} = r_p - \frac{FEt}{V} \tag{5.3d}$$

where the variables F, X_v, Gl, Et, and V denote the feed flow rate (m^3/h), the biomass concentration (kg/m^3), the substrate (glucose) concentration (kg/m^3), the product (ethanol) concentration (kg/m^3) and the fermentation medium volume (m^3), respectively.

Most of the biotechnological processes are assumed to consist of pure culture with a single growth limiting substrate. In this work, an unstructured model is adopted for its simplicity and practicality in describing the modeling of microbial kinetics in most fermentation processes. The growth rate of microorganism r_x is described using a modified Haldane kinetics in (5.4), which includes the effects of the inhibition imposed by high substrate and product concentration whilst

the death rate of microorganism via catabolism, which represents the rate of endogenous metabolism r_d is expressed in (5.5).

$$r_x = \frac{\mu_0 Gl X_v}{K_{s0} + Gl + K_{s1} Gl^2} exp\left(- \frac{Et}{Et_{max}} \right) \tag{5.4}$$

$$r_d = K_d X_v \tag{5.5}$$

The rate of substrate consumption r_s based on *Pirt* equation and the rate of product formation r_p based on *Luedeking-Piret* equation [96] are

$$r_s = Y_s r_x + m_s X_v \tag{5.6}$$

$$r_p = Y_p r_x + m_p X_v \tag{5.7}$$

The notations: Y_s (kg/kg), Y_p (kg/kg), m_s (kg/kg h) and m_p (kg/kg h) represent the coefficients for substrate yield over biomass, product yield over biomass, substrate maintenance and product maintenance, respectively.

5.1.2 Linearization

It is interesting to note that, a linearization at any given operating point of the simplest DAE system with only four state variables and one input variable can lead to a fourth-order integrating system. Depending on the point at which the system is linearized, the fourth-order integrating system can take several different forms of complex dynamic behaviors. One of the particular forms which can be very difficult to stabilized is given by

$$P(s) = \frac{z_i}{u} = \frac{K_p \prod_{j=1}^{3} (\tau_{zj} s + 1)}{s(\tau_p s + 1)(\tau_u^2 s^2 + 2\zeta \tau_u s + 1)} \tag{5.8}$$

with the following parameter assumptions

- A.1: two RHP zeros, $\tau_{z1} < 0$, $\tau_{z2} < 0$ and $\tau_{z3} > 0$.
- A.2: unstable-oscillatory, $\tau_p > 0$, $\tau_u > 0$ and $-1 < \zeta < 0$.

Here, z_i and u denote one of the state variables (e.g., substrate concentration) and input variable (e.g., fresh feed flow rate), respectively. It should be emphasized that not all fed-batch processes will demonstrate such a complex dynamic behavior. In some common cases of fermentation, the process involved can even be simplified to a second- or even first-order system with delay. The nature of fermentation dynamics depends on the types of applications and microrganisms involved.

5.1.3 Problem Statement

It can be readily shown that a linearization of the model (5.3) with respect to the input variable F and the state variables X_v, Gl, Et, and V at any initial set of values $\overline{F}$, $\overline{X_v}$, $\overline{Gl}$, $\overline{Et}$ and $\overline{V}$ followed by Laplace Transform can take a number of different transfer function forms. One of the forms of a transfer function from F to Gl is

$$P(s) = \frac{K_p \prod_{i=1}^{3}(\tau_{zi}s + 1)}{s(\tau_p s + 1)(\alpha_2 s^2 + \alpha_1 s + 1)} \tag{5.9}$$

Another form is given by

$$P(s) = \frac{K_p \prod_{i=1}^{3}(\tau_{zi}s + 1)}{s \prod_{i=1}^{3}(\tau_{pi}s + 1)} \tag{5.10}$$

Note that, the model parameters and detailed procedures for obtaining such a linearized model in (5.9) or (5.10) are presented in Appendix D.1 and D.2.

Table 5.1: Model parameter values

Model parameters	Values	Units
μ_0	0.4	h^{-1}
K_{s0}	0.5	kg/m^3
K_{s1}	0.05	kg/m^3
Et_{max}	40	kg/m^3
K_d	0.01	kg/kg h
Y_s	1.5	kg/kg
m_s	0.1	kg/kg h
Y_p	1.2	kg/kg
m_p	0.05	kg/kg h

Table 5.1 shows the values of model parameters used in this work to simulate the fed-batch process (5.3). For the fed-batch process (5.3), five different forms of possible transfer functions with respect to state variables $\boldsymbol{\chi_s} = [Gl, X_v, Et, V]^\intercal$ and inputs $\boldsymbol{U} = [F, Gl_{in}]^\intercal$ are as follows:

$$P_1(s) = \frac{Gl(s)}{F(s)} = \frac{298.7(-7.73s + 1)(-10s + 1)(10.2s + 1)}{s(10s + 1)(157.7s^2 + 11.9s + 1)}, \boldsymbol{U} = [0.1, 150]^\intercal, \boldsymbol{\chi_s} = [1, 1, 1, 1]^\intercal$$

$$P_2(s) = \frac{Gl(s)}{F(s)} = \frac{11.3(-4.7s + 1)(-60s + 1)(66.8s + 1)}{s(60s + 1)(142.9s^2 - 13s + 1)}, \boldsymbol{U} = [0.1, 150]^\intercal, \boldsymbol{\chi_s} = [1, 1, 1, 6]^\intercal$$

$$P_3(s) = \frac{Gl(s)}{F(s)} = \frac{0.73(-66.7s+1)(5000s^2 - 36.2s + 1)}{s(-13.5s+1)(33.5s+1)(66.7s+1)}, \boldsymbol{U} = [0.3, 170]^\intercal, \boldsymbol{\chi_s} = [10, 10, 50, 20]^\intercal$$

$$P_4(s) = \frac{Gl(s)}{F(s)} = \frac{1.22(-100s+1)(120s+1)(573.4s+1)}{s(93.7s+1)(100s+1)(-229.3s+1)}, \boldsymbol{U} = [0.5, 200]^\intercal, \boldsymbol{\chi_s} = [4, 5, 100, 50]^\intercal$$

$$P_5(s) = \frac{Gl(s)}{F(s)} = \frac{-0.04(-100s+1)(9390s^2 + 62.5s + 1)}{s(100s+1)(81.3s^2 + 11.5s + 1)}, \boldsymbol{U} = [0.4, 200]^\intercal, \boldsymbol{\chi_s} = [1, 9, 80, 40]^\intercal$$

From the aforementioned examples, the transfer function given by P_2 is the most difficult to stabilize and control as it simultaneously possesses multiple right-hand side (RHP) or unstable zeros (i.e., that cause complex inverse-responses and impose serious limitation on control performance) and integrating plus unstable second-order underdamped dynamics. The next difficult to control transfer functions are of the forms given by P_3 and P_4 but as they do not possess underdamped dynamics and have only one unstable zero, these transfer functions are relatively easy to stabilize compared with P_2. Meanwhile, the transfer functions represented by P_1 and P_5 are the easiest to stabilize because both do not have unstable dynamics, i.e., only an integrating mode.

In short, we can draw a general conclusion about the typical fed-batch process (5.3), that is, the process dynamics often vary nonlinearly with the operating conditions, where at some points the process can simultaneously exhibit complex inverse-responses and integrating plus unstable underdamped dynamics while at others, its behaviors can be much less complex. Understanding of the detailed fed-batch transient behaviors and rigorous methods to deal with them are vital in the adaptive and self-tuning PID controller designs, which are common strategies proposed by several researchers to control fed-batch processes. Most of the existing adaptive or self-tuning PID strategies are based on single-loop feedback structure. However, in view of some of the complex dynamics at certain operating points (e.g., P_2) which could not be easily stabilized using the single-loop feedback structure, those control strategies might not be able to deliver satisfactory performance overall.

In a case where the transfer function obtained is of the form given in (5.9), the system can exhibit simultaneous integrating, unstable and underdamped dynamic behaviors (e.g., P_2), which can pose a daunting challenge to designing a stabilizing control system based on the single-loop structure.

5.2 Fourth-order Integrating Process

In the present work, we consider a fourth-order integrating process as

$$P(s) = \frac{K_p \prod_{i=1}^{3}(\tau_{zi}s + 1)}{s(\tau_p s + 1)(\alpha_2 s^2 + \alpha_1 s + 1)} \tag{5.11}$$

It can also be presented in another form given by

$$P(s) = \frac{K_p \prod_{i=1}^{3}(\tau_{zi}s + 1)}{s \prod_{i=1}^{3}(\tau_{pi}s + 1)}$$

where K_p, τ_{zi}, $i = 1, 2, 3$ and τ_{pi}, $i = 1, 2, 3$ represent the process gain, lead time constant and time constant respectively. The following assumptions are made based on (5.11).

I. P is an integrating process with $\tau_p > 0$, $\alpha_2 > 0$ and $\alpha_1 > 0$

II. Two right-half plane (RHP) zeros, i.e., $\tau_{z1} < 0$, $\tau_{z2} < 0$ and $\tau_{z3} > 0$

For simplicity, the following terms q_1, q_2 and q_3 are defined as

$$\begin{bmatrix} q_1 \\ q_2 \\ q_3 \end{bmatrix} \triangleq \begin{bmatrix} \tau_{z1}\tau_{z2} + \tau_{z1}\tau_{z3} + \tau_{z2}\tau_{z3} \\ \sum_{i=1}^{3} \tau_{zi} \\ \prod_{i=1}^{3} \tau_{zi} \end{bmatrix} \tag{5.12}$$

In terms of the three simplified terms in (5.12), the characteristic polynomial of the closed-loop system in (4.1) can be written as

$$\begin{aligned} &(\tau_p\alpha_2\tau_I + K\tau_D\tau_I q_3)s^5 + [\tau_I(\alpha_2 + \tau_p\alpha_1) + K(\tau_D\tau_I q_1 \\ &\quad + \tau_I q_3)]s^4 + [\tau_I(\alpha_1 + \tau_p) + K(\tau_D\tau_I q_2 + \tau_I q_1 + q_3)]s^3 \\ &\quad + [\tau_I + K(\tau_D\tau_I + \tau_I q_2 + q_1)]s^2 \\ &\quad + K(\tau_I + q_2)s + K = 0 \end{aligned} \tag{5.13}$$

where $K = K_c K_p$ denotes the loop gain.

The notations λ_1 and λ_2 are introduced and used to identify the possible ranges of the relation between $|\tau_{z1}|$ and $|\tau_{z2}|$ to τ_{z3} based on the conditions given in each case of stabilizing PID controller region (to be discussed in the next section). The ratios of $|\tau_{z1}|$ and $|\tau_{z2}|$ to τ_{z3} are defined as follows:

$$\begin{bmatrix} \lambda_1 \\ \lambda_2 \end{bmatrix} \triangleq \begin{bmatrix} \frac{|\tau_{z1}|}{\tau_{z3}} \\ \frac{|\tau_{z2}|}{\tau_{z3}} \end{bmatrix}$$

Thus, q_1, q_2 and q_3 can be further simplified in terms of λ_1, λ_2 and τ_{z3}:

$$\begin{bmatrix} q_1 \\ q_2 \\ q_3 \end{bmatrix} \triangleq \begin{bmatrix} \tau_{z3}^2(\lambda_1\lambda_2 - \lambda_1 - \lambda_2) \\ \tau_{z3}(1 - \lambda_1 - \lambda_2) \\ \lambda_1\lambda_2\tau_{z3}^3 \end{bmatrix} \tag{5.14}$$

where $\lambda_1 > 0$ and $\lambda_2 > 0$.

5.3 PID Stability Analysis

5.3.1 Necessary Stability Conditions

Upon applying the necessary criterion of Routh stability (i.e., Theorem 4.2.1) to the characteristic equation (5.13), the ranges or limits on the loop gain, derivative time and integral time can be established, which render the coefficients in the characteristic polynomial positive. From the coefficient of s^5, a lower limit on the loop gain can be obtained as follows

$$K > -\frac{\tau_p\alpha_2\tau_I}{\tau_D\tau_I q_3}$$

Notice that, the lower limit based on the coefficient of s^5 is always negative in value, thus, it will not be taken into account, i.e., we consider the maximum positive lower limit. On the other hand, the coefficient of s^0 leads to another lower limit on the loop gain:

$$K > \underline{K}_o^{nc} = 0 \tag{5.15}$$

The q_3 is always greater than zero as long as the assumption of two right-half plane (RHP) zeros holds. Meanwhile, the limits on the loop gain from the coefficients of s^4, s^3, s^2 and s might be formed depending on which of the following 3 conditions holds:

Case 1 $q_1 < 0$ and $q_2 < 0$

Case 2 $q_1 > 0$ and $q_2 < 0$

Case 3 $q_1 < 0$ and $q_2 > 0$

Remark 13. *The case 4 (i.e., $q_1 > 0$ and $q_2 > 0$) is not possible. When $q_1 > 0$, it gives a lower limit $\lambda_1 > \frac{\lambda_2}{\lambda_2 - 1}$. Meanwhile, an upper limit of λ_1 is given as $\lambda_1 < 1 - \lambda_2$ when $q_2 > 0$. To ensure that the upper limit is always greater than the lower limit of λ_1, the quadratic equation is obtained as $\lambda_2^2 - \lambda_2 + 1 < 0$, which always form complex roots. Therefore, this implies that case 4 is not possible.*

For cases 1-3, the ranges and limits on the loop gain based on the coefficients of s^4, s^3 and s^2 can also be established. It is important to point out that the ranges of loop gain are affected by the coefficients of loop gain in the closed-loop characteristic equation, i.e. positive or negative value. Hence, the following terms are defined for the coefficients of loop gain from s^4, s^3 and s^2 respectively:

$$\begin{bmatrix} \zeta_1 \\ \zeta_2 \\ \zeta_3 \end{bmatrix} \triangleq \begin{bmatrix} \tau_D\tau_I q_1 + \tau_I q_3 \\ \tau_D\tau_I q_2 + \tau_I q_1 + q_3 \\ \tau_D\tau_I + \tau_I q_2 + q_1 \end{bmatrix} \tag{5.16}$$

Note that, the cases 1-3 can be further divided into several sub-cases based on the values (i.e. positive or negative value) given by ζ_1, ζ_2 and ζ_3, which will be demonstrated in the following sections.

5.3.1.1 Case 1: $q_1 < 0$ and $q_2 < 0$

Under case 1, there are two conditions which can hold for different ranges of λ_1.

$$\lambda_1 : \begin{cases} \lambda_1 > 1 - \lambda_2 & \text{for } 0 < \lambda_2 < 1 \\ 0 < \lambda_1 < \dfrac{\lambda_2}{\lambda_2 - 1} & \text{for } \lambda_2 > 1 \end{cases} \tag{5.17}$$

There are 8 different sub-cases which can arise from case 1 depending upon the values of ζ_1, ζ_2 and ζ_3 described as follows

Case 1.1 $\zeta_1 > 0$, $\zeta_2 > 0$ and $\zeta_3 > 0$
Case 1.2 $\zeta_1 > 0$, $\zeta_2 > 0$ and $\zeta_3 < 0$
Case 1.3 $\zeta_1 > 0$, $\zeta_2 < 0$ and $\zeta_3 > 0$
Case 1.4 $\zeta_1 > 0$, $\zeta_2 < 0$ and $\zeta_3 < 0$
Case 1.5 $\zeta_1 < 0$, $\zeta_2 > 0$ and $\zeta_3 > 0$
Case 1.6 $\zeta_1 < 0$, $\zeta_2 > 0$ and $\zeta_3 < 0$
Case 1.7 $\zeta_1 < 0$, $\zeta_2 < 0$ and $\zeta_3 > 0$
Case 1.8 $\zeta_1 < 0$, $\zeta_2 < 0$ and $\zeta_3 < 0$

Notice that, the coefficient of s always leads to a lower limit on the integral time:

$$\tau_I > \underline{I}_1^{nc} = |q_2| \tag{5.18}$$

It can be readily shown that, a negative value of lower limit on the loop gain is obtained when ζ_i, $i = 1, 2, 3$ are greater than zero while upper limit is obtained instead if ζ_i, $i = 1, 2, 3$ are less than zero.

If $\zeta_1 > 0$, a negative value of lower limit on the loop gain is produced:

$$K > -\frac{\tau_I(\alpha_2 + \tau_p\alpha_1)}{-\tau_D\tau_I|q_1| + \tau_I q_3}$$

If $\zeta_2 > 0$, a negative value of lower limit on the loop gain is obtained:

$$K > -\frac{\tau_I(\alpha_1 + \tau_p)}{-\tau_D\tau_I|q_2| - \tau_I|q_1| + q_3}$$

If $\zeta_3 > 0$, a negative value of lower limit on the loop gain is given as:

$$K > -\frac{\tau_I}{\tau_D\tau_I - \tau_I|q_2| - |q_1|}$$

The negative value of lower limits will not be taken into account as only the maximum positive lower limit will be considered. On the other hand, the upper limits on the loop gain are given as follows.

If $\zeta_1 < 0$, an upper limit on the loop gain is obtained:

$$K < \overline{K}_{1a}^{nc} = \frac{\tau_I(\alpha_2 + \tau_p\alpha_1)}{|-\tau_D\tau_I|q_1| + \tau_I q_3|} \tag{5.19}$$

If $\zeta_2 < 0$, another upper limit on the loop gain is produced:

$$K < \overline{K}_{1b}^{nc} = \frac{\tau_I(\alpha_1 + \tau_p)}{|-\tau_D\tau_I|q_2| - \tau_I|q_1| + q_3|} \tag{5.20}$$

Also if $\zeta_3 < 0$, one more upper limit on the loop gain is given as:

$$K < \overline{K}_{1c}^{nc} = \frac{\tau_I}{|\tau_D\tau_I - \tau_I|q_2| - |q_1||} \tag{5.21}$$

The necessary regions of PID controller for case 1 based on Theorem 4.2.1 is shown in Table 5.2. The difference between the maximum lower limit and minimum upper limit on the derivative time can be determined as:

$$R = \overline{D}_{min} - \underline{D}_{max} \tag{5.22}$$

Let us take an exponential function on R and further by logarithms function as follows:

$$log(R) = log_{10}(e^R) \tag{5.23}$$

If $log(R)$ is positive, it means the necessary criterion of stability is fulfilled, otherwise negative implies the criterion is not fulfilled. The detailed calculation on the necessary region of each PID parameter for the sub-cases 1.1 and 1.2 are demonstrated in Appendix B.1.

Remark 14. *It should be noted that, although the closed-loop region based on Theorem 4.2.1 is satisfied, i.e., the necessary criterion of Routh stability is met; this does not guarantee that the sufficient criterion for closed-loop stability is fulfilled. The Theorem 4.2.2 will be further applied to establishing the stabilizing regions of PID tuning parameters.*

Table 5.2: Regions of PID controller for case 1 based on Theorem 4.2.1

case 1: $q_1 < 0$ and $q_2 < 0$			
Sub-cases	K	τ_I	τ_D
1.1 $\zeta_1 > 0$ $\zeta_2 > 0$ $\zeta_3 > 0$	$K > \underline{K}_0^{nc}$	$max(0, \underline{I}_1, \underline{I}_{1.1,1}) <$ $\tau_I < \overline{I}_{1.1,1}$ $\underline{I}_1 = \lvert q_2 \rvert$ $\underline{I}_{1.1,1} = \frac{\lvert q_1 \rvert}{\tau_D - \lvert q_2 \rvert}$ $\overline{I}_{1.1,1} = \frac{q_3}{\tau_D \lvert q_2 \rvert + \lvert q_1 \rvert}$	$max(0, \underline{D}_{1.1,1}, \underline{D}_{1.1,2}) <$ $\tau_D <$ $min(\overline{D}_{1.1,1}, \overline{D}_{1.1,2})$ $\underline{D}_{1.1,1} = \lvert q_2 \rvert$ $\underline{D}_{1.1,2} = \frac{\lvert q_1 \rvert^2 + q_3 \lvert q_2 \rvert}{q_3 - \lvert q_1 \rvert \lvert q_2 \rvert}$; where $q_3 > \lvert q_1 \rvert \lvert q_2 \rvert$ $\overline{D}_{1.1,1} = \frac{q_3}{\lvert q_1 \rvert}$ $\overline{D}_{1.1,2} = \frac{q_3 - \lvert q_1 \rvert \lvert q_2 \rvert}{\lvert q_2 \rvert^2}$; where $q_3 > \lvert q_1 \rvert \lvert q_2 \rvert$
	Refer to Figure 5.1a, the closed-loop system cannot satisfy the necessary criterion.		
1.2 $\zeta_1 > 0$ $\zeta_2 > 0$ $\zeta_3 < 0$	$\underline{K}_0^{nc} < K < \overline{K}_{1c}^{nc}$	$max(0, \underline{I}_1) < \tau_I <$ $\overline{I}_{1.2,1}$ $\underline{I}_1 = \lvert q_2 \rvert$ $\overline{I}_{1.2,1} = \frac{q_3}{\tau_D \lvert q_2 \rvert + \lvert q_1 \rvert}$	$0 < \tau_D < min(\overline{D}_{1.2,1},$ $\overline{D}_{1.2,2}, \overline{D}_{1.2,3})$ $\overline{D}_{1.2,1} = \frac{q_3}{\lvert q_1 \rvert}$ $\overline{D}_{1.2,2} = \lvert q_2 \rvert$ $\overline{D}_{1.2,3} = \frac{q_3 - \lvert q_1 \rvert \lvert q_2 \rvert}{\lvert q_2 \rvert^2}$; where $q_3 > \lvert q_1 \rvert \lvert q_2 \rvert$
	Refer to Figure 5.1b, the closed-loop system might be marginally stable when $\lambda_2 < 1$ & $1 - \lambda_2 < \lambda_1 < 1$ or when $\lambda_2 > 1$ & $1 < \lambda_1 < \frac{\lambda_2}{\lambda_2 - 1}$ based on necessary criterion.		
1.3 $\zeta_1 > 0$ $\zeta_2 < 0$ $\zeta_3 > 0$	$\underline{K}_0^{nc} < K < \overline{K}_{1c}^{nc}$	$\tau_I >$ $max(0, \underline{I}_1, \underline{I}_{1.3,1}, \underline{I}_{1.3,2})$ $\underline{I}_1 = \lvert q_2 \rvert$ $\underline{I}_{1.3,1} = \frac{q_3}{\tau_D \lvert q_2 \rvert + \lvert q_1 \rvert}$ $\underline{I}_{1.3,2} = \frac{\lvert q_1 \rvert}{\tau_D - \lvert q_2 \rvert}$	$max(0, \underline{D}_{1.3,1}) < \tau_D <$ $\overline{D}_{1.3,1}$ $\underline{D}_{1.3,1} = \lvert q_2 \rvert$ $\overline{D}_{1.3,1} = \frac{q_3}{\lvert q_1 \rvert}$

Table 5.2: continued

Sub-cases	K	τ_I	τ_D
	Refer to Figure 5.1c, the closed-loop system might be marginally stable when $\lambda_2 < 1$ & $1 - \lambda_2 < \lambda_1 < 1$ or when $\lambda_2 > 1$ & $1 < \lambda_1 < \frac{\lambda_2}{\lambda_2 - 1}$ based on necessary criterion.		
1.4 $\zeta_1 > 0$ $\zeta_2 < 0$ $\zeta_3 < 0$	$\underline{K}_0^{nc} < K <$ $min(\overline{K}_{1b}^{nc}, \overline{K}_{1c}^{nc})$	$\tau_I > max(0, \underline{I}_1, \underline{I}_{1.4,1})$ $\underline{I}_1 = \lvert q_2 \rvert$ $\underline{I}_{1.4,1} = \frac{q_3}{\tau_D \lvert q_2 \rvert + \lvert q_1 \rvert}$	$0 < \tau_D <$ $min(\overline{D}_{1.4,1}, \overline{D}_{1.4,2})$ $\tau_D < \overline{D}_{1.4,1} = \frac{q_3}{\lvert q_1 \rvert}$ $\tau_D < \overline{D}_{1.4,2} = \lvert q_2 \rvert$
	Refer to Figure 5.1d, the closed-loop system might be stable when $\lambda_2 < 1$ & $\lambda_1 > 1 - \lambda_2$ or when $\lambda_2 > 1$ & $0 < \lambda_1 < \frac{\lambda_2}{\lambda_2 - 1}$ based on necessary criterion.		
1.5 $\zeta_1 < 0$ $\zeta_2 > 0$ $\zeta_3 > 0$	$\underline{K}_0^{nc} < K < \overline{K}_{1a}^{nc}$	$max(0, \underline{I}_1, \underline{I}_{1.5,1}) <$ $\tau_I < \overline{I}_{1.5,1}$ $\underline{I}_1 = \lvert q_2 \rvert$ $\underline{I}_{1.5,1} = \frac{\lvert q_1 \rvert}{\tau_D - \lvert q_2 \rvert}$ $\overline{I}_{1.5,1} = \frac{q_3}{\tau_D \lvert q_2 \rvert + \lvert q_1 \rvert}$	$max(0, \underline{D}_{1.5,1}, \underline{D}_{1.5,2},$ $\underline{D}_{1.5,3}) < \tau_D < \overline{D}_{1.5,1}$ $\underline{D}_{1.5,1} = \frac{q_3}{\lvert q_1 \rvert}$ $\underline{D}_{1.5,2} = \lvert q_2 \rvert$ $\underline{D}_{1.5,3} = \frac{\lvert q_1 \rvert^2 + q_3 \lvert q_2 \rvert}{q_3 - \lvert q_1 \rvert \lvert q_2 \rvert}$; where $q_3 > \lvert q_1 \rvert \lvert q_2 \rvert$ $\overline{D}_{1.5,1} = \frac{q_3 - \lvert q_1 \rvert \lvert q_2 \rvert}{\lvert q_2 \rvert^2}$; where $q_3 > \lvert q_1 \rvert \lvert q_2 \rvert$
	Refer to Figure 5.1e, the closed-loop system might be marginally stable with small regions when $\lambda_2 < 1$ based on necessary criterion.		
1.6 $\zeta_1 < 0$ $\zeta_2 > 0$ $\zeta_3 < 0$	$\underline{K}_0^{nc} < K <$ $min(\overline{K}_{1a}^{nc}, \overline{K}_{1c}^{nc})$	$max(0, \underline{I}_1) < \tau_I <$ $\overline{I}_{1.6,1}$ $\underline{I}_1 = \lvert q_2 \rvert$ $\overline{I}_{1.6,1} = \frac{q_3}{\tau_D \lvert q_2 \rvert + \lvert q_1 \rvert}$	$max(0, \underline{D}_{1.6,1}) < \tau_D <$ $min(\overline{D}_{1.6,1}, \overline{D}_{1.6,2})$ $\underline{D}_{1.6,1} = \frac{q_3}{\lvert q_1 \rvert}$ $\overline{D}_{1.6,1} = \lvert q_2 \rvert$ $\overline{D}_{1.6,2} = \frac{q_3 - \lvert q_1 \rvert \lvert q_2 \rvert}{\lvert q_2 \rvert^2}$; where $q_3 > \lvert q_1 \rvert \lvert q_2 \rvert$
	Refer to Figure 5.1f, the closed-loop system cannot satisfy the necessary criterion.		
1.7 $\zeta_1 < 0$ $\zeta_2 < 0$ $\zeta_3 > 0$	$\underline{K}_0^{nc} < K <$ $min(\overline{K}_{1a}^{nc}, \overline{K}_{1b}^{nc})$	$\tau_I >$ $max(0, \underline{I}_1, \underline{I}_{1.7,1}, \underline{I}_{1.7,2})$ $\underline{I}_1 = \lvert q_2 \rvert$ $\underline{I}_{1.7,1} = \frac{q_3}{\tau_D \lvert q_2 \rvert + \lvert q_1 \rvert}$ $\underline{I}_{1.7,2} = \frac{\lvert q_1 \rvert}{\tau_D - \lvert q_2 \rvert}$	$\tau_D >$ $max(0, \underline{D}_{1.7,1}, \underline{D}_{1.7,2})$ $\underline{D}_{1.7,1} = \frac{q_3}{\lvert q_1 \rvert}$ $\underline{D}_{1.7,2} = \lvert q_2 \rvert$

Table 5.2: continued

Sub-cases	K	τ_I	τ_D
	Refer to Figure 5.1g, the closed-loop system might be stable when $\lambda_2 < 1$ & $\lambda_1 > 1 - \lambda_2$ or when $\lambda_2 > 1$ & $0 < \lambda_1 < \frac{\lambda_2}{\lambda_2 - 1}$ based on necessary criterion.		
1.8 $\zeta_1 < 0$ $\zeta_2 < 0$ $\zeta_3 < 0$	$\underline{K}_0^{nc} < K < min(\overline{K}_{1a}^{nc}, \overline{K}_{1b}^{nc}, \overline{K}_{1c}^{nc})$	$\tau_I > max(0, \underline{I}_1, \underline{I}_{1.8,1})$ $\underline{I}_1 = \lvert q_2 \rvert$ $\underline{I}_{1.8,1} = \frac{q_3}{\tau_D \lvert q_2 \rvert + \lvert q_1 \rvert}$	$max(0, \underline{D}_{1.8,1}) < \tau_D < \overline{D}_{1.8,1}$ $\underline{D}_{1.8,1} = \frac{q_3}{\lvert q_1 \rvert}$ $\overline{D}_{1.8,1} = \lvert q_2 \rvert$
	Refer to Figure 5.1h, the closed-loop system might be marginally stable when $\lambda_2 < 1$ & $\lambda_1 > 1$ or when $\lambda_2 > 1$ & $0 < \lambda_1 < 1$ based on necessary criterion.		

5.3.1.2 Case 2: $q_1 > 0$ and $q_2 < 0$

The range of λ_1 for case 2 is given as:

$$\lambda_1 > \frac{\lambda_2}{\lambda_2 - 1} \quad \text{for } \lambda_2 > 1 \tag{5.24}$$

In this case 2, $q_1 > 0$ and $q_3 > 0$ result in $\zeta_1 > 0$. Thus, there are only 4 different sub-cases that can arise depending upon the values of ζ_1, ζ_2 and ζ_3 as follows

Sub-case 2.1 $\zeta_1 > 0$, $\zeta_2 > 0$ and $\zeta_3 > 0$
Sub-case 2.2 $\zeta_1 > 0$, $\zeta_2 > 0$ and $\zeta_3 < 0$
Sub-case 2.3 $\zeta_1 > 0$, $\zeta_2 < 0$ and $\zeta_3 > 0$
Sub-case 2.4 $\zeta_1 > 0$, $\zeta_2 < 0$ and $\zeta_3 < 0$

The coefficient of s always leads to a lower limit on the integral time given by

$$\tau_I > \underline{I}_2^{nc} = \lvert q_2 \rvert \tag{5.25}$$

A negative value of lower limit on the loop gain is obtained when ζ_i, $i = 1, 2, 3$ are greater than zero.

As $\zeta_1 > 0$, a negative value of lower limit on the loop gain is always formed:

$$K > -\frac{\tau_I(\alpha_2 + \tau_p \alpha_1)}{\tau_D \tau_I q_1 + \tau_I q_3} \tag{5.26}$$

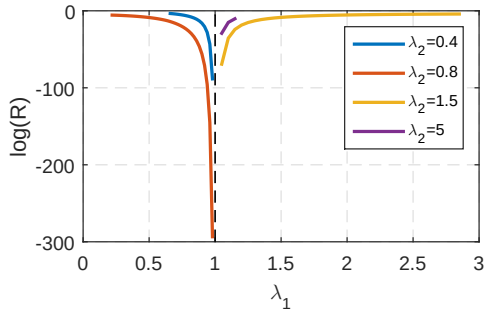

(a) Sub-case 1.1

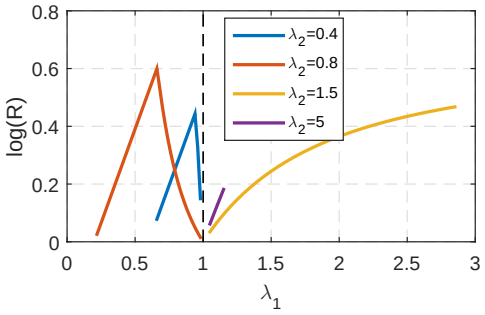

(b) Sub-case 1.2

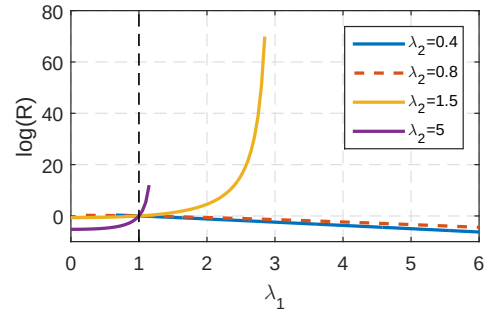

(c) Sub-case 1.3

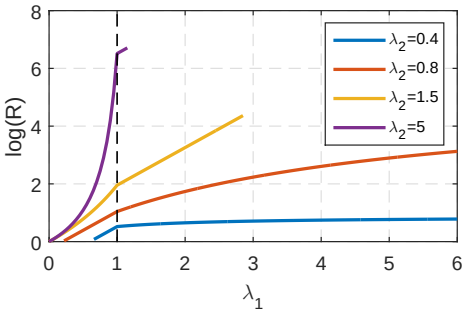

(d) Sub-case 1.4

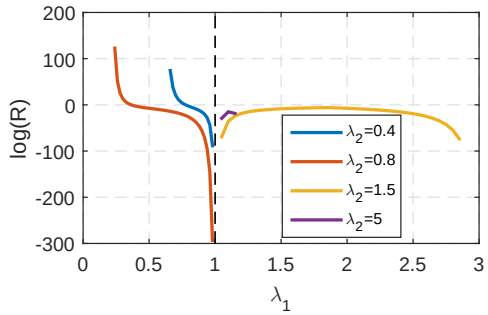

(e) Sub-case 1.5

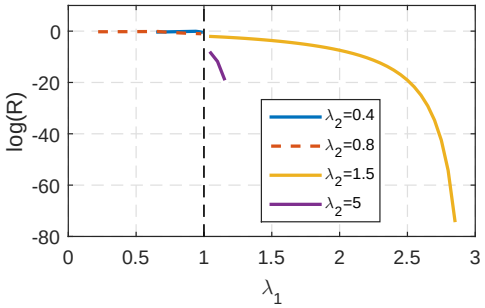

(f) Sub-case 1.6

If $\zeta_2 > 0$, a negative value of lower limit on the loop gain is obtained:

$$K > -\frac{\tau_I(\alpha_1 + \tau_p)}{-\tau_D\tau_I|q_2| + \tau_I q_1 + q_3} \tag{5.27}$$

If $\zeta_3 > 0$, a negative value of lower limit on the loop gain is given as:

$$K > -\frac{\tau_I}{\tau_D\tau_I - \tau_I|q_2| + q_1} \tag{5.28}$$

Meanwhile, the upper limits on the loop gain are produced when ζ_i, $i = 2, 3$ are less than zero.

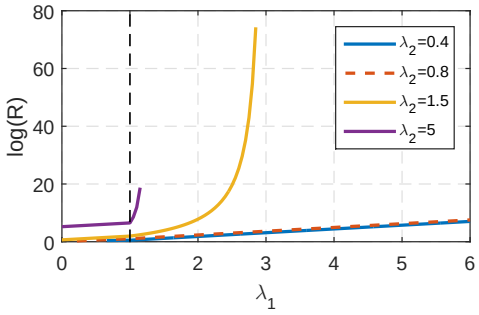

(g) Sub-case 1.7

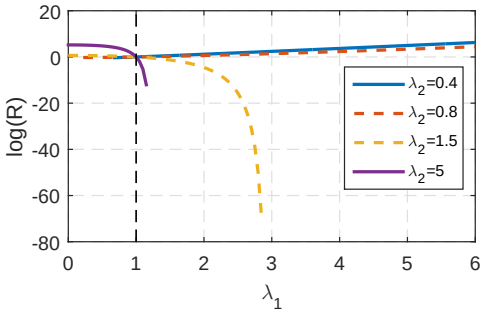

(h) Sub-case 1.8

Figure 5.1: Case 1

If $\zeta_2 < 0$, another upper limit on the loop gain is produced:

$$K < \overline{K}_{2a}^{nc} = \frac{\tau_I(\alpha_1 + \tau_p)}{|-\tau_D\tau_I|q_2| + \tau_I q_1 + q_3|} \tag{5.29}$$

Also if $\zeta_3 < 0$, one more upper limit on the loop gain is given as:

$$K < \overline{K}_{2b}^{nc} = \frac{\tau_I}{|\tau_D\tau_I - \tau|q_2| + q_1|} \tag{5.30}$$

The negative value of lower limits on the loop gain are neglected as only the maximum positive lower limits are considered. The necessary regions of PID controller for case 2 based on Theorem 4.2.1 is shown in Table 5.3. In view of remark 14, the stability analysis in Table 5.3 does not guarantee the closed-loop stability. Theorem 4.2.2 have to be applied in order to further confirm the closed-loop stability. The detailed calculation on the necessary region of each PID parameter for the sub-case 2.1 is demonstrated in Appendix B.2.

Table 5.3: Regions of PID controller for case 2 based on Theorem 4.2.1

case 2: $q_1 > 0$ and $q_2 < 0$			
Sub-cases	K	τ_I	τ_D
2.1 $\zeta_1 > 0$ $\zeta_2 > 0$ $\zeta_3 > 0$	$K > \underline{K}_0^{nc}$	$\tau_I > max(0, \underline{I}_2)$ $\underline{I}_2 = \lvert q_2 \rvert$	$max(0, \underline{D}_{2.1,1}) < \tau_D < \overline{D}_{2.1,1}$ $\underline{D}_{2.1,1} = \lvert q_2 \rvert$ $\overline{D}_{2.1,1} = \frac{q_1}{\lvert q_2 \rvert}$
	Refer to Figure 5.2a, the closed-loop system cannot be fulfilled the necessary criterion.		

Table 5.3: continued

Sub-cases	K	τ_I	τ_D
2.2 $\zeta_1 > 0$ $\zeta_2 > 0$ $\zeta_3 < 0$	$\underline{K}_0^{nc} < K < \overline{K}_{2b}^{nc}$	$\tau_I > max(0, \underline{I}_2, \underline{I}_{2.2,1})$ $\underline{I}_2 = \lvert q_2 \rvert$ $\underline{I}_{2.2,1} = \frac{q_1}{\lvert q_2 \rvert - \tau_D}$	$0 < \tau_D <$ $min(\overline{D}_{2.2,1}, \overline{D}_{2.2,2})$ $\overline{D}_{2.2,1} = \frac{q_1}{\lvert q_2 \rvert}$ $\overline{D}_{2.2,2} = \lvert q_2 \rvert$
	Refer to Figure 5.2b, the closed-loop system is able to fulfill the necessary criterion.		
2.3 $\zeta_1 > 0$ $\zeta_2 < 0$ $\zeta_3 > 0$	$\underline{K}_0^{nc} < K < \overline{K}_{2a}^{nc}$	$\tau_I > max(0, \underline{I}_2, \underline{I}_{2.3,1})$ $\underline{I}_2 = \lvert q_2 \rvert$ $\underline{I}_{2.3,1} = \frac{q_3}{\tau_D \lvert q_2 \rvert - q_1}$	$\tau_D >$ $max(0, \underline{D}_{2.3,1}, \underline{D}_{2.3,2})$ $\underline{D}_{2.3,1} = \frac{q_1}{\lvert q_2 \rvert}$ $\underline{D}_{2.3,2} = \lvert q_2 \rvert$
	Refer to Figure 5.2c, the closed-loop system is able to fulfill the necessary criterion.		
2.4 $\zeta_1 > 0$ $\zeta_2 < 0$ $\zeta_3 < 0$	$\underline{K}_0^{nc} < K <$ $min(\overline{K}_{2a}^{nc}, \overline{K}_{2b}^{nc})$	$\tau_I >$ $max(0, \underline{I}_2, \underline{I}_{2.4,1}, \underline{I}_{2.4,2})$ $\underline{I}_2 = \lvert q_2 \rvert$ $\underline{I}_{2.4,1} = \frac{q_3}{\tau_D \lvert q_2 \rvert - q_1}$ $\underline{I}_{2.4,2} = \frac{q_1}{\lvert q_2 \rvert - \tau_D}$	$max(0, \overline{D}_{2.4,1}) < \tau_D <$ $\underline{D}_{2.4,1}$ $\underline{D}_{2.4,1} = \frac{q_1}{\lvert q_2 \rvert}$ $\overline{D}_{2.4,1} = \lvert q_2 \rvert$
	Refer to Figure 5.2d, the closed-loop system is able to fulfill the necessary criterion.		

5.3.1.3 Case 3: $q_1 < 0$ and $q_2 > 0$

In this case 3, the range of λ_1 only valid when

$$0 < \lambda_1 < 1 - \lambda_2 \quad \text{for } \lambda_2 < 1 \tag{5.31}$$

There are 8 different sub-cases in case 3, which can happen depending upon the values of ζ_1, ζ_2 and ζ_3 described as follows

Sub-case 3.1 $\zeta_1 > 0$, $\zeta_2 > 0$ and $\zeta_3 > 0$

Sub-case 3.2 $\zeta_1 > 0$, $\zeta_2 > 0$ and $\zeta_3 < 0$

Sub-case 3.3 $\zeta_1 > 0$, $\zeta_2 < 0$ and $\zeta_3 > 0$

Sub-case 3.4 $\zeta_1 > 0$, $\zeta_2 < 0$ and $\zeta_3 < 0$

Sub-case 3.5 $\zeta_1 < 0$, $\zeta_2 > 0$ and $\zeta_3 > 0$

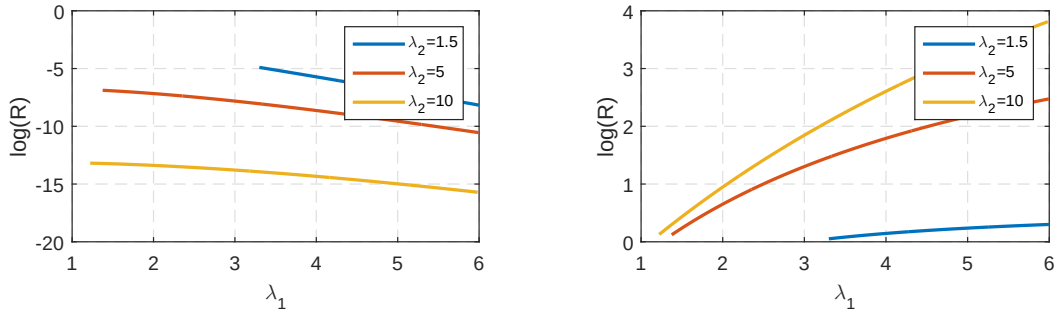

(a) Sub-case 2.1

(b) Sub-case 2.2

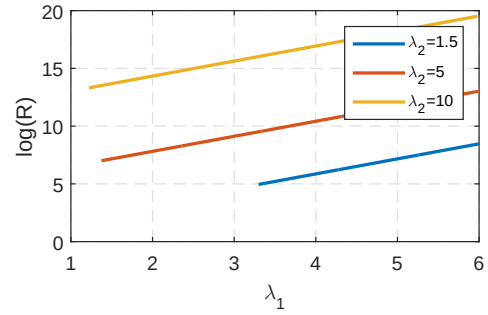

(c) Sub-case 2.3

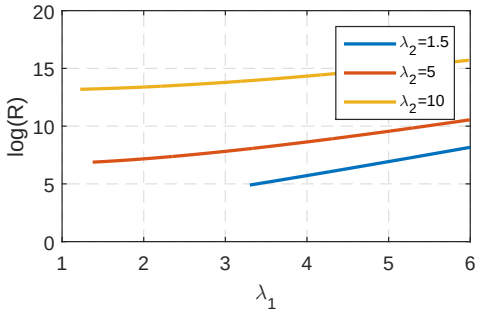

(d) Sub-case 2.4

Figure 5.2: Case 2

Sub-case 3.6 $\zeta_1 < 0$, $\zeta_2 > 0$ and $\zeta_3 < 0$
Sub-case 3.7 $\zeta_1 < 0$, $\zeta_2 < 0$ and $\zeta_3 > 0$
Sub-case 3.8 $\zeta_1 < 0$, $\zeta_2 < 0$ and $\zeta_3 < 0$

Under this case 3, the coefficient of s in the closed-loop characteristic polynomial always leads to a negative value of lower limit on the integral time, i.e. $\tau_I > -q_2$, which will not be considered as we consider only $\tau_I > 0$.

Similar to case 1 and case 2, a negative value of lower limit on the loop gain is obtained when ζ_i, $i = 1, 2, 3$ are greater than zero as follows:

If $\zeta_1 > 0$, a negative value of lower limit on the loop gain is formed:

$$K > -\frac{\tau_I(\alpha_2 + \tau_p\alpha_1)}{-\tau_D\tau_I|q_1| + \tau_I q_3} \tag{5.32}$$

If $\zeta_2 > 0$, a negative value of lower limit on the loop gain is obtained:

$$K > -\frac{\tau_I(\alpha_1 + \tau_p)}{\tau_D\tau_I q_2 - \tau_I|q_1| + q_3} \tag{5.33}$$

If $\zeta_3 > 0$, a negative value of lower limit on the loop gain is given as:

$$K > -\frac{\tau_I}{\tau_D\tau_I + \tau_I q_2 - |q_1|} \tag{5.34}$$

Since only the maximum positive lower limit on the loop gain is considered, the negative value of lower limits on the loop gain are neglected. On the other hand, the upper limits on the loop gain are formed when ζ_i, $i = 2, 3$ less than zero. If $\zeta_1 < 0$, an upper limit on the loop gain is given as:

$$K < \overline{K}_{3a}^{nc} = \frac{\tau_I(\alpha_2 + \tau_p\alpha_1)}{|-\tau_D\tau_I|q_1| + \tau_I q_3|} \tag{5.35}$$

If $\zeta_2 < 0$, another upper limit on the loop gain is produced:

$$K < \overline{K}_{3b}^{nc} = \frac{\tau_I(\alpha_1 + \tau_p)}{|\tau_D\tau_I q_2 - \tau_I|q_1| + q_3|} \tag{5.36}$$

Also if $\zeta_3 < 0$, one more upper limit on the loop gain is given as:

$$K < \overline{K}_{3c}^{nc} = \frac{\tau_I}{|\tau_D\tau_I + \tau_I q_2 - |q_1||} \tag{5.37}$$

The necessary regions of PID controller for case 3 based on Theorem 4.2.1 is shown in Table 5.4. In view of remark 14, the stability analysis in Table 5.4 does not guarantee the closed-loop stability, i.e. Theorem 4.2.2 have to be applied. The detailed calculation on the necessary region of each PID parameter for the sub-case 3.1 is demonstrated as illustrations in Appendix B.3.

Table 5.4: Regions of PID controller for case 3 based on Theorem 4.2.1

case 3: $q_1 < 0$ and $q_2 > 0$			
Sub-cases	K	τ_I	τ_D
3.1 $\zeta_1 > 0$ $\zeta_2 > 0$ $\zeta_3 > 0$	$K > \underline{K}_0^{nc}$	$\tau_I > max(0, \underline{I}_{3.1,1})$ $\underline{I}_{3.1,1} = \frac{\lvert q_1\rvert}{\tau_D + q2}$	$max(0, \underline{D}_{3.1,1}) < \tau_D < \overline{D}_{3.1,1}$ $\underline{D}_{3.1,1} = \frac{\lvert q_1\rvert}{q_2}$ $\overline{D}_{3.1,1} = \frac{q_3}{\lvert q_1\rvert}$
	Refer to Figure 5.3a, the closed-loop system cannot fulfill the necessary criterion.		
3.2 $\zeta_1 > 0$ $\zeta_2 > 0$ $\zeta_3 < 0$	$\underline{K}_0^{nc} < K < \overline{K}_{3c}^{nc}$	$0 < \tau_I < \overline{I}_{3.2,1}$ $\overline{I}_{3.2,1} = \frac{\lvert q_1\rvert}{\tau_D + q2}$	$max(0, \underline{D}_{3.2,1}) < \tau_D < \overline{D}_{3.2,1}$ $\underline{D}_{3.2,1} = \frac{\lvert q_1\rvert}{q_2}$ $\overline{D}_{3.2,1} = \frac{q_3}{\lvert q_1\rvert}$
	Refer to Figure 5.3b, the closed-loop system cannot fulfill the necessary criterion.		

Table 5.4: continued

Sub-cases	K	τ_I	τ_D
3.3 $\zeta_1 > 0$ $\zeta_2 < 0$ $\zeta_3 > 0$	$\underline{K}_0^{nc} < K < \overline{K}_{3b}^{nc}$	$\tau_I >$ $max(0, \underline{I}_{3.3,1}, \underline{I}_{3.3,2})$ $\underline{I}_{3.3,1} = \frac{q_3}{\lvert q_1\rvert - \tau_D q_2}$ $\underline{I}_{3.3,2} = \frac{\lvert q_1\rvert}{\tau_D + q_2}$	$0 < \tau_D <$ $min(\overline{D}_{3.3,1}, \overline{D}_{3.3,2})$ $\overline{D}_{3.3,1} = \frac{q_3}{\lvert q_1\rvert}$ $\overline{D}_{3.3,2} = \frac{\lvert q_1\rvert}{q_2}$
	Refer to Figure 5.3c, the closed-loop system can fulfill the necessary criterion.		
3.4 $\zeta_1 > 0$ $\zeta_2 < 0$ $\zeta_3 < 0$	$\underline{K}_0^{nc} < K <$ $min(\overline{K}_{3b}^{nc}, \overline{K}_{3c}^{nc})$	$max(0, \underline{I}_{3.4,1}) < \tau_I <$ $\overline{I}_{3.4,1}$ $\underline{I}_{3.4,1} = \frac{q_3}{\lvert q_1\rvert - \tau_D q_2}$ $\overline{I}_{3.4,1} = \frac{\lvert q_1\rvert}{\tau_D + \lvert q_2\rvert}$	$0 < \tau_D < min(\overline{D}_{3.4,1},$ $\overline{D}_{3.4,2}, \overline{D}_{3.4,3})$ $\overline{D}_{3.4,1} = \frac{q_3}{\lvert q_1\rvert}$ $\overline{D}_{3.4,2} = \frac{\lvert q_1\rvert}{q_2}$ $\overline{D}_{3.4,3} = \frac{\lvert q_1\rvert^2 - q_2 q_3}{q_3 + q_2 \lvert q_1\rvert}$; where $\lvert q_1\rvert^2 > q_2 q_3$
	Refer to Figure 5.3d, the closed-loop system can fulfill the necessary criterion.		
3.5 $\zeta_1 < 0$ $\zeta_2 > 0$ $\zeta_3 > 0$	$\underline{K}_0^{nc} < K < \overline{K}_{3a}^{nc}$	$\tau_I > max(0, \underline{I}_{3.5,1})$ $\underline{I}_{3.5,1} = \frac{\lvert q_1\rvert}{\tau_D + q_2}$	$\tau_D >$ $max(0, \underline{D}_{3.5,1}, \underline{D}_{3.5,2})$ $\underline{D}_{3.5,1} = \frac{q_3}{\lvert q_1\rvert}$ $\underline{D}_{3.5,2} = \frac{\lvert q_1\rvert}{q_2}$
	Refer to Figure 5.3e, the closed-loop system can fulfill the necessary criterion.		
3.6 $\zeta_1 < 0$ $\zeta_2 > 0$ $\zeta_3 < 0$	$\underline{K}_0^{nc} < K <$ $min(\overline{K}_{3a}^{nc}, \overline{K}_{3c}^{nc})$	$0 < \tau_I < \overline{I}_{3.6,1}$ $\overline{I}_{3.6,1} = \frac{\lvert q_1\rvert}{\tau_D + \lvert q_2\rvert}$	$\tau_D >$ $max(0, \underline{D}_{3.6,1}, \underline{D}_{3.6,2})$ $\underline{D}_{3.6,1} = \frac{q_3}{\lvert q_1\rvert}$ $\underline{D}_{3.6,2} = \frac{\lvert q_1\rvert}{q_2}$
	Refer to Figure 5.3f, the closed-loop system can fulfill the necessary criterion.		
3.7 $\zeta_1 < 0$ $\zeta_2 < 0$ $\zeta_3 > 0$	$\underline{K}_0^{nc} < K <$ $min(\overline{K}_{3a}^{nc}, \overline{K}_{3b}^{nc})$	$\tau_I >$ $max(0, \underline{I}_{3.7,1}, \underline{I}_{3.7,2})$ $\underline{I}_{3.7,1} = \frac{q_3}{\lvert q_1\rvert - \tau_D q_2}$ $\underline{I}_{3.7,2} = \frac{\lvert q_1\rvert}{\tau_D + q_2}$	$max(0, \underline{D}_{3.7,1}) < \tau_D <$ $\overline{D}_{3.7,1}$ $\underline{D}_{3.7,1} = \frac{q_3}{\lvert q_1\rvert}$ $\overline{D}_{3.7,1} = \frac{\lvert q_1\rvert}{q_2}$
	Refer to Figure 5.3g, the closed-loop system can fulfill the necessary criterion.		

Table 5.4: continued

Sub-cases	K	τ_I	τ_D
3.8 $\zeta_1 < 0$ $\zeta_2 < 0$ $\zeta_3 < 0$	$\underline{K}_0^{nc} < K <$ $min(\overline{K}_{3a}^{nc}, \overline{K}_{3b}^{nc},$ $\overline{K}_{3c}^{nc})$	$max(0, \underline{I}_{3.8,1}) < \tau_I <$ $\overline{I}_{3.8,1}$ $\underline{I}_{3.8,1} = \frac{q_3}{\lvert q_1\rvert - \tau_D q_2}$ $\overline{I}_{3.8,1} = \frac{\lvert q_1\rvert}{\tau_D + \lvert q_2\rvert}$	$max(0, \underline{D}_{3.8,1}) < \tau_D <$ $\overline{D}_{3.8,1}$ $\underline{D}_{3.8,1} = \frac{q_3}{\lvert q_1\rvert}$ $\overline{D}_{3.8,1} = \frac{\lvert q_1\rvert}{q_2}$ $\overline{D}_{3.8,2} = \frac{\lvert q_1\rvert^2 - q_2 q_3}{q_3 + q_2\lvert q_1\rvert}$; where $\lvert q_1\rvert^2 > q_2 q_3$
	Refer to Figure 5.3h, the closed-loop system can fulfill the necessary criterion.		

5.3.2 Sufficient Stability Conditions

In view of remark 14, all coefficients of the closed-loop characteristic polynomial are positive only if the conditions given by the Theorem 4.2.1 are fulfilled. However, the sufficient criterion for closed-loop stability are not guaranteed, i.e., some of the elements in the left column of Routh array might be negative values. Therefore, Theorem 4.2.2 is used to establish the limits on the integral time in order to assure the sufficient criterion of Routh stability for the given closed-loop characteristic polynomial.

Based on closed-loop characteristic polynomial (4.2), the following terms a_i, $i = 0, 1, 2 \ldots 5$ are defined in term of integral time as

$$\begin{bmatrix} a_5 \\ a_4 \\ a_3 \\ a_2 \\ a_1 \\ a_0 \end{bmatrix} \triangleq \begin{bmatrix} \tau_I(e_1 + Ke_2) \\ \tau_I(g_1 + Kg_2) \\ \tau_I j_1 + K(\tau_I j_2 + j_3) \\ \tau_I + K(\tau_I m_1 + m_2) \\ K(\tau_I + n_1) \\ K \end{bmatrix} \tag{5.38}$$

where $e_1 = \tau_p \alpha_2$, $e_2 = \tau_D q_3$, $g_1 = \alpha_2 + \tau_p \alpha_1$, $g_2 = \tau_D q_1 + q_3$, $j_1 = \alpha_1 + \tau_p$, $j_2 = \tau_D q_2 + q_1$, $j_3 = q_3$, $m_1 = \tau_D + q_2$, $m_2 = q_1$ and $n_1 = q_2$.

The Routh array is formed by taking all the coefficients a_i, $i = 0, 1, 2, 3, 4, 5$ of characteristic polynomial (4.2), and staggering them in array form as shown

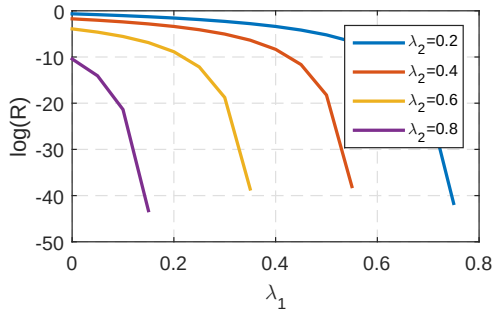

(a) Sub-case 3.1

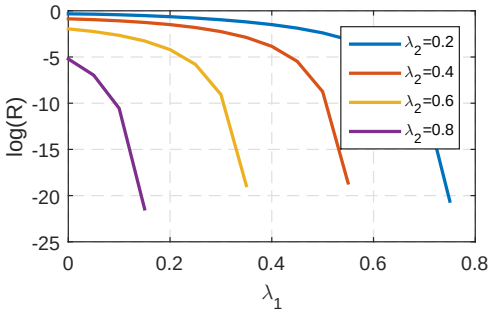

(b) Sub-case 3.2

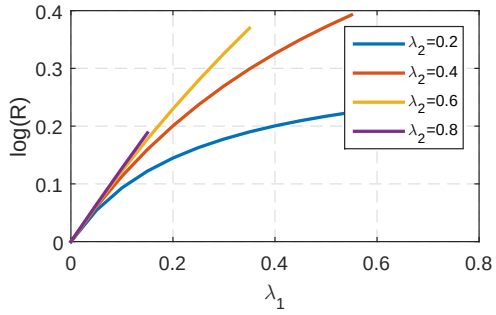

(c) Sub-case 3.3

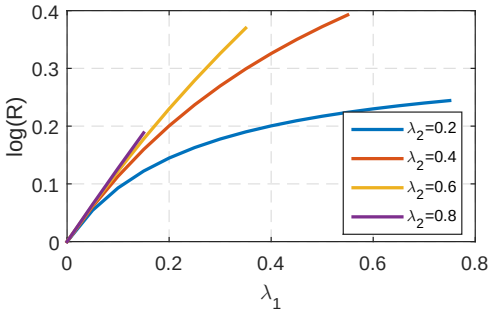

(d) Sub-case 3.4

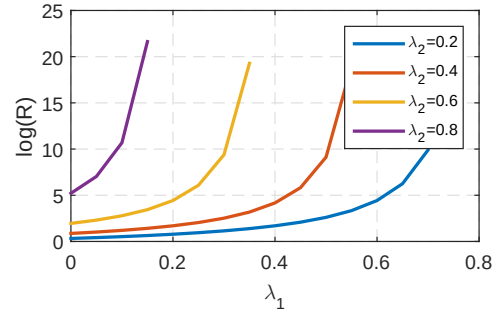

(e) Sub-case 3.5

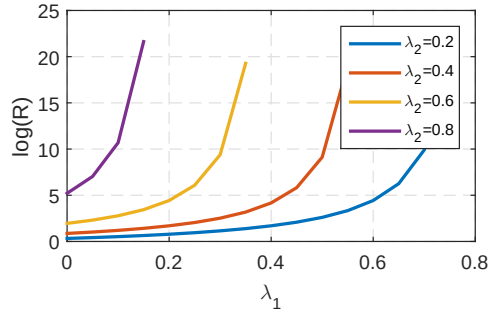

(f) Sub-case 3.6

in (5.39).

$$\mathbf{RA} = \begin{vmatrix} a_5 & a_3 & a_1 & 0 \\ a_4 & a_2 & a_0 & 0 \\ b_1 & b_2 & 0 & 0 \\ c_1 & c_2 & 0 & 0 \\ d_1 & 0 & 0 & 0 \\ c_2 & 0 & 0 & 0 \end{vmatrix} \tag{5.39}$$

It is noticed that, the coefficients a_i, $i = 0, 1, 2, 3, 4, 5$ are always greater than zero based on necessary stability criterion (Theorem 4.2.1 is obeyed). Meanwhile, the elements b_1, b_2, c_1, c_2 and d_1 must be greater than zero in order to fulfill the

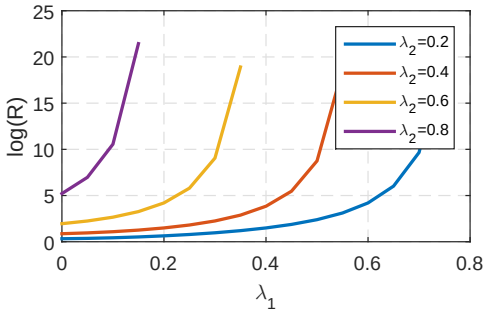

(g) Sub-case 3.7

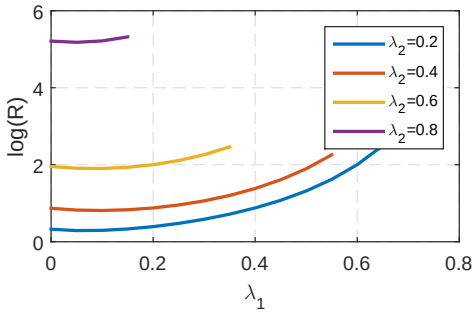

(h) Sub-case 3.8

Figure 5.3: Case 3

sufficient stability criterion (Theorem 4.2.2) as follows

$$b_1 = a_3 - \frac{a_5 a_2}{a_4} > 0$$

$$b_2 = a_1 - \frac{a_5 a_0}{a_4} > 0$$

$$c_1 = a_2 - \frac{a_4 b_2}{b_1} > 0$$

$$c_2 = a_0 > 0$$

$$d_1 = b_2 - \frac{b_1 c_2}{c_1} > 0$$

Notice that, the elements in the Routh array are functions of K, τ_D and τ_I where $\tau_D = f_1(\Theta)$, $\tau_I = f_2(\tau_D, \Theta)$ and $K = f_3(\tau_D, \tau_I, \Theta)$. We can fix the values of the derivative time, integral time and loop gain first to be within the ranges established in the Theorem 4.2.1, such that $\tau_D \in (\tau^{nc}_{D,min}, \tau^{nc}_{D,max})$, $\tau_I \in (\tau^{nc}_{I,min}, \tau^{nc}_{I,max})$ and $K \in (K^{nc}_{min}, K^{nc}_{max})$ if the necessary criterion of Routh stability is met, then obtain the limit on the integral time as a function of K, τ_D and model parameters based on the elements b_1, b_2, c_1, c_2 and d_1.

Remark 15. *The closed-loop stability is difficult to be satisfied when upper limits on the integral time are imposed. Thus, it is desirable to form lower limit on the integral time rather than upper limit on the integral time from the sufficient criterion of Routh stability (Theorem 4.2.2).*

Based on the inequality obtained from elements b_1 and b_2, the limits on integral time is given as

$$\tau_I > \underline{I}^{sc}_{b1} = \frac{K(A_1 m_2 - j_3)}{j_1 + K j_2 - A_1(1 + K m_1)} \tag{5.40}$$

$$\tau_I > \underline{I}_{b2}^{sc} = A_1 - n_1 \tag{5.41}$$

where $A_1 = \frac{e_1+Ke_2}{g_1+Kg_2}$. Since we want the denominator of (5.40) to be positive, otherwise, if the denominator is negative, (5.40) will become the upper limit on the integral time - this upper limit is negative and lower than the lower limit. It should be pointed out that for the lower limit on the integral time (5.40) to be valid, a lower bound on the loop gain is given by

$$K > \underline{K}_{b1}^{sc} = \frac{-B_2 + \sqrt{B_2^2 - 4B_1B_3}}{2B_1} \tag{5.42}$$

where $B_1 = g_2j_2 - e_2m_1$, $B_2 = j_2g_1 + j_1g_2 - e_2 - e_1m_1$ and $B_3 = j_1g_1 - e_1$. Notice that, if $B_1 < 0$, we choose the maximum root as the upper limit on the loop gain, otherwise, choose the maximum root as the lower limit on the loop gain.

On the other hand, another limit on the integral time is established from the element c_1 as follows

$$\tau_I > \underline{I}_{c1}^{sc} = \frac{-C_2 \pm \sqrt{C_2^2 - 4C_1C_3}}{2C_1} \tag{5.43}$$

where $C_1 = A_2(1 + Km_1) - K(g_1 + Kg_2)$, $C_2 = K[(n_1 - A_1)(g_1 + Kg_2) - (1 + Km_1)(A_1m_2 - j_3) + A_2m_2]$, $C_3 = K^2m_2(A_1m_2 - j_3)$ and $A_2 = j_1 + Kj_2 - A_1(1 + Km_1)$. The maximum root is chosen as the lower limit on the integral time if $C_1 > 0$.

Obviously, the element $c_2 = a_0$ which is always greater than zero. Lastly, the limit on the integral time can be obtained from the element d_1, which forms a third order polynomial as follows:

$$D_1\tau_I^3 + D_2\tau_I^2 + D_3\tau_I + D_4 > 0$$

where $D_1 = KC_1$, $D_2 = KC_2 + KC_1(n_1 - A_1)$, $D_3 = KC_2(n_1 - A_1) + KC_3 - KA_2$ and $D_4 = KC_3(n_1 - A_1) + K^2(A_1m_2 - j_3)$. Assume that $D_1 > 0$, we choose the maximum root as the lower limit on the integral time as follows:

$$\tau_I > \underline{I}_{d1}^{sc} \tag{5.44}$$

A simple iterative tuning to determine the range of integral time from sufficient condition of Routh stability is presented below.

Step 1: Set the K, τ_I and τ_D within the ranges based on necessary criterion of Routh stability (Theorem 4.2.1) such that $\tau_D \in (\tau_{D,min}^{nc}, \tau_{D,max}^{nc})$, $\tau_I \in (\tau_{I,min}^{nc}, \tau_{I,max}^{nc})$ and $K \in (K_{min}^{nc}, K_{max}^{nc})$. Note that, the K is obtained based on the range of τ_I obtained from necessary criterion.

Step 2: Calculate the τ_I based on sufficient condition of Routh stability. If the lower limit on τ_I from sufficient condition is less and/or the upper limit on τ_I is greater than the range of τ_I given by step 1, i.e., $\tau_{I,min}^{nc} < \tau_I < \tau_{I,max}^{nc}$, the tuning is completed for closed-loop stability. Otherwise, continue with the iterative tuning until the value of τ_I falls within the range based on the sufficient condition of Routh stability.

The summaries of the stabilizing regions of PID parameters for case 1, case 2 and case 3 based on the sufficient criterion of Routh stability are shown in Table 5.5, 5.6 and 5.7 respectively. From Table 5.5, 5.6 and 5.7, it can be noticed that sub-cases 1.2, 1.5, 3.4, 3.6 and 3.8 cannot be stabilized, the sub-cases 1.3, 1.4, 1.7 and 1.8 can be marginally stabilized and the sub-cases 2.2, 2.3, 2.4, 3.3, 3.5 and 3.7 can be stabilized with PID controller.

Table 5.5: Summary of the stabilizing regions of PID parameter for case 1

<table>
<tr><td colspan="4">case 1: $q_1 < 0$ and $q_2 < 0$</td></tr>
<tr><td>Sub-cases</td><td>K</td><td>τ_I</td><td>τ_D</td></tr>
<tr><td>1.2
$\zeta_1 > 0$
$\zeta_2 > 0$
$\zeta_3 < 0$</td><td>$\underline{K}_0^{nc} < K < \overline{K}_{1c}^{nc}$</td><td>$max(0, \underline{I}_1, \underline{I}_{b1}^{sc}, \underline{I}_{b2}^{sc}, \underline{I}_{c1}^{sc}, \underline{I}_{d1}^{sc}) < \tau_I < \overline{I}_{1.2,1}$</td><td>$0 < \tau_D < min(\overline{D}_{1.2,1}, \overline{D}_{1.2,2}, \overline{D}_{1.2,3})$</td></tr>
<tr><td></td><td colspan="3">In view of remark 15, the system is difficult to be stabilized. The closed-loop system cannot fulfill the sufficient criterion of Routh stability.</td></tr>
<tr><td>1.3
$\zeta_1 > 0$
$\zeta_2 < 0$
$\zeta_3 > 0$</td><td>$\underline{K}_0^{nc} < K < \overline{K}_{1c}^{nc}$</td><td>$\tau_I > max(0, \underline{I}_1, \underline{I}_{1.3,1}, \underline{I}_{1.3,2}, \underline{I}_{b1}^{sc}, \underline{I}_{b2}^{sc}, \underline{I}_{c1}^{sc}, \underline{I}_{d1}^{sc})$</td><td>$max(0, \underline{D}_{1.3,1}) < \tau_D < \overline{D}_{1.3,1}$</td></tr>
<tr><td></td><td colspan="3">The closed-loop system is marginally stable when $\lambda_2 < 1$ & $1 - \lambda_2 < \lambda_1 < 1$ or when $\lambda_2 > 1$ & $1 < \lambda_1 < \frac{\lambda_2}{\lambda_2 - 1}$ based on necessary and sufficient criteria of Routh stability.</td></tr>
<tr><td>1.4
$\zeta_1 > 0$
$\zeta_2 < 0$
$\zeta_3 < 0$</td><td>$\underline{K}_0^{nc} < K < min(\overline{K}_{1b}^{nc}, \overline{K}_{1c}^{nc})$</td><td>$\tau_I > max(0, \underline{I}_1, \underline{I}_{1.4,1}, \underline{I}_{b1}^{sc}, \underline{I}_{b2}^{sc}, \underline{I}_{c1}^{sc}, \underline{I}_{d1}^{sc})$</td><td>$0 < \tau_D < min(\overline{D}_{1.4,1}, \overline{D}_{1.4,2})$</td></tr>
</table>

Table 5.5: continued

Sub-cases	K	τ_I	τ_D
	The closed-loop system is marginally stable when $\lambda_2 < 1$ & $\lambda_1 > 1 - \lambda_2$ or when $\lambda_2 > 1$ & $0 < \lambda_1 < \frac{\lambda_2}{\lambda_2 - 1}$ based on necessary and sufficient criteria of Routh stability.		
1.5 $\zeta_1 < 0$ $\zeta_2 > 0$ $\zeta_3 > 0$	$\underline{K}_0^{nc} < K < \overline{K}_{1a}^{nc}$	$max(0, \underline{I}_1, \underline{I}_{1.5,1}, \underline{I}_{b1}^{sc}, \underline{I}_{b2}^{sc}, \underline{I}_{c1}^{sc}, \underline{I}_{d1}^{sc}) < \tau_I < \overline{I}_{1.5,1}$	$max(0, \underline{D}_{1.5,1}, \underline{D}_{1.5,2}, \underline{D}_{1.5,3}) < \tau_D < \overline{D}_{1.5,1}$
	In view of remark 15, the system is difficult to be stabilized. The closed-loop system cannot fulfill the sufficient criterion of Routh stability.		
1.7 $\zeta_1 < 0$ $\zeta_2 < 0$ $\zeta_3 > 0$	$\underline{K}_0^{nc} < K < min(\overline{K}_{1a}^{nc}, \overline{K}_{1b}^{nc})$	$\tau_I > max(0, \underline{I}_1, \underline{I}_{1.7,1}, \underline{I}_{1.7,2}, \underline{I}_{b1}^{sc}, \underline{I}_{b2}^{sc}, \underline{I}_{c1}^{sc}, \underline{I}_{d1}^{sc})$	$\tau_D > max(0, \underline{D}_{1.7,1}, \underline{D}_{1.7,2})$
	The closed-loop system is marginally stable when $\lambda_2 < 1$ & $\lambda_1 > 1 - \lambda_2$ or when $\lambda_2 > 1$ & $0 < \lambda_1 < \frac{\lambda_2}{\lambda_2 - 1}$ based on necessary and sufficient criteria of Routh stability.		
1.8 $\zeta_1 < 0$ $\zeta_2 < 0$ $\zeta_3 < 0$	$\underline{K}_0^{nc} < K < min(\overline{K}_{1a}^{nc}, \overline{K}_{1b}^{nc}, \overline{K}_{1c}^{nc})$	$\tau_I > max(0, \underline{I}_1, \underline{I}_{1.8,1}, \underline{I}_{b1}^{sc}, \underline{I}_{b2}^{sc}, \underline{I}_{c1}^{sc}, \underline{I}_{d1}^{sc})$	$max(0, \underline{D}_{1.8,1}) < \tau_D < \overline{D}_{1.8,1}$
	The closed-loop system is marginally stable when $\lambda_2 < 1$ & $\lambda_1 > 1$ or when $\lambda_2 > 1$ & $0 < \lambda_1 < 1$ based on necessary and sufficient criteria of Routh stability.		

Table 5.6: Summary of the stabilizing regions of PID parameter for case 2

case 2: $q_1 > 0$ and $q_2 < 0$			
Sub-cases	K	τ_I	τ_D
2.2 $\zeta_1 > 0$ $\zeta_2 > 0$ $\zeta_3 < 0$	$\underline{K}_0^{nc} < K < \overline{K}_{2b}^{nc}$	$\tau_I > max(0, \underline{I}_2, \underline{I}_{2.2,1}, \underline{I}_{b1}^{sc}, \underline{I}_{b2}^{sc}, \underline{I}_{c1}^{sc}, \underline{I}_{d1}^{sc})$	$0 < \tau_D < min(\overline{D}_{2.2,1}, \overline{D}_{2.2,2})$

Table 5.6: continued

Sub-cases	K	τ_I	τ_D
	The closed-loop system can fulfill the necessary and sufficient criteria of Routh stability.		
2.3 $\zeta_1 > 0$ $\zeta_2 < 0$ $\zeta_3 > 0$	$\underline{K}_0^{nc} < K < \overline{K}_{2a}^{nc}$	$\tau_I > max(0, \underline{I}_2, \underline{I}_{2.3,1}, \underline{I}_{b1}^{sc}, \underline{I}_{b2}^{sc}, \underline{I}_{c1}^{sc}, \underline{I}_{d1}^{sc})$	$\tau_D > max(0, \underline{D}_{2.3,1}, \underline{D}_{2.3,2})$
	The closed-loop system can fulfill the necessary and sufficient criteria of Routh stability.		
2.4 $\zeta_1 > 0$ $\zeta_2 < 0$ $\zeta_3 < 0$	$\underline{K}_0^{nc} < K < min(\overline{K}_{2a}^{nc}, \overline{K}_{2b}^{nc})$	$\tau_I > max(0, \underline{I}_2, \underline{I}_{2.4,1}, \underline{I}_{2.4,2}, \underline{I}_{b1}^{sc}, \underline{I}_{b2}^{sc}, \underline{I}_{c1}^{sc}, \underline{I}_{d1}^{sc})$	$max(0, \overline{D}_{2.4,1}) < \tau_D < \underline{D}_{2.4,1}$
	The closed-loop system can fulfill the necessary and sufficient criteria of Routh stability.		

Table 5.7: Summary of the stabilizing regions of PID parameter for case 3

case 3: $q_1 < 0$ and $q_2 > 0$			
Sub-cases	K	τ_I	τ_D
3.3 $\zeta_1 > 0$ $\zeta_2 < 0$ $\zeta_3 > 0$	$\underline{K}_0^{nc} < K < \overline{K}_{3b}^{nc}$	$\tau_I > max(0, \underline{I}_{3.3,1}, \underline{I}_{3.3,2}, \underline{I}_{b1}^{sc}, \underline{I}_{b2}^{sc}, \underline{I}_{c1}^{sc}, \underline{I}_{d1}^{sc})$	$0 < \tau_D < min(\overline{D}_{3.3,1}, \overline{D}_{3.3,2})$
	The closed-loop stability system can fulfill the necessary and sufficient criteria of Routh stability.		
3.4 $\zeta_1 > 0$ $\zeta_2 < 0$ $\zeta_3 < 0$	$\underline{K}_0^{nc} < K < min(\overline{K}_{3b}^{nc}, \overline{K}_{3c}^{nc})$	$max(0, \underline{I}_{3.4,1}, \underline{I}_{b1}^{sc}, \underline{I}_{b2}^{sc}, \underline{I}_{c1}^{sc}, \underline{I}_{d1}^{sc}) < \tau_I < \overline{I}_{3.4,1}$	$0 < \tau_D < min(\overline{D}_{3.4,1}, \overline{D}_{3.4,2}, \overline{D}_{3.4,3})$
	In view of remark 15, the system is difficult to be stabilized. The closed-loop system cannot fulfill the sufficient criterion of Routh stability.		

Table 5.7: continued

Sub-cases	K	τ_I	τ_D
3.5 $\zeta_1 < 0$ $\zeta_2 > 0$ $\zeta_3 > 0$	$\underline{K}_0^{nc} < K < \overline{K}_{3a}^{nc}$	$\tau_I > max(0, \underline{I}_{3.5,1}, \underline{I}_{b1}^{sc}, \underline{I}_{b2}^{sc}, \underline{I}_{c1}^{sc}, \underline{I}_{d1}^{sc})$	$\tau_D > max(0, \underline{D}_{3.5,1}, \underline{D}_{3.5,2})$
	The closed-loop system can fulfill the necessary and sufficient criteria of Routh stability.		
3.6 $\zeta_1 < 0$ $\zeta_2 > 0$ $\zeta_3 < 0$	$\underline{K}_0^{nc} < K < min(\overline{K}_{3a}^{nc}, \overline{K}_{3c}^{nc})$	$max(0, \underline{I}_{b1}^{sc}, \underline{I}_{b2}^{sc}, \underline{I}_{c1}^{sc}, \underline{I}_{d1}^{sc}) < \tau_I < \overline{I}_{3.6,1}$	$\tau_D > max(0, \underline{D}_{3.6,1}, \underline{D}_{3.6,2})$
	In view of remark 15, the system is difficult to be stabilized. The closed-loop system cannot fulfill the sufficient criterion of Routh stability.		
3.7 $\zeta_1 < 0$ $\zeta_2 < 0$ $\zeta_3 > 0$	$\underline{K}_0^{nc} < K < min(\overline{K}_{3a}^{nc}, \overline{K}_{3b}^{nc})$	$\tau_I > max(0, \underline{I}_{3.7,1}, \underline{I}_{3.7,2}, \underline{I}_{b1}^{sc}, \underline{I}_{b2}^{sc}, \underline{I}_{c1}^{sc}, \underline{I}_{d1}^{sc})$	$max(0, \underline{D}_{3.7,1}) < \tau_D < \overline{D}_{3.7,1}$
	The closed-loop system can fulfill the necessary and sufficient criteria of Routh stability.		
3.8 $\zeta_1 < 0$ $\zeta_2 < 0$ $\zeta_3 < 0$	$\underline{K}_0^{nc} < K < min(\overline{K}_{3a}^{nc}, \overline{K}_{3b}^{nc}, \overline{K}_{3c}^{nc})$	$max(0, \underline{I}_{3.8,1}, \underline{I}_{b1}^{sc}, \underline{I}_{b2}^{sc}, \underline{I}_{c1}^{sc}, \underline{I}_{d1}^{sc}) < \tau_I < \overline{I}_{3.8,1}$	$max(0, \underline{D}_{3.8,1}) < \tau_D < \overline{D}_{3.8,1}$
	In view of remark 15, the system is difficult to be stabilized. The closed-loop system cannot fulfill the sufficient criterion of Routh stability.		

5.4 PID Tuning Algorithm

The K_c, τ_I and τ_D are tuned within the established stabilizing PID regions shown in Tables 5.5, 5.6 and 5.7 in order to provide a desired or acceptable control performance/robustness. As a prerequisite for the proposed tuning algorithms, we introduce 3 new tuning or scaling parameters, namely r_c, r_d and r_i which are

used to calculate for the values of conventional PID parameters, K_c, τ_D and τ_I respectively.

Step 1: From the given model (5.11), determine λ_1 and λ_2; then calculate q_1, q_2 and q_3 based on which determine the main case (1, or 2, or 3) involved.

Step 2: Identify which sub-cases can be stabilized using a PID controller from Tables 5.5-5.7. Choose one of the sub-cases which can be stabilized using the PID controller and proceed to step 3.

Step 3: Calculate the following:

If there are no upper limits on K_c, τ_I and τ_D, the maximum lower limits are selected as the basis for PID parameter tuning. For this reason, we introduce 3 scaling or tuning parameters r_{c1}, r_{i1} and r_{d1} are given as follows:

$$\begin{bmatrix} K_c \\ \tau_I \\ \tau_D \end{bmatrix} \triangleq \begin{bmatrix} \frac{r_{c1}\underline{K}_{max}}{K_p} \\ r_{i1}\underline{I}_{max} \\ r_{d1}\underline{D}_{max} \end{bmatrix} \tag{5.45}$$

where $r_{c1} > 1$, $r_{i1} > 1$ and $r_{d1} > 1$.

On the other hand, if there are upper and lower limits on K_c, τ_I and τ_D, then we propose a tuning formula in the form of

$$\begin{bmatrix} K_c \\ \tau_I \\ \tau_D \end{bmatrix} \triangleq \begin{bmatrix} \frac{r_{c2}\Delta K + \underline{K}_{max}}{K_p} \\ r_{i2}\Delta\tau_I + \underline{I}_{max} \\ r_{d2}\Delta\tau_D + \underline{D}_{max} \end{bmatrix} \tag{5.46}$$

where $\Delta K = \underline{K}_{max} - \overline{K}_{min}$, $\Delta\tau_I = \underline{I}_{max} - \overline{I}_{min}$ and $\Delta\tau_D = \underline{D}_{max} - \overline{D}_{min}$, while $0 < r_{c1} < 1$, $0 < r_{i1} < 1$ and $0 < r_{d1} < 1$

Step 4: Calculate the minimum of integral time based on the sufficient condition, i.e., $\underline{I}^{sc}$; if $\tau_I > \underline{I}^{sc}$, then go to next Step 5, otherwise $\tau_I < \underline{I}^{sc}$, go back to Step 3 and increase the value of r_i such that the integral time is larger than its lower limit based on the sufficient condition.

Step 5: Evaluate the closed-loop robustness via gain margin (GM) and phase margin (PM) analysis using Nyquist diagram. Evaluate the responses to step changes in setpoint and disturbance. If the robustness and performance meet desired specification, then the tuning task is completed, otherwise, repeat Step 3 by adjusting the values of r_c, r_d and r_i until acceptable or desired robustness-performance is obtained. Note that, a set point pre-filter (F_r) is suggested in order to reduce the overshoot response in setpoint tracking. The setpoint pre-filter is expressed by

$$F_r = \frac{\frac{\tau_I}{\epsilon}s + 1}{\tau_I s + 1}, \quad 1.5 < \epsilon < 5 \tag{5.47}$$

Remark 16. *In the step 3 calculation of PID parameters, the limits are taken from the necessary criterion as we have not obtained the integral time limits based on the sufficient condition. In other words, we need to specify first the loop gain, integral time and derivative time within the maximum lower and minimum upper limit given by the necessary criterion (Theorem 4.2.1). To check whether sufficient condition is fulfilled or not, we then need to calculate the integral time limits based on Theorem 4.2.2 (sufficient criterion of stability) in step 4. If the integral time set in step 3 is within the limits (i.e., assuming sufficient condition imposes upper and lower limits on the integral time), or is above the minimum limits given by the sufficient criterion, then the PID controller is guaranteed stable, hence proceed to step 5.*

Remark 17. *If there are impulsive spikes on the manipulated variable with set-point tracking and output disturbance rejection, a lag filter is suggested to augment with the proposed PID controller in order to reduce the impulsive spikes as follows:*

$$F_a = \frac{1}{\tau_f s + 1}, \quad 0.001 < \tau_f < 0.005 \tag{5.48}$$

5.5 Illustrative Example

Based on P_2 from Section 5.1.3, a linearized model from F to Gl is obtained at the operating condition for controller design as follows:

$$P_s = \frac{Gl(s)}{F(s)} = \frac{298.7(-7.73s + 1)(-10s + 1)(10.2s + 1)}{s(10s + 1)(157.7s^2 + 11.9s + 1)} \tag{5.49}$$

It can be noticed that the transfer function belongs to case 1 as $q_1 < 0$, $q_2 < 0$ and $q_3 > 0$ are given. Note that, the sub-cases 1.3, 1.4, 1.7 and 1.8 can be marginally stabilized for case 1. By using sub-case 1.3, we obtain $G_c(s) = 3.7181 \times 10^{-5}(1 + 1/1.2241 \times 10^4 s + 7.5723s)$ after a trial-and-error tuning with $r_c = 8$, $r_i = 5$ and $r_d = 0.5$ augmented with a lag filter $F_a = (1/(0.001s + 1))$ to reduce the impulsive spikes on manipulated variable with setpoint tracking and output disturbance rejection. The proposed PID controller has a GM and PM of 10.1 dB and 75° respectively. Moreover, we obtain $G_c(s) = 3.3769 \times 10^{-5}(1 + 1/263.55s + 22.8438s)$ with $r_c = 5$, $r_i = 8$ and $r_d = 1.5$ augmented with a lag filter $F_a = (1/(0.001s + 1))$ by using sub-case 1.7 for further comparison purpose, which leads to GM and PM of 8.86 dB and 55.9° respectively. The set-point prefilter is not implemented in both cases as the overshoot is not large.

For comparison purpose, two controllers, i.e., via LQG synthesis and Ziegler-Nichols (ZN) frequency response tuning, are designed based on (5.49). The LQG controller has a GM and PM of 8.32 dB and 38.1°, respectively. A stabilizing fifth-order LQG controller is obtained as follows:

$$G_c(s) = 4.8134 \times 10^{-7} \times \frac{(10s+1)(120s+1)(169s^2+13s+1)}{s(0.00067s+1)(10s+1)(37.21s^2+8.1s+1)} \tag{5.50}$$

Meanwhile, the PID controller with filter designed based on Ziegler-Nichols (ZN) frequency response tuning has a GM of 3.11 dB and a PM of 34.1°, which can be expressed as follows:

$$G_c(s) = 1.0998 \times 10^{-6} \times \frac{1156s^2+65s+1}{s(1.6s+1)} \tag{5.51}$$

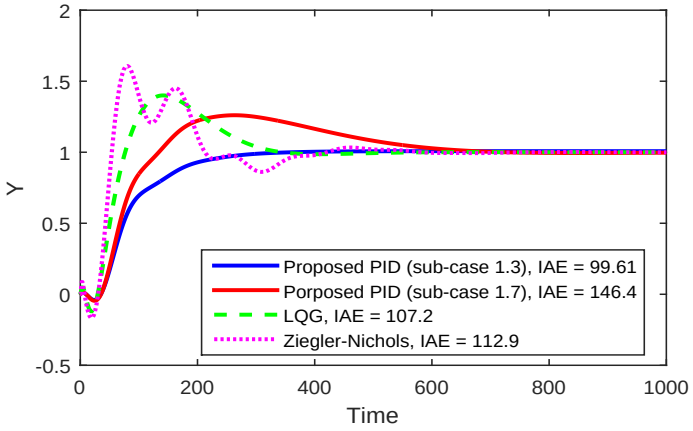

Figure 5.4: Responses of setpoint tracking at nominal condition

The closed-loop responses of the PID controllers are evaluated on the basis of separate step changes of magnitude 1 unit each in the setpoint at $t = 1$ unit and output disturbance (glucose concentration in feed) at $t = 50$ units. Figure 5.4 and Figure 5.5 demonstrate the responses of setpoint tracking and output disturbance rejection at nominal condition, respectively. In Figure 5.4, the results show that both proposed PID controllers from sub-cases 1.3 and 1.7 outperform the high-order LQG controller and PID controller based on Ziegler-Nichols tuning, both in the responses of setpoint tracking and output disturbance rejection. In Figure 5.5, it appears that the output disturbance rejection of proposed PID controller from sub-case 1.7 is a bit sluggish compared to PID controllers from sub-case 1.3, LQG controller and PID controller based on Ziegler-Nichols tuning. The responses of manipulated variable for each control schemes with setpoint tracking

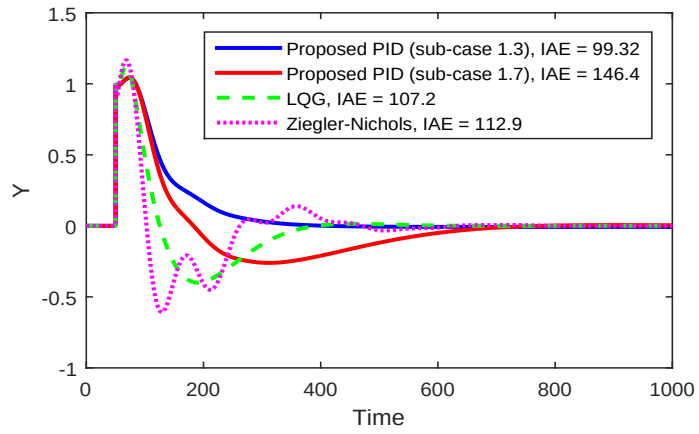

Figure 5.5: Responses of output disturbance at nominal condition

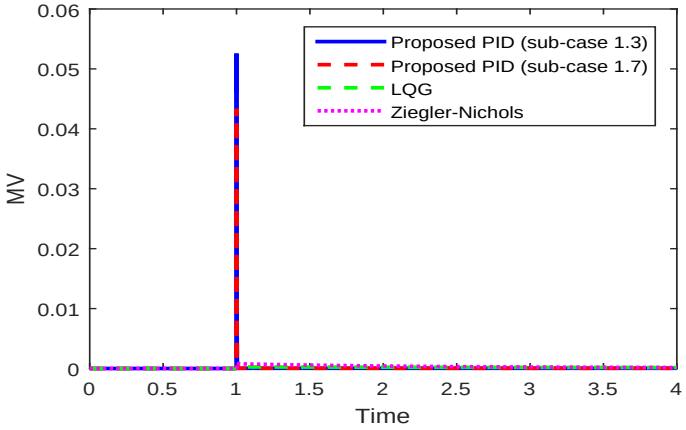

Figure 5.6: Responses of manipulated variable for setpoint tracking

are shown in Figure 5.6, which shows no obvious impulsive spikes occurred on the manipulated variable for each control schemes. Besides, the simulation of the responses of manipulated variable for disturbance rejection has been done but no impulsive spikes were observed instead.

5.6 Summary

Most of the existing reports on PID controller design and tuning are based on the first- and second-order models, which are assumed to be able to represent many real processes of interest. However, there are classes of important processes which could not be simply reduced to a first- or second-order model without the risk of losing information on significant dynamic behaviors. One such class of processes

is the fed-batch fermentation, which are commonly used in the biotechnology industry. Interestingly, these processes can be adequately represented by a class of fourth-order integrating model with multiple right-half plane (RHP) zeros, e.g., two RHP zeros. Unfortunately, so far there has been no report on PID stabilization or tuning for such a class of fourth-order integrating system. The present work aims to address this gap by establishing a set of stabilizing PID controller parameter regions based on the Routh-Hurwitz stability criteria, with the aid of two theorems recently published in the literature [179]. It has been found that via the numerical study, a PID controller tuned based on the proposed procedure can substantially outperform a high-order controller, e.g., the fifth-order optimal LQG controller. This shows that for such high order systems, e.g., fourth-order integrating system, one does not need a high-order controller to provide closed-loop stability in fact, a low-order PID controller can do the job well provided the stabilizing parameter regions are known beforehand. It should be bear in mind that, the class of fourth-order integrating system currently under investigation is not the only form that a fed-batch fermentation process can show during the course of the batch operation period. Indeed, it has been shown (unpublished) that a fed-batch process can show half a dozen forms of high-order integrating dynamics. Addressing the stabilization via PID control of these other forms of high-order integrating dynamics will remain an open problem for at least in the next few years. The presented chapter could provide a meaningful direction towards this future research direction. The work covered in this chapter has been submitted to International Journal of Control[1].

[1]Qiu Han Seer and Jobrun Nandong. Stabilizing PID Tuning for a class of fourth-order integrating nonminimum-phase systems. *Submitted to International Journal of Control - under first revision May 2017.*

Chapter 6

Multi-scale Control Scheme

In bioprocesses, several complex dynamics are frequently encountered in practice. From Chapter 4 and 5, it can be noticed that the stabilizing PID parameter regions are limited for such complex dynamic processes by using standard single-loop PID control. This chapter presents a multi-scale control (MSC) scheme which is applicable to both stable and unstable/integrating processes. The MSC scheme aims to achieve good cooperation among the different plant modes. For instance, a decentralized control and double-loop structure control strategies have been developed based on the MSC scheme. Decentralized control strategies have the advantages in controlling multi-inputs and multi-outputs processes. Meanwhile, double-loop structure control strategy can also be implemented to convert the integrating system into pre-stabilized second-order system first before the MSC scheme is employed to design the primary controller. This chapter presents the fundamental of MSC scheme and its applications to designing multi-loop PID control and double-loop PID control systems for some typical bioprocesses.

6.1 Fundamental of Multi-scale Control Scheme

The details of multi-scale control (MSC) scheme can be found in [154–157]. It has been shown that the multi-scale control scheme can be used to synthesize practical PID controller augmented with a filter. The multi-scale control scheme provides significant performance and robustness improvements over the conventional PID control for processes with long deadtime and inverse-response behaviors.

6.1.1 Plant Decomposition

A brief overview of the MSC scheme is presented. The basic idea of the MSC scheme is first to decompose a given plant system into a sum of basic factors or modes with distinct speeds of responses to a manipulated variable (input). Assume that a plant P is given by rational transfer function, which can be decomposed into a sum of factors or modes by applying partial fraction expansion as follows:

$$P(s) = P_0(s) + P_1(s) + P_2(s) + ... + P_n(s) \tag{6.1}$$

where P_i, $\forall i \in 0, 1, 2, ..., n$ is the plant factor, which can be first or second order system with real coefficients. P_0 is the outermost factor while P_i, $\forall i \in 0, 1, 2, ..., n$ is the inner-layer factor, where the response of P_j is slower that P_{j+1}, $\forall j \in 0, 1, 2, ..., n-1$. A set of sub-controllers is designed based on the basic modes, which are then combined in such a way to enhance cooperation among these different modes.

6.1.2 Realization of 2-layer Multi-scale Control Scheme

The block diagram of a 2-layer structure of multi-scale control (MSC) scheme is shown in Figure 6.1, where the plant P can be decomposed into a sum of two basic modes as follows:

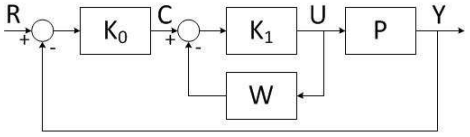

Figure 6.1: Two-layer MSC scheme block diagram

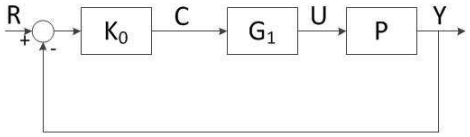

Figure 6.2: Equivalent reduced single-loop feedback control of two-layer MSC scheme block diagram

The plant P can be decomposed into a sum of two basic modes as follows:

$$P(s) = m_0(s) + m_1(s) \tag{6.2}$$

where m_0 represent the outermost (slow) mode and m_1 represent the inner-layer (fast) mode. In Figure 6.1, K_i, $i = 0, 1$ represent the sub-controller of outermost and inner-layer modes, W is the multi-scale predictor, R and Y denote the setpoint and controlled variable signals respectively. The closed-loop transfer function for the inner-layer is defined as

$$G_1(s) = \frac{U(s)}{C(s)} = \frac{K_1(s)}{1 + K_1(s)W(s)} \tag{6.3}$$

The two-layer MSC scheme can now be reduced to single-loop feedback control as shown in Figure 6.2. The overall MSC controller can be defined as follows:

$$G_c(s) = K_0(s)G_1(s) \tag{6.4}$$

6.2 Multi-loop PID Controller Design

The details of multi-scale control scheme for multivariable processes has been reported in [133, 180]. The multi-loop PID control has been widely used in multi-input and multi-output (MIMO) industrial processes. The MSC scheme is proposed to improve the effectiveness of multi-loop PID control in MIMO processes.

6.2.1 Case Study - Extractive Fermentation Process

In fact, the conventional alcoholic fermentation is typically inhibited by high product concentration, i.e., ethanol concentration above 12% (v/v) would reduce growth and production of conventional microorganisms, e.g., Baker's yeast [20]. In order to achieve high productivity in the fermentor, extractive fermentation technique has been implemented to partially remove the inhibiting ethanol (products). Refer to Figure 6.3, the extractive alcoholic fermentation process is constituted by four units: fermentor (ethanol production unit), centrifuge (cell separation unit), cell treatment unit and vacuum flash vessel (ethanol-water separation unit) [20, 181].

The control of extractive alcoholic fermentation process using Bakers yeast based on the decentralized partial control strategy was studied in [182]. In the present study, the application of partial control strategy based on 3x3 extractive fermentation system using *Z. mobilis* is proposed. The kinetics data for *Z. mobilis* is obtained from [183]. The detailed mechanistic model of extractive fermentation process is presented in Appendix C. The manipulated variables are: liquid flash

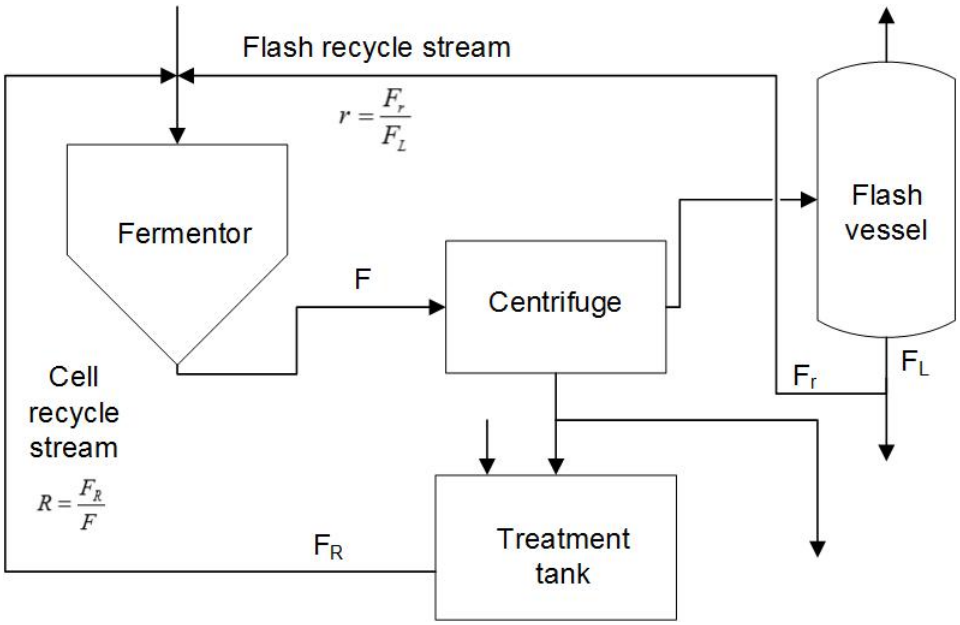

Figure 6.3: Extractive alcoholic fermentation

recycle ratio (r), cell recycle ratio (R) and flowrate of fresh feed (F_0, m^3/hr). The controlled variables are: concentration of glucose (C_g, kg/m^3), concentration of ethanol (C_e, kg/m^3) and liquid level in fermentor (L, m). The PID controllers required are designed based on the principle of multi-scale control scheme [154, 155]. The transfer function matrix for the 3x3 extractive fermentation system is given by (6.5):

$$G_p = \begin{bmatrix} \frac{3.25(s-0.849)}{(s+0.165)(s+0.485)} & \frac{28.43(s-0.077)(s+0.01)}{(s+0.456)(s+0.204)(s+0.034)} & \frac{5.49}{(s+0.216)} \\ \frac{-7}{(s+0.106)} & \frac{16.1(s+0.021)(s-0.873)}{(s+0.125)(s+0.046)} & \frac{6.08}{(s+0.219)} \\ \frac{0.5(s-0.074)(s+1.45)}{(s+9.23)(s+0.503)(s+0.16)} & \frac{0.19(s^2+0.05s+0.001)}{(s+0.11)(s^2+0.53s+0.109)} & \frac{0.029(s+0.028)}{(s+0.21)(s+0.03)} \end{bmatrix} \tag{6.5}$$

where the controlled variables $Y = [C_g\ C_e\ L]^T$ and manipulated variables $U = [r\ R\ F_0]^T$.

The Relative Gain Array (RGA) is used to determine the controller pairings, which given by (6.6):

$$RGA = \begin{bmatrix} 45.7 & -33.0 & -11.7 \\ -5.1 & 17.0 & -10.9 \\ -39.6 & 17.1 & 23.5 \end{bmatrix} \tag{6.6}$$

Based on the RGA, the pairing of inputs and outputs are (r, C_g), (R, C_e) and (F_0, L). The transfer function of g_{11} for pairing of inputs and outputs (r, C_g) is

used as an illustration, which is given by

$$g_{11}(s) = P(s) = \frac{K_p(\tau_z s + 1)}{(\tau_0 s + 1)(\tau_1 s + 1)} \tag{6.7}$$

where K_p, τ_z and τ_i, $i = 0, 1$ represent the process gain, lead time constant and time constant respectively. Upon decomposition, a sum of two basic modes are expressed by

$$P(s) = \underbrace{\frac{k_0}{\tau_0 s + 1}}_{m_0} + \underbrace{\frac{k_1}{\tau_1 s + 1}}_{m_1} \tag{6.8}$$

where m_0 and m_1 denote the outermost and inner-layer modes, respectively and the mode gains are given by

$$k_0 = \frac{K_p(\tau_z - \tau_0)}{\tau_1 - \tau_0} \tag{6.9}$$

$$k_1 = \frac{K_p(\tau_z - \tau_1)}{\tau_0 - \tau_1} \tag{6.10}$$

Design the K_1 based on the predictor W. First, assume that a P-only controller is used for controlling the inner-layer mode m_1 (predictor) and the sub-controller for inner-layer mode is given by

$$K_1 = k_{c1} \tag{6.11}$$

where k_{c1} denotes the sub-controller gain of inner-layer mode. The IMC Tuning is applied with dominant closed-loop time constant τ_{c1} in order to define the sub-controller for inner-layer mode. Assume that the closed-loop time constant will be improved four times compared to open-loop time constant. Thus, the inner-layer closed-loop transfer function can be defined as

$$G_1(s) = \frac{k_{c1}}{1 + k_{c1} W(s)} \tag{6.12}$$

where the predictor $W(s) = \frac{k_1}{\tau_1 s + 1}$ is substituted into (6.12). Construct the overall plant transfer function as follows:

$$P_c = G_1 P \tag{6.13}$$

A PI controller is used for controlling the outermost mode. The sub-controller for outermost modes is designed based on the overall plant transfer function. The IMC Tuning is applied with dominant closed-loop time constant τ_{c2} in order to define the sub-controller for outermost mode. Assume that the closed-loop time

constant will be improved four times compared to open-loop time constant, which is given by

$$K_0 = k_{c0}(1 + \frac{1}{\tau_{I0}s}) \tag{6.14}$$

where k_{c0} denotes the sub-controller gain of outermost mode whilst τ_{I0} is the integral time for the outermost mode sub-controller.

Thus, the overall MSC controller can be arranged as a PID controller with filter in the classical PID form as follows:

$$K_{msc} = K_0 G_1 = K_c(1 + \frac{1}{\tau_I s})(\frac{\tau_D s + 1}{\tau_f s + 1})S(k_{c1}) \tag{6.15}$$

where K_c, τ_I, τ_D and τ_f represent the controller gain, integral time, derivative time and filter time constant respectively. Here, $S(k_{c1})$ represents the sign of controller gain k_{c1}.

The MSC controller for g_{22} and g_{33}, which represent the pairing of inputs and outputs (R, C_e) and (F_0, L), can be designed in similar way. The tunings employed are as shown in Table 6.1.

Table 6.1: PID controller design based on the multi-scale control scheme

Loop	**Model**	**Input**	**Output**	**Inner loop**		**Outer loop**	
1	g_{11}	r	C_g	IMC tuning	P controller	IMC tuning	PI controller
2	g_{22}	R	C_e	IMC tuning	P controller	Ziegler-Nichols	PI controller
3	g_{33}	F_0	L	IMC tuning	P controller	IMC tuning	PI controller

Note that, the IMC tuning is applied to design the sub-controllers for inner-layer and outermost modes. However, the PI controller for the outermost mode in loop 2 could not be designed by applying IMC tuning. Thus, Ziegler-Nichols tuning is applied instead.

The PID controllers of loop 1, loop 2 and loop 3 are given as follows:
Loop 1:

$$G_{c1}(s) = -0.0078 \times \left(\frac{1 + 6s}{s}\right) \times \left(\frac{2.0668s + 1}{0.4148s + 1}\right) \tag{6.16}$$

Loop 2:

$$G_{c2}(s) = 3.75 \times 10^{-5} \times \left(\frac{1 + 53s}{s}\right) \times \left(\frac{7.94s + 1}{1.3219s + 1}\right) \tag{6.17}$$

Loop 3:

$$G_{c3}(s) = 51.4921 \times \left(\frac{1 + 0.72s}{s}\right) \times \left(\frac{4.7596s + 1}{0.9598s + 1}\right) \tag{6.18}$$

6.2.2 Results and Discussion

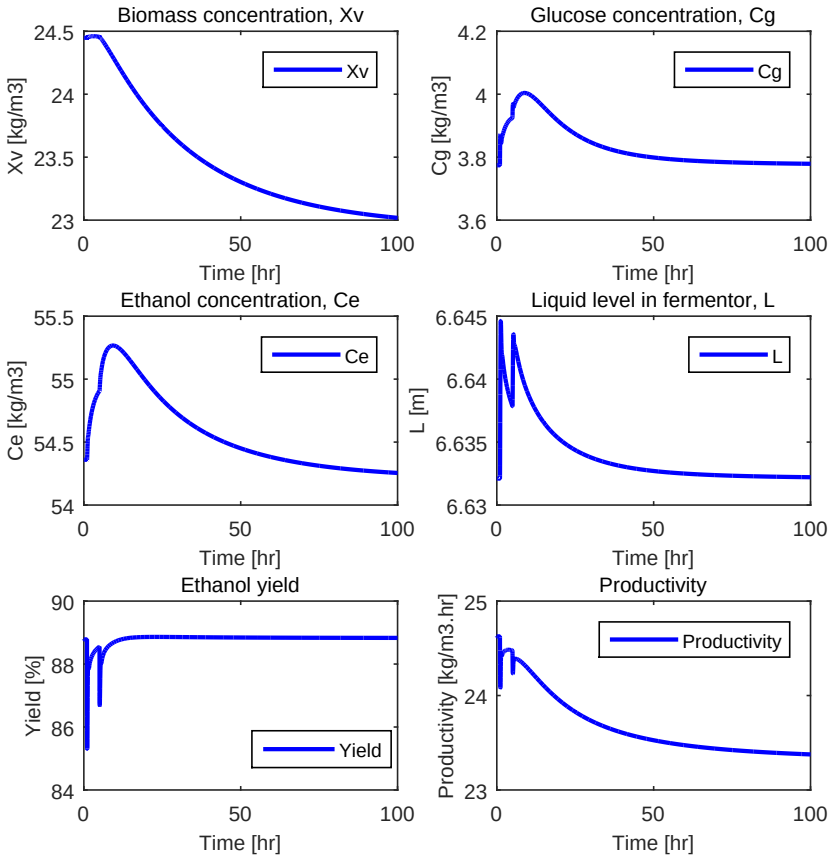

Figure 6.4: Closed-loop performances of 3×3 multi-scale control system with disturbances

The operating conditions of biomass, glucose, ethanol and liquid level in the fermentor are 24.4 kg/m^3, 3.8 kg/m^3, 54.4 kg/m^3 and 6.6321 m, respectively. At these conditions, the ethanol yield and productivity are 88.8% and 24.6 kg/m^3.hr respectively. It should be noted that the typical maximum yield and productivity for the extractive fermentation using Bakers yeast are about 82% and 21 kg/m^3.hr, respectively. Thus, the application of the *Z. mobilis* substantial increases both yield and productivity. The closed-loop performances subject to disturbances in fresh feed glucose concentration (S_{go}) and fresh feed xylose concentration (S_{xo}) of the 3×3 multi-scale control system are shown in Figure 6.4; the responses are based on sequential step changes of 5 kg/m^3 in the S_{go} and followed by 3 kg/m^3 in the S_{xo}. As can be seen, all the controlled parameters are restored

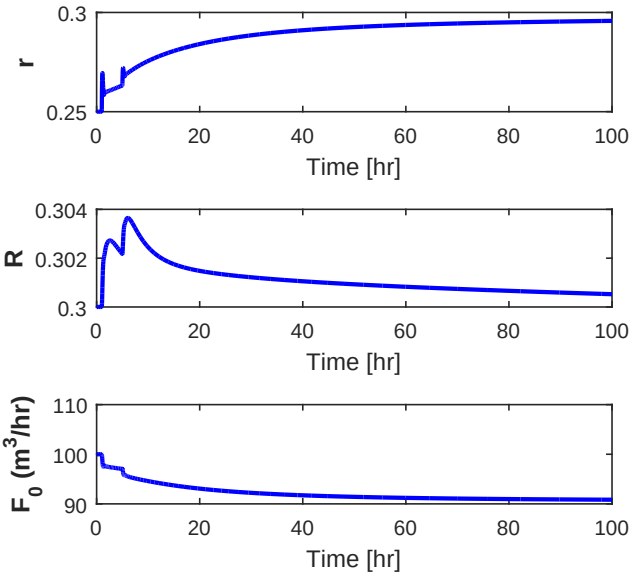

Figure 6.5: Responses of manipulated variables for 3×3 multi-scale control system

back the set point mentioned above. The steady-state drop in the productivity (not directly controlled) is within 1 kg/m^3.hr while the drop in yield is quite negligible. This suggests that the 3×3 partial control strategy with three PID controllers designed using the multi-scale control scheme is effective for the complex nonlinear extractive fermentation process. Figure 6.5 shows the responses of manipulated variables for 3×3 multi-scale control system. There is no impulsive spikes occurred on the manipulated variables, i.e., liquid flash recycle ratio (r), cell recycle ratio (R) and flowrate of fresh feed (F_0, m^3/hr).

Instead of applying 3×3 multi-scale control system, a 2×2 control system with the control-loop 2 (R, C_e) turned off is used instead. Again subject to the similar disturbances as mentioned previously, the closed-loop responses under the 2×2 control strategy is shown in Figure 6.6. As the loop control for ethanol concentration was eliminated, the ethanol concentration reach higher concentration in the beginning compared to 3×3 multi-scale control system (refer to Figure 6.4). Other than this, the responses are pretty much the same as in the case of the 3x3 control strategy. Thus In this case, it can be concluded that a simple 2×2 control strategy is quite sufficient to control the alcoholic fermentation process application of the 2×2 control strategy could be better in practice in term of the cost savings related to the control instrumentation.

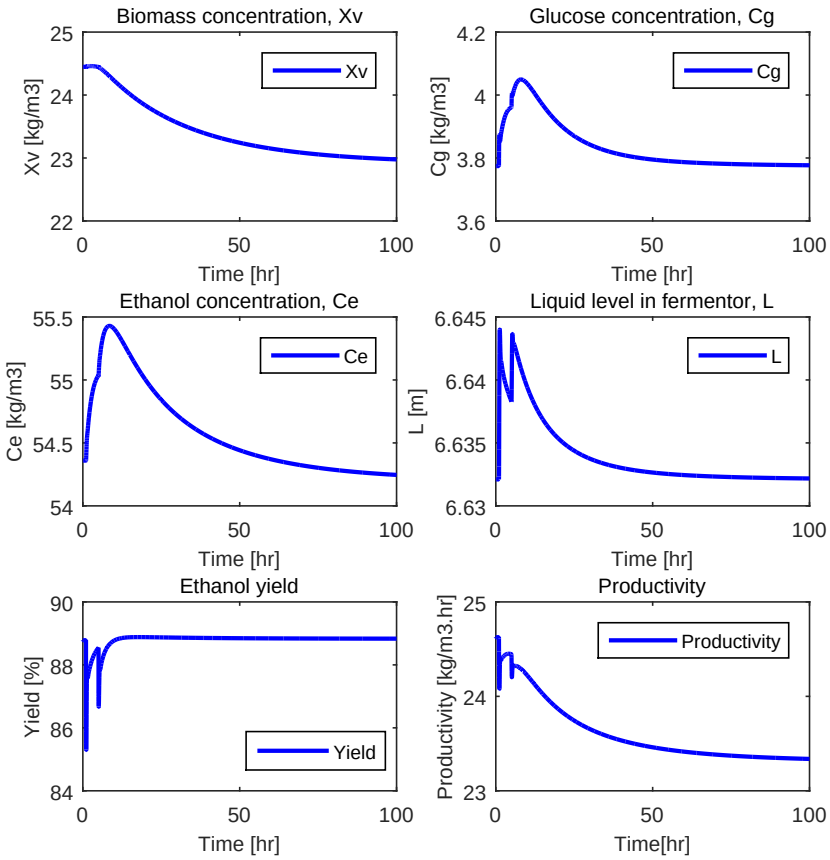

Figure 6.6: Closed-loop performances of 2×2 multi-scale control system with disturbances

6.3 Double-Loop Control Strategy for Integrating Systems

The integrating processes are frequently encountered in practice, especially in chemical plants and electromechanical processes [130, 184], such as heating boilers, liquid storing tanks with pump, heat exchanger and batch chemical reactors [127, 185, 186]. In real processes, the presence of integrating dynamic can cause poor control performance due to difficulty in stabilizing the unstable poles. Moreover, the high overshoot or inverse response is frequently encountered in integrating processes due to the presence of negative or positive zero respectively, which is highly undesirable [127, 184].

The main focus of this section is on the control of integrating systems com-

monly encountered in bioprocesses, e.g., fed-batch fermentation. Two control schemes are combined to address challenging control design in integrating processes: (1) double-loop control structure and (2) multi-scale control (MSC) scheme. The multi-scale control (MSC) scheme has been reported in [133], which offers a systematic approach to designing multi-loop PID controllers augmented with filters. The double-loop structure is implemented as to enable the use of the existing MSC-PID tuning procedure. It shall be shown that the proposed tuning method substantially simplifies the difficult PID tuning task for integrating systems. The idea of double-loop control structure was used in [187], in which an inner feedback loop is used to first pre-stabilize the integrating process.

6.3.1 Block Diagram of Double-loop Control

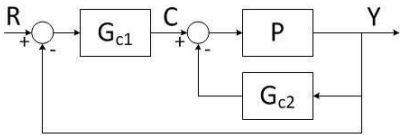

Figure 6.7: Double-loop structure of feedback control scheme block diagram

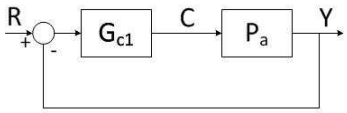

Figure 6.8: Equivalent reduced single-loop feedback control of double-loop structure block diagram

The double-loop control structure for integrating process is shown in Figure 6.7. The basic idea is to first pre-stabilize the integrating process using the inner feedback controller. This conversion of the integrating system to a stable one enables a PID (main) controller to be tuned as in the standard-single loop control scheme, as shown in Figure 6.8. Here, P is the integrating plant transfer function; R and Y denote the setpoint and controlled variable signals respectively. There are two controllers in a double-loop control structure, which is an inner controller G_{c2} and main controller G_{c1}. The plant transfer function P is first stabilized using inner controller G_{c2} and the main controller G_{c1} is tuned to provide certain performance and robustness improvements based on the overall process P_a. In this work, a MSC-PID tuning method is used to tune the main PID controller, where the construction of MSC-PID tuning method can be referred to next Section 6.1.

6.3.2 Derivation of MSC-PID Tuning Formula

A brief construction procedure of MSC-PID tuning formula is presented for a second order process, where the transfer function is represented as follows:

$$P(s) = \frac{K_p(\tau_z s + 1)}{(\tau_0 s + 1)(\tau_1 s + 1)} \tag{6.19}$$

where K_p, τ_z and τ_i, $i = 0, 1$ represent the process gain, lead time constant and time constant respectively.

The partial fraction expansion is applied to decompose (6.19) into a sum of two basic modes given by

$$P(s) = \underbrace{\frac{k_0}{\tau_0 s + 1}}_{m_0} + \underbrace{\frac{k_1}{\tau_1 s + 1}}_{m_1} \tag{6.20}$$

where the mode gains are

$$k_0 = \frac{K_p(\tau_z - \tau_0)}{\tau_1 - \tau_0} \tag{6.21}$$

$$k_1 = \frac{K_p(\tau_z - \tau_1)}{\tau_0 - \tau_1} \tag{6.22}$$

Assume that a P-only controller is used for controlling the inner-layer mode m_1 and a PI controller is used for controlling the outermost mode m_0. The sub-controllers for inner-layer and outermost modes are given by

$$K_1 = k_{c1} \tag{6.23}$$

$$K_0 = k_{c0}(1 + \frac{1}{\tau_{I0} s}) \tag{6.24}$$

where k_{c1} and k_{c0} denote the sub-controller gains of inner-layer and outermost mode respectively; τ_{I0} is the integral time for the outermost mode sub-controller. The inner-layer transfer function can be defined in term of

$$G_1(s) = \frac{k_{c1}}{1 + k_{c1} W(s)} \tag{6.25}$$

After substituting $W(s) = \frac{k_1}{\tau_1 s + 1}$ into (6.25), and followed by simplification as follows

$$G_1(s) = \frac{k_{c1}^0}{\tau_{c1} s + 1} \tag{6.26}$$

where the overall gain and closed-loop time constant are given by (6.27) and (6.28) respectively

$$k_{c1}^0 = \frac{k_{c1}}{1 + k_{c1} k_1} \tag{6.27}$$

$$\tau_{c1} = \frac{\tau_1}{1 + k_{c1}k_1} \tag{6.28}$$

The ratio of open-loop time constant to closed-loop time constant is defined as follows

$$\lambda_1 = \frac{\tau_1}{\tau_{c1}} \; ; \quad \lambda_1 > 1 \tag{6.29}$$

From (6.28) and (6.29), k_{c1} can be expressed as follows:

$$k_{c1} = \frac{\lambda_1 - 1}{k_1} \; ; \quad \lambda_1 > 1 \tag{6.30}$$

Meanwhile, PI controller is chosen to control the outermost mode. However, P-only controller is assumed first in order to determine the λ_0 and k_{c0}, which can be determined in the same way as the inner-layer mode.

$$\lambda_0 = \frac{\tau_0}{\tau_{c0}} \; ; \quad \lambda_0 > 1 \tag{6.31}$$

$$k_{c0} = \frac{\lambda_0 - 1}{k_0} S(k_{c1}) \; ; \quad \lambda_0 > 1 \tag{6.32}$$

Here, $S(k_{c1})$ represents the sign of controller gain k_{c1} which is included in order to get the correct sign for the controller gain k_{c0}. Also, the integral time for outermost mode is expressed based on a desired fraction γ of the open-loop time constant.

$$\tau_{I0} = \gamma\tau_0 \tag{6.33}$$

where $0.1 \leq \gamma \leq 1.5$.

The overall MSC controller can be arranged as a PID controller augmented with filter in the classical PID form

$$G_c(s) = K_c(1 + \frac{1}{\tau_I s})(\frac{\tau_D s + 1}{\tau_f s + 1}) \tag{6.34}$$

where K_c, τ_I, τ_D and τ_f represent the controller gain, integral time, derivative time and filter time constant respectively, which can be expressed as follows:

$$K_c = \frac{(\lambda_0 - 1)(\lambda_1 - 1)(\tau_0 - \tau_1)^2}{\lambda_1(\tau_0 - \tau_z)(\tau_1 - \tau_z)|K_p|K_p} \tag{6.35}$$

$$\tau_I = \gamma\tau_0 \tag{6.36}$$

$$\tau_D = \tau_1 \tag{6.37}$$

$$\tau_f = \frac{\tau_1}{\lambda_1} \tag{6.38}$$

Here, $|K_p|$ denotes the absolute value of K_p. Equations (6.35)-(6.38) represent the MSC-PID tuning relations, which can be tuned by adjusting the dimensionless parameters λ_0, λ_1 and γ.

6.3.3 Double-loop Control System Design

6.3.3.1 Tuning Relations for Secondary Controller

The proposed double-loop control scheme can be referred in Section 6.3.1. Consider a transfer function of a second order integrating process represented in the form of

$$P = \frac{K_p(\tau_z s + 1)}{s(\tau s + 1)} \tag{6.39}$$

where K_p, τ_z and τ represent the process gain, lead time constant and lag time constant for the integrating process, respectively.

From Figure 6.8, the closed-loop transfer function P_a is written as follows:

$$P_a(s) = \frac{Y(s)}{U(s)} = \frac{P(s)}{1 + G_{c2}(s)P(s)} \tag{6.40}$$

Assume that the secondary controller is selected as a P controller, i.e. $G_{c2} = K_{c2}$. Based on (6.40), the characteristic equation is shown to be

$$1 + K_{c2}P = 0 \tag{6.41}$$

By substituting (6.39) into (6.41), the characteristic equation is expressed in the form of

$$\tau s^2 + (1 + K_{c2}K_p\tau_z)s + K_{c2}K_p = 0 \tag{6.42}$$

The standard second-order form is given by

$$a_2 s^2 + a_1 s + a_0 = 0 \tag{6.43}$$

where $a_2 = \tau$, $a_1 = 1 + K_{c2}K_p\tau_z$ and $a_0 = K_{c2}K_p$.

From the necessary condition of Routh Stability criterion, $a_2, a_1, a_0 > 0$. Based on the necessary stability condition, two cases can be encountered.

Case 1: If $\tau_z > 0$

$$1 + K_{c2}K_p\tau_z > 0 \tag{6.44}$$

Upon simplification of (6.44), the stability range is

$$K_{c2}K_p > -\frac{1}{\tau_z} \tag{6.45}$$

Also, the Routh stability stipulates that $a_0 = K_{c2}K_p > 0$. So, the lower limit for $K_{c2}K_p$, which ensures closed-loop stability is

$$K_{c2}K_p > 0 \tag{6.46}$$

For simple tuning, let a parameter ω_1 be defined as follows:

$$K_{c2}K_p = \omega_1 \; ; \quad \omega_1 > 0 \tag{6.47}$$

Then, the secondary controller gain is given by

$$K_{c2} = \frac{\omega_1}{K_p} \; ; \quad \omega_1 > 0 \tag{6.48}$$

Based on the second-order characteristic equation (6.42), the roots x_0 and x_1 of the equation can be obtained

$$x_0, x_1 = \frac{-a_1 \pm \sqrt{a_1^2 - 4a_0a_2}}{2a_2} \tag{6.49}$$

To avoid the formation of imaginary roots, $a_1^2 - 4a_0a_2 > 0$. For real roots, it can be readily shown that

$$\omega_1 > \omega_{cric1} = \frac{4\tau - 2\tau_z + \sqrt{(2\tau_z - 4\tau)^2 - 4\tau_z^2}}{2\tau_z^2} \tag{6.50}$$

where ω_{cric1} indicates a critical value below which the system has complex imaginary poles.

In (6.50), ω_1 is specified in order to avoid unstable or complex imaginary poles. Note that, ω_1 is obtained by considering the requirements from (6.47) and (6.50) in order to avoid unstable poles.

Case 2: If $\tau_z < 0$

$$1 - K_{c2}K_p|\tau_z| > 0 \tag{6.51}$$

$$K_{c2}K_p < \frac{1}{|\tau_z|} \tag{6.52}$$

The Routh stability requires that $a_0 = K_{c2}K_p > 0$. There are upper and lower limits for $K_{c2}K_p$, which ensure closed-loop stability

$$0 < K_{c2}K_p < \frac{1}{|\tau_z|} \tag{6.53}$$

Let us define a tuning parameter ω_2 as follows:

$$K_{c2}K_p = \frac{1}{\omega_2|\tau_z|} \; ; \quad \omega_2 > 1 \tag{6.54}$$

$$K_{c2} = \frac{1}{\omega_2 K_p|\tau_z|} \; ; \quad \omega_2 > 1 \tag{6.55}$$

The same condition as in case 1 is applied in order to avoid the imaginary roots. It can be shown that, the tuning parameter ω_2 has to be

$$\omega_2 > \omega_{cric2} = \frac{2 + \frac{4\tau}{|\tau_z|} + \sqrt{[-(2 + \frac{4\tau}{|\tau_z|})]^2 - 4}}{2} \tag{6.56}$$

where ω_{cric2} denotes a critical value below which the system has complex imaginary poles.

In (6.56), ω_2 is specified in order to avoid unstable or complex imaginary poles. Here, ω_2 is obtained by considering the requirements from (6.54) and (6.56).

The closed-loop transfer function P_a in (6.40) can now be expressed as follows

$$P_a = \frac{K_{pa}(\tau_z s + 1)}{(\tau_{p0} s + 1)(\tau_{p1} s + 1)} \tag{6.57}$$

where the overall process gain is given by

$$K_{pa} = \frac{K_p \tau_{p0} \tau_{p1}}{\tau} \tag{6.58}$$

Also, where the time constant $\tau_{p0} = -\frac{1}{x_0}$ and $\tau_{p1} = -\frac{1}{x_1}$ and $\tau_{p0} > \tau_{p1}$.

For Case 1, the τ_{p0} and τ_{p1} can be expressed as follows

$$\tau_{p0} = \frac{2\tau}{1 + \omega_1 \tau_z - \sqrt{(1 + \omega_1 \tau_z)^2 - 4\omega_1 \tau}} \tag{6.59}$$

$$\tau_{p1} = \frac{2\tau}{1 + \omega_1 \tau_z + \sqrt{(1 + \omega_1 \tau_z)^2 - 4\omega_1 \tau}} \tag{6.60}$$

For Case 2, the τ_{p0} and τ_{p1} can be expressed as follows

$$\tau_{p0} = \frac{2\tau}{1 - \frac{1}{\omega_2} - \sqrt{(1 - \frac{1}{\omega_2})^2 - \frac{4\tau}{\omega_2 |\tau_z|}}} \tag{6.61}$$

$$\tau_{p1} = \frac{2\tau}{1 - \frac{1}{\omega_2} + \sqrt{(1 - \frac{1}{\omega_2})^2 - \frac{4\tau}{\omega_2 |\tau_z|}}} \tag{6.62}$$

Based on (6.57), the main controller (MSC-PID controller) parameters can be tuned by referring to (6.35)-(6.38) which are shown in Section 6.1.

6.3.3.2 Modification of MSC Tuning Relations

The modification of the expression of filter time constant in main controller from (6.38) is proposed in order to increase the overall closed-loop robustness, particularly to increase the Phase Margin (PM).

$$\tau_f = F_a \frac{\tau_1}{\lambda_1} \tag{6.63}$$

where the modifying factor of F_a is recommended in the range of $0.1 \leq F_a \leq 1.0$. The filter is implemented in order to reduce the high frequency noise presents in the process variable with a very slow right-half plane (RHP) zero, i.e., large $|\tau_z|$ in the case 2.

6.3.3.3 Robustness Criteria

In order to get additional insight into the performance-robustness of the system, sensitivity function plays an important role in judging the performance of the controller. The maximum peak of sensitivity function in frequency domain is defined as follows:

$$M_s = \|[1 + G_{c1}(j\omega)P_a(j\omega)]^{-1}\|_\infty \tag{6.64}$$

where the maximum peak of sensitivity function should be in the range of $M_s < 2.0$ [188]. The lower value of maximum peak of sensitivity function leads to higher robustness of controller but results in a sluggish response. A range of $1.0 < M_s < 2.0$ is recommended to give a practical response.

6.3.3.4 Design Procedure

The general design procedure is proposed as follows:

Step 1: Obtain ω_{cric1} using (6.50) or ω_{cric2} using (6.56) for case 1 or 2 respectively. Set $\omega_i = f\omega_{crici}$, $1.2 \leq f \leq 1.6$, $i = 1$ or 2. Calculate K_{c2} via (6.48) or (6.55) for case 1 or 2 respectively.

Step 2: The closed-loop transfer function P_a as shown in (6.57) is obtained by calculating the value of K_{pa} via (6.58); τ_{p0} and τ_{p1} via (6.59) and (6.60) for case 1 and (6.61) and (6.62) for case 2 respectively.

Step 3: The main controller G_{c1} in (6.34) is tuned by specifying the three MSC tuning parameters, which are λ_0, λ_1 and γ via (6.35)-(6.37) and (6.63) for the controller gain K_c, integral time τ_I, derivative time τ_D and filter time constant τ_f is calculated using the modified relation in (6.63) respectively. As a suggestion, set $F_a = 0.1$ and $\lambda_0 = 1.1$ while altering λ_1 and γ in order to achieve GM close to 7.5 dB - 8.5 dB, PM close to 50°- 60°and maximum peak of sensitivity function in the range of $1.0 < M_s < 2.0$ by referring to (6.64).

6.3.4 Illustrative Examples

6.3.4.1 Example 1

A linearized open-loop second order integrating process is obtained based on a real case of fed-batch bioethanol production [172].

$$P(s) = \frac{3.55(-20.64s + 1)}{s(42.81s + 1)} \tag{6.65}$$

The process parameters are given by: $K_p = 3.55$, $\tau_z = -20.64$ and $\tau = 42.81$. A characteristic of inverse response is significant with $\tau_z = -20.64$, case 2 is applied for the secondary controller design by referring to Section 6.3.3.1. From (6.54) and (6.56), the ω_2 is obtained with $\omega_2 > \omega_{cric2} = 10.20$ to avoid imaginary roots. Specify the value $\omega_2 = 1.2\omega_{cric2}$, i.e., 20% above the critical value, which leads to $\omega_2 = 12.24$ and $K_{c2} = 0.0011$ by using (6.55). For the main controller, the finalized MSC tuning values are $\lambda_0 = 1.1$, $\lambda_1 = 3$ and $\gamma = 0.7$ with $F_a = 0.1$, which leads to GM = 8.23 dB, PM = 57.6°and $M_s = 1.67$. The MSC-PID controller is given by

$$G_c(s) = 0.0035\left(1 + \frac{1}{117.13s}\right)\left(\frac{64.62s + 1}{2.15s + 1}\right) \tag{6.66}$$

Two other controllers are designed based on (6.65) in a standard single-loop control scheme, one via the LQG synthesis and another via the Ziegler-Nichols (ZN) frequency response tuning. Note that, the LQG controller can be expressed in the form of a PID controller with second-order filter given as follows:

$$G_c(s) = 4.56 \times 10^{-5}\left(\frac{44s + 1}{8.6s^2 + s}\right)\left(\frac{100s + 1}{0.0059s + 1}\right) \tag{6.67}$$

Also, the PID controller based on ZN tuning is expressed in the form of PID controller with lag filter as follows:

$$G_c(s) = 8.77 \times 10^{-5}\left(\frac{2401s^2 + 96s + 1}{2.3s^2 + s}\right) \tag{6.68}$$

Moreover, two others controllers are designed in a double-loop control scheme, i.e. via Skogestad IMC (SIMC) and Ziegler-Nichols (ZN) frequency response tuning, in order to compare the performances of MSC-PID control scheme with the others. The PID controller with filter designed based on double-loop SIMC tuning is shown as follows:

$$G_c(s) = 1.14 \times 10^{-5}\left(\frac{25s + 1}{s}\right)\left(\frac{2.1 \times 10^2 s + 1}{12s + 1}\right) \tag{6.69}$$

The PID controller with lag filter based on double-loop ZN tuning is given by

$$G_c(s) = 8.05 \times 10^{-5}\left(\frac{2401s^2 + 96s + 1}{2.3s^2 + s}\right) \tag{6.70}$$

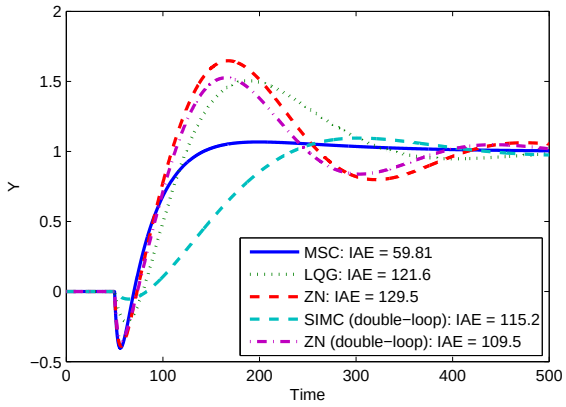

Figure 6.9: Nominal responses for setpoint tracking

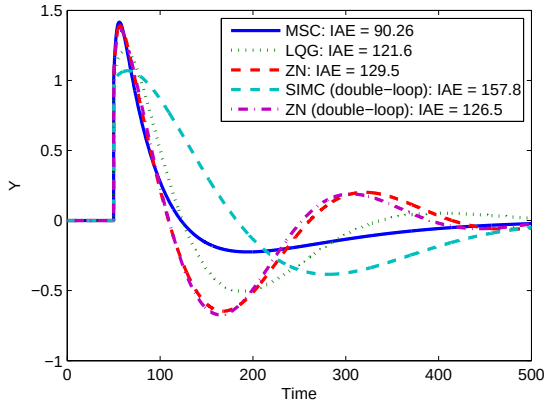

Figure 6.10: Nominal responses for disturbance rejection

The performances of these established control strategies are compared with the proposed MSC with double-loop control scheme. Figure 6.9 shows the set-point tracking responses while Figure 6.10 shows the output disturbance rejection responses. The performances of the five different control schemes are evaluated based on 1 unit step changes in the setpoint and output disturbance. In Figure 6.9, the settling time under the proposed MSC scheme is much improved compared to another four control schemes, i.e. under the proposed scheme is less than 170 units. Moreover, the Integral Absolute Error (IAE) values of the proposed

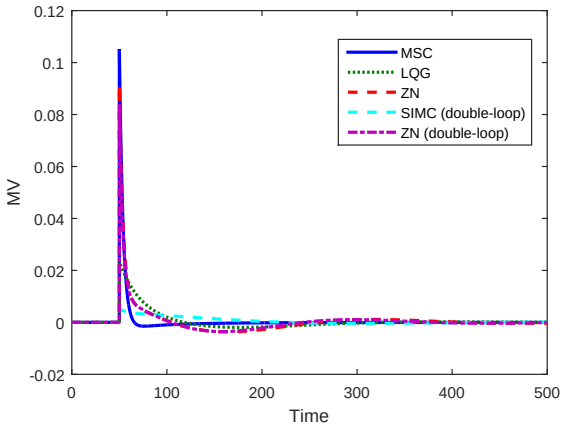

Figure 6.11: Responses of manipulated variable for setpoint tracking

scheme is much lower, which gives a smooth response and provides improvement on setpoint tracking performance over not only the single-loop LQG and PID controllers but also double-loop PID controllers. A high overshoot is undesirable in bioethanol production as this may retard the yeast activity and cause higher cell death rate, which in turn lead to lower productivity and ethanol yield. In Figure 6.10, it is obvious that the proposed MSC with double-loop control scheme shows improved output disturbance rejection performance, which provides fast response compared to the other four control schemes. Obviously, the standard single-loop control schemes, i.e. LQG synthesis and ZN tuning, unable to give good control performance for the nonminimum-phase integrating systems. Whilst, the proposed double-loop structure combining with MSC scheme shows the improved performance compared to those existing control schemes with double-loop structure, i.e. ZN and SIMC tuning. Moreover, Figure 6.11 shows the responses of manipulated variable for each control schemes with setpoint tracking. From the Figure 6.11, there is no sign of impulsive spikes occurred on the manipulated variable for each control schemes. The simulation of the responses of manipulated variable for disturbance rejection has been done but no impulsive spikes were observed instead.

The setpoint tracking and disturbance rejection with 1 unit step changes for $\pm 10\%$ modeling error in process gain and lead time constant are included and shown in Figure 6.12. It shows that the proposed control scheme remains stable in the presence of $\pm 10\%$ modeling error either in process gain or lead time constant.

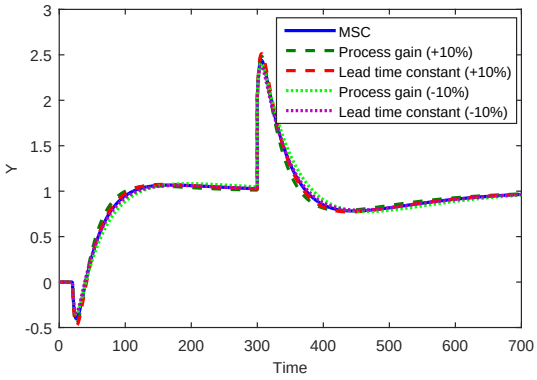

Figure 6.12: Nominal responses for setpoint tracking and disturbance rejection for modeling error of ±10%

6.3.4.2 Example 2

In this example, we use the P_5 from Section 5.1.3 to represent a less complex dynamics (only an integrating mode) which can arise from a fed-batch fermentation process and this model can be reduced to a second-order integrating process based on the model reduction algorithm from [189–191].

$$P_5 \cong \frac{298.74(-11.77s+1)}{s(35.3s+1)}$$

In here, since $\tau_z < 0$, case 2 is applied for the secondary controller design. The ω_2 is obtained with $\omega_2 > \omega_{cric2} = 13.92$ to avoid imaginary roots by referring to (6.54) and (6.56). The value $\omega_2 = 1.2\omega_{cric2} = 16.71$ and $K_{c2} = 1.7 \times 10^{-5}$ are specified by using (6.55). The main controller, i.e., MSC-PID is obtained as follows:

$$G_c(s) = 7.89 \times 10^{-5}\left(1 + \frac{1}{79.51s}\right)\left(\frac{52.39s+1}{0.81s+1}\right) \tag{6.71}$$

where the finalized MSC tuning values are $\lambda_0 = 13$, $\lambda_1 = 6.5$ and $\gamma = 0.6$ with $F_a = 0.1$, which has a GM = 7.67 dB, PM = 56.3°and $M_s = 1.74$.

For comparison purpose, two controllers, i.e., via LQG synthesis and Ziegler-Nichols (ZN) frequency response tuning, are designed based on (6.65) in a standard single-loop control scheme. The LQG controller and PID controller based on ZN tuning can be expressed respectively, as follows:

$$G_c(s) = 6.13 \times 10^{-7}\left(\frac{36s+1}{7.2s^2+s}\right)\left(\frac{99s+1}{0.001s+1}\right) \tag{6.72}$$

$$G_c(s) = 2.66 \times 10^{-6}\left(\frac{1156s^2+66s+1}{1.6s^2+s}\right) \tag{6.73}$$

Meanwhile, another two controllers are designed in a double-loop control scheme, i.e. via Skogestad IMC (SIMC) and Ziegler-Nichols (ZN) frequency response tuning. The PID controllers with filter designed based on double-loop SIMC tuning and double-loop ZN tuning are shown as follows:

$$G_c(s) = 2.48 \times 10^{-7}\left(\frac{17s+1}{s}\right)\left(\frac{1.7\times 10^2 s+1}{8.6s+1}\right) \tag{6.74}$$

$$G_c(s) = 2.51 \times 10^{-6}\left(\frac{1156s^2+66s+1}{1.6s^2+s}\right) \tag{6.75}$$

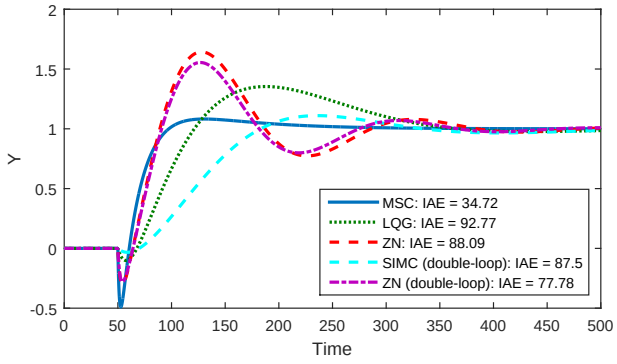

Figure 6.13: Nominal responses for setpoint tracking

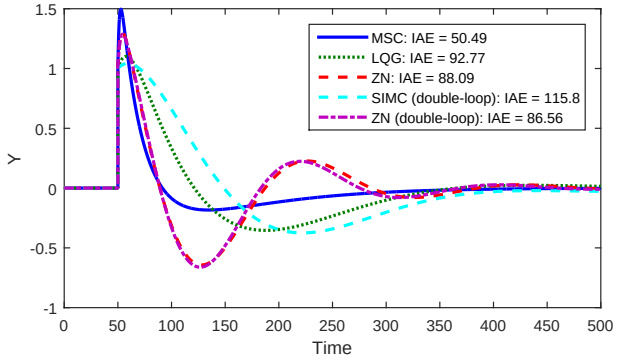

Figure 6.14: Nominal responses for disturbance rejection

The closed-loop responses of the five different control schemes are evaluated based on 1 unit step changes in the setpoint and output disturbance. Figure 6.13 and Figure 6.14 show the setpoint tracking responses and output disturbance rejection responses respectively. It is interesting to note that, the Integral Absolute Error (IAE) values of the proposed scheme is much lower, which provides improvement on the performance of setpoint tracking and disturbance rejection

over the other four control schemes. The proposed MSC with double-loop control scheme outperforms not only the single-loop control schemes, i.e. LQG synthesis and ZN tuning, but also double-loop structure, i.e. ZN and SIMC tuning. The simulation of the responses of manipulated variable for setpoint tracking and disturbance rejection has been done but no impulsive spikes were observed.

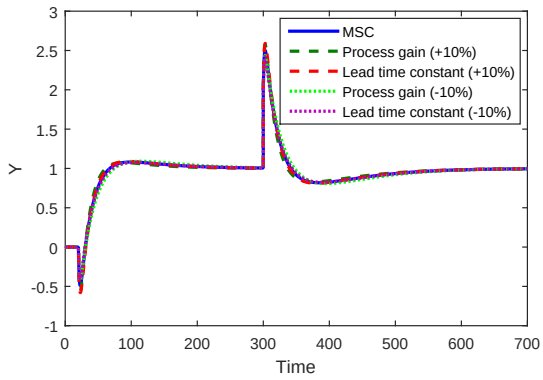

Figure 6.15: Nominal responses for setpoint tracking and disturbance rejection for modeling error of ±10%

Figure 6.15 shows the setpoint tracking and disturbance rejection with 1 unit step changes for ±10% modeling error in process gain and lead time constant. Interestingly, the proposed control scheme remains stable in the presence of ±10% modeling error either in process gain or lead time constant.

6.4 Summary

In this chapter, the applicability and effectiveness of the multi-scale control scheme are demonstrated through 2 different types of processes, i.e., multi-inputs and multi-outputs and second-order integrating processes. It can be noticed that, the unstable and NMP integrating processes are difficult to control using the standard single-loop control scheme. Note that, the MSC scheme can effectively control both stable and NMP integrating processes. Also, the MSC scheme outperforms some existing control schemes and PID tuning methods. The works reported in this chapter have been published in Trans Tech Publications[1] and

[1]Qiu Han Seer, Jobrun Nandong and Zhuquan Zang. Decentralized Control Design for Ethanol Fermentation by Zymomonas Mobilis Multi-scale Control Approach, *Applied Mechanics and Materials*, 625: 34-37, 2014.

IEEE Xplore[2].

[2]Qiu Han Seer and Jobrun Nandong. Tuning method for double-loop control structure for nonminimum-phase integrating systems. *2015 IEEE Conference on Control Applications (CCA)*, 589-594, 2015.

Chapter 7

Double-loop Multi-scale Control Scheme

The basic idea of the MSC scheme has been reported in Chapter 6. This chapter presents a new control strategy which unifies the direct and indirect multi-scale control schemes via a double-loop control structure. This unified control strategy is proposed for controlling a class of highly nonminimum-phase processes having both integrating and unstable modes. This type of systems is often encountered in fed-batch fermentation processes which are very difficult to stabilize via most of the existing well-established control strategies. The double-loop MSC (DL-MSC) scheme attempts to solve complex problem by breaking down the complex system into 2 simple sub-systems. The first loop acts as to pre-stabilize the unstable mode via the indirect MSC scheme, whilst the second loop provides overall control robustness and performance where the primary controller is designed via the direct MSC scheme.

7.1 DL-MSC Scheme for NMP Integrating- Unstable Systems

The unstable and integrating processes are frequently observed in process industries, such as batch reactors in the fermentation processes [186]. The unstable processes are difficult to control compared to open-loop stable processes due to the difficulty in stabilizing unstable poles, which can cause closed-loop instability of the system and lead to poor control performance. However, the conventional PID controllers are normally employed for stable processes [187], which are diffi-

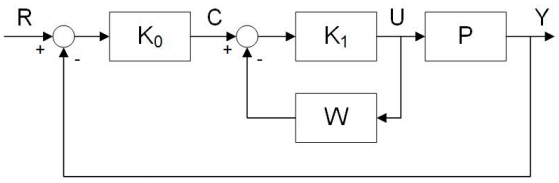

Figure 7.1: Direct MSC scheme

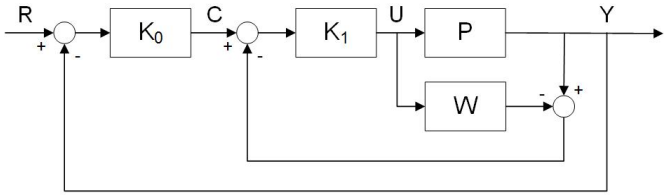

Figure 7.2: Indirect MSC scheme

cult to design for integrating and unstable processes [192].

This paper presents an idea of incorporating an inner feedback loop with the multi-scale control (MSC) scheme. The MSC scheme offers a systematic approach for designing PID controllers augmented with filters, which provide enhanced performance robustness. Meanwhile, the inner feedback loop is able to first pre-stabilize the unstable mode or pole, i.e. using a simple P controller, before the implementation of MSC-PID controller in the outer loop.

7.1.1 Direct and Indirect MSC Schemes

Figure 7.1 represents the block diagram of a 2-layer direct multi-scale control (MSC) scheme while the corresponding indirect MSC scheme is shown in Figure 7.2, where the plant P can be decomposed into a sum of two basic modes as follows:

$$P(s) = m_0(s) + m_1(s) \tag{7.1}$$

where m_0 represents the outermost (slow) mode and m_1 represents the inner-layer (fast) mode, which can be first or second order systems with real coefficients. For the direct MSC scheme, the multi-scale predictor is often chosen as the faster inner mode. On the other hand, the multi-scale predictor is chosen as the slower outermost mode for the indirect MSC scheme.

In Figure 7.1 and Figure 7.2, K_i, $i = 0, 1$ represent the sub-controllers of outermost and inner-layer modes, W is the multi-scale predictor, R and Y denote the setpoint and controlled variable signals respectively. The closed-loop transfer

function for the inner-layer is defined as

$$G_1(s) = \frac{U(s)}{C(s)} = \frac{K_1(s)}{1 + K_1(s)W(s)} \tag{7.2}$$

The two-layer MSC scheme can now be reduced to single-loop feedback control and the overall MSC controller can be defined as follows:

$$G_c(s) = K_0(s)G_1(s) \tag{7.3}$$

7.1.2 Derivation of MSC-PID Tuning Relations

A second order integrating-unstable process is considered after partial stabilization in order to present a brief construction procedure of MSC-PID tuning formula.

$$P(s) = \frac{K_p(-\tau_z s + 1)}{s(\tau_p s + 1)} \tag{7.4}$$

where K_p, τ_z and τ_p represent the process gain, lead time constant and time constant respectively.

The partial fraction expansion is applied to decompose (7.4) into a sum of two basic modes given by

$$P(s) = \underbrace{\frac{k_{p0}}{s}}_{m_0} + \underbrace{\frac{k_{p1}}{\tau_p s + 1}}_{m_1} \tag{7.5}$$

where m_0 and m_1 denote the outermost and inner-layer modes, respectively. The mode gains are given by

$$k_{p0} = K_p \tag{7.6}$$

$$k_{p1} = -K_p(\tau_z + \tau_p) \tag{7.7}$$

Assume that a P-only controller is used for controlling the inner-layer mode m_1 and a PI controller is used for controlling the outermost mode m_0. The sub-controllers for inner-layer and outermost modes are given by

$$K_1 = k_{c1} \tag{7.8}$$

$$K_0 = k_{c0}(1 + \frac{1}{\tau_{I0} s}) \tag{7.9}$$

where k_{c1} and k_{c0} denote the sub-controller gains of inner-layer and outermost mode respectively; τ_{I0} is the integral time for the outermost mode sub-controller.

Based on the direct MSC scheme (refer to Figure 7.1), assume that the multi-scale predictor is chosen as the fast inner mode, the inner-layer transfer function is defined as

$$G_1(s) = \frac{k_{c1}}{1 + k_{c1}W(s)} \tag{7.10}$$

After substituting the inner mode $W(s) = \frac{k_{p1}}{\tau_p s+1}$ into (7.10) and followed by simplification

$$G_1(s) = \frac{k_{c1}^0(\tau_p s + 1)}{\tau_{c1}s + 1} \tag{7.11}$$

where the overall gain and closed-loop time constant are given in term of

$$k_{c1}^0 = \frac{k_{c1}}{1 + k_{c1}k_{p1}} \tag{7.12}$$

$$\tau_{c1} = \frac{\tau_p}{1 + k_{c1}k_{p1}} \tag{7.13}$$

The ratio of open loop time constant to closed-loop time constant is defined as follows:

$$\lambda_1 = \frac{\tau_p}{\tau_{c1}} \; ; \quad \lambda_1 > 1 \tag{7.14}$$

From (7.13) and (7.14), k_{c1} can be expressed as follows:

$$k_{c1} = \frac{\lambda_1 - 1}{k_{p1}} \; ; \quad \lambda_1 > 1 \tag{7.15}$$

Meanwhile, PI controller is chosen to control the outermost mode. However, P-only controller is assumed first in order to determine the k_{c0} following the same way as the inner-layer mode.

$$k_{c0} = \frac{\lambda_0 - 1}{k_{p0}} \tag{7.16}$$

However, the open-loop time constant is undefined for an integrating mode. Thus, the range of λ_0 is unclear.

In order to calculate k_{c0}, P-only controller with gain k_{c0} is used based on the unity feedback control and the characteristic equation by using (7.4) is given by

$$\tau_p s^2 + (1 - k_{c0}K_p\tau_z)s + k_{c0}K_p = 0 \tag{7.17}$$

Based on the Routh Stability criterion, the upper limits can be written in term of a parameter r_1 as follows:

$$k_{c0}K_p < \frac{1}{\tau_z} = \frac{1}{r_1\tau_z} \; ; \quad r_1 > 1 \tag{7.18}$$

From (7.16) and (7.18), the k_{c0} can be calculated by applying (7.6) that $k_{p0} = K_p$ in the following manner.

$$k_{c0} = \frac{1}{r_1 \tau_z K_p} = \frac{\lambda_0 - 1}{K_p} \; ; \quad r_1 > 1 \tag{7.19}$$

Thus, the outermost time constant λ_0 can be obtained from (7.19) as follows:

$$\lambda_0 = \frac{r_1 \tau_z + 1}{r_1 \tau_z} \; ; \quad r_1 > 1 \tag{7.20}$$

Thus, $\lambda_0 > 1$ in order to stabilize the outermost mode.

Let us define an equivalent ('fictitious') open-loop time constant τ_∞ for the integrating mode, similar to (7.14).

$$\lambda_0 = \frac{\tau_\infty}{\tau_{c0}} \; ; \quad \lambda_0 > 1 \tag{7.21}$$

Note that, τ_{c0} represents the closed-loop time constant for the outermost mode as follows:

$$\tau_{c0} = \frac{1}{k_{c0} K_p} = r_1 \tau_z \tag{7.22}$$

Substitute (7.20) and (7.22) into (7.21) in order to get the open-loop time constant τ_∞.

$$\tau_\infty = r_1 \tau_z + 1 \tag{7.23}$$

The integral time for the outermost mode is expressed based on desired fraction γ of the open-loop time constant τ_∞.

$$\tau_{I0} = \gamma \tau_\infty \tag{7.24}$$

where a range of $0.5 \leq \gamma \leq 3.0$ is recommended.

The overall MSC controller for the partially stabilized plant can be arranged as a PID controller with filter in the classical PID form.

$$G_c(s) = K_c(1 + \frac{1}{\tau_I s})(\frac{\tau_D s + 1}{\tau_f s + 1}) S(k_{c1}) \tag{7.25}$$

where $S(k_{c1})$ represents the sign of controller gain k_{c1} which is included in order to get the correct sign for the controller gain k_{c0}. Also, K_c, τ_I, τ_D and τ_f represent the controller gain, integral time, derivative time and filter time constant respectively, which can be expressed as follows:

$$K_c = \frac{\lambda_1 - 1}{\lambda_1 r_1 \tau_z K_p |K_p| (\tau_p + \tau_z)} \tag{7.26}$$

where $|K_p|$ denoted the absolute value of K_p.

$$\tau_I = \gamma(1 + r_1\tau_z) \tag{7.27}$$

$$\tau_D = \tau_p \tag{7.28}$$

$$\tau_f = \frac{\tau_p}{\lambda_1} \tag{7.29}$$

7.1.3 Unified Double-Loop MSC Scheme

The key feature of the proposed scheme is to combine both direct and indirect MSC ideas. Figure 7.3 demonstrates the block diagram of the proposed MSC scheme for controlling (i.e., highly nonminimum-phase) integrating unstable process.

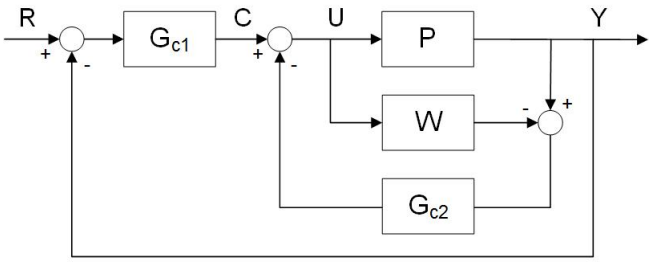

Figure 7.3: MSC with double-loop scheme

Guideline for choosing the predictor for DL-MSC scheme: choose as predictor the mode or sum of modes such that the secondary loop will stabilize the desired unstable mode/s. The indirect MSC scheme is used to design the secondary controller G_{c2} in order to first pre-stabilize the unstable process, whilst the direct MSC scheme is used to design the primary controller G_{c1}. Figure 7.4 shows the equivalent structure of the secondary loop with the implementation of indirect MSC scheme.

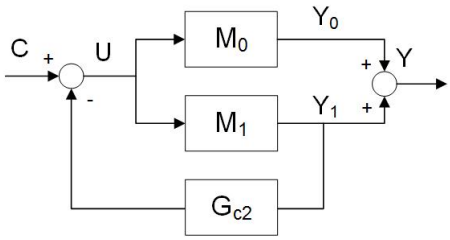

Figure 7.4: Equivalent structure of the secondary loop

7.1.3.1 Tuning Relations for Secondary Controller

Consider a second order unstable integrating process represented in term of

$$P(s) = \frac{K_p(-\tau_z s + 1)}{s(\tau_p s - 1)} \tag{7.30}$$

where K_p, τ_z and τ_p represent the process gain, lead time constant and time constant respectively. After the decomposition by partial fraction expansion, the sum of two basic modes written as

$$P(s) = \underbrace{\frac{k_{p0}}{s}}_{m_0} + \underbrace{\frac{k_{p1}}{\tau_p s - 1}}_{m_1} \tag{7.31}$$

where m_0 and m_1 denote the outermost and inner-layer modes, respectively and the mode gains are

$$k_{p0} = -K_p \tag{7.32}$$

$$k_{p1} = -K_p(\tau_z - \tau_p) \tag{7.33}$$

Referring to Figure 7.4, a transfer function from C to U is given as

$$H_u = \frac{K_u(\tau_p s - 1)}{\tau_{c2} s + 1} \tag{7.34}$$

A closed-loop transfer function from C to Y_1 can be defined as

$$G_2 = \frac{K_{c1}^0}{\tau_{c2} s + 1} \tag{7.35}$$

Also, a transfer function from C to Y_0 can be written in the form of

$$G_0 = \frac{K_{c0}^0(\tau_p s - 1)}{s(\tau_{c2} s + 1)} \tag{7.36}$$

where the parameters in (7.34)-(7.36) are given by

$$K_u = \frac{1}{K_{c2} k_{p1} - 1} \tag{7.37}$$

$$K_{c1}^0 = \frac{k_{p1}}{K_{c2} k_{p1} - 1} \tag{7.38}$$

$$K_{c0}^0 = \frac{k_{p0}}{K_{c2} k_{p1} - 1} \tag{7.39}$$

$$\tau_{c2} = \frac{\tau_p}{K_{c2} k_{p1} - 1} = \frac{\tau_p}{-K_{c2} K_p(\tau_z - \tau_p) - 1} \tag{7.40}$$

The augmented plant transfer function from C to Y is obtained by summing (7.35) and (7.36) as follows:

$$P_a(s) = G_0(s) + G_2(s) = H_u(s)P(s) \tag{7.41}$$

After the simplification of (7.41), the augmented plant transfer function P_a can be expressed as

$$P_a(s) = \frac{K_{pa}(-\tau_z s + 1)}{s(\tau_{c2} s + 1)} \tag{7.42}$$

where the augmented process gain is given by

$$K_{pa} = -K_{c0}^0 = \frac{K_p}{-K_{c2}K_p(\tau_z - \tau_p) - 1} \tag{7.43}$$

It is worth to note that, the ill-conditioned process of the form given by (7.30) can now be relieved to (7.42), i.e. similar to (7.4), which is relatively easy to stabilize.

7.1.3.2 Secondary Controller Setting

Referring to (7.10), by applying the Routh stability criterion to its characteristic equation to get the range $\tau_{c2} > 0$. Thus, the following limit can be obtained from (7.40). For simple tuning, let a parameter r_2 be defined as follows:

$$-K_{c2}K_p(\tau_z - \tau_p) = r_2 > 1 \; ; \quad r_2 > 1 \tag{7.44}$$

Here, r_2 is used as a tuning parameter to calculate K_{c2}, which ensures local stability of the mode m_1 with a range of $r_2 > 1$ as follows:

$$K_{c2} = \frac{r_2}{-K_p(\tau_z - \tau_p)} \; ; \quad r_2 > 1 \tag{7.45}$$

Also, the augmented process gain in (7.43) can now be rewritten as

$$K_{pa} = \frac{K_p}{r_2 - 1} \tag{7.46}$$

A recommended range of $0.5\tau_z \leq r_2 \leq \tau_z + \tau_p$ is sufficient for the partial stabilization purpose for secondary controller tuning.

7.1.3.3 Primary Controller Tuning

The overall system performance is to be attained via the tuning of the main controller G_{c1}, which can be referred to (7.26)-(7.29) in Section 7.1.2. Meanwhile,

the controller parameters based on the partially stabilized plant P_a in (7.42) can be expressed in the form of

$$K_c = \frac{(\lambda_1 - 1)(r_2 - 1)^3}{\lambda_1 r_1 \tau_z K_p |K_p| (\tau_p + \tau_z)} \tag{7.47}$$

$$\tau_I = \gamma(1 + r_1 \tau_z) \tag{7.48}$$

$$\tau_D = \tau_p \tag{7.49}$$

$$\tau_f = \frac{\tau_p}{\lambda_1} \tag{7.50}$$

From (7.47), an approximated linear relation which provides an inversely proportional relationship between the controller gain and the process gain is given as follows, i.e., one of the terms $|K_p|$ has been removed.

$$K_c = \frac{(\lambda_1 - 1)(r_2 - 1)^3}{\lambda_1 r_1 \tau_z K_p (\tau_p + \tau_z)} \tag{7.51}$$

For simple tuning task (approximate linear relation between K_c and K_p), we recommend a tuning formula where one of the K_p term is removed. Note that, in the exact synthesis there are both K_p and $|K_p|$ terms in the relation.

Thus, (7.48)-(7.51) represent the MSC-PID tuning relations, which can be tuned by adjusting λ_1, γ, r_1 and r_2.

7.1.3.4 Robustness Criteria

Sensitivity function plays an important role for judging the performance-robustness of the system. The maximum peak of sensitivity function in frequency domain is defined as follows:

$$M_s = \|[1 + G_{c1}(j\omega) P_a(j\omega)]^{-1}\|_\infty \tag{7.52}$$

where the maximum peak of sensitivity function is recommended in the range of $M_s < 2.0$ [188]. The lower value of maximum peak of sensitivity function leads to higher robustness of controller but results in a sluggish response. A range of $1.0 < M_s < 2.0$ is recommended to give a practical response.

7.1.3.5 Design Procedure

The general design procedure is generated based on the design of double-loop control structure for unstable integrating systems. The indirect MSC scheme is used to stabilize the unstable process in the secondary loop, while direct MSC scheme is used as the main controller. The design steps are as follows:

Step 1: Tune the secondary controller, i.e. obtain the value of controller gain K_{c2} via (7.45) by specifying the tuning parameter r_2 with a range of $0.5\tau_z \leq r_2 \leq \tau_z + \tau_p$.

Step 2: Obtain the augmented plant transfer function P_a as (7.42). The value of K_{pa} and τ_{c2} can be calculated by (7.40) and (7.43).

Step 3: The main controller G_{c1} in (7.25) is tuned by specifying the four MSC tuning parameters, which are λ_1, γ, r_1 and r_2 via (7.48)-(7.51) for the controller gain K_c, integral time τ_I, derivative time τ_D and filter time constant τ_f respectively. Note that, $\lambda_1 > 1$, $r_1 > 1$, $0.5\tau_z \leq r_2 \leq \tau_z + \tau_p$ and $0.5 \leq \gamma \leq 3.0$. As a suggestion, set $\lambda_1 = 5$ while altering r_1, r_2 and γ in order to achieve GM close to 7.5 dB - 8.5 dB, PM close to 45°- 60°and maximum peak of sensitivity function in the range of $1.0 < M_s < 2.0$ by referring to (7.52).

7.1.4 Closed-loop PID Stability Analysis

By using the ideal PID controller, the closed-loop characteristic polynomial of second-order integrating-unstable process (7.30) can be written as

$$\underbrace{\tau_I(\tau_p - K\tau_z\tau_D)}_{a_3} s^3 + \underbrace{\tau_I[K(\tau_D - \tau_z) - 1]}_{a_2} s^2 + \underbrace{[K(\tau_I - \tau_z)]}_{a_1} s + \underbrace{K}_{a_0} = 0 \quad (7.53)$$

where $K = K_c K_p$.

Theorem 4.2.1 (necessary criterion) is applied in order to establish the ranges or limits on the loop gain, derivative time and integral time which render all the coefficients in the characteristic equation (4.11) positive, i.e. $a_i > 0$, $i = 0, 1, 2, 3$. From the characteristic equation (7.53), an upper limit on the loop gain K can be established from the coefficient a_3 as follows

$$K < \frac{\tau_p}{\tau_z \tau_D} \quad (7.54)$$

and a lower limit based on the coefficient a_2

$$K > \frac{1}{\tau_D - \tau_z} \quad (7.55)$$

From the coefficient a_0, a lower limit on the integral time is given

$$\tau_I > \tau_z \quad (7.56)$$

There is a lower limit on the K which are obtained from the coefficients a_1 and a_0 where $\tau_I > \tau_z$:

$$K > 0$$

Since the upper limit must be greater than the lower limit on the loop gain, the lower bound on the derivative time is obtained

$$\tau_D > \frac{\tau_z \tau_p}{\tau_p - \tau_z} \tag{7.57}$$

where τ_p must be greater than τ_z. The derivative time must be bounded from above, otherwise, there is no stable PID controller exists for stabilizing the second-order integrating-unstable process.

Remark 18. *If $\tau_p < \tau_z$, we will get a lower limit on the derivative time given by*

$$\tau_D < \frac{-\tau_z \tau_p}{\tau_z - \tau_p}$$

Since the derivative time must be negative leads to a lower limit on the loop gain instead of upper limit from the coefficient a_3 as follows:

$$K > \frac{-\tau_p}{\tau_z |\tau_D|}$$

and a negative upper limit will be obtained from coefficient a_2 as

$$K < \frac{-1}{\tau_z + |\tau_D|}$$

Since this upper limit is less than maximum lower limit $K > 0$, so this implies that PID controller cannot stabilize the process (7.30) *if $\tau_p < \tau_z$.*

On the other hand, Theorem 4.2.2 (sufficient criterion) stipulates that $b > 0$ in the Routh array, which give a lower limit on the integral time as

$$\tau_I > \frac{\tau_p - K\tau_z\tau_D}{K(\tau_D - \tau_z) - 1} + \tau_z \tag{7.58}$$

Based on the limits on K, τ_I and τ_D obtained, it can be readily shown that the stabilizing regions of those parameters are limited for the given standard single-loop PID controller. Thus, this motivates the use of DL-MSC scheme.

7.1.5 Illustrative Examples

7.1.5.1 Example 1

A real case of nonlinear fed-batch bioethanol production is used as a case study in this paper [193]. A linearized open-loop second order unstable integrating process (SOUIP) is used to demonstrate the effectiveness of the proposed control scheme as follows:

$$P(s) = \frac{Gl(s)}{F(s)} = \frac{-13.99(-3.81s+1)}{s(3.83s-1)} \tag{7.59}$$

Based on (7.30), the process parameters are stated as: $K_p = -13.99$, $\tau_z = 3.81$ and $\tau_p = 3.83$. Following (7.59) shows that the lower limit on the derivative (7.57) given by

$$\tau_D = \frac{(3.81)(3.83)}{(3.83-3.81)} = 729.6$$

Since τ_p is very close to τ_z, this indicates that the system will be very difficult to control using a standard single-loop PID controller. Within a very limited stabilizing region, we need a very high value of derivative time to deliver closed-loop stability. In practice, this closed-loop system will be very sensitive to uncertainties and noise in measurement will seriously degrade the controller due to a very large action from derivative mode. Hence, even if the system can be stabilized by a PID controller, it is unlikely that we can obtain a satisfactory performance in practice. So this shall motive the use of DL-MSC scheme which can not only stabilize the system but also can provide better performance within adequate robustness margin.

The $-\tau_z$ and negative pole value causes the inverse response and unstable open-loop system respectively. Note that, the process is extremely difficult to stabilize with the conventional PID controller including with some of the advanced control techniques, e.g., Linear-Quadratic Gaussian (LQG) and robust control. So far, there is no report in the open literature of a control scheme which can stabilize such a type of processes.

The design procedure of the proposed control system is shown in Section 6.3.3.4. The secondary controller is obtained by specifying the tuning parameter $r_2 = 7.5$ in order to pre-stabilize the unstable process, which leads to $K_{c2} = -29.14$ by using (7.45). For the main controller, the finalized MSC tuning values are $\lambda_1 = 5$, $r_1 = 3$ and $\gamma = 2$, which leads to GM = 8.04dB and PM = 46.1°. Thus, the MSC-PID controller is given by

$$G_c(s) = -0.0481\left(1 + \frac{1}{24.8480s}\right)\left(\frac{0.5887s+1}{0.1177s+1}\right) \tag{7.60}$$

The maximum peak of sensitivity function is given as $M_s = 1.67$, which is within the recommended range. Note that, a set point pre-filter (F_r) is suggested in order to reduce the overshoot response in setpoint tracking. The setpoint pre-filter is expressed by

$$F_r = \frac{\frac{\tau_I}{3}s + 1}{\tau_I s + 1} \tag{7.61}$$

In order to compare the performances of proposed MSC scheme, a Skogestad IMC (SIMC) tuning are designed based on a double-loop control scheme [194]. The PID with filter based on double-loop SIMC tuning is shown as follows:

$$G_c(s) = -0.00034\left(\frac{2.2s + 1}{s}\right)\left(\frac{35s + 1}{1.1s + 1}\right) \tag{7.62}$$

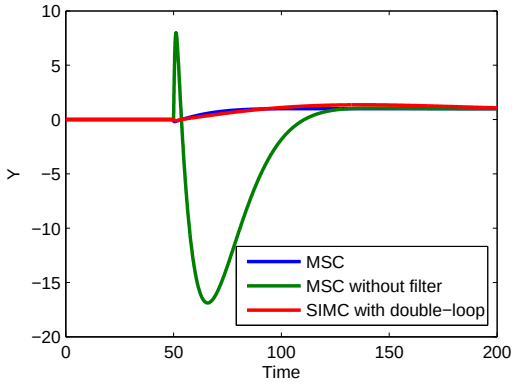

Figure 7.5: Nominal response for setpoint tracking

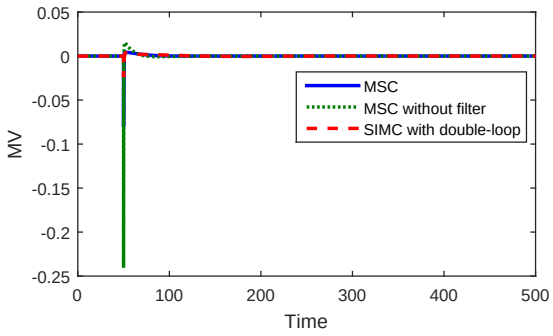

Figure 7.6: Response of manipulated variable for setpoint tracking

The performances of the proposed control system design are presented based on the response of setpoint tracking, output disturbance and input distrubance with 1 unit step changes. In Figure 7.5, the settling time of the proposed MSC

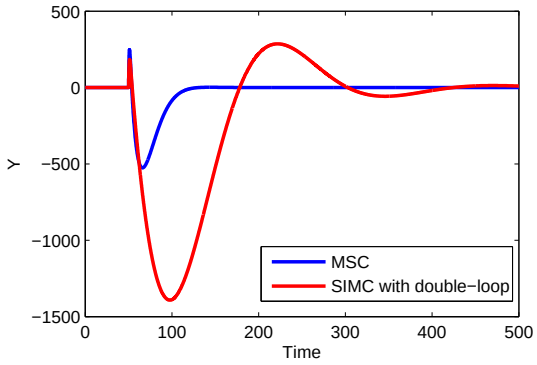

Figure 7.7: Nominal response for output disturbance rejection

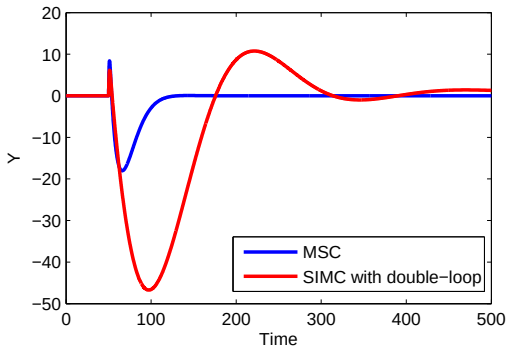

Figure 7.8: Nominal response for input disturbance rejection

scheme is much improved with the employ of setpoint pre-filter and SIMC tuning, i.e. 63 units, which gives a smooth response and faster settling time. Noted that, the setpoint pre-filter is able to reduce the overshoot and underdamped responses in setpoint tracking, which does not affect the disturbances rejection performance. Figure 7.7 and Figure 7.8 demonstrate the output and input disturbance rejection responses respectively. Obviously, the proposed MSC scheme shows improved performance compared to the established control strategy, i.e. SIMC tuning. The responses of manipulated variable for each control schemes with setpoint tracking are shown in Figure 7.6, which shows no obvious impulsive spikes occurred on the manipulated variable for DL-MSC scheme. The simulation of the responses of manipulated variable for disturbance rejection has been done but no impulsive spikes were observed instead.

7.1.5.2 Example 2

We consider the P_4 from Section 5.1.3, which can be reduced to a second-order integrating-unstable process based on the model reduction algorithm from [189–191].

$$P(s) = \frac{Gl(s)}{F(s)} \cong \frac{-0.73(-79.7s+1)}{s(13.5s-1)} \tag{7.63}$$

Note that, this dynamics cannot be controlled using a standard single-loop PID controller as $\tau_p < \tau_z$ giving a negative upper limit of τ_D which leads to negative upper limit on the loop gain, hence unstable closed-loop system will result. Thus, the DL-MSC scheme can be used in order to provide better control performance.

Base on the proposed control system design, the secondary controller obtained is $K_{c2} = 1.86$ by specifying the tuning parameter $r_2 = 90$, which convert the integrating system into the pre-stabilized system. By setting (through a trial-and-error) the MSC tuning parameter $\lambda_1 = 2.5$, $r_1 = 9$ and $\gamma = 2.6$, the MSC-PID controller is obtained

$$G_c(s) = -0.6062\left(1 + \frac{1}{520.65s}\right)\left(\frac{0.1517s+1}{0.0169s+1}\right) \tag{7.64}$$

which has a GM = 8.04 dB, PM = 46.9°and $M_s = 1.66$ respectively. Note that, the setpoint prefilter is not applied in this case as the overshoot is not significant.

The integrating-unstable system is difficult to control by using some existing control schemes. It is worth to highlight that, the Skogestad IMC (SIMC), Ziegler-Nichols (ZN) frequency response tuning and LQG synthesis are unable to design the controller based on a double-loop control scheme.

The performances of the proposed DL-MSC scheme are evaluated based on 1 unit step changes in the response of setpoint tracking, output disturbance and input disturbance, which are shown in Figure 7.9, Figure 7.10 and Figure 7.11 respectively. The simulation of the responses of manipulated variable for setpoint tracking and disturbance rejection has been done but no impulsive spikes were observed.

7.2 Summary

A new variant of an MSC scheme with double-loop control structure which unifies the direct and indirect MSC schemes has been presented for NMP integrating-unstable systems, which are difficult to control using standard single-loop feedback structure, or even the double-loop structure employing some existing PID

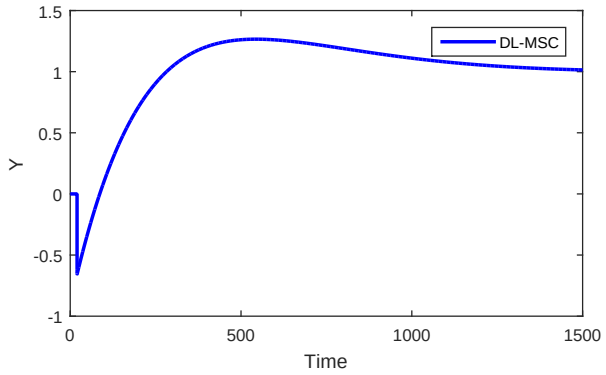

Figure 7.9: Nominal response for setpoint tracking

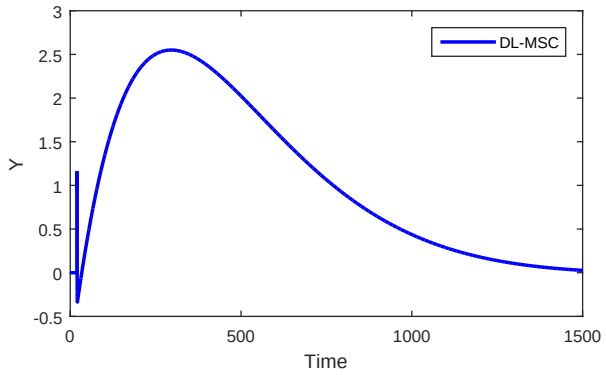

Figure 7.10: Nominal response for output disturbance rejection

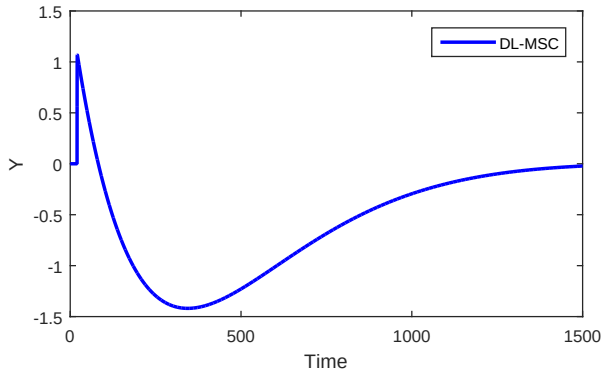

Figure 7.11: Nominal response for input disturbance rejection

tuning methods, e.g., well-known LQG, SIMC and ZN tuning methods. Note that, the DL-MSC scheme can be extended into triple-loop multi-scale control scheme (TL-MSC), which will be presented in Chapter 8. The TL-MSC scheme can be used to control some of the most complex forms of dynamic behavior which

cannot be stabilized using existing single-loop controllers. These very complex dynamic behaviors can occur during a fed-batch fermentation process. These complex dynamic behaviors can be represented by fourth-order integrating-unstable models with multiple RHP zeros. Please note that, part of the work described in this chapter has been published in IOP Science[1].

[1]Qiu Han Seer and Jobrun Nandong. A unified double-loop multi-scale control strategy for NMP integrating-unstable systems. *IOP Conference Series: Materials Science and Engineering*, 121 (1): 12-21, 2016.

Chapter 8

Triple-loop Multi-scale Control Scheme

It is worth to highlight that, a linearization at any given operating point of even the simplest fed-batch system of differential algebraic equations (DAE system), e.g., with only four state variables and one input variable can lead to a complex fourth-order integrating dynamics as previously reported in Chapter 5. One of the most intriguing form of dynamic behaviors that can occur at some points during the fed-batch operation is a fourth-order integrating-unstable plus oscillatory system with multiple RHP zeros. To deal with the stabilization of this complex dynamics, a new triple-loop multi-scale control (TL-MSC) scheme is proposed. This scheme aims to first decompose the complex dynamics into three simpler sub-systems, which are then separately addressed within the proposed multi-scale structure. This chapter presents both the fundamental of TL-MSC scheme and the details of its design. A typical fed-batch alcoholic fermentation reported in Chapter 5 is used as an example to demonstrate the applicability of the new scheme.

8.1 Fundamental of Triple-loop Multi-scale Control Scheme

8.1.1 Realization Block Diagram

The model in (5.8) can be decomposed into 3 basic modes

$$P = \underbrace{\frac{k_1}{s}}_{M_0} + \underbrace{\frac{k_2}{\tau_p s + 1}}_{M_1} + \underbrace{\frac{k_3 s + k_4}{\alpha_2 s^2 + \alpha_1 s + 1}}_{M_2} \tag{8.1}$$

where the mode parameters k_j, $j = 1, 2, 3, 4$ are obtained via the procedure in the Appendix D.3.

The decomposition in (8.1) assumes that in term of dynamics, the integrating mode M_0 is the slowest, followed by the stable first-order mode M_1 and the second-order underdamped unstable mode M_2 is the fastest. An interesting point to note is that, the third mode M_2 is not only unstable (i.e., $\alpha_2 > 0$ and $\alpha_1 < 0$) but also it exhibits an inverse-response, i.e., $b = k_3/k_4 < 0$.

A process which has a combination of integrating and unstable underdamped modes as in (8.1) is extremely difficult to control (or might be even impossible to stabilize using a PID-type controller) via a standard single-loop feedback control structure. For the process given in (8.1), it is imperative to introduce a more advanced control structure, which not only can stabilize the process but also can provide good closed-loop performance and robustness. A possible choice of an advanced control structure is the proposed triple-loop multi-scale control (TL-MSC) scheme.

The details of multi-scale control (MSC) scheme can be found in [133, 154]. The block-diagram of the proposed TL-MSC scheme is shown in Figure 8.1. The scheme has three controllers. First, the tertiary controller G_{c2} is used to stabilize the unstable underdamped mode M_2 leading to a pre-stabilized system but it still exhibits both integrating mode and stable underdamped mode with an unstable zero, i.e., nonminimum-phase mode. This pre-stabilized system is still quite difficult to control due to the presence of the nonminimum-phase underdamped mode. Thus, the secondary controller G_{c1} is then needed to provide further stabilization of the pre-stabilized integrating-underdamped system, thereby it is desired to convert the process P into an overdamped self-regulating system. This overdamped self-regulating system is quite easy to control compared with the original process P. Finally the primary controller G_{c0} is required as to provide a desired control performance-robustness trade-off of the overall system.

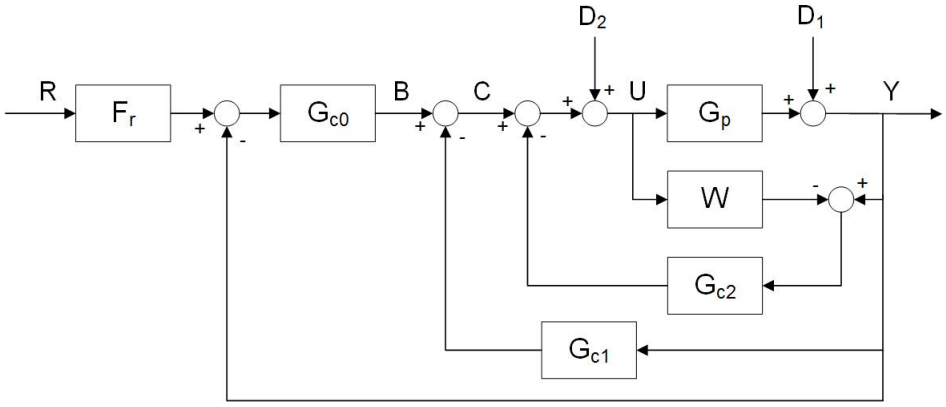

Figure 8.1: Block diagram of the triple-loop MSC scheme

In Figure 8.1, R, Y, D_1 and D_2 denote the setpoint, output variable, output disturbance and input disturbance signals respectively; W represents the multi-scale predictor.

The multi-scale predictor in the proposed scheme is chosen to be the slower M_0 and M_1 modes as follows:

$$W = \frac{k_1}{s} + \frac{k_2}{\tau_p s + 1} \tag{8.2}$$

In other words, the tertiary controller is designed based on the indirect MSC scheme [155] where the controller is primarily intended to stabilize the unstable M_2 mode. It is interesting to point out that under a perfect model assumption, the tertiary loop in Figure 8.1 can be represented as in Figure 8.2. Figure 8.2 clearly shows that G_{c2} only serves to directly control (stabilize) the M_2 mode.

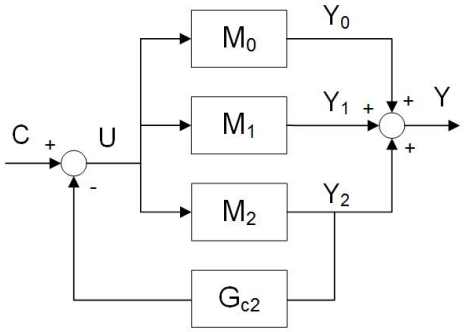

Figure 8.2: Equivalent block-diagram representation of the tertiary inner-loop

Based on Figure 8.2, corresponding to the tertiary loop the closed-loop transfer

function from C to Y is given by

$$P_{a1} = \frac{Y}{C} = \frac{P}{1 + G_{c2}M_2} \tag{8.3}$$

The equation (8.3) represents the first pre-stabilized process.

8.1.2 Stabilization of the Unstable Mode

Case 1: $\tau_p > 0$, $\alpha_2 > 0$ and $\alpha_1 < 0$

We consider a case where the second order M_2 mode is unstable, i.e., $\alpha_1 < 0$. Let us re-write the unstable mode as follows:

$$M_2 = \frac{k_{p2}(bs + 1)}{\alpha_2 s^2 + \alpha_1 s + 1} \tag{8.4}$$

where $k_{p2} = k_4$ and $b = \frac{k_3}{k_4}$.

Referring to Figure 8.2, the transfer function from C to U is given by

$$H_u = \frac{U}{C} = \frac{1}{1 + G_{c2}M_2} \tag{8.5}$$

In the present work, the tertiary controller is chosen to be a proportional-derivative (PD) controller, i.e.:

$$G_{c2} = K_{c2}(1 + \tau_{D2}s) \tag{8.6}$$

Remark 19. *It is desired to use a simple controller algorithm for the tertiary loop for easy controller design. It can easily be shown that the simplest P-only controller is unable to stabilize the unstable M_2 mode with the presence of an unstable zero in the mode. Thus, a PD controller is chosen as it can stabilize the mode and the controller is quite simple to use in practice.*

Notice that, the characteristic equation in (8.5) is given by

$$(\alpha_2 + K_{c2}k_{p2}b\tau_{D2})s^2 + [\alpha_1 + K_{c2}k_{p2}(b + \tau_{D2})]s + K_{c2}k_{p2} + 1 = 0 \tag{8.7}$$

Upon applying the necessary criterion of Routh stability to the characteristic equation, the following inequalities are obtained

$$K_{c2}k_{p2} > -1 \tag{8.8}$$

$$\alpha_1 + K_{c2}k_{p2}(b + \tau_{D2}) > 0 \tag{8.9}$$

$$\alpha_2 + K_{c2}k_{p2}b\tau_{D2} > 0 \tag{8.10}$$

In order to obtain the lower and upper limits on the loop gain, we propose to further divide the case 1 into two sub-cases detailed as follows.

Case 1.1: $b < 0$ and $\tau_{D2} > 0$

From (8.10), an upper limit on the loop gain can be described as

$$K_{c2}k_{p2} < \frac{\alpha_2}{|b|\tau_{D2}} \tag{8.11}$$

The lower limit on loop gain is obtained from (8.9)

$$K_{c2}k_{p2} > \frac{|\alpha_1|}{\tau_{D2} - |b|} \tag{8.12}$$

Note that, the upper limit (8.11) must be greater than the lower limit (8.12) for stability. Upon simplification, the range of derivative time is given by

$$\tau_{D2} > \frac{|b|\alpha_2}{\alpha_2 - |b||\alpha_1|} \tag{8.13}$$

The range of derivative time (8.13) holds for stability only if

$$\alpha_2 - |b||\alpha_1| > 0 \tag{8.14}$$

Otherwise, the derivative time has to change sign (i.e., negative) to produce closed-loop stability, and this issue is dealt with in the following case 1.2.

Case 1.2: $b < 0$ and $\tau_{D2} < 0$

From (8.10), a lower limit on the loop gain is obtained

$$K_{c2}k_{p2} > \frac{-\alpha_2}{|b||\tau_{D2}|} \tag{8.15}$$

whereas (8.9) leads to an upper limit given as

$$K_{c2}k_{p2} < \frac{-|\alpha_1|}{|\tau_{D2}| + |b|} \tag{8.16}$$

To stabilize the unstable M_2 mode (tertiary loop), it is necessary that the upper limit (8.16) is greater than the lower limit (8.15). Hence, absolute value for the derivative time that leads to stability must be

$$|\tau_D| < \frac{|b|\alpha_2}{|b||\alpha_1| - \alpha_2} \tag{8.17}$$

More specifically, the range of derivative time that provides stability is

$$\tau_D > \frac{|b|\alpha_2}{\alpha_2 - |b||\alpha_1|} \tag{8.18}$$

where the range of derivative time (8.18) holds for stability only if

$$\alpha_2 - |b||\alpha_1| < 0 \tag{8.19}$$

8.1.2.1 Tertiary Controller Tuning

Note that, choosing an appropriate value for the derivative time is important to ensure closed-loop stability of the tertiary loop. We propose to first specify the value for the derivative time before specifying the value for the controller gain. Here, two PD controller tuning rules are proposed as follows.

PD Controller Tuning for Case 1.1:

Based on the range of derivative time (8.13), the value of the derivative time can be determined as follows

$$\tau_{D2} = F_{TD}\left(\frac{|b|\alpha_2}{\alpha_2 - |b||\alpha_1|}\right) \tag{8.20}$$

where the tuning parameter $F_{TD} > 1$ is introduced.

After the derivative time is determined, the controller gain can be obtained based on the upper limit in (8.11) which yields the following relation

$$K_{c2} = \frac{F_{TC}}{k_{p2}}\left(\frac{\alpha_2}{|b|\tau_{D2}}\right) \tag{8.21}$$

where the tuning parameter F_{TC} is introduced and for ensuring stability its range is

$$\frac{|b||\alpha_1|\tau_{D2}}{\alpha_2(\tau_{D2} - |b|)} < F_{TC} < 1 \tag{8.22}$$

Notice that, the application of the tuning relations (8.20) and (8.21) requires the determination of appropriate values for F_{TD} and F_{TC}, which can be done manually or by some optimization techniques. Such tuning task can be eliminated by establishing some fixed tuning relations, which can directly ensure that the tertiary controller is able to stabilize the unstable M_2 mode. At this stage, it is not necessary to achieve a specific control performance, i.e., only stabilization of the mode is required. Thus, it is important to specify the values for the derivative time and controller gain that lead to stability. This can be easily done via the proposed Average Value Tuning (AVT) rule described in the following section.

Average Value Tuning Rule

The AVT rule is proposed to remove the need for tedious manual tuning of the tertiary controller. The AVT rule is established as follows.

First, notice that the value of τ_D affects both the upper and lower limits shown in (8.11) and (8.12) respectively. It is desired that the difference (i.e., ratio of the

upper to lower limit) between these limits to be large enough to ensure sufficient controller robustness, hence closed-loop stabilization. The ratio between the two limits is expressed by

$$\kappa_{UL} = \frac{\alpha_2(\tau_{D2} - |b|)}{\tau_{D2}|\alpha_1||b|}, \quad \kappa_{UL} > 1 \tag{8.23}$$

Hence, the derivative time can be written in the form of

$$\tau_{D2} = \frac{|b|\alpha_2}{\alpha_2 - \kappa_{UL}|b||\alpha_1|} \tag{8.24}$$

In (8.24), the denominator must be positive, i.e., $\alpha_2 - \kappa_{UL}|b||\alpha_1| > 0$. To ensure the denominator is always positive, the following equality is imposed

$$\kappa_{UL}|b||\alpha_1| = \frac{\alpha_2 + |b||\alpha_1|}{2} \tag{8.25}$$

After substituting (8.25) into (8.24), the derivative time is expressed by

$$\tau_{D2} = \frac{2|b|\alpha_2}{\alpha_2 - |b||\alpha_1|} \tag{8.26}$$

Next, let us specify the value of loop gain such that it is equal to the average value between the upper limit (8.11) and lower limit (8.12), which leads to the controller gain relation

$$K_{c2} = \frac{1}{2k_{p2}}\left(\frac{\alpha_2}{|b|\tau_{D2}} + \frac{|\alpha_1|}{\tau_{D2} - |b|}\right) \tag{8.27}$$

Please note that, the relations in (8.26) and (8.27) for calculating τ_{D2} and K_{c2} represent the AVT rule for PD controller design.

PD Controller Tuning for Case 1.2:

For this case, the derivative time is written as

$$\tau_{D2} = F'_{TD}\left(\frac{|b|\alpha_2}{\alpha_2 - |b||\alpha_1|}\right) \tag{8.28}$$

Here, the tuning parameter $F'_{TD} < 1$ is imposed to be consistent with the lower limit in (8.18).

To ensure stability, the ratio of the lower limit (8.15) to the upper limit (8.16) must be greater than unity, where

$$\kappa_{LU} = \frac{\alpha_2(|\tau_{D2}| + |b|)}{|\tau_{D2}||\alpha_1||b|}, \quad \kappa_{LU} > 1 \tag{8.29}$$

Hence, the derivative time can also be written in the form of

$$\tau_{D2} = \frac{|b|\alpha_2}{\alpha_2 - \kappa_{LU}|b||\alpha_1|} \tag{8.30}$$

Note that, the denominator in (8.30) must be negative, i.e., $\alpha_2 - \kappa_{LU}|b||\alpha_1| < 0$. Let us specify $\kappa_{LU}|b||\alpha_1|$ as follows:

$$\kappa_{LU}|b||\alpha_1| = |b||\alpha_1| + \frac{|b||\alpha_1| + \alpha_2}{2} \tag{8.31}$$

Upon substituting (8.31) into (8.30), the derivative time can be determined by

$$\tau_{D2} = \frac{2|b|\alpha_2}{\alpha_2 - 3|b||\alpha_1|} \tag{8.32}$$

The controller gain can be determined from the knowledge of the upper limit from (8.16)

$$K_{c2} = \frac{F'_{TC}}{k_{p2}} \frac{-|\alpha_1|}{|\tau_{D2}| + |b|} \tag{8.33}$$

For stability, the tuning parameter must lie in the following range

$$F'_{TC} = 1 < F'_{TC} < \frac{\alpha_2(|\tau_{D2}| + |b|)}{|\tau_{D2}||\alpha_1||b|} \tag{8.34}$$

Alternatively, by using the AVT rule the value of the controller gain is specified as follows:

$$K_{c2} = \frac{1}{2k_{p2}} \left(- \frac{\alpha_2}{|b||\tau_D|} - \frac{|\alpha_1|}{|\tau_D| + |b|} \right) \tag{8.35}$$

Remark 20. *The controller gain relation* (8.35) *for the case 1.2 gives more conservative value than that of the case 1.1 in* (8.27)*. The reason is that, for the case 1.2 the mode has an unstable zero ($b < 0$) which imposes a serious limitation on the control performance. In contrast, for the case 1.1 the mode has a stable zero which does not impose serious limitation on the control performance, hence, the controller can afford to be more aggressive.*

8.1.3 Secondary Controller Tuning

After stabilizing the unstable M_2 mode, the first pre-stabilized overall process becomes

$$P_{a1} = \frac{K_{pa1} \prod_{i=1}^{3} (\tau_{zi} s + 1)}{s(\tau_p s + 1)(\beta_2 s^2 + \beta_1 s + 1)} \tag{8.36}$$

where $\beta_j > 0$, $j = 1, 2$ and $K_{pa1} = \frac{K_p}{1 + K_{c2} k_{p2}}$.

The pre-stabilized process remains an integrating one and which probably possesses underdamped but stable mode. Unlike in the original process (5.9), the pre-stabilized process (8.36) can be stabilized using the simplest P-only controller. Thus, the secondary controller is chosen to be a P-only controller, i.e., $G_{c1} = K_{c1}$.

Corresponding to the secondary loop, the characteristic equation is given as

$$\begin{aligned} &\tau_p\beta_2 s^4 + (\tau_p\beta_1 + \beta_2 + K_{c1}K_{pa1}\tau_{z1}\tau_{z2}\tau_{z3})s^3 \\ &+ [\tau_p + \beta_1 + K_{c1}K_{pa1}(\tau_{z1}(\tau_{z2} + \tau_{z3}) + \tau_{z2}\tau_{z3})]s^2 \\ &+ [1 + K_{c1}K_{pa1}(\tau_{z1} + \tau_{z2} + \tau_{z3})]s + K_{c1}K_{pa1} = 0 \end{aligned} \tag{8.37}$$

Based on the necessary criterion of Routh stability, all of the coefficients in (8.37) must be positive. Obviously, regardless of the values of the model parameters in (8.36), one of the lower limits is fixed as

$$K_{c1}K_{pa1} > 0 \tag{8.38}$$

In view of the assumption that $\tau_{z1} < 0$, $\tau_{z2} < 0$, $\tau_{z3} > 0$ and $\tau_p > 0$, it is noticed that the coefficient of s^3 can also leads to a lower limit. However, it is always smaller than (8.38), which can be ignored.

With regard to the coefficients of s^2 and s, either upper or lower limit might be formed depending on which one of the following 3 conditions holds.

C.1. $\tau_{z1}(\tau_{z2} + \tau_{z3}) + \tau_{z2}\tau_{z3} < 0$ and $\tau_{z1} + \tau_{z2} + \tau_{z3} < 0$

C.2. $\tau_{z1}(\tau_{z2} + \tau_{z3}) + \tau_{z2}\tau_{z3} > 0$ and $\tau_{z1} + \tau_{z2} + \tau_{z3} < 0$

C.3. $\tau_{z1}(\tau_{z2} + \tau_{z3}) + \tau_{z2}\tau_{z3} < 0$ and $\tau_{z1} + \tau_{z2} + \tau_{z3} > 0$

Notice that, case 4 (i.e., both terms greater than 0) is not possible.

Given the condition C.1, the following upper limits U_{L1} and U_{L2} are obtained

$$K_{c1}K_{pa1} < U_{L1} = \frac{\tau_p + \beta_1}{|\tau_{z1}(\tau_{z2} + \tau_{z3}) + \tau_{z2}\tau_{z3}|} \tag{8.39}$$

$$K_{c1}K_{pa1} < U_{L2} = \frac{1}{|\tau_{z1} + \tau_{z2} + \tau_{z3}|} \tag{8.40}$$

As for the condition C.2, another lower limit is obtained as follows

$$K_{c1}K_{pa1} > -\frac{\tau_p + \beta_1}{\tau_{z1}(\tau_{z2} + \tau_{z3}) + \tau_{z2}\tau_{z3}} \tag{8.41}$$

while an upper limit is as (8.40).

Corresponding to the condition C.3, an upper limit is as (8.39) while another lower limit is

$$K_{c1}K_{pa1} < -\frac{1}{\tau_{z1} + \tau_{z2} + \tau_{z3}} \tag{8.42}$$

Remark 21. *The lower limit given by* (8.38) *is a common limit for all conditions. Another lower limit in* (8.41) *is imposed by the condition C.2 and* (8.42) *imposed by C.3. Under C.1, 2 upper limits* (8.39) *and* (8.40) *exist but the lowest one should be cosnidered to ensure stability. Under C.2, the upper limit is given only by* (8.40) *and under C.3 the upper limit is only by* (8.39).

P Controller Tuning Rules

Please note that, a new tuning parameter R_1 is introduced in order to obtain K_{c1} via the following tuning rules.

In the case when the condition C.1 holds, the controller gain is expressed as follows

$$K_{c1} = \begin{cases} \dfrac{U_{L1}}{R_1 K_{pa1}} & \text{for } U_{L1} < U_{L2},\ R_1 > 1 \\ \dfrac{U_{L2}}{R_1 K_{pa1}} & \text{for } U_{L2} < U_{L1},\ R_1 > 1 \end{cases} \tag{8.43}$$

If the condition C.2 holds, then the controller gain is given as

$$K_{c1} = \frac{U_{L2}}{R_1 K_{pa1}}, \quad R_1 > 1 \tag{8.44}$$

If the condition C.3 holds, then

$$K_{c1} = \frac{U_{L1}}{R_1 K_{pa1}}, \quad R_1 > 1 \tag{8.45}$$

where U_{L1} and U_{L2} are as in (8.39) and (8.40) respectively.

Remark 22. *In order to ensure closed-loop stability, it is important to impose $R_1 > 1$. The larger the value of R_1 the less aggressive is the controller action, i.e., as the loop gain moves further away from the lowest upper limit. It is proposed to set a value for R_1 which simultaneously gives a maximum peak of sensitivity function M_{s1} of the secondary loop in the range of $M_{s1} = [1.5 \quad 2.5]$, and such that the closed-loop poles are all real and distinct.*

The controller gain K_{c1} is calculated by specifying an appropriate value for the tuning parameter R_1. Since we propose to set R_1 to a value which will lead to real and distinct closed-loop poles of the secondary loop, the closed-loop transfer function from B to Y can be written in the form of

$$P_{a0} = \frac{P_{a1}}{1 + G_{c1} P_{a1}} = \frac{K_{pa0} \prod_{i=1}^{3} (\tau_{zi} s + 1)}{\prod_{j=0}^{3} (\tau_j s + 1)} \tag{8.46}$$

Here, the closed-loop time constants $\tau_j > \tau_{j+1}$, $j = 0, 1, 2, 3$ and the overall gain $K_{pa0} = K_{c1}^{-1}$.

The maximum peak of sensitivity function for the secondary loop is calculated as follows

$$M_{s1} = \max_{\omega} \|[1 + K_{c1}(j\omega)G_{pa1}(j\omega)]^{-1}\|_{\infty} \tag{8.47}$$

8.1.4 Primary Controller Tuning

8.1.4.1 Model Reduction

For the main (primary) controller G_{c0}, we propose to use a PID controller augmented with a filter based on the second pre-stabilized process (8.46). As the pre-stabilized process (8.46) is complex and high-order, it is recommended to design the controller via the multi-scale control (MSC) scheme for effective controller tuning. In view of the assumption that one of the process zeros, i.e., $\tau_{z3} > 0$, the model in (8.46) can be further simplified to a third-order system using the Skogestad half-rule [194], which leads to a reduced model in the form of

$$\overline{P}_{a0} \cong \frac{K_0(\tau_{z1}s + 1)(\tau_{z2}s + 1)}{(\tau_1 s + 1)(\tau_2 s + 1)(\tau_3 s + 1)} \tag{8.48}$$

where the process gain is $K_0 = \frac{\tau_{z3}}{\tau_0 K_{c1}}$. Bear in mind that, the process model in (8.48) is used to design the primary controller. The first step in the MSC scheme is to decompose the given process model (8.48) into its 3 basic factors or modes, which in this case are all first order systems with real coefficients.

8.1.4.2 Model Decomposition

The model decomposition is carried out by applying the partial fraction expansion to the reduced process model (8.48), which leads to 3 basic modes, i.e., m_1, m_2 and m_3.

$$\overline{P}_{a0} = \underbrace{\frac{k_{m1}}{\tau_1 s + 1}}_{m_1} + \underbrace{\frac{k_{m2}}{\tau_2 s + 1}}_{m_2} + \underbrace{\frac{k_{m3}}{\tau_3 s + 1}}_{m_3} \tag{8.49}$$

where m_j is slower than m_{j+1} for $j = 1, 2$. The mode gains are given by

$$k_{m1} = \frac{K_0(\tau_1 - \tau_{z1})(\tau_1 - \tau_{z2})}{(\tau_1 - \tau_2)(\tau_1 - \tau_3)} \tag{8.50}$$

$$k_{m2} = \frac{K_0(\tau_2 - \tau_{z1})(\tau_2 - \tau_{z2})}{(\tau_2 - \tau_1)(\tau_2 - \tau_3)} \tag{8.51}$$

$$k_{m3} = \frac{K_0(\tau_3 - \tau_{z1})(\tau_3 - \tau_{z2})}{(\tau_3 - \tau_1)(\tau_3 - \tau_2)} \tag{8.52}$$

The next step after the model decomposition is to design a sub-controller for each of the three basic modes. For simplicity, P-only controller form is chosen for the sub-controllers controlling the second and third modes while for the outermost (slowest) mode a PI controller form is used.

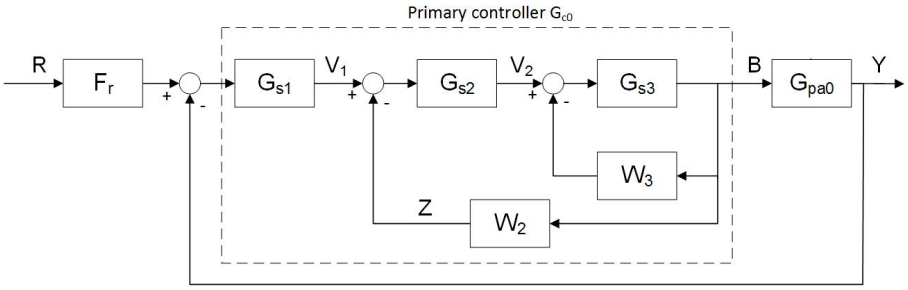

Figure 8.3: Block diagram illustrating the primary controller design via the MSC scheme

Figure 8.3 shows the block diagram of the primary controller design via the direct multi-scale control (MSC) scheme. Note that, G_{s1}, G_{s2} and G_{s3} denote the outermost, inner-layer and innermost sub-controllers; P_{a0} is the pre-stabilized process in (8.46); W_i, $i = 2, 3$ represent the multi-scale predictors selected to be $W_3 = m_3$ and $W_2 = m_2$.

8.1.4.3 Sub-controller Design for the Innermost Mode m_3

Consider a P-only controller with the gain $G_{s3} = k_{s3}$ which can be calculated via [133]

$$k_{s3} = \frac{\lambda_3 - 1}{k_{m3}}, \quad \lambda_3 > 1 \tag{8.53}$$

where λ_3 represents a ratio of the open loop time constant to the closed time constant corresponding to the mode m_3, i.e., $\lambda_3 = \frac{\tau_3}{\tau_{3c}} = k_{m3}k_{s3} + 1$ where the closed-loop time constant is $\tau_{3c} = \frac{\tau_3}{k_{m3}k_{s3}+1} = \frac{\tau_3}{\lambda_3}$.

The corresponding closed-loop inner layer transfer function is

$$g_3 = \frac{B}{V_2} = \frac{k_{s3}^0(\tau_3 s + 1)}{\tau_{3c}s + 1} \tag{8.54}$$

where the overall gain is $k_{s3}^0 = \frac{\lambda_3 - 1}{\lambda_3 k_{m3}}$.

The augmented transfer function of the mode m_2 becomes

$$h_2 = \frac{Z}{V_2} = \frac{k_{m2}^0(\tau_3 s + 1)}{(\tau_{3c}s + 1)(\tau_2 s + 1)} \tag{8.55}$$

where the augmented gain is $k_{m2}^0 = \frac{k_{m2}(\lambda_3 - 1)}{\lambda_3 k_{m3}}$.

Please note that, the next sub-controller is designed based on the augmented mode m_2 in (8.55).

8.1.4.4 Sub-controller Design for the Inner-layer Mode m_2

Again a P-only controller ($G_{s2} = k_{s2}$) is used to control the second (inner) mode, which can be calculated in the same way as the innermost sub-controller

$$k_{s2} = \frac{\lambda_2 - 1}{k_{m2}^0} = \frac{\lambda_3 k_{m3}(\lambda_2 - 1)}{k_{m2}(\lambda_3 - 1)} \tag{8.56}$$

where the sub-controller is designed based on the augmented mode m_2 in (8.55). As τ_{3c} and τ_3 are very small, it can be ignored in the closed-loop transfer function

$$g_2 = \frac{B}{V_1} = \frac{k_{s2}^0(\tau_2 s + 1)}{\tau_{2c} s + 1} \tag{8.57}$$

where the overall gain is $k_{s2}^0 = \frac{k_{s2}}{1 + k_{s2} k_{m2}^0}$ and τ_{2c} is the closed-loop time constant corresponding to the second mode.

The characteristic equation of the transfer function from V_1 to B is written as follows

$$\left(\frac{\tau_{3c}\tau_2}{1 + k_{s2}k_{m2}^0}\right)s^2 + \left(\frac{\tau_{3c} + \tau_2 + k_{s2}k_{m2}^0\tau_3}{1 + k_{s2}k_{m2}^0}\right)s + 1 = 0 \tag{8.58}$$

From the characteristic equation (8.58), notice that the closed-loop damping factor can be expressed in term of λ_i, $i = 2, 3$

$$\zeta_{2c} = \frac{\tau_3 + \lambda_3(\tau_2 + \tau_3(\lambda_2 - 1))}{2\sqrt{\lambda_3\lambda_2\tau_3\tau_2}} \tag{8.59}$$

where the closed-loop time constant is given as

$$\tau_{2c} = \sqrt{\frac{\tau_3\tau_2}{\lambda_3\lambda_2}} \tag{8.60}$$

We propose to tune λ_2 with a value above unity which leads to an overdamped behaviour $\zeta_{2c} > 1$. Specifically, it is proposed in this work to set λ_2 such that the closed-loop damping factor lies in the range of $\zeta_{2c} = [1.1 \quad 3]$. Since the closed-loop behaviour is overdamped, the augmented transfer function of the second loop simplifies to

$$q_2 = \frac{k_{s2}g_3}{1 + k_{s2}h_2} = \frac{k_{s2}^0(\tau_2 s + 1)(\tau_3 s + 1)}{(\tau_{2c1} s + 1)(\tau_{2c2} s + 1)} \tag{8.61}$$

where the overall gain in (8.61) is written in terms of λ_2

$$k_{s2}^0 = \frac{\lambda_2 - 1}{k_{m2}\lambda_2} \tag{8.62}$$

Meanwhile, the closed-loop time constants in (8.61) are

$$\tau_{2c1} = \frac{\tau_{2c}}{\zeta_{2c} - \sqrt{\zeta_{2c}^2 - 1}} \tag{8.63}$$

$$\tau_{2c2} = \frac{\tau_{2c}}{\zeta_{2c} + \sqrt{\zeta_{2c}^2 - 1}} \tag{8.64}$$

The augmented overall plant transfer function can be arranged as follows

$$P_0 = \overline{P}_{a0} q_2 = \frac{K_P^0(\tau_{z1}s + 1)(\tau_{z2}s + 1)}{(\tau_1 s + 1)(\tau_{2c1}s + 1)(\tau_{2c2}s + 1)} \tag{8.65}$$

where the overall augmented process gain expressed in terms of the tuning parameters λ_2

$$K_P^0 = \frac{\tau_{z3}(\lambda_2 - 1)}{k_{m2}\lambda_2\tau_0 K_{c1}} \tag{8.66}$$

The augmented overall plant transfer function (8.65) is used to design the outermost sub-controller which is chosen to take the form of a PI controller as

$$G_{s1} = k_{s1}\left(1 + \frac{1}{\tau_{I1}s}\right) \tag{8.67}$$

where k_{s1} and τ_{I1} denote the sub-controller gain and reset time respectively. One simple way to obtain these two parameters are discussed in the next section.

8.1.4.5 Sub-controller Design for the Outermost Mode m_1

The characteristic equation corresponding to the augmented overall plant in (8.65) assuming the outermost sub-controller is of the form (8.67)

$$\begin{aligned} &\tau_{I1}\tau_1\tau_{2c}^2 s^4 + [\tau_{I1}(2\tau_1\tau_{2c}\zeta_{2c} + \tau_{2c}^2) + k_{s1}K_P^0\tau_{I1}\tau_{z1}\tau_{z2}]s^3 \\ &+ [\tau_{I1}(\tau_1 + 2\tau_{2c}\zeta_{2c}) + k_{s1}K_P^0(\tau_{I1}(\tau_{z1} + \tau_{z2}) + \tau_{z1}\tau_{z2})]s^2 \\ &+ [\tau_{I1} + k_{s1}K_P^0(\tau_{I1} + \tau_{z1} + \tau_{z2})]s + k_{s1}K_P^0 = 0 \end{aligned} \tag{8.68}$$

Recall that, it has been assumed that $\tau_{z1} < 0$, $\tau_{z2} < 0$. Let us further assume that the reset time is set to a value greater than the sum of absolute values of τ_{z1} and τ_{z2}, i.e.:

$$\tau_{I1} = \mu|\tau_{z1} + \tau_{z2}|, \quad \mu > 1 \tag{8.69}$$

Due to the specification imposed in (8.69), from the characteristic equation in (8.68) the following limits are concluded

$$k_{s1}K_P^0 > 0 \tag{8.70}$$

$$k_{s1}K_P^0 > -\frac{\mu}{\mu-1}, \quad \mu > 1 \tag{8.71}$$

$$k_{s1}K_P^0 > -\frac{2\tau_1\tau_{2c}\zeta_{2c} + \tau_{2c}^2}{\tau_{z1}\tau_{z2}} \tag{8.72}$$

$$k_{s1}K_P^0 < \frac{\mu|\tau_{z1}+\tau_{z2}|(\tau_1 + 2\tau_{2c}\zeta_{2c})}{\mu(\tau_{z1}+\tau_{z2})^2 - \tau_{z1}\tau_{z2}} \tag{8.73}$$

Note that, there are three lower limits (8.70)-(8.72) and one upper limit (8.73) exist. We propose to use the upper limit (8.73) as a basis to calculate the value of k_{s1} by adjusting a parameter λ_1 as

$$k_{s1} = \frac{1}{\lambda_1 K_P^0}\left(\frac{\mu|\tau_{z1}+\tau_{z2}|(\tau_1 + 2\tau_{2c}\zeta_{2c})}{\mu(\tau_{z1}+\tau_{z2})^2 - \tau_{z1}\tau_{z2}}\right), \quad \lambda > 1 \tag{8.74}$$

Note that, the primary controller can be arranged as in the form of a classical PID controller augmented with a lead-lag filter, i.e.:

$$G_{c0} = G_{s1}q_2 = K_{c0}\left(1 + \frac{1}{\tau_{I1}s}\right)\left(\frac{\tau_2 s + 1}{\tau_{2c1}s + 1}\right)G_f \tag{8.75}$$

where the lead-lag filter is given as

$$G_f = \frac{\tau_3 s + 1}{\tau_{2c2}s + 1} \tag{8.76}$$

The primary controller gain in (8.75) is $K_{c0} = k_{s1}k_{s2}^0$ which can be simplified to

$$K_{c0} = \frac{\tau_0 K_{c1}}{\lambda_1 \tau_{z3}}\left(\frac{\mu|\tau_{z1}+\tau_{z2}|(\tau_1 + 2\tau_{2c}\zeta_{2c})}{\mu(\tau_{z1}+\tau_{z2})^2 - \tau_{z1}\tau_{z2}}\right) \tag{8.77}$$

Here, K_{c1} denotes the secondary controller gain given by either (8.43) or (8.44) or (8.45).

In summary, the tuning parameters for the primary controller G_{c0} are:λ_1, λ_2, λ_3 and μ. It should be noted that, λ_2 and λ_3 implicitly affect K_{c0} via the terms ζ_{2c} and τ_{2c} respectively.

The maximum peak of sensitivity function corresponding to the overall control system is

$$M_{s0} = \max_{\omega} \|[1 + G_{c0}(j\omega)G_{pa0}(j\omega)]^{-1}\|_\infty \tag{8.78}$$

Sometimes, it is necessary to include a setpoint pre-filter F_r to avoid impulsive spikes in both controller output and output variable responses following a step

change in the setpoint. Here, it is proposed to use a lead-lag pre-filter given in the form of

$$F_r = \frac{(\tau_{I1} + \tau_2)s/\epsilon + 1}{(\tau_{I1} + \tau_2)s + 1}, \quad \epsilon = [2 \quad 5] \tag{8.79}$$

8.2 Proposed Control Design Procedure

A simple procedure based on the established relationships in this work is proposed.

Step 1: Tune the tertiary controller $G_{c2} = K_{c2}(1 + \tau_{D2}s)$. If case 1.1, first calculate τ_{D2} using (8.26) and then K_{c2} via (8.27). If case 1.2, first calculate τ_{D2} using (8.32) and then K_{c2} via (8.35).

Step 2: Tune the secondary controller $G_{c1} = K_{c1}$. First, determine which one of the 3 conditions (C.1 or C.2 or C.3) holds: if C.1 then calculate K_{c1} via (8.43), else if C.2 calculate K_{c1} via (8.44), else C.3 use (8.45). Specify the value of the tuning parameter $R_1 > 1$ such that (a) the closed-loop poles are all real and distinct, and (b) the maximum peak of sensitivity function M_{s1} lies in the range of 1.5 and 2.5.

Step 3: Tune the primary controller G_{c0} in (8.75): set $\lambda_3 = 10$ and a value for λ_2 that gives damping factor in (8.59), i.e., $\zeta_{2c} = [1.1 \quad 3]$. Next, set $\mu = 1.1$ and tune λ_1 such that the maximum peak of sensitivity function M_{s0} lies between 1.5 and 2.5. Finally, the reset time is calculated using (8.69) while the controller gain using (8.77); the augmented filter is given in (8.76). Use (8.79) to tune the setpoint pre-filter by using a default value $\epsilon = 3$.

8.3 Illustrative Examples

From the aforementioned examples, the transfer function P_2 is chosen to demonstrate the effectiveness of the proposed control scheme as it is the most difficult to stabilize and control, which is given as follows:

$$P(s) = \frac{11.3}{s} + \frac{131.3}{60s + 1} + \frac{-638.7(-2.5s + 1)}{142.9s^2 - 13s + 1} \tag{8.80}$$

Two control schemes are used for controlling the process given in (8.80), i.e., triple-loop multi-scale control (TL-MSC) and robust control schemes. The control performances of these control schemes are evaluated via both simulation and Nyquist stability plot. Sequential step changes in setpoint, input disturbance and output disturbance are used to determine the nominal performances while

the general Nyquist stability plot is adopted for stability/robustness analysis. The dynamic simulation is performed by using Matlab Simulink, where the ode45 solver is used.

8.3.1 Triple-loop MSC scheme

The triple-loop MSC scheme is selected where three controllers are included. For the tertiary controller, the multi-scale predictor is chosen as:

$$W = \frac{11.3}{s} + \frac{131.3}{60s+1} \tag{8.81}$$

The tertiary controller is obtained by applying Average Value Tuning (AVT) rule, which is given by

$$G_{c2} = -0.0092(1 + 6.6043s) \tag{8.82}$$

The secondary controller is obtained as follows:

$$K_{c1} = 0.0046 \tag{8.83}$$

where $R_1 = 2$ and $M_{s1} = 2.2387$.

The finalized MSC tuning values for the primary controller are $\lambda_3 = 10$, $\lambda_2 = 5$, $\lambda_1 = 2.5$ and $\mu = 1.1$. The primary controller can be arranged as in the form of a classical PID controller augmented with a lead-lag filter, which is given by

$$G_{c0}(s) = 0.0014\left(1 + \frac{1}{71.16s}\right)\left(\frac{9.11s+1}{3.45s+1}\right)G_f \tag{8.84}$$

where the lead-lag filter is given as

$$G_f = \frac{2.12s+1}{0.11s+1} \tag{8.85}$$

which leads to Gain Margin (GM) = 7.49 dB, Phase Margin (PM) = 85.5°and $M_{s0} = 1.74$, which is within the recommended range.

Note that, a set point pre-filter (Fr) is suggested in order to reduce the overshoot response in setpoint tracking. The setpoint pre-filter for the proposed MSC scheme is expressed as follows:

$$F_r = \frac{\frac{80.27}{3}s+1}{80.27s+1} \tag{8.86}$$

8.3.2 Robust control

In order to compare the performances of proposed MSC scheme, a loop shaping design method of McFarlane and Glover [195] is used to synthesize the primary controller (G_{c0}). In this case, the secondary and tertiary controllers used are the same as in the previous scheme. Note that, the loop shaping design is unable to produce stable controller based on original plant transfer function, i.e., direct application of loop shaping method in the standard single-loop feedback control structure. Thus, the primary controller is designed based on the reduced closed-loop transfer function from B to Y, i.e., $\overline{P}_{a0}$, which is given by

$$\overline{P}_{a0} \cong \frac{153.7(-4.7s+1)(-60s+1)}{(2.1s+1)(9.1s+1)(28.3s+1)} \tag{8.87}$$

Using the loop shaping control design, the primary controller is obtained based on (8.87) is given as follows:

$$G_c(s) = -0.0017\frac{(s+0.4629)(s+0.0985)(s+0.0392)(s+0.0112)}{s(s+0.0159)(s^2+0.4213s+0.1424)} \tag{8.88}$$

where the stable minimum-phase LTI weight is designed based on Ziegler-Nicholas frequency response, which is given as

$$w_1(s) = 1.7 \times 10^{-5}\left(\frac{1+89s}{s}\right) \tag{8.89}$$

It should be noted that, the input weight w_1 is designed based on $\overline{P}_{a0}$ (8.87). The stability margin gives a good indication of robustness to a wide class of unstructured plant variations. The value of stability margin of robust control is 0.6643, with Gain Margin (GM) = 14 dB, Phase Margin (PM) = 84.1°and $M_s = 1.25$. Notice that, the primary controller designed based on loop shaping method produces 4^{th} order controller while that designed via the proposed method is 3^{rd} order. Thus, this leads to the difference in the stability margins between the two controllers in (8.84) and (8.88). For practicality, it is desired to have a low-order controller.

Furthermore, the performance robustness of the two different control schemes are evaluated under perturbed conditions of the fed-batch process (5.3), i.e., $\boldsymbol{U} = [0.15, 100]^\intercal$, $\boldsymbol{\chi_s} = [1, 1, 1, 6]^\intercal$. The ν-gap metric [196] between the system at the nominal level and perturbed level is 0.2016. The performances of the two different control schemes are evaluated based on 1 unit step changes in the setpoint and output disturbance and 0.05 unit in the input disturbance.

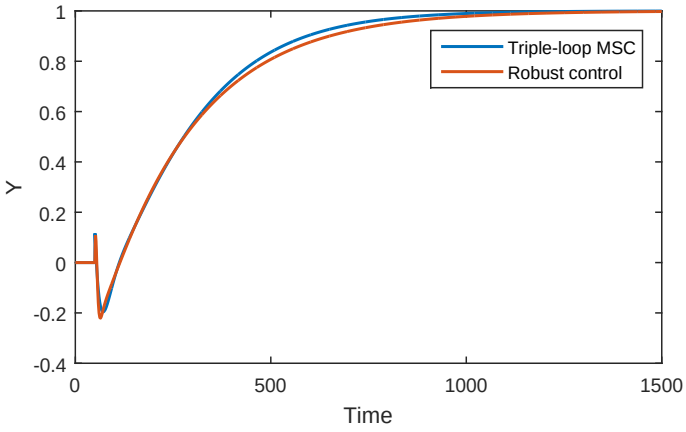

Figure 8.4: Responses of setpoint tracking at nominal condition

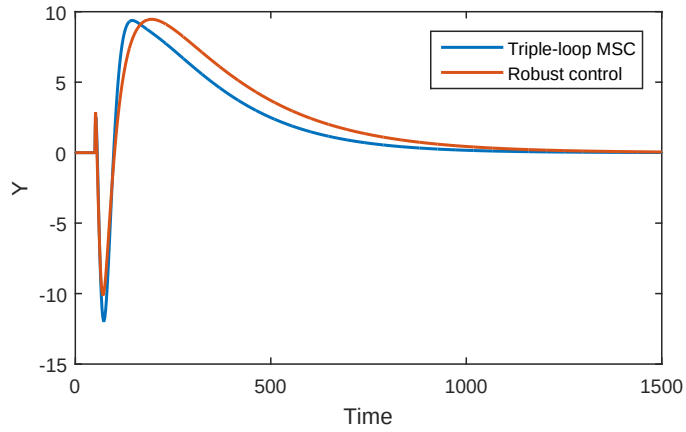

Figure 8.5: Responses of input disturbance at nominal condition

Table 8.1 shows the Integral Absolute Error (IAE) values for the two control schemes, i.e., proposed MSC and robust control at the nominal and perturbed conditions. Meanwhile, Figure 8.4 , Figure 8.5 and Figure 8.6 show the setpoint tracking, input disturbance rejection and output disturbance rejection

Table 8.1: The IAE value at nominal and perturbed conditions

	Nominal condition		Perturbed condition	
	MSC	Robust control	MSC	Robust control
Setpoint tracking	233.7	304.6	233.1	303.2
Input disturbance	3152	3835	3013	3706
Output disturbance	467.4	608.7	466.4	605.7

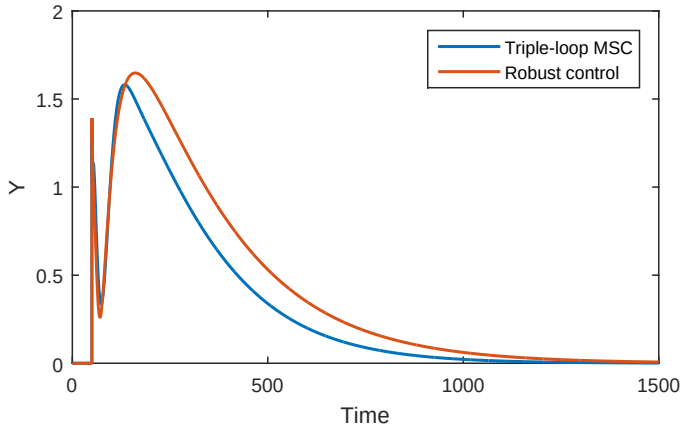

Figure 8.6: Responses of output disturbance at nominal condition

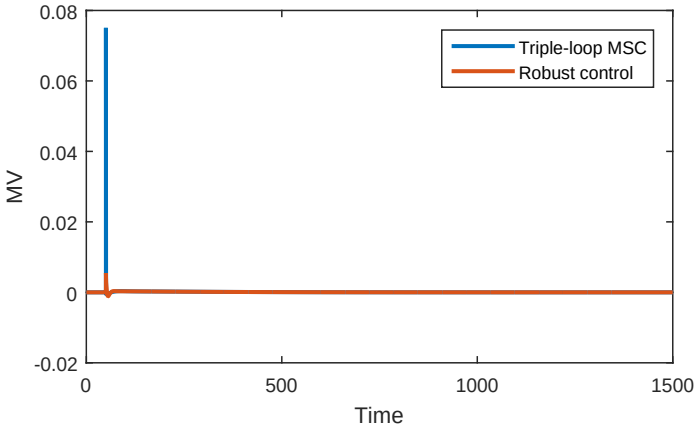

Figure 8.7: Responses of manipulated variable for setpoint tracking at nominal condition

responses at nominal condition respectively. As shown by the Table 8.1 and figures, the proposed MSC scheme achieves substantial improvement in nominal performance over the robust control scheme. Figure 8.7 shows the responses of manipulated variable for setpoint tracking at nominal condition. The proposed TL-MSC scheme and robust control scheme shows not obvious impulsive spikes on the manipulated variable for setpoint tracking. Moreover, the simulation of the responses of manipulated variable for output disturbance rejection has been done but no impulsive spikes were observed.

Figure 8.8 , Figure 8.9 and Figure 8.10 show the setpoint tracking, input disturbance rejection and output disturbance rejection responses at perturbed condition respectively. Based on the figures and Table 8.1, the proposed MSC

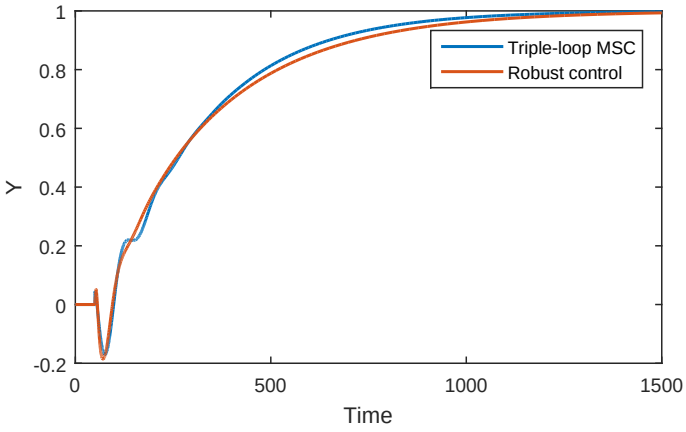

Figure 8.8: Responses of setpoint tracking at perturbed condition

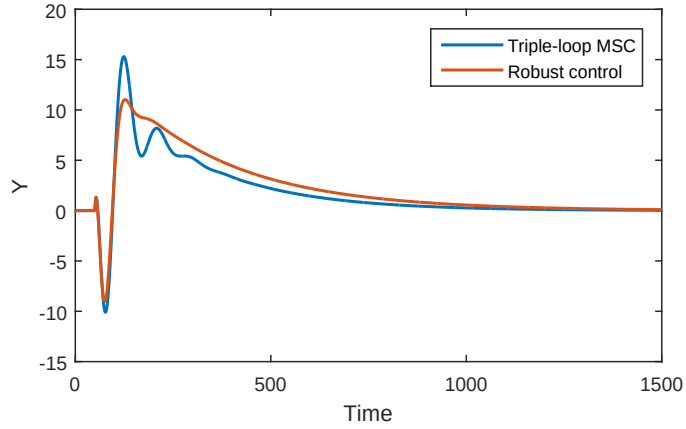

Figure 8.9: Responses of input disturbance at perturbed condition

scheme is still stable and gives improved performance robustness compared to robust control scheme especially for the input-output disturbance rejection.

8.4 Summary

This chapter has demonstrated that a fed-batch fermentation can show several forms of complex dynamic behaviors throughout the course of its operation, e.g., a fourth-order integrating-unstable plus oscillatory system with multiple RHP zeros. This form of fourth-order integrating-unstable system has never been reported in the open literature. Noteworthy, this type of system is very difficult to stabilize using a single-loop PID controller, and even with a robust loop shaping method (in Matlab 2008b), a minimum of a tenth-order controller form is required

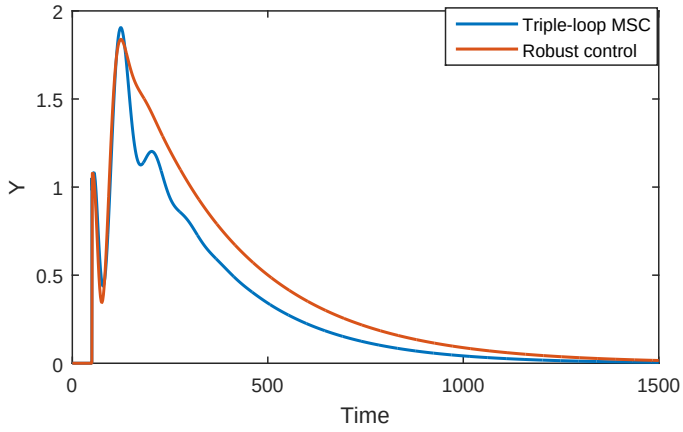

Figure 8.10: Responses of output disturbance at perturbed condition

for possible stabilization of the system. It is worth highlighting that, the proposed TL-MSC scheme not only can stabilize the complex system but also can give good closed-loop performance by using a combination of three traditional PID-type controllers. Although in the presented design procedure a low-order PID controller augmented with filter has been proposed for the primary controller, it should be noted that an advanced controller such as the loop-shaping robust controller can also be used in the primary loop. However, the use of such an advanced controller will lead to a high-order controller form, e.g., a fourth-order robust controller. Despite its higher order form, the simulation study has shown that the high-order robust controller in the primary loop could not necessarily lead to a better performance than that of a well-tuned low-order PID controller. This implies that the structure of control scheme itself is more important than the individual control laws involved. The work presented in this chapter has been submitted to Journal of Franklin Institute[1].

[1]Qiu Han Seer and Jobrun Nandong. Multi-scale control scheme: stabilization of a class of fourth-order integrating-unstable systems. *Submitted to Journal of Franklin Institute - under first revision May 2017.*

Chapter 9

Conclusions and Recommendations

9.1 Conclusions

From the literature review, we can conclude that fed-batch control remains an open-ended issue in both academia and industry. In fed-batch fermentation, due to the process variability and the complexity of biological systems, often results in strong nonlinear and complex dynamics, which become major concerns in control system design. The nonlinearity problem has been addressed by using some advanced control strategies as mentioned in the literature. An interesting point is that, so far, there has been limited studies regarding the challenges of several complex dynamics which can arise from the fermentation process; these dynamics can be described using fourth-order integrating models. Even more surprising is that, there has been very few reports on PID stabilization and tuning for cases of complex dynamics represented by such high-order integrating models. In response to this research gap, this dissertation has presented the results of an investigation into the design and application of several control strategies, i.e., using standard single-loop as well as non-standard PID feedback control structures, which can be used not only to stabilize such complex dynamics but also to provide improved performance robustness of the closed-loop system.

In this regard, this dissertation answers three important questions: (1) how microbial kinetics models affect the controllability of the fed-batch system, (2) how complex dynamics in fed-batch fermentation process affect the stability of standard PID feedback controllers, and (3) how to improve control performance by using a non-standard PID controller to address the complex dynamics. Hence,

the conclusions are discussed as follows:

9.1.1 Experimental and Kinetics Modeling of Batch Fermentation Process

The microbial kinetics model represents an important part of the mathematical model of the fed-batch fermentation process, which can be used to obtain satisfactory results in optimization and control studies. An experimental study was required to develop the kinetics model of the fermentation process. In this case study, mixed mango waste and cassava were used as feedstock and the effects of pH and mixing intensity (i.e., aeration rate and stirrer speed) were studied. The test results showed the fermentation was affected more significantly by the changes in the pH and aeration rate compared to the stirrer speed. In kinetics modeling, the proposed Herbert-Haldane microbial model provided an appropriate fit, which is uniquely capable in capturing the death phase of biomass concentration during the end of fermentation. The proposed microbial model is simple and can be implemented for process optimization and control studies. For example, an advanced expanded microbial kinetics (EMK) model has been constructed based on the proposed Herbert-Haldane model (reported in [173]), which can provide greater accuracy in estimating the kinetic parameters value in a case of a highly nonlinear dynamic fermentation process. The advanced EMK model can be used in bioreactor simulation, optimization and control studies.

9.1.2 PID stabilization

There has been a limited number of studies addressing the stabilization of some specific complex dynamic behaviors inherent in fed-batch fermentation processes. In this dissertation, the characterization of the boundaries of stabilizing PID parameter regions was evaluated based on the necessary and sufficient criterion of the Routh-Hurwitz stability analysis. In Chapter 4, the stabilization by a PID controller of second-order unstable processes, i.e., second-order deadtime with an unstable pole (SODUP) and second-order deadtime with two unstable poles (SODTUP), was performed. In Chapter 5, several different forms of complex dynamics that can arise from a typical fed-batch fermentation process have been presented. A class of fourth-order integrating-unstable model was used to adequately represent the most complex forms of dynamic behavior encountered in the fed-batch fermentation process. The novelty of this PID stabilization approach

can be summarized as follows:

- An interesting feature of this approach is that, explicit upper and lower limits on K, τ_I and τ_D were systematically established. Some of the existing methods reported in open literature rely quite a lot on the graphical plots representing the stability regions, whereas the proposed method requires no such plots because it yields explicit stabilizing regions in mathematical expressions. Therefore, the proposed method can provide a practical alternative way to construct systematically the stabilizing PID parameter regions.

- A low-order controller can provide closed-loop stability for such complex and high order systems, e.g., second-order unstable and fourth-order integrating-unstable processes, when the stabilizing parameter regions are known beforehand, rather than using a high-order controller.

9.1.3 Extended Multi-scale Control Scheme

This dissertation intend to provide a solution to achieve an improved closed-loop performance for addressing some of the complex dynamics inherent in fed-batch system with the combination of 2 or 3 PID-type controllers. With respect to this goal, some novel basic multi-scale control, double-loop multi-scale control (DL-MSC) and triple-loop multi-scale control (TL-MSC) schemes have been proposed in order to address each linearized form of complex dynamics, where the behaviors changed throughout the course of the fed-batch operation.

- In Chapter 6, the application of the multi-scale control scheme to design the multi-loop PID control for an extractive alcoholic fermentation by *Zymomonas mobilis* has been presented. The results showed that the 2×2 and 3×3 partial control strategies with 2 to 3 PID controllers, which were designed using the multi-scale control scheme were effective for the complex nonlinear extractive fermentation process.

- A new control scheme combining the direct multi-scale control and double-loop structure has been presented in Chapter 6. The proposed scheme provides a simple way to design an effective control system for a second-order nonminimum-phase integrating processes, which may be exhibited occasionally in a fed-batch system.

- A new extended control strategy which unifies the direct and indirect multi-scale control schemes via a double-loop control structure has been presented in Chapter 7. This unified control strategy has been proposed for controlling a class of highly nonminimum-phase processes having both integrating and unstable modes using two controllers, i.e., a P controller in the inner loop and a PID controller in the external loop. The secondary controller was designed via indirect MSC scheme, which can always guarantee the pre-stabilization of unstable pole and the finalized MSC controller provides the overall system performance.

- The triple-loop MSC scheme has been presented to stabilize the most complex forms of dynamic behavior, i.e., a fourth-order integrating-unstable system with multiple right-half plane (RHP) zeros, encountered in the fed-batch fermentation process by using a combination of 3 PID-type controllers. The proposed scheme provided an improved closed-loop performance compared to other advanced controllers, such as the loop-shaping robust controller.

9.2 Recommendations

Some future research directions extending the work in this dissertation are suggested as follows:

1. *Kinetics modeling*
   The product inhibition can be evaluated via experimental study so the kinetics of ethanol inhibition can be examined in order to provide a better description on cell population especially in fed-batch bioprocesses with a higher ethanol concentration.

2. *Expanding the developed control approach to address the nonlinearity problem*
   The proposed MSC schemes can be combined with some advanced control strategies such as robust, adaptive, and nonlinear control, to address the nonlinearity problem in order to provide an integrated control system for fed-batch fermentation processes.

3. *Separation processes in fed-batch bioprocesses*
   The separation approaches (i.e., membrane separation, vacuum fermentation, liquid-liquid extraction, adsorption and etc.) can be implemented

in the bioprocesses in order to remove the products simultaneously from fed-batch systems whereby reducing the product inhibition and increasing yields.

References

[1] C. E. Wyman, Biomass ethanol: Technical progress, opportunities, and commercial challenges, Annual Review of Energy and the Environment 24 (1) (1999) 189–226.

[2] M. Balat, H. Balat, Recent trends in global production and utilization of bio-ethanol fuel, Applied Energy 86 (11) (2009) 2273–2282.

[3] D. Mazaheri, S. A. Shojaosadati, S. M. Mousavia, P. Hejazi, S. Saharkhiz, Bioethanol production from carob pods by solid-state fermentation with zymomonas mobilis, Applied Energy 99 (2012) 372–378.

[4] F. W. Bai, W. A. Anderson, M. Moo-Young, Ethanol fermentation technologies from sugar and starch feedstocks, Biotechnology Advances 26 (2008) 89–105.

[5] S. Alfenore, X. Cameleyre, L. Benbadis, C. Bideaux, J.-L. Uribelarrea, G. Goma, C. Molina-Jouve, S. E. Guillouet, Aeration strategy a need for very high ethanol performance in saccharomyces cerevisiae fed-batch process, Applied Microbiology Biotechnology 63 (5) (2004) 537–542.

[6] J. Cheng (Ed.), Biomass to Renewable Energy Processes, CRC Press Inc., Taylor & Francis Group, Florida, 2010.

[7] P. Kumar, D. M. Barrett, M. J. Delwiche, P. Stroeve, Methods for pretreatment of lignocellulosic biomass for efficient hydrolysis and biofuel production, Industrial & Engineering Chemistry Research 48 (8) (2009) 3713–3729.

[8] P. Binod, R. Sindhu, R. R. Singhania, S. Vikram, L. Devi, S. Nagalakshmi, N. Kurien, R. K. Sukumaran, A. Pandey, Bioethanol production from rice straw: An overview, Bioresource Technology 101 (13) (2010) 4767–4774, special Issue on Lignocellulosic Bioethanol: Current Status and Perspectives.

[9] R. S. Parker, F. J. Doyle, Optimal control of a continuous bioreactor using an empirical nonlinear model, Industrial & engineering chemistry research 40 (8) (2001) 1939–1951.

[10] M. D. Kapadi, R. D. Gudi, Optimal control of fed-batch fermentation involving multiple feeds using differential evolution, Process Biochemistry 39 (11) (2004) 1709–1721.

[11] F. Renard, A. V. Wouwer, S. Valentinotti, D. Dumur, A practical robust control scheme for yeast fed-batch cultures–an experimental validation, Journal of Process Control 16 (8) (2006) 855–864.

[12] R. Aguilar, J. González, M. Barrón, R. Martınez-Guerra, R. Maya-Yescas, Robust PI^2 controller for continuous bioreactors, Process Biochemistry 36 (10) (2001) 1007–1013.

[13] T. T. Lee, F. Y. Wang, R. B. Newell, Robust multivariable control of complex biological processes, Journal of Process Control 14 (2) (2004) 193–209.

[14] E. Petre, D. Selişteanu, Adaptive control of a fermentation bioprocess for lactic acid production, Mathematical Problems in Engineering 2012.

[15] L. Chen, G. Bastin, V. V. Breusegem, A case study of adaptive nonlinear regulation of fed-batch biological reactors, Automatica 31 (1) (1995) 55–65.

[16] C. B. Youssef, V. Guillou, A. Olmos-Dichara, Modelling and adaptive control strategy in a lactic fermentation process, Control Engineering Practice 8 (11) (2000) 1297–1307.

[17] D. G. Rao, Introduction to Biochemical Engineering, Tata McGraw-Hill, 2006.

[18] A. Cinar, S. J. Parulekar, C. Ündey, G. Birol, Batch Fermentation: Modeling, Monitoring and Control, Marcel Dekker, Inc., 2003.

[19] D. M. Díaz-Montaño, Continuous Agave Juice Fermentation for Producing Bioethanol, Creative Commons, 2013.

[20] M. Minier, G. Goma, Ethanol production by extractive fermentation, Biotechnology and Bioengineering 24 (1982) 1565–1579.

[21] M. J. Taherzadeh, K. Karimi, Alternative Feedstocks and Conversion Processes, Elsevier, 2011.

[22] G. M. Walker, Bioethanol: Science and technology of fuel alcohol, Ventus Publishing Aps, 2010.

[23] E. Tomás-Pejó, J. Oliva, A. Gonzlez, I. Ballesteros, M. Ballesteros, Bioethanol production from wheat straw by the thermotolerant yeast kluyveromyces marxianus CECT 10875 in a simultaneous saccharification and fermentation fed-batch process, Fuel 88 (2009) 2142–2147.

[24] J. Lu, X. Li, R. Yang, L. Yang, J. Zhao, Y. Liu, Y. Qu, Fed-batch semi-simultaneous saccharification and fermentation of reed pretreated with liquid hot water for bio-ethanol production using saccharomyces cerevisiae, Bioresource Technology 144 (2013) 539–547.

[25] A. Rudolf, M. Alkasrawi, G. Zacchi, G. Lidén, A comparison between batch and fed-batch simultaneous saccharification and fermentation of steam pretreated spruce, Enzyme and Microbial Technology 37 (2005) 195–204.

[26] L. Laopaiboon, P. Thanonkeo, P. Jaisil, P. Laopaiboon, Ethanol production from sweet sorghum juice in batch and fed-batch fermentations by saccharomyces cerevisiae, World J Microbiol Biotechnol 23 (2007) 14971501.

[27] I. S. I. Snoek, H. Y. Steensma, Factors involved in anaerobic growth of saccharomyces cerevisiae, Yeast 24 (1) (2007) 1–10.

[28] J. Zaldivar, J. Nielsen, L. Olsson, Fuel ethanol production from lignocellulose: a challenge for metabolic engineering and process integration, Appl Microbiol Biotechnol 56 (1-2) (2001) 17–34.

[29] M. Cot, M.-O. Loret, J. Francois, L. Benbadis, Physiological behavior of saccharomyces cerevisiae in aerated fed-batch fermentation for high level production of bioethanol, FEMS Yeast Research 7 (1) (2007) 22–32.

[30] M. T. Flikweert, Physiological roles of pyruvate decarboxylase in saccharomyces cerevisiae, Ph.D. thesis, Delft University of Technology (1999).

[31] L. W. T. Emily, J. Nandong, Y. Samyudia, Experimental investigation on the impact of aeration rate and stirrer speed on micro-aerobic batch fermentation, Journal of Applied Sciences 9 (17) (2009) 3126–3130.

[32] A. W. Bhutto, K. Harijan, K. Qureshi, A. A. Bazmi, A. Bahadori, Perspectives for the production of ethanol from lignocellulosic feedstock - a case study, Journal of Cleaner Production 95 (0) (2015) 184 – 193.

[33] C. M. Drapcho, N. P. Nhuan, T. H. Walker, Biofuels Engineering Process Technology, United States of America: McGraw-Hill, 2008.

[34] M. Balat, H. Balat, C. Öz, Progress in bioethanol processing, Progress in Energy and Combustion Science.

[35] N. Sarkar, S. K. Ghosh, S. Bannerjee, K. Aikat, Bioethanol production from agricultural wastes: An overview, Renewable Energy 37 (1) (2012) 19–27.

[36] I. C. Onwueme, Cassava in asia and the pacific, Cassava: Biology, production and utilization (2002) 55–65.

[37] R. Liu, F. Shen, Impacts of main factors on bioethanol fermentation from stalk juice of sweet sorghum by immobilized saccharomyces cerevisiae (CICC 1308), Bioresource Technology 99 (4) (2008) 847 – 854.

[38] Y. Lin, W. Zhang, C. Li, K. Sakakibara, S. Tanaka, H. Kong, Factors affecting ethanol fermentation using saccharomyces cerevisiae BY4742, Biomass and Bioenergy 47 (2012) 395–401.

[39] J. Eed, Factors affecting enzyme activity, ESSAI 10 (1) (2012) 19.

[40] W. Zhang, Y. Lin, Q. Zhang, X. Wang, D. Wu, H. Kong, Optimisation of simultaneous saccharification and fermentation of wheat straw for ethanol production, Fuel 112 (2013) 331–337.

[41] M. J. Torija, N. Rozùs, M. Poblet, J. M. Guillamón, A. Mas, Effects of fermentation temperature on the strain population of saccharomyces cerevisiae, International Journal of Food Microbiology 80 (1) (2003) 47 – 53.

[42] M. J. Torija, G. Beltran, M. Novo, M. Poblet, J. M. Guillamón, A. Mas, N. Rozès, Effects of fermentation temperature and saccharomyces species on the cell fatty acid composition and presence of volatile compounds in wine, International Journal of Food Microbiology 85 (12) (2003) 127 – 136.

[43] W. A. Khattak, M. Ul-Islam, M. W. Ullah, B. Yu, S. Khan, J. K. Park, Yeast cell-free enzyme system for bio-ethanol productionat elevated temperatures, Process Biochemistry.

[44] C.-L. Wong, H.-W. Yen, C.-L. Lin, J.-S. Chang, Effects of pH and fermentation strategies on 2, 3-butanediol production with an isolated klebsiella sp. zmd30 strain, Bioresource technology 152 (2014) 169–176.

[45] H. Akin, C. Brandam, X.-M. Meyer, P. Strehaiano, A model for pH determination during alcoholic fermentation of a grape must by saccharomyces cerevisiae, Chemical Engineering and Processing: Process Intensification 47 (11) (2008) 1986 – 1993.

[46] D. Infantes, A. G. del Campo, F. F. J. Villaseñor, Kinetic model and study of the influence of pH, temperature and undissociated acids on acidogenic fermentation, Biochemical Engineering Journal 66 (2012) 66–72.

[47] J. Kim, K.-J. Cho, G. Han, C. Lee, S. Hwang, Effects of temperature and pH on the biokinetic properties of thiocyanate biodegradation under autotrophic conditions, Water Research 47 (1) (2013) 251–258.

[48] Y. Tan, Z.-X. Wang, K. C. Marshall, Modeling pH effects on microbial growth: A statistical thermodynamic approach, Biotechnology and Bioengineering 59 (6) (1998) 724–731.

[49] I. Tang, M. R. Okos, , S.-T. Yang, Effects of pH and acetic acid on homoacetic fermentation of lactate by clostridium formicoaceticum, Biotechnology and bioengineering 34 (8) (1989) 1063–1074.

[50] Y. Combet-Blanc, K. Kalamba, P. Kergoat, Effect of pH on bacillus thermoamylovorans growth and glucose fermentation., Applied and environmental microbiology 61 (2) (1995) 656–659.

[51] A.-P. Zeng, A. Ross, H. Biebl, C. Tag, B. Günzel, W.-D. Deckwer, Multiple product inhibition and growth modeling of clostridium butyricum and klebsiella pneumoniae in glycerol fermentation, Biotechnology and Bioengineering 44 (8) (1994) 902–911.

[52] N. V. Narendranath, R. Power, Relationship between pH and medium dissolved solids in terms of growth and metabolism of Lactobacilli and Saccharomyces cerevisiae during ethanol production, Applied and Environmental Microbiology 71 (5) (2005) 2239–2243.

[53] N. V. Narendranath, K. C. Thomas, W. M. Ingledew, Acetic acid and lactic acid inhibition of growth of Saccharomyces cerevisiae by different

mechanisms, Journal of the American Society of Brewing Chemists 59 (4) (2001) 187–194.

[54] K. C. Thomas, S. H. Hynes, W. M. Ingledew, Influence of medium buffering capacity on inhibition of saccharomyces cerevisiae growth by acetic and lactic acids, Applied and Environmental Microbiology 68 (4) (2002) 1616–1623.

[55] E. W. T. Liew, Modeling and control of non-ideally mized bioreactors, Ph.D. thesis, Curtin University (2011).

[56] F. Garcia-Ochoa, E. Gomez, Bioreactor scale-up and oxygen transfer rate in microbial processes: An overview, Biotechnology Advances 27 (2) (2009) 153 – 176.

[57] Y. H. Lin, W. S. Chien, K. J. Duan, P. R. Chang, Effect of aeration timing and interval during very-high-gravity ethanol fermentation, Process Biochemistry 46 (4) (2011) 1025–1028.

[58] C. Fornairon-Bonnefond, V. Demaretz, E. Rosenfeld, J.-M. Salmon, Oxygen addition and sterol synthesis in saccharomyces cerevisiae during enological fermentation, Journal of Bioscience and Bioengineering 93 (2) (2002) 176 – 182.

[59] F. G. Priest, G. G. Stewart, Handbook of Brewing, CRC Press Inc., Taylor & Francis Group, Florida, 2006.

[60] Ó. J. Sánchez, C. A. Cardona, Trends in biotechnological production of fuel ethanol from different feedstocks, Bioresource Technology 99 (2008) 5270–5295.

[61] H.-B. Seo, J.-H. Yeon, M. H. Chung, D. H. Kang, H.-Y. Lee, K.-H. Jung, Long-term repeated fed-batch ethanol fermentation in aerated condition, Biotechnology and Bioprocess Engineering 15 (2) (2010) 324–328.

[62] H.-B. Seo, S. S. Kim, H.-Y. Lee, K.-H. Jung, High-level production of ethanol during fed-batch ethanol fermentation with a controlled aeration rate and non-sterile glucose powder feeding of saccharomyces cerevisiae, Biotechnology and Bioprocess Engineering 14 (5) (2009) 591–598.

[63] C. D. L. Roza, A. Laca, L. A. Garca, M. Diaz, Stirring and mixing effects at different cider fermentation scales, Food and Bioproducts Processing 80 (2) (2002) 129 – 134.

[64] M. Okabe, M. Katoh, F. Furugoori, M. Yoshida, S. Mitsui, Growth and fermentation characteristics of bottom brewer's yeast under mechanical stirring, Journal of Fermentation and Bioengineering 73 (2) (1992) 148 – 152.

[65] E. Riscaldati, M. Moresi, M. Petruccioli, F. Federici, Effect of pH and stirring rate on itaconate production by Aspergillus terreus, Journal of Biotechnology 83 (3) (2000) 219 – 230.

[66] M. M. Toma, U. Kalnenieks, A. Berzins, A. Vigants, M. Rikmanis, U. Viesturs, The effect of mixing on glucose fermentation by zymomonas mobilis continuous culture, Process Biochemistry 38 (9) (2003) 1347 – 1350.

[67] J. E. Bailey, Mathematical modeling and analysis in biochemical engineering: Past accomplishments and future opportunities, Biotechnology Progress 14 (1) (1998) 8–20.

[68] J. L. Casti, Reality Rules: II. Picturing the world in mathematics, the frontier, New York: John Wiley and sons, 1992.

[69] C. L. Dym, Principles of Mathematical Modeling, Academic Press, 2004.

[70] J. H. T. Luong, Kinetics of ethanol inhibition in alcoholic fermentation, Biotechnology and Bioengineering 27 (3) (1985) 280–285.

[71] M. Novak, P. Strehaiano, M. Moreno, G. Goma, Alcoholic fermentation: On the inhibitory effect of ethanol, Biotechnology and Bioengineering 23 (1) (1981) 201–211.

[72] K. Han, O. Levenspiel, Extended monod kinetics for substrate, product, and cell inhibition, Biotechnology and Bioengineering 32 (4) (1988) 430–447.

[73] S. K. C. Lin, C. Du, A. Koutinas, R. Wang, C. Webb, Substrate and product inhibition kinetics in succinic acid production by actinobacillus succinogenes, Biochemical Engineering 41 (2008) 128–135.

[74] A. J. Daugulis, D. E. Swaine, Examination of substrate and product inhibition kinetics on the production of ethanol by suspended and immobilized cell reactors, Biotechnology and Bioengineering 29 (5) (1987) 639–645.

[75] A. B. Jarzebski, J. J. Malinowski, G. Goma, Modeling of ethanol fermentation at high yeast concentrations, Biotechnology and Bioengineering 34 (1989) 1225–1230.

[76] F. N. Arroyo-López, S. Orlić, A. Querol, E. Barrio, Effects of temperature, pH and sugar concentration on the growth parameters of saccharomyces cerevisiae, s. kudriavzevii and their interspecific hybrid, International Journal of Food Microbiology 131 (2009) 120–127.

[77] R. R. de Andrade, E. C. Rivera, A. C. Costa, D. I. P. Atala, F. M. Filho, R. M. Filho, Estimation of temperature dependent parameters of a batch alcoholic fermentation process, Applied Biochemistry and Biotechnology 136-140 (2007) 753–763.

[78] M. Starzak, L. Kryzstek, L. Nowicki, H. Michalski, Macroapproach kinetics of ethanol fermentation by saccharomyces cerevisiae: experimental studies and mathematical modelling, The Chemical Engineering Journal and the Biochemical Engineering Journal 54 (3) (1994) 221 – 240.

[79] G. K. Hoppe, G. S. Hansford, The effect of micro-aerobic conditions on continuous ethanol production by Saccharomyces cerevisiae, Biotechnology 6 (10) (1984) 681–686.

[80] R. Grosz, G. Stephanopoulos, Physiological, biochemical, and mathematical studies of micro-aerobic continuous ethanol fermentation by saccharomyces cerevisiae. iii: Mathematical model of cellular energetics and catabolism, Biotechnology and Bioengineering 36 (10) (1990) 1030–1040.

[81] J. M. Laplace, J. P. Delgenes, R. Moletta, J. M. Navarro, Alcoholic fermentation of glucose and xylose by pichia stipitis, candida shehatae, saccharomyces cerevisiae and zymomonas mobilis : oxygen requirement as a key factor, Applied Microbiology and Biotechnology 36 (2) (1991) 158–162.

[82] E. W.-T. Liew, J. Nandong, Y. Samyudia, Multi-scale models for the optimization of batch bioreactors, Chemical Engineering Science 95 (2013) 257–266.

[83] G. Birol, P. Doruker, B. Kirdar, Z. İ. Önsan, K. Ülgen, Mathematical description of ethanol fermentation by immobilised saccharomyces cerevisiae, Process Biochemistry 33 (7) (1998) 763 – 771.

[84] S. Kumar, P. Dheeran, S. P. Singh, I. M. Mishrac, D. K. Adhikaric, Kinetic studies of ethanol fermentation using kluyveromyces sp. IIPE453, Journal of Chemical Technology and Biotechnology 88 (10) (2013) 1874–1884.

[85] J. F. Andrews, A mathematical model for the continuous culture of microorganisms utilizing inhibitory substrates, Biotechnology and Bioengineering 10 (6) (1968) 707–723.

[86] M. Phisalaphong, N. Srirattana, W. Tanthapanichakoon, Mathematical modmodel to investigate temperature effect on kinetic parameter of ethanol fermentation, Biochemical Engineering Journal 28 (2006) 36–43.

[87] J. B. S. Haldane, Enzymes, MIT Press, Cambridge, MA, 1965.

[88] R. D. Tyagi, T. K. Ghose, Studies on immobilized saccharomyces cerevisiae. i. analysis of continuous rapid ethanol fermentation in immobilized cell reactor, Biotechnology and Bioengineering 24 (4) (1982) 781–795.

[89] V. H. Edwards, The influence of high substrate concentrations on microbial kinetics, Biotechnology and Bioengineering 12 (5) (1970) 679–712.

[90] S. Aiba, M. Shoda, M. Nagatani, Kinetics of product inhibition in alcohol fermentation, Biotechnology and Bioengineering 10 (6) (1968) 845–864.

[91] T. K. Ghose, R. D. Tyagi, Rapid ethanol fermentation of cellulose hydrolysate. ii. product and substrate inhibition and optimization of fermentor design, Biotechnology and Bioengineering 21 (8) (1979) 1401–1420.

[92] I. Holzberg, R. K. Finn, K. H. Steinkraus, A kinetic study of the alcoholic fermentation of grape juice, Biotechnology and Bioengineering 9 (3) (1967) 413–427.

[93] G. K. Hoppe, G. S. Hansford, Ethanol inhibition of continuous anaerobic yeast growth, Biotechnology 4 (1) (1982) 39–44.

[94] O. Levenspiel, The monod equation: A revisit and a generalization to product inhibition situations, Biotechnology and Bioengineering 22 (8) (1980) 1671–1687.

[95] R. R. de Andrade, F. M. Filho, R. M. Filho, A. C. da Costa, Kinetics of ethanol production from sugarcane bagasse enzymatic hydrolysate concentrated with molasses under cell recycle, Bioresource Technology 130 (2013) 351 – 359.

[96] O. A. Garro, E. Rodríguez, R. P. Unda, D. A. S. Callieri, Mathematical modelling of the alcoholic fermentation of glucose by zymomonas mobilis, Journal of Chemical Technology & Biotechnology 63 (4) (1995) 367–373.

[97] A. S. Soni, R. S. Parker, Fed-batch bioreactor control using a multi-scale model, in: American Control Conference, 2003. Proceedings of the 2003, Vol. 3, 2003, pp. 2371–2376.

[98] S. Ochoa, A new approach for finding smooth optimal feeding profiles in fed-batch fermentations, Biochemical Engineering Journal 105 (2016) 177 – 188.

[99] G. Birol, C. Ündey, A. Cinar, A modular simulation package for fed-batch fermentation: penicillin production, Computers & Chemical Engineering 26 (11) (2002) 1553–1565.

[100] X. Han, W. Song, G. Liu, Z. Li, P. Yang, Y. Qu, Improving cellulase productivity of penicillium oxalicum re-10 by repeated fed-batch fermentation strategy, Bioresource Technology 227 (2017) 155 – 163.

[101] J. C. Menezes, S. S. Alves, J. M. Lemos, S. F. de Azevedo, Mathematical modelling of industrial pilot-plant penicillin-g fed-batch fermentations, Journal of Chemical Technology and Biotechnology 61 (2) (1994) 123–138.

[102] Y. Xie, Y. Jin, X. Zeng, J. Chen, Y. Lu, K. Jing, Fed-batch strategy for enhancing cell growth and c-phycocyanin production of arthrospira (spirulina) platensis under phototrophic cultivation, Bioresource Technology 180 (2015) 281 – 287.

[103] D. Soletto, L. Binaghi, L. Ferrari, A. Lodi, J. Carvalho, M. Zilli, A. Converti, Effects of carbon dioxide feeding rate and light intensity on the fed-batch pulse-feeding cultivation of spirulina platensis in helical photobioreactor, Biochemical Engineering Journal 39 (2) (2008) 369 – 375.

[104] D. Soletto, L. Binaghi, A. Lodi, J. Carvalho, A. Converti, Batch and fed-batch cultivations of spirulina platensis using ammonium sulphate and urea as nitrogen sources, Aquaculture 243 (14) (2005) 217 – 224.

[105] M. Rodrigues, L. Ferreira, A. Converti, S. Sato, J. Carvalho, Fed-batch cultivation of arthrospira (spirulina) platensis: Potassium nitrate and ammonium chloride as simultaneous nitrogen sources, Bioresource Technology 101 (12) (2010) 4491 – 4498.

[106] M. Weiner, C. Albermann, K. Gottlieb, G. A. Sprenger, D. Weuster-Botz, Fed-batch production of l-phenylalanine from glycerol and ammonia with recombinant escherichia coli, Biochemical Engineering Journal 83 (2014) 62–69.

[107] S. K. Maiti, A. E. Lantz, M. Bhushan, P. P. Wangikar, Multi-objective optimization of glycopeptide antibiotic production in batch and fed batch processes, Bioresource Technology 102 (13) (2011) 6951 – 6958.

[108] M. Kawohl, T. Heine, R. King, Model based estimation and optimal control of fed-batch fermentation processes for the production of antibiotics, Chemical Engineering and Processing: Process Intensification 46 (11) (2007) 1223–1241.

[109] M. Pecyna, M. Bizukojc, Lovastatin biosynthesis by aspergillus terreus with the simultaneous use of lactose and glycerol in a discontinuous fed-batch culture, Journal of biotechnology 151 (1) (2011) 77–86.

[110] N. Novak, S. Gerdin, M. Berovic, Increased lovastatin formation by aspergillus terreus using repeated fed-batch process, Biotechnology Letters 19 (10) (1997) 947–948.

[111] L. Yee, H. W. Blanch, Recombinant protein expression in high cell density fed-batch cultures of escherichia coli, Nature Biotechnology 10 (12) (1992) 1550–1556.

[112] G. P. Longobardi, Fed-batch versus batch fermentation, Bioprocess and biosystems engineering 10 (5) (1994) 185–194.

[113] C. A. Frohman, R. M. de Orduña, Cellular viability and kinetics of osmotic stress associated metabolites of saccharomyces cerevisiae during traditional

batch and fed-batch alcoholic fermentations at constant sugar concentrations, Food Research International 53 (2013) 551–555.

[114] Y. Bakri, Y. Akeed, P. Thonart, Comparison between continuous and batch processing to produce xylanase by penicillium canescens 10-10c, Brazilian Journal of Chemical Engineering 29 (3) (2012) 441–447.

[115] J. S. Alford, Bioprocess control: Advances and challenges, Computers and Chemical Engineering 30 (2006) 1464–1475.

[116] R. Oliveira, R. Simutis, S. F. de Azevedo, Design of a stable adaptive controller for driving aerobic fermentation processes near maximum oxygen transfer capacity, Journal of process control 14 (6) (2004) 617–626.

[117] R. Oliveira, J. J. Clemente, A. E. Cunha, M. J. T. Carrondo, Adaptive dissolved oxygen control through the glycerol feeding in a recombinant pichia pastoris cultivation in conditions of oxygen transfer limitation, Journal of biotechnology 116 (1) (2005) 35–50.

[118] Z. I. T. A. Soons, J. A. Voogt, G. Van Straten, A. J. B. Van Boxtel, Constant specific growth rate in fed-batch cultivation of bordetella pertussis using adaptive control, Journal of biotechnology 125 (2) (2006) 252–268.

[119] A. P. Ranjan, J. Gomes, Decoupled adaptive control of glucose and dissolved oxygen for fed-batch methionine production using linear reference model, in: American Control Conference (ACC), 2010, IEEE, 2010, pp. 5862–5867.

[120] S. Tebbani, D. Dumur, G. Hafidi, Alain, Nonlinear predictive control of fed-batch cultures of escherichia coli, Chemical Engineering & Technology 33 (7) (2010) 1112–1124.

[121] A. Ashoori, B. Moshiri, A. Khaki-Sedigh, M. R. Bakhtiari, Optimal control of a nonlinear fed-batch fermentation process using model predictive approach, Journal of Process Control 19 (7) (2009) 1162–1173.

[122] S. Craven, J. Whelan, B. Glennon, Glucose concentration control of a fed-batch mammalian cell bioprocess using a nonlinear model predictive controller, Journal of Process Control 24 (4) (2014) 344–357.

[123] V. G. Nyttle, M. Chidambaram, Fuzzy logic control of a fed-batch fermentor, Bioprocess and Biosystems Engineering 9 (2) (1993) 115–118.

[124] M. A. H. Hisbullah, K. B. Ramachandran, Design of a fuzzy logic controller for regulating substrate feed to fed-batch fermentation, Food and Bioproducts Processing 81 (2) (2003) 138–146.

[125] J. Peng, F. Meng, Y. Ai, Time-dependent fermentation control strategies for enhancing synthesis of marine bacteriocin 1701 using artificial neural network and genetic algorithm, Bioresource technology 138 (2013) 345–352.

[126] Q.-G. Wang, Z. Ye, W.-J. Cai, C.-C. Hang, PID control for multivariable processes, Vol. 373, Springer Science & Business Media, 2008.

[127] R. C. Panda, Synthesis of PID controller for unstable and integrating processes, Chemical Engineering Science 64 (12) (2009) 2807–2816.

[128] A. M. D. Paor, M. O'Malley, Controllers of Ziegler-Nichols type for unstable process with time delay, International Journal of Control 49 (4) (1989) 1273–1284.

[129] K. J. Åström, T. Hägglund, Revisiting the Ziegler–Nichols step response method for PID control, Journal of process control 14 (6) (2004) 635–650.

[130] Y. Lee, J. Lee, S. Park, PID controller tuning for integrating and unstable processes with time delay, Chemical Engineering Science 55 (2000) 3481–3493.

[131] X. P. Yang, Q. G. Wang, C. C. Hang, C. Lin, IMC-based control system design for unstable processes, Industrial & engineering chemistry research 41 (17) (2002) 4288–4294.

[132] W. Tan, J. Liu, P. K. S. Tam, PID tuning based on loop-shaping h_∞ control, IEE Proceedings-Control Theory and Applications 145 (6) (1998) 485–490.

[133] J. Nandong, Z. Zang, Multi-loop design of multi-scale controllers for multivariable processes, Journal of Process Control 24 (5) (2014) 600 – 612.

[134] A. O'Dwyer, Handbook of PI and PID controller tuning rules, Vol. 57, World Scientific, 2009.

[135] S. C. Lee, Stabilization and control of unstable time delay systems, Ph.D. thesis, National University of Singapore (2012).

[136] S. Das, S. Saha, S. Das, A. Gupta, On the selection of tuning methodology of FOPID controllers for the control of higher order processes, ISA transactions 50 (3) (2011) 376–388.

[137] G. M. Malwatkar, S. H. Sonawane, L. M. Waghmare, Tuning PID controllers for higher-order oscillatory systems with improved performance, ISA transactions 48 (3) (2009) 347–353.

[138] M. Kubalčík, V. Bobál, Predictive control of higher order systems approximated by lower order time-delay models, WSEAS Transactions on Systems.

[139] K. J. Åström, Limitations on control system performance, European Journal of Control 6 (1) (2000) 2–20.

[140] W. A. Malik, S. Darbha, S. P. Bhattacharyya, A linear programming approach to the synthesis of fixed-structure controllers, IEEE Transactions on Automatic Control 53 (6) (2008) 1341–1352.

[141] V. Blondel, M. Gevers, A. Lindquist, Survey on the state of systems and control, European Journal of Control 1 (1) (1995) 5–23.

[142] M.-T. Ho, A. Datta, S. Bhattacharyya, A new approach to feedback stabilization, in: Proceedings of the 35th IEEE Conference on Decision and Control, Vol. 4, IEEE, 1996, pp. 4643–4648.

[143] M.-T. Ho, A. Datta, S. Bhattacharyya, A linear programming characterization of all stabilizing PID controllers, in: Proceedings of the American Control Conference, Vol. 6, IEEE, 1997, pp. 3922–3928.

[144] N. Tan, Computation of stabilizing PI and PID controllers for processes with time delay, ISA transactions 44 (2) (2005) 213–223.

[145] N. Tan, I. Kaya, C. Yeroglu, D. P. Atherton, Computation of stabilizing PI and PID controllers using the stability boundary locus, Energy Conversion and Management 47 (18) (2006) 3045–3058.

[146] G. J. Silva, A. Datta, S. P. Bhattacharyya, PI stabilization of first-order systems with time delay, Automatica 37 (12) (2001) 2025–2031.

[147] G. J. Silva, A. Datta, S. P. Bhattacharyya, New results on the synthesis of PID controllers, IEEE transactions on automatic control 47 (2) (2002) 241–252.

[148] M. T. Söylemez, N. Munro, H. Baki, Fast calculation of stabilizing PID controllers, Automatica 39 (1) (2003) 121–126.

[149] M. A. Hernández-Pérez, B. Muro-Cuéllar, M. Velasco-Villa, PID for the stabilization of high-order unstable delayed systems with possible complex conjugate poles, Asia-Pacific Journal of Chemical Engineering 10 (5) (2015) 687–699.

[150] L. Ou, W. Zhang, D. Gu, Nominal and robust stability regions of optimization-based PID controllers, ISA transactions 45 (3) (2006) 361–371.

[151] Q. B. Jin, Q. Liu, B. Huang, New results on the robust stability of PID controllers with gain and phase margins for UFOPTD processes, ISA transactions 61 (2016) 240–250.

[152] S. Srivastava, V. S. Pandit, A PI/PID controller for time delay systems with desired closed loop time response and guaranteed gain and phase margins, Journal of Process Control 37 (2016) 70–77.

[153] C.-H. Lee, A survey of PID controller design based on gain and phase margins, International Journal of Computational Cognition 2 (3) (2004) 63–100.

[154] J. Nandong, Z. Zang, High-performance multi-scale control scheme for stable, integrating and unstable time-delay processes, Journal of Process Control 23 (2013) 1333–1343.

[155] J. Nandong, Z. Zang, Novel multiscale control scheme for nonminimum-phase processes, Industrial & Engineering Chemistry Research 52 (24) (2013) 8248–8259.

[156] J. Nandong, Z. Zang, Multi-scale control: Improved technique to overcome time-delay limitation, in: Industrial Electronics and Applications (ICIEA), 2013 8th IEEE Conference on IEEE, IEEE, 2013, pp. 1527–1532.

[157] B. Ugon, J. Nandong, Z. Zang, Advanced PID controller synthesis using multiscale control scheme, in: Industrial Electronics and Applications (ICIEA), 2014 IEEE 9th Conference, 2014, pp. 775–780.

[158] K. Y. Rani, V. S. R. Rao, Control of fermenters–a review, Bioprocess Engineering 21 (1) (1999) 77–88.

[159] I. Y. Smets, J. E. Claes, E. J. November, G. P. Bastin, J. F. V. Impe, Optimal adaptive control of (bio)chemical reactors: past, present and future, Journal of Process Control 14 (1) (2004) 795–805.

[160] J.-J. E. Slotine, W. Li, Applied nonlinear control, Prentice-Hall Englewood Cliffs, NJ, 1991.

[161] F. Renard, A. V. Wouwer, Robust adaptive control of yeast fed-batch cultures, Computers & Chemical Engineering 32 (6) (2008) 1238–1248.

[162] Y. Zhou, G.-l. Wang, P. Yang, D.-Q. Kang, Fuzzy immune adaptive PID control for fermentation process, in: Intelligent Information Technology Application, 2008. IITA'08. Second International Symposium on, Vol. 2, IEEE, 2008, pp. 678–682.

[163] S. Duan, Z. Shi, H. Feng, Z. Duan, Z. Mao, An on-line adaptive control based on DO/pH measurements and ANN pattern recognition model for fed-batch cultivation, Biochemical engineering journal 30 (1) (2006) 88–96.

[164] R. Ketata, D. De Geest, A. Titli, Fuzzy controller: design, evaluation, parallel and hierarchial combination with a PID controller, Fuzzy sets and systems 71 (1) (1995) 113–129.

[165] C. G. Alfafara, K. Miura, H. Shimizu, S. Shioya, K.-i. Suga, K. Suzuki, Fuzzy control of ethanol concentration its application to maximum glutathione production in yeast fed-batch culture, Biotechnology and bioengineering 41 (4) (1993) 493–501.

[166] L. Wang, W. Du, H. Wang, H. Wu, Fuzzy self-tuning PID control of the operation temperatures in a two-staged membrane separation process, Journal of Natural Gas Chemistry 17 (4) (2008) 409–414.

[167] A. Altınten, F. Ketevanlioğlu, S. Erdoğan, H. Hapoğlu, M. Alpbaz, Self-tuning PID control of jacketed batch polystyrene reactor using genetic algorithm, Chemical Engineering Journal 138 (1) (2008) 490–497.

[168] H. De Battista, J. Picó, E. Picó-Marco, Nonlinear PI control of fed-batch processes for growth rate regulation, Journal of Process Control 22 (4) (2012) 789–797.

[169] D. C. Montgomery, Design and Analysis of Experiments, John Wiley & Sons, Inc., 2001.

[170] A. A. K. M. Ghareib, K. A. Youssef, Ethanol tolerance of saccharomyces cerevisiae and its relationship to lipid content and composition, Folia Microbiol 33 (1988) 447–452.

[171] D. Herbert, In Recent Progress in Microbiology, Almquist and Wiksell, Stockholm, Sweden, 1958.

[172] E. C. Rivera, C. K. Yamakawa, M. H. Garcia, V. C. Geraldo, C. E. Rossell, R. M. Filho, A. Bonomia, A procedure for estimation of fermentation kinetic parameters in fed-batch bioethanol production process with cell recycle, Chemical Engineering Transactions 32 (2013) 1369–1374.

[173] Q. H. Seer, J. Nandong, Advanced expanded microbial kinetics (EMK) model for ethanol production from mixed cassava and fruit wastes, Procedia Engineering 148 (2016) 417–425.

[174] D. E. Seborg, T. F. Edgar, D. A. Mellichamp, F. J. D. III, Process Dynamics and Control, John Wiley & Sons, Inc., 2010.

[175] W. Cho, J. Lee, T. F. Edgar, Simple analytic proportional-integral-derivative (PID) controller tuning rules for unstable processes, Industrial & Engineering Chemistry Research 53 (13) (2014) 5048–5054.

[176] M. K. Jhunjhunwala, M. Chidambaram, PID controller tuning for unstable systems by optimization method, Chemical Engineering Communications 185 (1) (2001) 91–113.

[177] P. Agrawal, H. C. Lim, Analyses of various control schemes for continuous bioreactors, in: Bioprocess Parameter Control, Springer Berlin Heidelberg, 1984, pp. 61–90.

[178] J. Nandong, Guaranteed stable PID controller tuning rules for first-order dead-time unstable processes, in: 2015 IEEE 10th Conference on Industrial Electronics and Applications (ICIEA),, IEEE, 2015, pp. 1443–1448.

[179] Q. H. Seer, J. Nandong, Stabilization and PID tuning algorithms for second-order unstable processes with time-delays, ISA transactions 67 (2017) 233–245.

[180] J. Nandong, Heuristic-based multi-scale control procedure of simultaneous multi-loop pid tuning for multivariable processes, Journal of Process Control 35 (2015) 101–112.

[181] F. L. H. da Silva, M. I. Rodrigues, F. Maugeri, Dynamic modelling, simulation and optimization of an extractive continuous alcoholic fermentation process, Journal of Chemical Technology and Biotechnology 74 (1999) 176–182.

[182] J. Nandong, Y. Samyudia, M. O. Tadé, Novel PCA-based technique for identification of dominant variables for partial control, Chemical Product and Process Modeling 5 (1).

[183] N. Leksawasdi, E. L. Joachimsthal, P. L. Rogers, Mathematical modeling of ethanol production from glucose/xylose mixtures by recombinant zymomonas mobilis, Biotechnology Letters 23 (2001) 1087–1093.

[184] D. Simhachalam, R. K. Mudi, Self-tuning fuzzy PID controller for integrating processes, in: 2014 International Conference on Control, Instrumentation, Energy & Communication(CIEC), 2014, pp. 51–55.

[185] Y. Chen, S. Won, Simple fuzzy PID controller tuning of integrating process with dead-time, in: International Conference on Control, Automation and Systems 2008, 2008, pp. 618–626.

[186] G. E. Rotstein, D. R. Lewin, Control of an unstable batch chemical reactor, Computers & chemical engineering 16 (1) (1992) 27–49.

[187] J. H. Park, S. W. Sung, I.-B. Lee, An enhanced PID control strategy for unstable processes, Automatica 34 (6) (1998) 751–756.

[188] H. Panagopoulos, K. J. Aström, PID control design and h_∞ loop shaping, International Journal of Robust and Nonlinear Control 10 (2000) 1249–1261.

[189] M. G. Safonov, R. Y. Chiang, Model reduction for robust control: A schur relative error method, International journal of adaptive control and signal processing 2 (4) (1988) 259–272.

[190] M. G. Safonov, R. Y. Chiang, A schur method for balanced model reduction, in: American Control Conference, 1988, IEEE, 1988, pp. 1036–1040.

[191] M. G. Safonov, R. Y. Chiang, D. J. N. Limebeer, Optimal hankel model reduction for nonminimal systems, IEEE Transactions on Automatic Control 35 (4) (1990) 496–502.

[192] Y.-G. Wang, W.-J. Cai, Advanced proportional-integral-derivative tuning for integrating and unstable processes with gain and phase margin specifications, Industrial & engineering chemistry research 41 (12) (2002) 2910–2914.

[193] B. Sonnleitnert, O. Käppeli, Growth of saccharomyces cerevisiae is controlled by its limited respiratory capacity: formulation and verification of a hypothesis, Biotechnology and bioengineering 28 (6) (1986) 927–937.

[194] S. Skogestad, Simple analytic rules for model reduction and PID controller tuning, Journal of Process Control 13 (4) (2003) 291 – 309.

[195] D. McFarlane, K. Glover, A loop-shaping design procedure using H_∞ synthesis, IEEE Transactions on Automatic Control 37 (6) (1992) 759–769.

[196] G. Vinnicombe, Uncertainty and Feedback: H_∞ loop-shaping and the ν-gap metric, Imperial College Press, 2000.

[197] R. Thatipamala, S. Rohani, G. A. Hill, Effects of high product and substrate inhibitions on the kinetics and biomass and product yields during ethanol batch fermentation, Biotechnology and Bioengineering 40 (2).

Appendix A

Experimental Procedure and Analysis

A set of experiments was executed in batch mode by using a BIOSTAT A-plus 2 L, MO-Assembly bioreactor. Rejected mango juice and hydrolyzed cassava were used as a carbon source for the fermentation process. The batch experiments were run for a period of about 60 hours until the substrate was used up. In this study, the effect of pH, stirrer speed (SS) and aeration rate (AR) on the rates of microbial growth, substrate consumption and ethanol production were studied throughout the experiments.

A.1 Medium Preparation

The preparation of medium is outlined in Table A.1. The cassava medium was prepared to be used for fermentation. The formulation is similar to inoculum, except that the glucose is changed into cassava.

1.5 L of culture medium was prepared. First, 150 g of cassava powder was mixed with 562.5 mL of 1 N H_2SO_4 solution. The cassava culture medium was cooked at 121℃ for 20 minutes in order to break down the cassava starch into fermentable sugars and then cooled down to room temperature, approximately at 30℃. All the chemicals listed in Table A.1 were dissolved in 562.5 mL of distilled water and mixed with the hydrolyzed cassava culture medium. 375 mL of pure filtered fresh mango juice was then added into the hydrolyzed cassava culture medium according to a volume ratio of 75:25. The culture medium was adjusted to desired pH by using solutions of 1 N of NaOH and 1 N of H_2SO_4. The culture medium was sterilized at 121℃ for 20 minutes to avoid contamination

Table A.1: Medium preparation formulation

Constituents	Amounts (g/L)
Cassava	100
Yeast extract	1.0
NH_4CL	2.5
NA_2HPO_4	2.91
KH_2PO_4	3.0
$MgSO_4$	0.25
$CaCl_2$	0.08
Citric acid	4.3
Sodium citrate	3.0

and then cooled down to room temperature. 4% (v/v) of inoculum was added to the fermentation medium prior to fermentation start-up. Figure A.1 shows the cassava culture medium after sterilization, which is brownish in colour.

Figure A.1: Cassava culture medium

A.2 Inoculum Preparation

The inoculum was prepared by using Baker's yeast incubated in glucose solution. The preparation of inoculum is referred to formulation based on [197], which is outlined in Table A.2.

Table A.2: Inoculum preparation formulation

Constituents	Amounts (g/L)
Glucose	100
Yeast extract	1.0
NH_4CL	2.5
NA_2HPO_4	2.91
KH_2PO_4	3.0
$MgSO_4$	0.25
$CaCl_2$	0.08
Citric acid	4.3
Sodium citrate	3.0

250 mL of inoculum was prepared in a conical flask by adding all the chemicals listed in Table A.2. The inoculum was adjusted to pH 5 by using solutions of 1 N of NaOH and 1 N of H_2SO_4. The inoculum is covered with cotton wool and aluminium foil and sterilized at 121℃ for 20 minutes to avoid contamination and then cooled down to room temperature. 1 g of Baker's yeast is added and stand for 8-10 hours for microbial growth. Cotton wool and aluminium foil are used to cover the conical flask to prevent contamination. The appearance of inoculum after 8-10 hours is shown in Figure A.2.

A.3 Preparation of Mango Juice

The rejected mango fruits were needed for mango juice preparation. The damaged parts of fruits were removed. The mango fruits were blended into juice by using blender and the juice was filtered by using a filter bag. The pure filtered fresh mango juice was ready for used.

Figure A.2: Inoculum after 8-10 hours

A.4 Sample Analysis

A number of samples were taken throughout the experiment for every 2-3 hours of sampling interval. The concentrations of glucose and ethanol were analyzed by using R-Biopharm test kits and UV spectrophotometer (Lambda 25) at a wavelength of 340 nm under room temperature. The preparations were done based on the procedures provided by the manuals of the test kits under different concentration measurements. Semi-micro (1.5 L) methacrylate cuvettes are used during the analysis process. Figure A.3 shows the R-Biopharm test kits for glucose and ethanol, whilst Figure fig:UV shows the UV spectrophotometer used for analysis.

On the other hand, the biomass concentration was analyzed by using UV spectrophotometer at a wavelength of 340 nm for cell concentration. Prior to analysis, the sample was diluted to appropriate concentrations so that the range of absorbance range was between 0.1 and 0.4.

Figure A.3: R-Biopharm test kits for glucose and ethanol

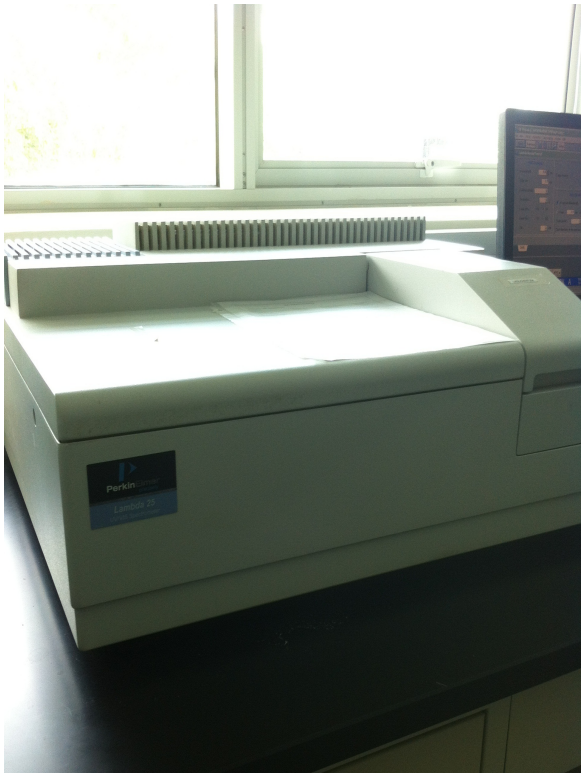

Figure A.4: UV spectrophotometer (Lambda 25)

A.4.1 Calculation of Glucose Concentration

The calculation of glucose concentration was done based on the manual provided by glucose test kit. The absorbances of the solutions were measured by using UV

spectrophotometer at a wavelength of 340 nm under temperature of 25℃, whereby the absorbance value were recorded for the calculation of glucose concentration based on the equation as follows:

$$\Delta A = (A_1 - A_2)_{sample} - (A_1 - A_2)_{blank} \tag{A.1}$$

where A_1 is the absorbance value upon reaction after approximately 3 minutes before adding suspension 2.

A_2 is the absorbance value upon reaction after approximately 10-15 minutes after adding suspension 2.

$$c = \frac{V \times MW}{\epsilon \times d \times v \times 1000} \times \Delta A[g/L] \tag{A.2}$$

where V = final volume [mL]

v = sample volume [mL]

MW = molecular weight of the substance to be assayed [g/mol]

d = light path = 1 cm

ϵ = extinction coefficient of NADPH at 340 nm = 6.3 $[L \times mmol^{-1} \times cm^{-1}]$

Notice that, the result have to multiply by dilution factor F.

A.4.2 Calculation of Ethanol Concentration

The calculation of ethanol concentration was measured in the similar way as the analysis of glucose concentration at a wavelength of 340 nm under temperature of 25℃. The absorbance value were recorded for the calculation of ethanol concentration as follows:

$$\Delta A = (A_1 - A_2)_{sample} - (A_1 - A_2)_{blank} \tag{A.3}$$

where A_1 is the absorbance value upon reaction after approximately 3 minutes before adding suspension 2.

A_2 is the absorbance value upon reaction after approximately 5-10 minutes after adding suspension 2.

$$c = \frac{V \times MW}{\epsilon \times d \times v \times 1000} \times \Delta A[g/L] \tag{A.4}$$

where V = final volume [mL]

v = sample volume [mL]

MW = molecular weight of the substance to be assayed [g/mol]

d = light path = 1 cm

ϵ = extinction coefficient of NADPH at 340 nm = 6.3 $[L \times mmol^{-1} \times cm^{-1}]$

Note that, the result have to multiply by dilution factor F.

Appendix B

Detailed Calculations on the Necessary Region for Fourth-order Integrating Nonminimum-phase System

B.1 Case 1: Example

Sub-case 1.1: $\zeta_1 > 0$, $\zeta_2 > 0$ and $\zeta_3 > 0$

For this sub-case 1.1, since $\zeta_1 > 0$, $\zeta_2 > 0$ and $\zeta_3 > 0$, there exists only 1 lower limit ($\underline{K}_o^{nc}$) on the loop gain from the coefficient of s^0 as

$$K > \underline{K}_o^{nc} = 0 \tag{B.1}$$

In addition to the lower limit on the integral time ($\underline{I}_1^{nc}$) in (5.18), the ranges of derivative time and integral time can be determined from the conditions given in sub-case 1.1 where $\zeta_1 > 0$, $\zeta_2 > 0$ and $\zeta_3 > 0$ as follows. In view of $\zeta_1 > 0$, the derivative time must be bounded from below

$$\tau_D < \overline{D}_{1.1,1}^{nc} = \frac{q_3}{|q_1|} \tag{B.2}$$

For $\zeta_2 > 0$ to occur, it is required that the integral time must be bounded as follows

$$\tau_I < \overline{I}_{1.1,1}^{nc} = \frac{q_3}{\tau_D|q_2| + |q_1|} \tag{B.3}$$

Notice that, to ensure that the upper limit on the integral time (B.3) holds, the denominator of (B.3) must be positive. Otherwise, the integral time will become

a negative upper limit - $\tau_I > 0$ violated. Hence, by assuming that denominator of (B.3) is always positive, the negative lower bound on the derivative time is given, i.e., $\tau_D > -\frac{|q_1|}{|q_2|}$, which can be ignored as only $\tau_D > 0$ is considered in this case. In view of $\zeta_3 > 0$, another lower bound on the integral time is produced

$$\tau_I > \underline{I}^{nc}_{1.1,1} = \frac{|q_1|}{\tau_D - |q_2|} \tag{B.4}$$

where the denominator of (B.4) must be positive to guarantee a positive lower bound on the integral time. Hence, the derivative time must be limited by a lower bound as follows

$$\tau_D > \underline{D}^{nc}_{1.1,1} = |q_2| \tag{B.5}$$

Remark 23. *Based on Theorem 4.2.1 states, the upper limit on the integral time must always be greater than the lower limit to ensure that the necessary criterion of the Routh stability is obeyed, otherwise, no stable PID controller exists to stabilize the process.*

In view of remark 23, we have to ensure that the upper limit on the integral time (B.3) is always greater than the lower limit (5.18), thus another upper limit on the derivative time is imposed:

$$\tau_D < \overline{D}^{nc}_{1.1,2} = \frac{q_3 - |q_1||q_2|}{|q_2|^2} \tag{B.6}$$

Also, the upper limit on the integral time (B.3) must be greater than the lower limit (B.4), another lower limit on the derivative time is obtained:

$$\tau_D > \underline{D}^{nc}_{1.1,2} = \frac{|q_1|^2 + q_3|q_2|}{q_3 - |q_1||q_2|} \tag{B.7}$$

where the limits $q_3 > |q_1||q_2|$ is given to ensure the numerator of (B.6) and denominator of (B.7) must be positive.

Since there are multiple upper and lower limits, to meet the Routh stability necessary criterion, Theorem 4.2.1 stipulates that the derivative time have to be bounded between its maximum lower limit and minimum upper limit, i.e.:

$$max(0, \underline{D}^{nc}_{1.1,1}, \underline{D}^{nc}_{1.1,2}) < \tau_D < min(\overline{D}^{nc}_{1.1,1}, \overline{D}^{nc}_{1.1,2}) \tag{B.8}$$

The ranges of derivative time are used to verify the stability of PID controller. The minimum upper limit must always greater than the maximum lower limit, otherwise, there is no stable PID controller exists for stabilizing the given process -

violate the necessary condition for closed-loop stability as stated by the Theorem 4.2.1. However, the inequality above is hard to prove analytically; due to the complexity of the equation. Alternatively, the results can be proved graphically.

The difference between the maximum lower limit and minimum upper limit on the derivative time can be determined as:

$$R = \overline{D}_{min} - \underline{D}_{max} \tag{B.9}$$

Let us take an exponential function on R and further by logarithms function as follows:

$$log(R) = log_{10}(e^R) \tag{B.10}$$

The graph of $log(R)$ versus λ_1 are shown in Figure B.1 where $\lambda_2 = 0.4, 0.8, 1.5, 5$ and $\tau_{z3} = 3$ for validation. As illustrations, $\lambda_2 = 0.4, 0.8$ and $\lambda_2 = 1.5, 5$ are used as examples to illustrate $\lambda_2 < 1$ and $\lambda_2 > 1$ respectively.

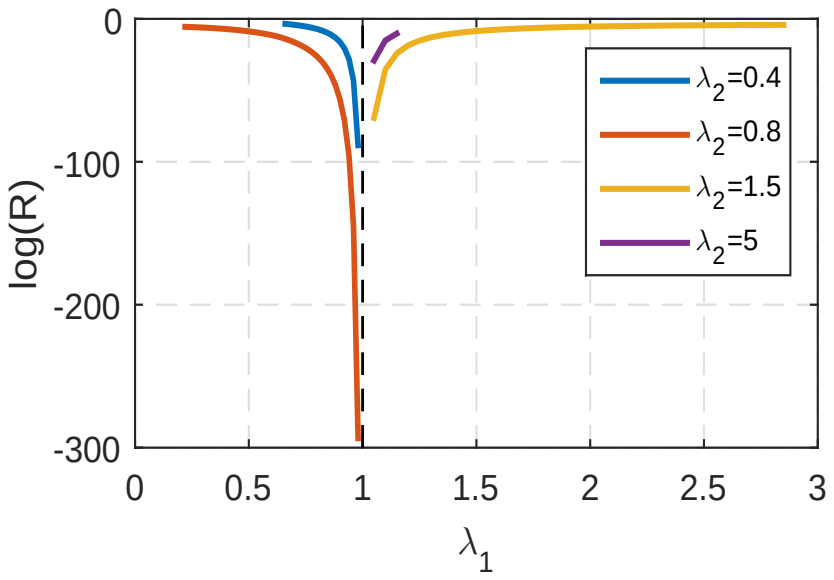

Figure B.1: Sub-case 1.1 - $log(R)$ versus λ_1

Figure B.1 shows that the $log(R)$ gives negative value when $\lambda_2 = 0.4, 0.8, 1.5, 5$ and $\tau_{z3} = 3$, which means that the minimum upper limit on derivative time is always lower than its maximum lower limit - Theorem 4.2.1 is violated. Thus, it can be proved that the closed-loop stability cannot be satisfied, thus there is no stable PID controller exists to stabilize this sub-cases 1.1.

Sub-case 1.2: $\zeta_1 > 0$, $\zeta_2 > 0$ and $\zeta_3 < 0$

Under the sub-case 1.2, there exists only 1 lower limit ($\underline{K}_o^{nc}$) and 1 upper limit ($\overline{K}_{1c}^{nc}$) on the loop gain. For closed-loop stability, it is necessary that the range of

loop gain must lie between these lower limit and upper limit. As such, the range of loop gain is given as:

$$\underline{K}_o^{nc} < K < \overline{K}_{1c}^{nc} \tag{B.11}$$

From the closed-loop characteristic polynomial, the coefficient of s always leads to a lower limit on the integral time (5.18). Moreover, the upper and lower limits on the derivative time and integral time can be obtained from ζ_1, ζ_2 and ζ_3. When $\zeta_1 > 0$, the upper limit on the derivative time is given as

$$\tau_D < \overline{D}_{1.2,1}^{nc} = \frac{q_3}{|q_1|} \tag{B.12}$$

Additionally, the integral time must be bounded from below when $\zeta_2 > 0$.

$$\tau_I < \overline{I}_{1.2,1}^{nc} = \frac{q_3}{\tau_D|q_2| + |q_1|} \tag{B.13}$$

By assuming the denominator of (B.13) is always positive, a negative lower bound on the derivative time is given as $\tau_D > -\frac{|q_1|}{|q_2|}$. It should be note that only $\tau_D > 0$ is considered, thus, the given negative lower bound on the derivative time can be neglected in this case.

By rearranging the coefficient of the loop gain given by $\zeta_3 < 0$, it can either form a positive upper limit or a negative lower limit on the integral time. The upper bound on the integral time is undesired as it give a limitation on selecting the range of integral time. Hence, the negative lower limit on the integral time is preferred in this case, which give a larger range on integral time as follows:

$$\tau_I > \underline{I}_{1.2,1}^{nc} = -\frac{|q_1|}{|q_2| - \tau_D} \tag{B.14}$$

Note that, the negative lower limit on the integral time above (B.14) can be neglected as only $\tau_I > 0$ is considered in this case. However, the denominator of (B.14) must be positive to ensure this negative lower limit on the integral time holds, which means that the derivative time has to be restricted by an upper limit as follows:

$$\tau_D < \overline{D}_{1.2,2}^{nc} = |q_2| \tag{B.15}$$

In view of remark 23, to ensure that the upper limit on the integral time (B.13) is greater than the maximum lower limit (5.18), a upper limit on the derivative time has to be imposed:

$$\tau_D < \overline{D}_{1.2,3}^{nc} = \frac{q_3 - |q_1||q_2|}{|q_2|^2} \tag{B.16}$$

where the inequality $q_3 > |q_1||q_2|$ is established to ensure the numerator of (B.16) must be positive.

For this sub-case 1.2, only upper limits on the derivative time are encountered. Since $\tau_D > 0$, in order to fulfill the Theorem 4.2.1 - necessary criterion of Routh stability, the range of derivative time is bounded as:

$$0 < \tau_D < min(\overline{D}^{nc}_{1.2,1}, \overline{D}^{nc}_{1.2,2}, \overline{D}^{nc}_{1.2,3}) \tag{B.17}$$

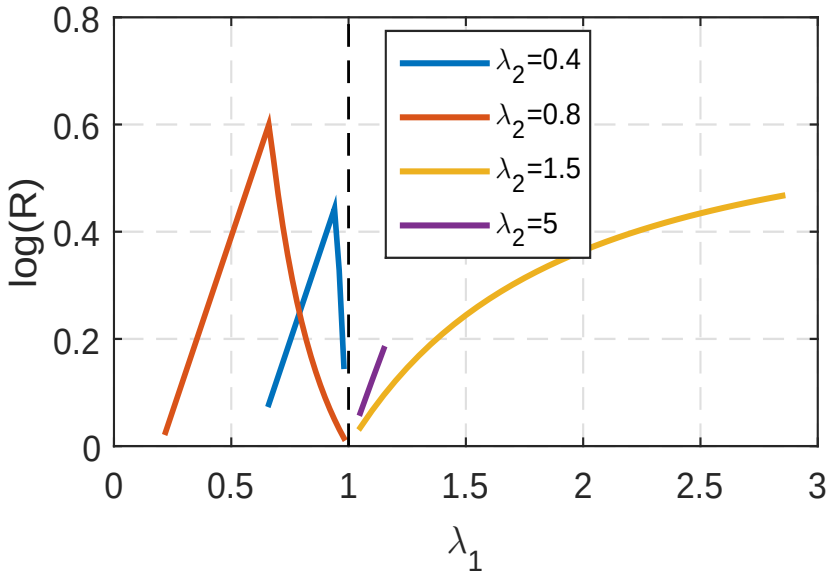

Figure B.2: Sub-case 1.2 - $log(R)$ versus λ_1

The limits on the derivative time are used to verify the closed-loop stability of a PID controller. For this sub-case 1.2, the graph of $log(R)$ versus λ_1 is shown in Figure B.2 where $\lambda_2 = 0.4, 0.8, 1.5, 5$ and $\tau_{z3} = 3$ are used for validation. $\lambda_2 = 0.4, 0.8$ are used to illustrate $\lambda_2 < 1$ while $\lambda_2 = 1.5, 5$ are used as examples to describe $\lambda_2 > 1$. In Figure B.2, the results show that the positive values of $log(R)$ can be attained when $\lambda_1 < 0$, $\lambda_2 < 0$ and when $\lambda_1 > 0$, $\lambda_2 > 0$. It can be proved that for this sub-case 1.2, it can only be stabilized by using a PID controller when $\lambda_1 < 0$, $\lambda_2 < 0$ or when $\lambda_1 > 0$, $\lambda_2 > 0$ in certain range given in Figure B.2.

B.2 Case 2: Example

The sub-case 2.1 is used as illustration as follows.

Sub-case 2.1: $\zeta_1 > 0$, $\zeta_2 > 0$ and $\zeta_3 > 0$

Under the sub-case 2.1, the conditions $\zeta_1 > 0$, $\zeta_2 > 0$ and $\zeta_3 > 0$ result in only 1 non-negative lower limit ($\underline{K}_o^{nc}$) on the loop gain as

$$K > \underline{K}_o^{nc} = 0 \tag{B.18}$$

The coefficient of s in the characteristic equation always lead to a lower limit on the integral time as in (5.25). The upper and lower limits on the integral time and derivative time can be determined based on ζ_1, ζ_2 and ζ_3. For $\zeta_1 > 0$ to be valid, the derivative time has to be greater than certain value, i.e., $\tau_D > -\frac{q_3}{q_1}$, which will not be taken into account as we assume $\tau_D > 0$.

When $\zeta_2 > 0$ occurred, a negative lower limit on the integral time is given based on the coefficient of s^3 in characteristic equation as follows

$$\tau_I > -\frac{q_3}{-\tau_D|q_2| + q_1}$$

To ensure this negative lower limit on the integral time holds, the denominator must be positive, which the derivative time limited by an upper limit

$$\tau_D < \overline{D}_{2.1,1}^{nc} = \frac{q_1}{|q_2|} \tag{B.19}$$

On the other hand, when $\zeta_3 > 0$, another negative lower limit on the integral time is obtained as

$$\tau_I > -\frac{q_1}{\tau_D - |q_2|}$$

Thus, the lower bound on the derivative time is given to ensure that the denominator of the lower limit on the integral time above to be valid.

$$\tau_D > \underline{D}_{2.1,1}^{nc} = |q_2| \tag{B.20}$$

In this sub-case 2.1, there exists only 1 lower limit on the integral time (5.25) based on necessary criterion of Routh stability. There is no extra limits on the derivative time to be imposed to ensure that the upper limit on the integral time is always greater than its lower limit.

The range of the derivative time is imposed as to fulfill the necessary criterion of Routh stability (Theorem 4.2.1), i.e.:

$$max(0, \underline{D}_{2.1,1}^{nc}) < \tau_D < \overline{D}_{2.1,1}^{nc} \tag{B.21}$$

The upper and lower limits on the derivative time are used to verify the stability of PID controller for the given process. The graph of $log(R)$ versus λ_1

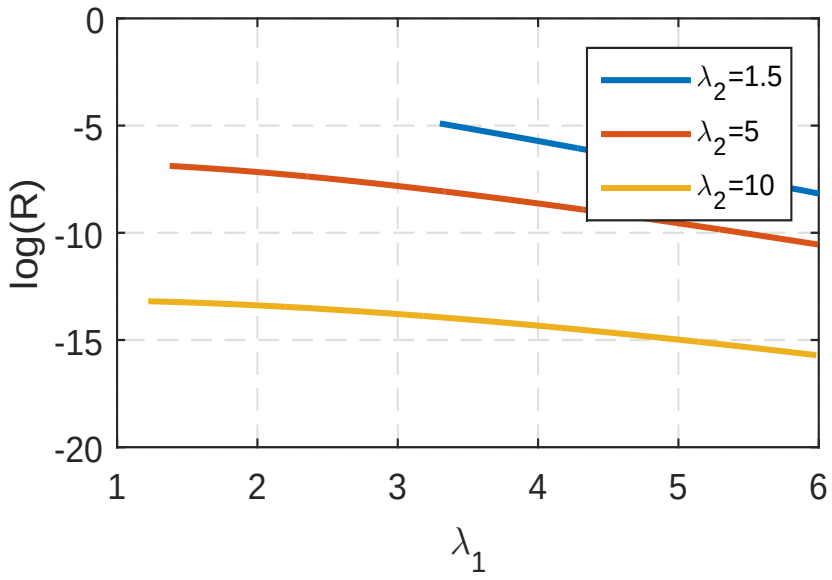

Figure B.3: Sub-case 2.1 - $log(R)$ versus λ_1

is shown in Figure B.3. Consider $\lambda_2 > 1$, for an illustration, $\lambda_2 = 1.5, 5, 10$ and $\tau_{z3} = 3$ are used for the validation of the range of derivative time.

The results show that the $log(R)$ is always negative value when $\lambda_2 = 1.5, 5, 10$ and $\tau_{z3} = 3$, which means that the minimum upper limit on the derivative time is always lower than its maximum lower limit - violation of Theorem 4.2.1. It can be proved that the closed-loop stability of the given process is not stable.

B.3 Case 3: Example

The sub-cases 3.1 is demonstrated as illustration as follows.

Sub-case 3.1: $\zeta_1 > 0$, $\zeta_2 > 0$ and $\zeta_3 > 0$

For this sub-case 3.1 to occur, there exists only 1 lower limit on the loop gain from the coefficient s^0.

$$K > \underline{K}_o^{nc} = 0 \tag{B.22}$$

When $\zeta_1 > 0$, we have an upper limit on the derivative time

$$\tau_D < \overline{D}_{3.1,1}^{nc} = \frac{q_3}{|q_1|} \tag{B.23}$$

Based on the $\zeta_2 > 0$, we can further obtain a negative value of lower limit on the integral time.

$$\tau_I > -\frac{q_3}{\tau_D q_2 - |q_1|}$$

which the denominator must be positive, it stipulates the derivative time must be bounded from below, hence

$$\tau_D > \underline{D}^{nc}_{3.1,1} = \frac{|q_1|}{q_2} \tag{B.24}$$

For the $\zeta_3 > 0$ to be valid, the integral time has to be greater than a certain value given by

$$\tau_I > \underline{I}^{nc}_{3.1,1} = \frac{q_1}{\tau_D + q_2} \tag{B.25}$$

The denominator of (B.25) must be positive to guarantee the lower limit on the integral time holds, which deliver a negative value of lower limit on the derivative time, i.e., $\tau_D > q_2$. This negative lower bound on the derivative time can be neglected as we only consider $\tau_D > 0$ in this case.

The range of derivative time is used to guarantee the stability of PID controller as follows

$$max(0, \underline{D}^{nc}_{3.1,1}) < \tau_D < min(\overline{D}^{nc}_{3.1,1}) \tag{B.26}$$

According to necessary critetion of Routh stability, the minimum upper limit on the derivative time (B.23) must be greater than its lower limit (B.24). It should be note that, there is no stable PID controller exists for stabilizing this sub-case 3.1 as the upper limit on the derivative time (B.23) is always less than the lower limit (B.24), which can be proved analytically - violate the Theorem 4.2.1. Additionally, the graph of $log(R)$ versus λ_1 is shown in Figure B.4.

In Figure B.4, it can be readily shown that the $log(R)$ is always in negative value when $\lambda_2 = 0.2, 0.4, 0.6, 0.8$ and $\tau_{z3} = 3$, which means that the minimum upper limit on the derivative time is lower than its maximum lower limit, i.e. Theorem 4.2.1 is violated. Thus, it can be proved that the closed-loop stability of this sub-case 3.1 is not stable.

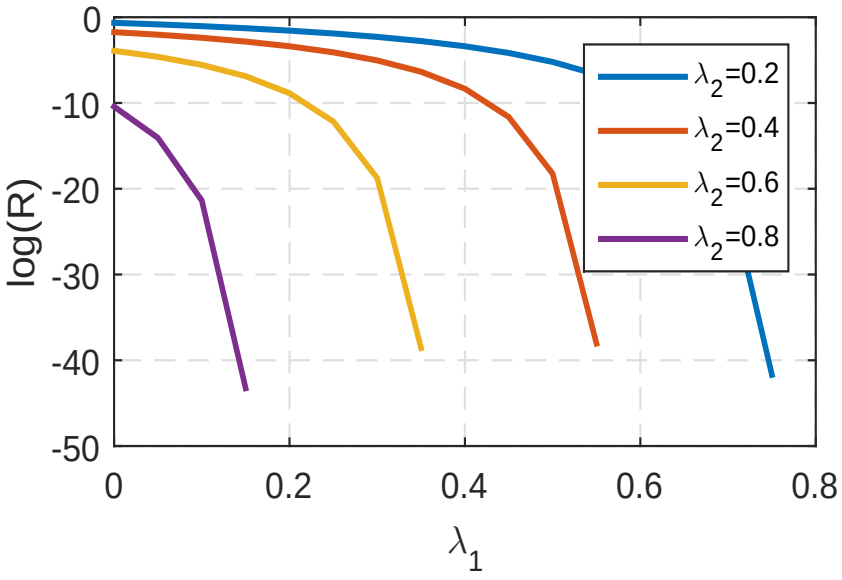

Figure B.4: Sub-case 3.1 - $log(R)$ versus λ_1

Appendix C

Extractive Alcoholic Fermentation Model

C.1 System Model

The dynamic model of a extractive bioreactor system of ethanol fermentation are shown as follows:

$$\frac{dL}{dt} = \frac{F_{in} - F}{A} \tag{C.1a}$$

$$\frac{dX_v}{dt} = \alpha r_{x,1} + (1-\alpha) r_{x,2} - \left(\frac{FX_v - F_{in}X_{v,in}}{V}\right) - \frac{X_v dL}{L} \tag{C.1b}$$

$$\frac{dC_g}{dt} = -\alpha r_{s,1} + \left(\frac{F_{in}C_{g,in} - FC_g}{V}\right) - \frac{C_g dL}{L} \tag{C.1c}$$

$$\frac{dC_x}{dt} = -(1-\alpha) r_{s,2} + \left(\frac{F_{in}C_{x,in} - FC_x}{V}\right) - \frac{C_x dL}{L} \tag{C.1d}$$

$$\frac{dC_e}{dt} = \alpha r_{p,1} + (1-\alpha) r_{p,2} - \left(\frac{FC_e - F_{in}C_{e,in}}{V}\right) - \frac{C_e dL}{L} \tag{C.1e}$$

$$\frac{dT}{dt} = \left(\frac{F_{in}T_{in} - FT}{V}\right) + \frac{\Delta H(\alpha r_{s,1} + (1-\alpha) r_{s,2})}{\rho C_p} - \frac{T dL}{L} \tag{C.1f}$$

where the variables L, X_v, C_g, C_x, C_e, and T denote the medium level (m), biomass concentration (kg/m^3), glucose concentration (kg/m^3), xylose concentration (kg/m^3), ethanol concentration (kg/m^3) and temperature (℃) respectively. The cross-sectional area of fermentor (A) is given as 50 m^2. The weighting factor of substrate consumptions is given as

$$\alpha = \frac{r_{s,1}}{r_{s,1} + r_{s,2}} \tag{C.2}$$

The cell growth on glucose (1) and xylose (2) is represented by the specific growth rates of recombinant *Z. mobilis* ZM4(pZB5) are shown as

$$r_{x,1} = \mu_{max,1}\left(\frac{C_g}{K_{sx,1}+C_g}\right)\left(1-\frac{C_e-P_{ix,1}}{P_{mx,1}-P_{ix,1}}\right)\left(\frac{K_{ix,1}}{K_{ix,1}+C_g}\right) \tag{C.3}$$

$$r_{x,2} = \mu_{max,2}\left(\frac{C_x}{K_{sx,2}+C_x}\right)\left(1-\frac{C_e-P_{ix,2}}{P_{mx,2}-P_{ix,2}}\right)\left(\frac{K_{ix,2}}{K_{ix,2}+C_x}\right) \tag{C.4}$$

The rates of glucose (1) and xylose (2) consumption on are represented as

$$r_{s,1} = q_{s,max,1}\left(\frac{C_g}{K_{ss,1}+C_g}\right)\left(1-\frac{C_e-P_{is,1}}{P_{ms,1}-P_{is,1}}\right)\left(\frac{K_{is,1}}{K_{is,1}+C_g}\right) \tag{C.5}$$

$$r_{s,2} = q_{s,max,2}\left(\frac{C_x}{K_{ss,2}+C_x}\right)\left(1-\frac{C_e-P_{is,2}}{P_{ms,2}-P_{is,2}}\right)\left(\frac{K_{is,2}}{K_{is,2}+C_x}\right) \tag{C.6}$$

The rate of ethanol production on glucose (1) and xylose (2) are

$$r_{p,1} = q_{p,max,1}\left(\frac{C_g}{K_{sp,1}+C_g}\right)\left(1-\frac{C_e-P_{ip,1}}{P_{mp,1}-P_{ip,1}}\right)\left(\frac{K_{ip,1}}{K_{ip,1}+C_g}\right) \tag{C.7}$$

$$r_{p,2} = q_{p,max,2}\left(\frac{C_x}{K_{sp,2}+C_x}\right)\left(1-\frac{C_e-P_{ip,2}}{P_{mp,2}-P_{ip,2}}\right)\left(\frac{K_{ip,2}}{K_{ip,2}+C_x}\right) \tag{C.8}$$

The kinetics parameters and physical constants adopted in this study can be found in Table C.1 and C.2. Furthermore, other algebraic equations describing the system are given as:

$$F_{in} = F_o + F_R + F_r \tag{C.9}$$

$$F_R = RF \tag{C.10}$$

$$F_r = rF_L \tag{C.11}$$

Table C.1: Kinetic parameters

Glucose		Xylose	
Specific growth rate			
$\mu_{max,1}$	0.31	$\mu_{max,2}$	0.1
$K_{sx,1}$	1.45	$K_{sx,2}$	4.91
$P_{mx,1}$	80	$P_{mx,2}$	80
$K_{ix,1}$	200	$K_{ix,2}$	600
$P_{ix,1}$	28.9	$P_{ix,2}$	26.6
Rate of substrate consumption			
$q_{s,max,1}$	10.9	$q_{s,max,2}$	3.27
$K_{ss,1}$	6.32	$K_{ss,2}$	0.03
$P_{ms,1}$	75.4	$P_{ms,2}$	81.2
$K_{is,1}$	186	$K_{is,2}$	600
$P_{is,1}$	42.6	$P_{is,2}$	53.1
Rate of ethanol production			
$q_{p,max,1}$	5.12	$q_{p,max,2}$	1.59
$K_{sp,1}$	6.32	$K_{sp,2}$	0.03
$P_{mp,1}$	75.4	$P_{mp,2}$	81.2
$K_{ip,1}$	186	$K_{ip,2}$	600
$P_{ip,1}$	42.6	$P_{ip,2}$	53.1

Table C.2: Physical constants

Physical constants	
ΔH (kJ/kg)	51.76
ρ (kg/m^3)	1000
C_p (kJ/kg ℃)	1.0

Appendix D

Linearization and Partial Fraction Expansion

D.1 Linearization

D.1.1 Linearized Rate Equations

The linearization of nonlinear rate equations of fed-batch bioreactor process using Taylor Series approximation is as follows.

$$r_x = \overline{r_x} + \beta_{xs}G' + \beta_{xx}X' + \beta_{xp}P' \tag{D.1}$$

$$r_p = \overline{r_p} + \beta_{ps}G' + \beta_{px}X' + \beta_{pp}P' \tag{D.2}$$

$$r_s = \overline{r_s} + \beta_{ss}G' + \beta_{sx}X' + \beta_{sp}P' \tag{D.3}$$

$$r_d = \overline{r_d} + k_d X' \tag{D.4}$$

where the parameters are given by

$$\overline{r_x} = \delta_1 \overline{GX} \tag{D.5}$$

$$\beta_{xs} = (\delta_1 - \delta_2 \overline{G})\overline{X} \tag{D.6}$$

$$\beta_{xx} = \delta_1 \overline{G} \tag{D.7}$$

$$\beta_{xp} = -\delta_3 \overline{GX} \tag{D.8}$$

$$\overline{r_p} = Y_p \overline{r_x} + m_p \overline{X} \tag{D.9}$$

$$\beta_{ps} = Y_p \beta_{xs} \tag{D.10}$$

$$\beta_{px} = Y_p \beta_{xx} + m_p \tag{D.11}$$

$$\beta_{pp} = Y_p \beta_{xp} \tag{D.12}$$

$$\overline{r_s} = Y_s \overline{r_x} + m_s \overline{X} \tag{D.13}$$

$$\beta_{ss} = Y_s \beta_{xs} \tag{D.14}$$

$$\beta_{sx} = Y_s \beta_{xx} + m_s \tag{D.15}$$

$$\beta_{sp} = Y_s \beta_{xp} \tag{D.16}$$

Others parameters:

$$\delta_1 = \frac{\mu_0}{K_{s0} + \overline{G} + K_{s1}\overline{G}^2} exp\left(- \frac{P}{P_{max}} \right) \tag{D.17}$$

$$\delta_2 = \frac{(1 + sK_{s1})\mu_0}{(K_{s0} + \overline{G} + K_{s1}\overline{G}^2)^2} exp\left(- \frac{P}{P_{max}} \right) \tag{D.18}$$

$$\delta_3 = \frac{\delta_1}{P_{max}} \tag{D.19}$$

D.1.2 Linearized Convective Terms

Let

$$f_x = \frac{FX}{V} \cong \frac{\overline{FX}}{\overline{V}} + \gamma_{xf} F' + \gamma_{xx} X' + \gamma_{xv} V' \tag{D.20}$$

where $\gamma_{xf} = \frac{\overline{X}}{\overline{V}}$, $\gamma_{xx} = \frac{\overline{F}}{\overline{V}}$, $\gamma_{xv} = -\frac{\overline{FX}}{\overline{V}^2}$ and $Y' = Y - \overline{Y}$ denote the deviated variable form and the value at which the linearization is made, respectively.

Let

$$f_s = \frac{F(G_{in} - G)}{V} \cong \frac{\overline{F}(G_{in} - \overline{G})}{\overline{V}} + \gamma_{sf}F' + \gamma_{ss}G' + \gamma_{sv}V' \tag{D.21}$$

where $\gamma_{sf} = \frac{G_{in}-\overline{G}}{\overline{V}}$, $\gamma_{ss} = -\frac{\overline{F}}{\overline{V}}$ and $\gamma_{sv} = -\frac{\overline{F}(G_{in}-\overline{G})}{\overline{V}^2}$.
Let

$$f_p = \frac{FP}{V} \cong \frac{\overline{FP}}{\overline{V}} + \gamma_{pf}F' + \gamma_{pp}P' + \gamma_{pv}V' \tag{D.22}$$

where $\gamma_{pf} = \frac{\overline{P}}{\overline{V}}$, $\gamma_{pp} = \frac{\overline{F}}{\overline{V}}$ and $\gamma_{pv} = -\frac{\overline{FP}}{\overline{V}^2}$.

D.2 Development of Linearized Model

Let us convert the model equations (5.3) into the deviated variable form:

$$\frac{dV'}{dt} = F' \tag{D.23}$$

$$\frac{dX'}{dt} = \beta_{xs}G' + \beta_{xx}X' + \beta_{xp}P' - k_dX' - (\gamma_{xf}F' + \gamma_{xx}X' + \gamma_{xv}V') \tag{D.24}$$

$$\frac{dG'}{dt} = -(\beta_{ss}G' + \beta_{sx}X' + \beta_{sp}P') + \gamma_{sf}F' + \gamma_{ss}G' + \gamma_{sv}V' \tag{D.25}$$

$$\frac{dP'}{dt} = \beta_{ps}G' + \beta_{px}X' + \beta_{pp}P' - (\gamma_{pf}F' + \gamma_{pp}P' + \gamma_{pv}V') \tag{D.26}$$

Laplace Transform is applied to all 4 of the model equations which leads to:

$$V'(s) = \frac{F'(s)}{s} \tag{D.27}$$

$$X'(s) = \frac{1}{L_1(s)}\left[\beta_{xs}G'(s) + \beta_{xp}P'(s) - \frac{N_1(s)}{s}F'(s)\right] \tag{D.28}$$

$$G'(s) = \frac{1}{L_2(s)}\left[\frac{N_3(s)}{s}F'(s) - \beta_{sx}X'(s) - \beta_{sp}P'(s)\right] \tag{D.29}$$

$$P'(s) = \frac{1}{L_3(s)}\left[\beta_{ps}G'(s) + \beta_{px}X'(s) - \frac{N_2(s)}{s}F'(s)\right] \tag{D.30}$$

where $L_1(s) = s + a_1$, $L_2(s) = s + a_2$, $L_3(s) = s + a_3$, $N_1(s) = \gamma_{xf}s + \gamma_{xv}$, $N_2(s) = \gamma_{pf}s + \gamma_{pv}$, $N_3(s) = \gamma_{sf}s + \gamma_{sv}$, $a_1 = \gamma_{xx} + k_d - \beta_{xx}$, $a_2 = \beta_{ss} - \gamma_{ss}$ and $a_3 = \gamma_{pp} - \beta_{pp}$.

It can be readily shown that the overall transfer function relating the input F to output G can be written in the form of

$$G_p = \frac{L_3(L_1N_3 + \beta_{sx}N_1) + \beta_{xp}(\beta sxN_2 - \beta_{px}N_3) + \beta_{sp}(L_1N_2 + \beta_{px}N_1)}{s[L_3(L_1L_2 + \beta_{sx}\beta_{xs}) + \beta_{sp}(L_1\beta_{ps} - \beta_{px}\beta_{xs}) + \beta_{xp}(L_2\beta_{px} - \beta_{sx}\beta_{ps})]} \quad \text{(D.31)}$$

D.3 Partial Fraction Expansion

The partial fraction expansion is applied to decompose process transfer function (5.9) into a sum of three basic factors as follows:

$$G_p = \frac{k_1}{s} + \frac{k_2}{\tau_p s + 1} + \frac{k_3 s + k_4}{\alpha_2 s^2 + \alpha_1 s + 1} \quad \text{(D.32)}$$

where the parameters k_j, $j = 1, 2, 3, 4$ are given by $k_1 = K_p$, $k_2 = \frac{-K_p \prod_{i=1}^{3}(\tau_p - \tau_{zi})}{\alpha_2 - \alpha_1\tau_p + \tau_p^2}$, $k_3 = 2\psi_2 - \psi_1$ and $k_4 = \frac{\psi_1 - \psi_2}{\tau_p}$. Here,

$$\psi_1 = \frac{1}{3\tau_p}[K_p \prod_{i=1}^{3}(\tau_{zi} + 2\tau_p) - A_{m2}(k_2 + 3\tau_p k_1)] \quad \text{(D.33)}$$

$$\psi_2 = \frac{1}{2\tau_p}[K_p \prod_{i=1}^{3}(\tau_{zi} + \tau_p) - A_{m1}(k_2 + 2\tau_p k_1)] \quad \text{(D.34)}$$

where $A_{m1} = \alpha_2 + \alpha_1\tau_p + \tau_p^2$ and $A_{m2} = \alpha_2 + 2\alpha_1\tau_p + 4\tau_p^2$.